TECHNISCHE UNIVERSITÄT MÜNCHEN
Lehrstuhl für Proteomik und Bioanalytik

PHOSPHOPROTEOMICS FOR MODE OF ACTION ANALYSIS OF TARGETED CANCER DRUGS

Svenja Wiechmann

Vollständiger Abdruck der von der Fakultät TUM School of Life Sciences der Technischen Universität München zur Erlangung des akademischen Grades eines

Doktors der Naturwissenschaften

genehmigten Dissertation.

Vorsitzende:	Prof. Angelika Schnieke, Ph.D.
Prüfer der Dissertation:	1. Prof. Dr. Bernhard Küster 2. Priv.-Doz. Dr. Günter Schneider

Die Dissertation wurde am 13.07.2020 bei der Technischen Universität München eingereicht und durch die Fakultät TUM School of Life Sciences am 27.10.2020 angenommen.

Table of contents

Abstract

Targeted cancer drugs that aim to perturb cancer-specific proteins and signaling networks promise enhanced efficacy and less toxic side effects than conventional approaches. However, the high prevalence of low responses, relapses and unwanted effects represents a major clinical obstacle. To obtain a better knowledge of the mode of actions of targeted cancer drugs, renowned clinical agents and different cancer types were subjected to a global and unbiased analysis by phosphoproteomics in this thesis.

The combination of radiation therapy with targeted agents could improve the limited therapeutic options for pancreatic cancer. In this regard, the (phospho)proteomes of radioresistant pancreatic ductal adenocarcinoma cells were analyzed to identify mechanisms of low response to radiation that may be overcome by targeted drugs. The common reaction of the cells to radiation engaged over 700 phosphorylation sites on more than 400 proteins, thereby uncovering novel members of the radiation-responsive signaling network. Among those, ten novel ATM substrates were confirmed by *in vitro* kinase assays. The radioresistant cells displayed a complex regulation of apoptotic processes that featured increased expression of NQO1. Moreover, comprehensive enrichment analysis pinpointed elevated Actin dynamics and FAK activity in radioresistant cells. These adaptions in cellular protein expression and signaling suggest pharmacological inhibition of NQO1 and FAK as putative new avenues towards radiosensitization.

Small molecule kinase inhibitors often bind to more than one target protein resulting in uncertain activities in patients. The combination of kinobeads affinity screening and phosphoproteomics enabled the study of the targets and effects on cellular signaling of the clinical AKT inhibitors AZD5363, GSK2110183, GSK690693, Ipatasertib and MK-2206 in HER2-overexpressing breast cancer cells. Between four and 29 nanomolar targets for each inhibitor and 1700 regulated phosphorylation sites were revealed. Common drug-responsive phosphorylation sites were based on AKT engagement and allowed an expanded view on the AKT signaling network. Within this network, 15 novel AKT substrates were corroborated by a recombinant kinase assay. Based on this data, a targeted PRM assay was established to reproducibly analyze further AKT inhibitors in higher throughput. Furthermore, a secretome analysis identified STC2 as a putative response marker in the cell culture model.

Another class of targeted agents are monoclonal antibodies that engage surface antigens and exert multiple actions. Here, the direct Fab-mediated effects of anti-HER2 pertuzumab and trastuzumab, in comparison to EGFR/HER2 inhibitor lapatinib, as well as anti-CD20 rituximab were analyzed by concentration- and time-dependent phosphoproteomics. A panel of breast cancer cell lines and B-cell lymphoma and lymphoblastoid cell lines were the basis to investigate both common effects and resistance mechanisms. Over 2000 responsive phosphorylation sites were mainly regulated by lapatinib, while trastuzumab and pertuzumab had only modest direct effects. In contrast, rituximab affected several thousands of phosphorylation events. Among these, phosphorylated MAPK1/3 can serve as s resistance and treatment marker. The role of MAPK1/3 for rituximab action was further confirmed by the sensitization of resistant cells by pharmacological inhibition of MAPK signaling pathway members. In addition, comprehensive pathway enrichment has uncovered the importance of an early activation of calcium-dependent NFAT signaling and a subsequent cell cycle arrest for the action of rituximab.

In conclusion, this thesis revealed the mode of actions of selected clinical small molecule inhibitors and monoclonal antibodies. It enabled a deep insight into the targets and effects of these agents on cancer signaling and shed light onto resistance mechanisms. Furthermore, this study enhanced our understanding of major signaling networks and may help to suggest novel targeted drugs for the application in patients. It can be considered a valuable resource for researchers in the field of medicine and cell biology.

Zusammenfassung

Zielgerichtete Krebsmedikamente, die darauf abzielen, krebsspezifische Proteine und Signalnetzwerke zu beeinträchtigen, versprechen eine verbesserte Wirksamkeit und weniger toxische Nebenwirkungen als herkömmliche Ansätze. Die hohe Prävalenz niedriger Ansprechraten, Rezidive und unerwünschter Wirkungen stellt jedoch ein großes klinisches Problem dar. Um ein besseres Verständnis der Wirkungsweise von zielgerichteten Krebsmedikamenten zu erhalten, wurden in dieser Dissertation renommierte klinische Wirkstoffe und verschiedene Krebsarten einer globalen und unvoreingenommenen Analyse durch die Phosphoproteomik unterzogen.

Die Kombination von Strahlentherapie mit zielgerichteten Wirkstoffen könnte die begrenzten therapeutischen Möglichkeiten bei Bauchspeicheldrüsenkrebs verbessern. In diesem Zusammenhang wurden die (Phospho)Proteome von strahlenresistenten duktalen Adenokarzinomzellen des Pankreas analysiert, um Mechanismen des geringen Ansprechens auf Strahlung zu identifizieren, die durch gezielte Medikamente überwunden werden könnten. Die gemeinsame Antwort der Zellen auf Strahlung umfasste über 700 Phosphorylierungsstellen an mehr als 400 Proteinen, wodurch neue Mitglieder des strahlenempfindlichen Signalnetzwerks aufgedeckt wurden. Darunter wurden zehn neuartige ATM-Substrate durch in vitro-Kinase-Assays bestätigt. Die strahlungsresistente Zellen zeigte eine komplexe Regulation apoptotischer Prozesse, die sich durch eine erhöhte Expression von NQO1 auszeichnet. Darüber hinaus konnte durch eine umfassende Anreicherungsanalyse eine erhöhte Aktindynamik und FAK-Aktivität in strahlenresistenten Zellen festgestellt werden. Diese Anpassungen in der zellulären Proteinexpression und Signalübertragung legen eine pharmakologische Hemmung von NQO1 und FAK als mutmaßlich neue Wege zur Strahlensensibilisierung nahe.

Niedermolekulare Kinaseinhibitoren binden oft an mehr als ein Zielprotein, was zu ungewissen Aktivitäten in Patienten beiträgt. Die Kombination von Affinitätsscreening mit Kinobeads und Phosphoproteomik ermöglichte die Untersuchung der Targets und der Auswirkungen der klinischen AKT-Inhibitoren AZD5363, GSK2110183, GSK690693, Ipatasertib und MK-2206 auf die zelluläre Signalübertragung in HER2-überexprimierenden Brustkrebszellen. Es wurden zwischen vier und 29 nanomolare Targets für jeden Inhibitor und 1700 regulierte Phosphorylierungsstellen gefunden. Häufige auf Medikamente ansprechende Phosphorylierungsstellen basierten auf der Bindung an AKT und erlaubten einen erweiterten Blick auf das AKT-Signalnetzwerk. Innerhalb dieses Netzwerks wurden 15 neuartige AKT-Substrate durch einen rekombinanten Kinase-Test bestätigt. Auf der Grundlage dieser Daten wurde ein zielgerichteter PRM-Assay etabliert, um weitere AKT-Inhibitoren bei höherem Durchsatz reproduzierbar zu analysieren. Darüber hinaus identifizierte die Sekretomanalyse STC2 als einen mutmaßlichen Behandlungsarker im Zellkulturmodell.

Eine weitere Klasse zielgerichteter Substanzen sind monoklonale Antikörper, die an Oberflächenantigenen angreifen und vielfältige Wirkungen ausüben. Hier wurden die direkten Fab-vermittelten Effekte von anti-HER2-Pertuzumab und Trastuzumab im Vergleich zum EGFR/HER2-Inhibitor Lapatinib sowie anti-CD20-Rituximab mittels konzentrations- und zeitabhängiger Phosphoproteomik analysiert. Ein Panel von Brustkrebs-Zelllinien sowie B-Zell-Lymphom- und Lymphoblastoid-Zelllinien bildeten die Grundlage für die Untersuchung sowohl der gemeinsamen Wirkungen als auch der Resistenzmechanismen. Über 2000 ansprechende Phosphorylierungsstellen wurden hauptsächlich durch Lapatinib reguliert, während Trastuzumab und Pertuzumab nur mäßige direkte Wirkungen hatten. Im Gegensatz dazu beeinflusste Rituximab mehrere tausend Phosphorylierungsereignisse. Unter diesen kann phosphoryliertes MAPK1/3 als Resistenz- und Behandlungsmarker dienen. Die Rolle von MAPK1/3 für die Wirkung von Rituximab wurde durch die Sensibilisierung resistenter Zellen durch pharmakologische Hemmung der Mitglieder des MAPK-Signalwegs weiter bestätigt. Schließlich wurde durch eine

umfassende Anreicherung der Signalwege die Bedeutung einer frühen Aktivierung des kalziumabhängigen NFAT-Signalweges und eines anschließenden Zellzyklus-Stillstands für die Wirkung von Rituximab aufgedeckt.

Zusammenfassend enthüllte diese Arbeit die Wirkungsweise ausgewählter klinischer niedermolekularer Inhibitoren und monoklonaler Antikörper. Sie ermöglichte einen tiefen Einblick in die Ziele und Wirkungen dieser Wirkstoffe auf die Krebssignalübertragung und beleuchtete Resistenzmechanismen. Darüber hinaus verbesserte diese Studie unser Verständnis wichtiger Signalnetzwerke und könnte dazu beitragen, neue zielgerichtete Medikamente für die Anwendung bei Patienten vorzuschlagen. Sie kann als eine wertvolle Ressource für Forschende auf dem Gebiet der Medizin und Zellbiologie angesehen werden.

I General introduction

Table of contents

1 Protein phosphorylation

1.1 Protein phosphorylation in cellular homeostasis

While the human genome was estimated to consist of > 20,000 genes [1], the human proteome is expected to be far more complex containing > 1 million species [2]. In addition to the prominent processes of genetic variations and alternative splicing of mRNA as a source of expanding protein diversity, post-translational modifications (PTMs) of proteins further increase the number of so-called 'proteoforms', which describe all molecular forms in which protein products of a single gene can exist [3]. By the covalent attachment of small chemical moieties or other proteins, PTMs can modulate manifold processes such as metabolism, signal transduction, and protein stability [4].

A key PTM in the regulation of cellular functions is protein phosphorylation, which is fine-tuned by the interplay of two enzyme groups: kinases and phosphatases. Protein kinases catalyze the process of phosphorylation, which is the transfer of the γ-phosphoryl group of adenosine triphosphate (ATP) to a specific residue on a protein by the formation of a phosphate ester linkage through a nucleophilic substitution reaction (Figure I-1). Dephosphorylation that is catalyzed by protein phosphatases reverses protein phosphorylation by hydrolyzing the phosphate ester and releasing the phosphate group into solution as a free ion. While protein phosphorylation itself was already discovered in 1906 [5], the role of ATP and the enzymatic nature of the attachment of the phosphate group was uncovered later. This happened in the 1950s when Fischer and Krebs as well as Burnett and Kennedy studied the conversion of phosphorylase b to phosphorylase a and mitochondrial extracts [6, 7]. It was later shown that the driving force behind phosphorylation is the energy released from the cleavage of the phosphoanhydride bond between the β- and γ-phosphate of ATP under a high cellular ATP/ADP ratio [8].

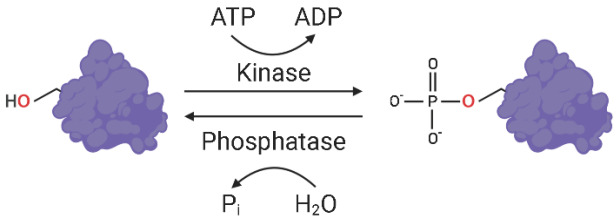

Figure I-1: The principle of reversible protein phosphorylation mediated by kinases and phosphatases. The transfer of the γ-phosphoryl group of ATP onto proteins is catalyzed by kinases. By hydrolyzing the phosphate ester, phosphatases reverse phosphorylation.

The first kinase was subsequently discovered in 1968, when Krebs purified cAMP-dependent protein kinase (PKA), which takes part in the activation cascade of phosphorylase a [9]. A study from 2002 reported that the human genome contains 518 genes that encode protein kinases, which can be further

categorized into nine groups based on their sequence similarity [10]. A more current report re-evaluated the annotation of kinases and found 555 members of the human kinome, from which 497 were allocated to the main class of eukaryotic protein kinases and 58 to the class of atypical protein kinases including lipid kinases [11]. Protein kinases share a conserved ensemble of secondary structures that include 12 subdomains folding into a bi-lobed catalytic core, which is connected by a flexible hinge region (Figure I-2). The ATP binding site is localized in a deep cleft between the two lobes [12]. The ribose and triphosphate groups of ATP bind in a hydrophilic channel, which further extends to the substrate binding site. Kinase activity is regulated by particular structures of the kinase that can adopt manifold conformations. The conserved DFG (aspartic acid, phenylalanine and glycine) sequence motif plays a pivotal role in the process of kinase activation and engages in a regulatory hydrophobic spine ('R-spine'). The DFG motif rotates and flips between the active state (DFG-in conformation; aspartate points into ATP pocket) and the inactive state of the kinase (DFG-out conformation) [13]. Phosphorylation of the conserved activation loop, 20-30 residues C-terminal of the DFG motif, is required for the activation of many kinases [14]. In addition, the largest fraction of phosphorylation in annotated pfam protein domains has been found for protein kinase domains, spanning not only the activation loop but the whole catalytic domain [15]. The activation of a kinase by an upstream kinase is the basis of cellular signaling cascades that enable fine-tuning and amplification of signal transduction [16]. Complete activation by interaction with binding partners is furthermore necessary for a few kinases such as cyclin-dependent kinases (CDKs) that engage cyclins forming catalytically active cyclin/CDK complexes [17].

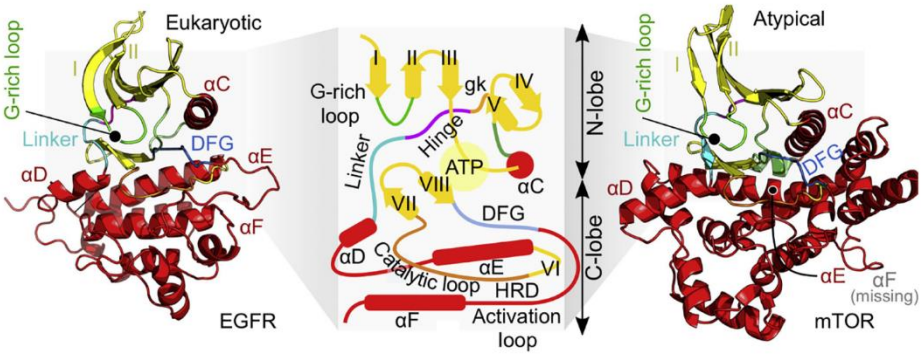

Figure I-2: Common structural characteristics of protein kinases. Typical features of the secondary structure of protein kinases, the ATP binding site and additional conserved elements, are shared among the kinome (middle). Exemplary structures for a eukaryotic (EGFR; left) and atypical kinase (mTOR; right) are displayed (adapted, with permission from [11]).

Despite the overall similar structural characteristics of kinases, large-scale studies in yeast have proven vast differences between the size of substrate spectra among the kinome which have ranged between 1 and 256 substrates for a kinase [18]. In a hypothetical calculation with ~ 10,000 different proteins of an

average length of ~ 400 amino acids kinases would need to specifically phosphorylate their substrates in a background of ~ 700,000 potential phosphorylation sites (p-sites) (without considering the exposure of these sites to the cytoplasm) [19, 20]. Mechanisms for kinase-substrate specificity are diverse and include the depth of the catalytic cleft allowing for the discrimination between tyrosine and serine/threonine residues, local interactions in proximity of the p-site, allosteric docking sites, distinct cellular localizations of kinases that increase local kinase concentrations, scaffolds that direct the interaction between kinases and substrates, competition between different putative p-sites and kinetic proofreading after aberrant off-target phosphorylation (reviewed in [20]). The number of counteracting phosphatases - ~ 200 - is far lower, which puts the question on how the reciprocity of phosphorylation and dephosphorylation is regulated in terms of substrate specificity [21]. One major principle on how the specificity of dephosphorylation is achieved appears to be driven by the interaction of the catalytic subunits of the phosphatase with regulatory domains. The catalytic subunit of protein phosphatase 1 (PP1), for instance, can form complexes with > 50 bona fide or putative regulatory subunits contributing to many different conformations of PP1, which have specific substrate specificities, restricted subcellular locations and diverse regulation [22].

Protein phosphorylation in eukaryotes occurs mainly by O-phosphorylation of the amino acids serine, threonine and tyrosine in the ratio of 90:10:0.05 [23]. It has been proposed that the lower stoichiometry of tyrosine phosphorylation is based on the higher specificity of signaling via phospho-tyrosine [24]. N-phosphorylation of arginine, histidine and lysine, as well as S-phosphorylation of cysteine and acylphosphorylation of aspartic and glutamic acid has been furthermore detected in predominantly prokaryotes but also eukaryotes. Most research has been accomplished on O-phosphorylation potentially due to the higher abundance and increased stability compared to other forms of phosphorylation [25]. The importance of phosphorylation in cellular regulation is highlighted by the fact that at least three quarters of all proteins are known to be phosphorylated at some point of their lifetime. Moreover, it has been proposed that more than 90 % of the human proteome would be covered with increasing depth of phosphoproteomic identifications [23].

The large hydrated shell and the multiple negative charges of the phosphate group alters its modified residues chemically in such a way that it is distinct from the appearance of all other naturally occurring amino acids. This even holds true for aspartic and glutamic acid, whose carboxyl side chains only carry a single negative charge and a smaller hydrated shell than the phosphate group [26]. Protein phosphorylation therefore increases the chemical diversity of the surface of proteins in specific locations.

Due to its chemical properties, the phosphate group can promote either hydrogen bonds or salt bridges. Especially the interaction with the guanidine group of arginine by the formation of an hydrogen bound is likely, which can occur within the protein itself or between proteins [27]. As a consequence, protein phosphorylation can regulate the interaction to another protein or, more frequently, provoke alterations in the conformation of the protein monomer or composition of a protein multimer thereby tuning the protein's function (Figure I-3). Protein phosphorylation furthermore enables specific and inducible recognition of the phosphorylated residues by binding domains of other proteins, thus promoting transient protein–protein interactions. Renowned examples include Src-homology-2/3 (SH2, SH3) and phosphotyrosine-binding (PTB) domain-containing proteins that bind to phosphorylated tyrosine residues, forkhead-associated (FHA) domains that engage phosphorylated threonine and 14-3-3 domains that interact with phosphorylated serine and threonine [28, 29]. Protein interactions established by phosphorylation are hence essential for inducing or inhibiting enzymatic activity and transducing cellular signals. Phosphorylation can also lead to a regulated subcellular location of a protein or create a phospho-degron that guides the protein towards ubiquitin-dependent degradation [30, 31].

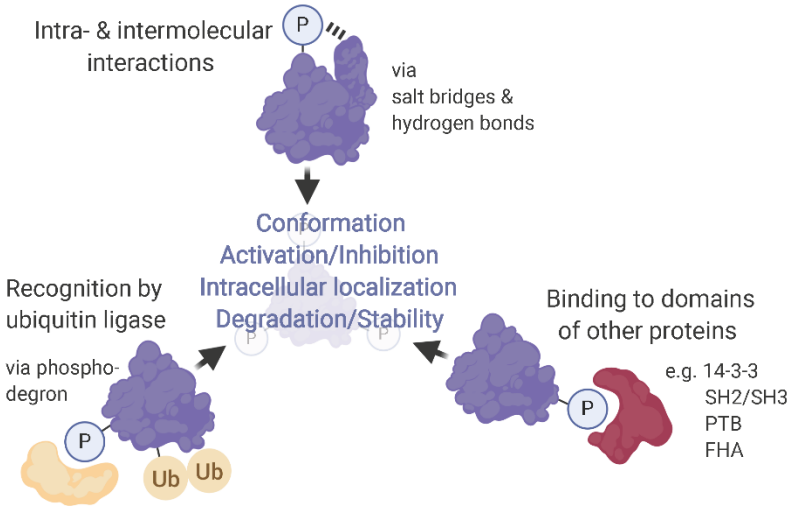

Figure I-3: Consequences of phosphorylation on protein function. Phosphorylation can exert multiple effects on proteins leading to the change of conformation, activation or inhibition of a protein with enzymatic function, adjusted intracellular localization, degradation or stability of the protein. Molecularly, phosphate groups can introduce intra- and intermolecular interactions, engage specific binding domains of other proteins or establish a phospho-degron enabling proteasomal degradation.

In order to anecdotally illustrate the functionalities of phosphorylation on protein function, the consequences of the activity of the serine/threonine kinase AKT will be discussed in more detail on the example of two renowned AKT substrates. In concert with PI3K and mTOR (consolidated to the PI3K-AKT-mTOR (PAM) pathway), AKT, is at one of the major hubs of cellular signaling that regulates

manifold processes such as cell growth, differentiation, and survival (reviewed in [32]). Phosphorylation of glycogen synthase kinase 3 (GSK3) on the N-terminus (Ser^{9} and Ser^{21}) by AKT leads to the formation of an intramolecular pseudosubstrate that precludes binding of substrates to GSK3. The blockade of catalytic activity of GSK3 by AKT-mediated phosphorylation is based on its substrate specificity, which favors substrates that have been primed by phosphorylation in +4 position to the intended residue [33]. Some GSK3 substrates such as prosurvival BCL-2 family member MCL-1 and transcription factor c-Myc are stabilized subsequent to GSK3 inhibition. Otherwise, phosphorylation would have created a phospho-degron leading to proteasomal degradation [34, 35]. Another group of well-studied AKT substrates are Forkhead Box O (FoxO) transcription factors, which are phosphorylated at the N-terminus and within a nuclear localization sequence (NLS) (Thr^{4} and Ser^{256} on FoxO1) leading to the recognition by 14-3-3 domain-containing proteins [36]. The interaction enables the export and retention of the transcription factors in the cytosol thereby inhibiting the expression of FoxO targets. Consequently, AKT activity impedes the formation of relevant proteins for apoptosis activation, cell-cycle arrest, catabolism and growth inhibition, whose expression would have been enabled by FoxO [37].

1.2 Perturbed protein phosphorylation in cancer

Given the importance of the catalytic activity of kinases on cellular functions, perturbations of the formerly tightly controlled process of protein phosphorylation can cause human diseases such as cancer. Cancer describes a group of disorders characterized by the occurrence of aberrant cells that are enabled to divide in an unregulated manner and invade nearby tissues but also distant organs. The biological basis of cancer is highly diverse. A framework to summarize underlying principles of tumor pathogenesis was established that recognizes cancer development as a multistep progress [38]. Among those characteristics are eight 'hallmarks of cancer', which include sustaining proliferative signaling, evading growth suppressors, resisting cell death, enabling replicative immortality, inducing angiogenesis, activating invasion and metastasis, reprogramming of energy metabolism and evading immune destruction. Genome instability and inflammation are further understood to enable the advent of the aforementioned hallmarks, which are fostered by non-malignant cells of the so-called tumor microenvironment. Despite the complex interactions of these step-wise processes, the malignant phenotype can be dependent on a single critical oncogene responsible for the malignant phenotype, which describes the concept of 'oncogene addiction' [39]. Oncogenes are therefore ideal targets of pharmacological intervention for cancer therapy. The discovery of the Rous sarcoma virus transforming factor (v-Src) as the first kinase oncogene [40] has since been followed by numerous additional cancer

genes, which arose by different genetic mechanisms. More recently, also a 'non-oncogene addiction' of cancer cells was proposed, which explains the perpetuation of the stress-phenotype of cancer cells [41, 42].

Mutations in kinase genes have been found to provoke several human diseases such as developmental and metabolic disorders and cancer. In a study from 2010, 50 kinases, from which half were tyrosine kinases, were prone to 915 mutations resulting in 67 single-gene diseases [43]. While the occurrence of mutations in congenital disorders rather affected residues that are involved in regulation and substrate binding of kinases, mutations in cancer commonly affected ATP binding and catalytic residues leading to the activation of oncogenes or inhibition of tumor suppressors. Comprehensive genomic analysis of multiple tumor entities has uncovered two to eight oncogenic driver mutations on average in a tumor. [44]. Mutated residues in the catalytic subunit of phosphoinositide 3-kinase (PI3K), for instance, hyperactivate the PI3K-AKT signaling cascade in different cancers [45]. Another prime example are activating mutations of BRAF (including V600E-as the most common mutation) initiating constitutive signaling of the mitogen-activated protein kinase (MAPK) pathway in ~ 40% of melanoma tumors [46]. Mutations in non-kinase proteins within kinase signaling cascades are also known to be frequently occurring in cancer. For example, tumor suppressor Phosphatase and Tensin homologue (PTEN) is highly affected by deletion or mutation in various human cancers, which again prompts aberrant AKT activity [45]. Moreover, a comparison between pathogenic human single-nucleotide variants, insertions, or deletions in the ClinVar database [47] and phosphorylated residues in the PhosphoSitePlus database [48] uncovered 762 pathogenic mutations covering 383 diseases, including cancer [15]. Despite the fact that impaired phosphorylation might not be the driver of pathogenesis for all p-sites, for some, it could be a putative mechanism. Interestingly, in more than 75 % of these p-sites the upstream kinase was not known, which could hint to completely new therapeutic lesions [15]. Another source of oncogenes can be gene fusions, a phenomenon which was first discovered in 1960. Back then the so-called 'Philadelphia chromosome' was detected in chronic myeloid leukemia (CML). This genomic arrangement creates chimeric mRNA and protein of fused BCR-ABL leading to constitutive ABL activity (reviewed in [49]). Further oncogenic gene fusions were for instance identified in acute leukemia [50], prostate cancer [51] and in Ewing sarcoma [52]. Furthermore, gene amplification and subsequent overexpression can provoke the emergence of oncogenes. In a comprehensive study from 2010 77 genes were discovered that provide evidence for an amplification and overexpression in cancer leading to oncogenesis [53]. A very prominent example is HER2, which is amplified and overexpressed in > 20 % of all breast cancer tumors as well as in certain other solid tumors such as gastric cancer [54].

2 Targeted drugs for cancer therapy

The majority of global deaths are nowadays provoked by non-communicable diseases such as cancer, which is the second leading cause, after cardiovascular diseases, of worldwide deaths [55]. A steady aging and growth of the population, and changes in the prevalence of the main risk factors for cancer play pivotal roles in even further escalating cancer incidence and mortality rates world-wide [56]. 18.1 million new cancer diagnoses and 9.6 million cancer deaths worldwide were estimated in 2018 [57]. Among all cancer types, lung cancer was the most frequently diagnosed cancer and the leading cause of cancer death (18.4 %). Incidents of female breast cancer (11.6 %), prostate cancer (7.1 %), and colorectal cancer (6.1 %) followed. Colorectal cancer (9.2 %), stomach cancer (8.2 %), and liver cancer (8.2 %) were subsequent for mortality. These numbers and the expected rise in cancer incidences and mortality highlight the enormous need for suitable treatment options for cancer patients.

First-line therapy for many cancer types regularly includes surgery, chemotherapy and radiation therapy. However, these conventional treatment options usually face highly limiting constraints. Treatment options are, for instance, confined for solid tumors that suffer from dramatic low resectability rates, such as pancreatic ductal adenocarcinoma (PDAC) [58]. Chemotherapy, on the other hand, likely provokes undesired side-effects that arise from the non-specific effects of intracellular toxic compounds like alkylating agents and platinants (e.g. cisplatin), cytotoxic antibiotics (e.g. anthracyclines), inhibitors of topoisomerase (e.g. daunorubicin and doxorubicin), antimetabolites (e.g. gemcitabine) and anti-microtubule agents (e.g. paclitaxel and docetaxel) (reviewed in [59]). The impairment of the essential cellular functionalities that are targeted by chemotherapeutic agents in both cancer and healthy cells regularly elicit acute and long-term toxicities affecting all organs and can even provoke leukemia [60]. Furthermore, a comprehensive study from 2004 has uncovered rather low therapeutic effects, as represented by the benefit to the 5-year survival rate in > 200,000 patients with 22 major adult malignancies that barely exceeded 2 % [61]. While there are chemotherapy-sensitive cancers, in particular testicular cancer, Hodgkin's and non-Hodgkin's lymphoma, cervical cancer and ovarian cancer, they account for less than 10 % of total cancer incidents [57]. Similarly, diminished responses towards radiation cancer therapy are encountered on a regular basis with varying response rates among different tissues [62]. As an example, high recurrence rates are faced in glioblastoma or non-small-cell lung cancer (NSCLC) [63, 64].

Consequently, the limitations and unsatisfactory therapeutic effects of conventional cancer therapy approaches prompted the development of a novel way to treat cancer patients: targeted cancer drugs. These agents hit molecular targets in a specific subpopulation of cancer patients. The underlying basis for unraveling targets for novel agents was molecular and genetic research that uncovered perturbed signaling networks initiating and sustaining tumor pathogenesis leading to the discovery of oncogenes (see 1.2). Additional targets have derived from proteins that are differentially expressed by the cancer cells and healthy cells or only expressed in a subset of the human cell types. Thereby, targeted cancer drugs aim to introduce pharmacological specificity. Hormone therapeutics, signal transduction inhibitors, gene expression modulators, apoptosis inducers, angiogenesis inhibitors and immune therapeutics constitute the ever-growing list of targeted cancer drugs. While they derive from different classes of pharmacological agents, targeted cancer drugs mostly target proteins. The two renowned classes of kinase inhibitors and monoclonal antibodies are discussed in further detail.

2.1 Kinase inhibitors

The development of kinase inhibitors was, as elaborated earlier, driven by the findings that perturbed kinase activity and protein phosphorylation play pivotal roles in the establishment and progression in cancer. The early clinical success of imatinib in CML targeting BCR-ABL in 2001 was a breakthrough in the development of targeted small molecule cancer drugs [65]. Further examples of renowned targeted inhibition of oncogenes are EGFR-inhibitors erlotinib and gefitinib for the treatment of NSCLC with sensitizing EGFR mutation [66, 67] and BRAF inhibitors dabrafenib and vemurafenib in cases of $BRAF^{V600E}$-mutation harboring melanoma [68, 69]. Until the end of 2019, 55 kinase inhibitors were approved by the FDA, from which 48 agents are in use for targeted cancer therapy (provided by https://www.icoa.fr/pkidb/; [70]). Over 100 additional kinase inhibitors are currently tested for multiple indications in clinical trials.

The current classification system divides kinase inhibitors, based on their mode of binding to the kinase, into the following groups: I (including I½), II, III, IV, V and VI [13] (Figure I-4). Most of the protein kinase inhibitors developed to date mimic the binding of ATP to the hydrophilic channel in the hinge region. These inhibitors are referred as to type I inhibitors, are ATP competitive and target the active conformation of the kinase, which means that the DFG-aspartate is pointing into the ATP binding pocket and the R spine is ordered and active. They typically contain a heterocyclic ring system that fits the ATP binding site. Side chains of the inhibitors are then able to occupy the adjacent hydrophobic regions. In case of type I½ inhibitors, a subtype of the type I inhibitors, the DFG-aspartate is pointing

into the pocket but the Cα is pointing out and the R spine is disordered [71]. Due to their binding to the structurally conserved, active kinase conformation, type I kinase inhibitors often face selectivity problems. A better selectivity towards the intended kinase is aimed to be addressed by considering the size, shape and polarity of the gatekeeper residue at the rear part of the hinge region [72]. By contrast, type II inhibitors target the structurally less conserved inactive conformation of the kinase. The inactive conformation of the kinase leads to the establishment of an additional hydrophobic binding site in the hinge region, which is targeted by the inhibitor. It has been proposed that these inhibitors usually show the same ATP competition as type I inhibitors [73], but offer increased selectivity [74]. However, more recent and comprehensive research has found evidence that this assumption does not hold true [75]. Type III inhibitors bind to the phospho-acceptor site next to the ATP binding pocket, while type IV inhibitors do not target the ATP-binding site but another distinct site of the kinase and are, as well as type III inhibitors, referred to as allosteric. While the approach of targeting allosteric sites within kinases is a promising tool to increase selectivity, these structures remain rare among the kinome [76]. The low incidence is well reflected by the modest number of approved allosteric inhibitors, which are comprised by solely MEK inhibitors trametinib and cobimetinib [77]. Inhibitors of the type V are bivalent inhibitors that target two different regions of the protein kinase domain. Type VI inhibitors bind covalently to the kinase. The binding often occurs via Michael addition to a distinct cysteine residue within the binding pocket of the kinase [78]. Consequently, the binding pocket is irreversibly blocked. The development of irreversible kinase inhibitors is one attempt to prevent resistance of tumor cells to already approved reversible inhibitors. As an example, irreversible inhibitors targeting EGFR were shown to circumvent not only the T790M mutation but also altered receptor trafficking in gefitinib- and erlotinib-resistant NSCLC [79].

As most kinase inhibitors target the well-conserved ATP-binding site, selectivities towards intended kinases are mostly compromised. A recent chemoproteomic profiling of 243 clinical kinase inhibitors revealed that only a small fraction exhibited high selectivity (for example capmatinib for MET, lapatinib for EGFR, and rabusertib for CHEK1) [80]. Selective inhibition of a single kinase can be clinically relevant when tumors carry the aforementioned ‘oncogene addiction’ causing the dependence on an overly high activity of the targeted kinase. Thereby, undesired or toxic side effects by inhibiting off-target kinases and non-kinase proteins can be reduced. In this regard, FECH is a common off-target of kinase inhibitors and its inhibition is described to cause phototoxicity in patients [81, 82]. Apart from the clinical perspective, the selectivity of kinase inhibitors is of utmost importance when used for basic research. Here, kinase inhibitors are utilized as a tool to perturb kinase activity in order to decipher

consequences on cellular signaling. However, cancer cells frequently bear complex perturbations of cellular signaling including the aberrant activity of multiple kinases. Therefore, polypharmacology, meaning the action on more than one target by promiscuous or multiple kinase inhibitors, might be beneficial [83]. Evidence for the clinical success of the principle of polypharmacology can be seen in the approval of highly unselective kinase inhibitors like dasatinib that binds to 67 proteins [80]. Furthermore, polypharmacology can enable the repurposing of kinase inhibitors. MET and ALK inhibitor crizotinib, for instance, has been found to additionally target FAK, which leads to responses in Neurofibromatosis Type 2 [84]. Moreover, BCR-ABL inhibitor imatinib has been successfully repurposed for gastro-intestinal stromal tumors due to its inhibition of KIT [85]. These findings suggest that the detailed knowledge of the targets as well as molecular consequences of the kinase inhibitors can be beneficial for an intelligent use such as in drug repurposing.

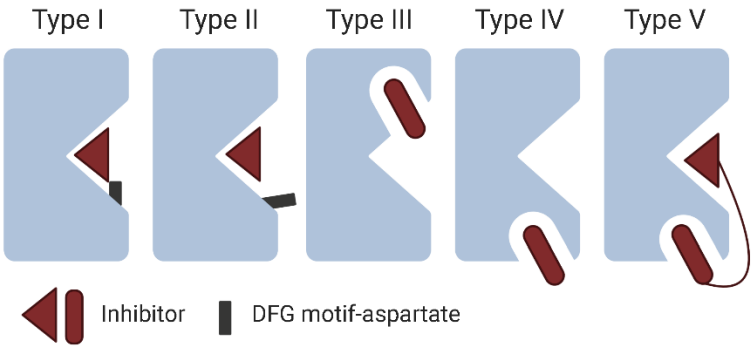

Figure I-4: Binding types of kinase inhibitors. While type I (including subtype I½), and II inhibitors bind to the ATP binding site, either of the active (I) or inactive (II) conformation, type III and VI inhibitors target allosteric sites. Bivalent inhibitors of type V target both the ATP pocket and an allosteric binding site.

2.2 Therapeutic antibodies

As a key component of the adaptive immune system, antibodies or immunoglobulins (Igs) do not depend on an enzymatic functionality to bind and inhibit the protein of interest, but instead reach intended proteins on the cellular surface via protein-protein-interactions. Igs belong to the immunoglobulin super-family (IgSF) and consist of each two heavy (H) and two light (L) chains [86] (Figure I-5A). Each chain contains one N-terminal variable (V) IgSF domain and one (L chain), three or four (H chain) C-terminal constant (C) IgSF domains. The proteolysis of Igs by papain led to the further partition of antibodies into the Fab (fragment, antigen-binding) and the Fc moiety (fragment, crystallizable). The three complementarity-determining regions (CDRs) on each IgSF domain are characterized by a considerably high sequence variability and mediate antigen binding. Following the

'magic bullets' concept as proposed by Paul Ehrlich, scientists have worked early on towards the application of antibodies to treat human diseases such as cancer. The hybridoma technique, which was introduced by Milstein and Köhler 1975, allowed for the first time the production of monoclonal antibodies (mAbs) [87], which bind tumor cell-surface antigens at high specificities and are unable to bind intracellular off-targets [88]. Nowadays, recombinant DNA technology using mammalian cell expression systems are the methods of choice for the production of mAbs. Most of the clinically successful antibodies are intact immunoglobulin G (IgG) molecules [89]. Yet, recent research has led to the development of additional antibody constructs including single-chain antibody fragments and bispecific antibodies provoking novel therapeutic actions.

The definition of cell surface antigens that are expressed on cancer cells or associated tissue has uncovered a multitude of antibody targets that are overexpressed, mutated or significantly expressed compared to healthy cells [90]. Ideally, those target antigens feature an abundant and homogeneous expression, which is consistently and exclusively found on the surface of cancer cells and surrounding tissue. In order to prevent antibody loss in the tumor interstitial space and blood circulation leading to hindered efficacy, increased systemic clearance and side-effects, antigen shedding and secretion should be minimal. Clinically successful cancer antigens, either for diagnostics or therapy, belong to different classes of proteins that include haematopoietic differentiation antigens (cluster of differentiation (CD) groupings; e.g. CD20, CD30, CD33 and CD52), glycoproteins on solid tumours (e.g. EpCAM, CEA, mucins), glycolipids (e.g. gangliosides), carbohydrates (e.g. Le^Y), angiogenesis-regulating proteins (e.g. VEGF, VEGFR), growth- and signaling-regulating proteins (e.g. EGFR, HER2, HER3, MET and IGF1R), stromal and extracellular matrix antigens (e.g. FAP and tenascin) and immune checkpoints (e.g. PD-1, PD-L1 and CTLA4) [89]. As of May 2020, 28 antibodies (excluding biosimilars) have received approval from the FDA and EMA for the treatment of various solid tumors and haematological malignancies and seven are currently under clinical review (as provided by https://www.antibodysociety.org).

Different factors enable the successful engagement of tumor antigens by antibodies. In particular, the penetration of the tumor, catabolism of the antibody and specificity are critical parameters that are greatly influenced by two related characteristics of antibodies: affinity and avidity. While affinity explains the strength of binding between a single antigen and a single region of the mAb, avidity is the accumulated strength of multiple affinities from multiple binding interactions [91]. For this reason, functional affinity is dependent on the affinity of the antibody for the antigen, the valency of the antibody and antigen and the geometric arrangement of the interacting components. Even though increased

binding affinity and valence is generally proposed to improve targeting of the tumor [92], maximal tumor engagement will be reached with intrinsic monovalent affinities in the low nanomolar range [93]. High-affinity antibodies that bind to internalizing tumor antigens, for instance, may be prone to a higher degree of degradation [94]. The general principle of this so-called 'binding-site barrier' therefore necessitates a tight balance between affinity and antigen/tumor engagement of the antibody [95].

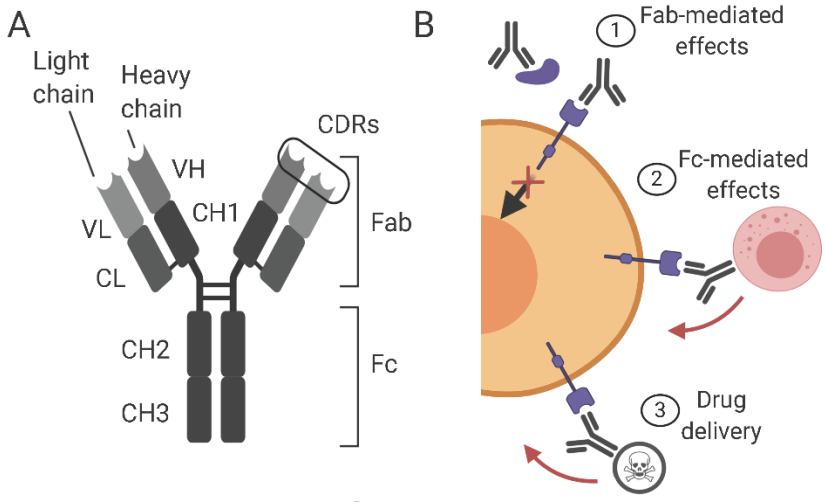

Figure I-5: Monoclonal antibodies as therapeutic agents in oncology. (A) Structural features of antibodies of the IgG type. (B) Multiple putative mode of actions shape the therapeutic effect of antibodies in patients. These can be mediated by the Fab terminus leading to the neutralization of soluble antigens or direct actions on the cancer cell (1). Additionally, the Fc terminus of the antibody might engage immune effector cells that themselves perturb the cancer cell (2). Furthermore, antibody-drug conjugates are used to deliver drugs specifically to cancer cells (3).

The unique composition of therapeutic antibodies accounts for their multiple modes of action (Figure I-5B). While the Fab moiety mediates the specific binding towards the cancer antigen, the Fc terminus can elicit binding, and activation or inhibition of immune effector cells. By disrupting the interaction with its binding partners, the binding of soluble ligands by antibodies can be regarded as the simplest mode of action. Bevacizumab, for instance, binds anti-vascular endothelial growth factor (VEGF) and is approved for multiple cancer types due to its anti-angiogenic effect [96]. Similarly (but not in the field of oncology), renowned agents for the treatment of autoimmune diseases infliximab, adalimumab and golimumab (among additional antibody constructs) target tumor necrosis factor alpha (TNFα) [97]. Due to their binding to a secreted cytokine, the limitations based on the 'binding-site barrier' principle are negligible which is reflected by picomolar affinities towards TNFα [98]. Perturbation of the cancer cell by direct binding of the antigen can be driven by single or multiple mechanisms including blocking ligand binding or receptor dimerization, inhibiting cell-cycle progression or DNA repair [99], hindering angiogenesis [100], increasing the internalization of receptors [101], reducing proteolytic cleavage of

receptors [102] or inducing apoptosis [103]. Aside from direct actions on cancer cells, antibodies can modulate the immune system by Fcγ receptor (FcγR)-binding on immune-effector cells [104]. The human FcγR family comprises six receptors in three subgroups, including FcγRI (CD64), FcγRIIa,b,c (CD32a,b,c) and FcγRIIIa,b (CD16a,b). These receptors are expressed by several immune cells such as neutrophils, macrophages, dendritic cells and natural killer (NK) cells. Especially NK cells are elucidating antibody-dependent, cell-mediated cytotoxicity (ADCC) upon activation via FcγRIIIa engagement by the Fc terminus. The interaction enables the formation of an immunological synapse that releases perforin and granzyme as well as initiates the Fas/FasL interaction, subsequently leading to apoptosis of the tumor cells. Recruitment of the other cell types mainly provokes antibody-dependent cellular phagocytosis (ADCP) [105]. Antibodies can additionally engage the complement system by either interacting with complement component C1q, leading to the formation of pores in the targeted cell membrane, or recruit effector cells by interaction with the C4b/C2b/C3b complement complex and the receptor complement receptor (CR1). Both processes will ultimately lead to complement-dependent cytotoxicity (CDC) [106]. The third putative mechanism of action is specific to antibody-drug conjugates that can deliver toxins, radioisotopes or small molecule agents to tumor cells by engaging the intended surface antigen [107]. Due to the guidance of the drugs directly to the tumor, toxic side effects on healthy tissue are limited. In this regard, trastuzumab-emtansine (T-DM1), which contains anti-HER2 antibody trastuzumab covalently linked to the highly potent anti-microtubule drug DM1 via a stable thioether linker, has been approved for HER2-positive locally advanced and metastatic breast cancer [108]. Most clinical mAbs feature activity of both Fab and Fc of the antibody resulting in complex effects on the tumor cells. Consequently, the actual mode of action, including the share of action of the putative mechanisms in the total action in patients is often not completely understood [109]. The first clinically approved mAb anti-CD20 rituximab, for instance, depletes CD20-positive B-cells by ADCC [110], CDC [111, 112], and caspase-dependent and -independent apoptosis [103, 113, 114]. Studies have demonstrated the pivotal role of ADCC in the MOA of rituximab by showing that the efficacy of the treatment is the highest in patients harboring the higher affinity form of FcγRIIIa (Val158) compared to patients with the lower affinity form (Phe158) [115, 116]. However, rituximab still demonstrated clinical efficacy in more than 50 % of the carriers with the lower affinity form. Furthermore, the beneficial effect of the higher affinity form of FcγRIIIa was less clear when rituximab was combined with chemotherapy [117]. This example highlights the interplay of different putative mechanisms shaping the effects of antibodies and the need to decipher the detailed consequences of antibody engagement for estimating the clinical impact on patients.

2.3 Resistance towards targeted cancer drugs

The advent of targeted cancer drugs that rely on the existence of certain specific cancer antigens or oncogenic drivers in tumors prompted the parallel development of companion diagnostics (CDx). CDx are defined as an *in vitro* diagnostic tools, which predict and thereby support the safety and efficacy of a corresponding targeted drug in patients [118]. This concept was introduced along with the approval of trastuzumab, an anti-HER2 mAb that was approved for HER2-positive breast cancer in 1998 [119] by an immunohistochemical assay for HER2 overexpression (HercepTest, Dako) [120].

Still, targeted cancer therapy regularly faces primary and acquired resistance. Even if initial responses towards targeted cancer drugs are striking, relapses often occur one to two years after treatment start. For instance, the overall response rate to trastuzumab-containing therapies is ~ 26 % when used as a single therapy and 40 - 60 % when used in combination with chemotherapy [121-123]. Genetic alterations of receptor tyrosine kinases (RTKs) and their downstream signaling targets are pivotal drivers of *de novo* resistances. In the case of trastuzumab, the resistance mechanisms frequently involve constitutive activation of the PAM pathway via PTEN loss [124] or activating PIK3CA gene mutations [125] and the presence of a truncated HER2 form (p95HER2) that lacks an extracellular trastuzumab-binding domain [126]. Since cancer is a dynamic disease indicated by a perpetual process of perturbed cellular functions [38, 44], the tumor of a patient can also develop over the course of a treatment leading to a cancer that is different from the diagnosed one. Distinct cancer subpopulations that harbor molecular features with ranging sensitivities to cancer drugs can foster the adaption towards the therapy and thereby provoke therapeutic failure [127]. The intratumoral heterogeneity may result from genetic, epigenetic, transcriptomic, proteomic or other phenotypic changes evolving at different disease sites (spatial heterogeneity) or over time (temporal heterogeneity). Acquired mutations, activation of bypass signaling and cell lineage changes are among the manifold mechanisms [128-131] and could be featured by distinct subpopulations leading to low responses during drug treatment. The overexpression of other RTKs, such as EGFR, insulin-like growth factor-1 receptor (IGF-1R) or hepatocyte growth factor receptor (MET) enables acquired resistance towards trastuzumab [132-134]. While these processes are often thought of as 'acquired', underlying genetic vulnerabilities may be present in low allele frequencies in treatment-naïve tumors, as it has been proven for the $EGFR^{T790M}$ mutation [135].

Consequently, defeating resistance to targeted cancer drugs became a major task in modern oncology that necessitates a thorough understanding of the mode of actions of these agents. Given that cancers generally become more heterogeneous and genomically complex during the course of a treatment,

common treatment regimens need to be revisited. Upfront combination treatments with multiple or promiscuous targeted agents might be more efficacious than subsequent lines of therapies. By a so-called vertical approach the same signaling pathway is hit by several inhibitors thereby decreasing the chance for the rise of resistance-conveying alterations. For example, the combined inhibition of BRAF and MEK by dabrafenib and trametinib is recommended for the therapy of melanoma [136]. More pre-clinical data is promising and further combinations are under clinical review. The combination of afatinib and cetuximab that doubly hits EGFR, for instance, prolonged the response and delayed the emergence of the $EGFR^{T790M}$ mutation in lung cancer cells [137]. The horizontal approach aims to prevent the emergence of a second pathway in response to the inhibition of the first one by targeting multiple signaling pathways in parallel. Here, *in vitro* data rise hope to more efficacious treatments such as the combination of an irreversible EGFR and a MAPK inhibitor that prevented multiple resistance mechanisms to occur in NSCLC cells [138]. However, increased toxicity by applying multiple targeted cancer drugs is a major limitation that needs to be tightly balanced with a gain in clinical response [139, 140]. Furthermore, cell populations with a low response towards the drug might ultimately still develop and give rise to resistance. Consequently, combinations with more systemic and local therapies might be key to sustainably combat resistance. In light of this, early clinical studies about combinations of kinase inhibitors with immune checkpoint mAbs have confirmed beneficial outcomes, such as lenvatinib and anti-PD1 pembrolizumab in endometrial and kidney cancer [141] as well as regorafenib and anti-PD1 nivolumab in advanced gastric or colorectal cancers [142].

3 Proteomics for studying drug targets and drug-perturbed cellular signaling

The comprehensive analysis of the action of targeted cancer drugs requires a global view on the cellular signaling network that can be supplied by the scientific approach of systems biology. Systems biology is a holistic framework to investigate the complex interactions of biological functions by applying key 'omic' techniques such as genomics, epigenomics, transcriptomics, proteomics and metabolomics [143]. Since the major drivers of cancer and effects of drugs are based on perturbed alterations of protein kinase activities, proteomics might be an optimal tool to study the action of drugs. Thereby, not only the composition but also the abundances and modification status of all proteins in complex biological mixtures can be uncovered, including the subproteomes of all kinases (kinome) and phosphorylated proteins (phosphoproteome) [144]. While low-throughput techniques such as Western Blotting are frequently used to study protein changes, technical development in the field of mass spectrometry allowed for the blossoming of proteomics [145, 146]. A milestone in this regard was the release of the first draft of the human proteome in 2014 [147, 148]. Today, bottom-up proteomics is mostly used to analyze protein mixtures by inferring from corresponding proteolytic peptides. In contrast, top-down proteomics directly investigates intact proteins [149, 150].

3.1 Sample preparation for bottom-up proteomics

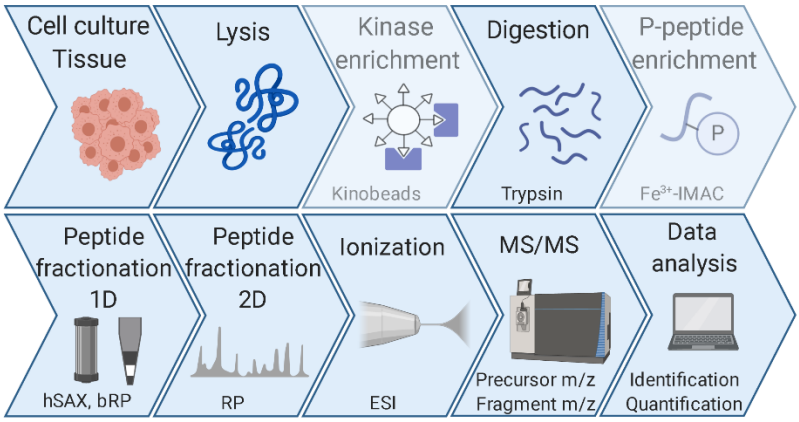

Figure I-6: Steps of the sample preparation for bottom-up proteomics. Proteins are extracted from cell culture or tissue samples and digested to peptides. Affinity enrichments of kinases or phosphorylated peptides might be utilized if needed (transparent boxes). Resultant peptides undergo two-dimensional peptide separation and ionization. Precursor and fragment m/z of peptide ions are determined by tandem mass spectrometry (MS/MS). Finally, data analysis identifies and quantifies peptides and proteins.

The preparation of complex biological samples for the analysis by bottom-up proteomics follows a few basic principles but the technical details always need to fit the purpose of the research question [149]

(Figure I-6). In this spirit, the method for the extraction of proteins from tissue or cell cultures needs to be selected according to the type of samples, the subsequent processing steps and whether modifications or the native structure of proteins need to be recovered [151]. Reduction of disulfide bridges and alkylation of free cysteines are generally conducted right before protein digestion to enable the detection of cysteine-containing peptides [152]. For the digestion of proteins, trypsin is mostly the protease of choice because of the high sequence specificity and the generation of short peptides (bearing the basic amino acids arginine or lysine at the C-terminus) [153]. Still, additional sequence-specific proteases such as AspN, chymotrypsin, GlucC, LysC, and LysN could be used to enhance the sequence coverage. However, this comes at the cost of decreased identification rates [154, 155]. The resultant thousands of proteolytic peptides derived from a proteome prompt an additional step of peptide separation in order to decrease the complexity and thus improve the depth of identification by mass spectrometry. A multitude of chromatographic principles is at hand that exert the separation of peptides based on the charge, polarity and hydrophobicity of the peptides. [156]. This first off-line fractionation approach should ideally prove a high orthogonality to the second ion-pairing reversed-phase (RP) chromatography that is typically performed on-line to the mass spectrometric analysis [157]. Strong anion exchange chromatography (SAX) [158] or basic RP chromatography (bRP) [159] are frequently applied in bottom-up proteomics. While high-performance liquid chromatography (HPLC) systems [158] are often applied, stop-and-go-extraction (STAGE) tips offer beneficial characteristics such as down-scaling capabilities [160].

The analysis of the kinome and phosphoproteome underlies technical obstacles that demand additional sample processing steps. Shortcomings arise from the low abundance of kinases and the dynamic nature and complexity of the phosphoproteome as well as the sub-stoichiometry of phosphorylated peptides. Thus, kinases and phosphorylated peptides need to be enriched selectively from complex cell lysates and peptide mixtures prior to the analysis with mass spectrometry [161, 162].

The kinome can be selectively enriched from complex lysates with immobilized promiscuous kinase inhibitors that have been introduced as Kinobeads [161]. By applying Kinobeads in the form of a competitive pulldown assay, proteins bound to kinase inhibitors can be deciphered on a kinome-wide scale including additional purine-binding proteins. Incubation of lysates with the free kinase inhibitor of interest prior to the addition of the affinity matrix results in the absence of the targets from the beads (Figure I-7A). Comparative analysis of the captured kinases and non-kinase proteins by mass spectrometry consequently enables the identification of the target space of the inhibitor, thereby

uncovering so far unknown off-targets. Several generations of Kinobeads have been developed over the time leading to the most recent version of Kinobeads ε with seven immobilized probes [163, 164]. It has been demonstrated that the combination of probes on Kinobeads ε is able to cover more than 300 kinases, including lipid kinases, corresponding to more than half of the human kinome.

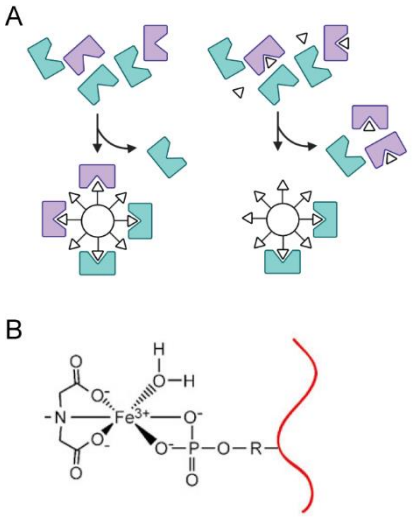

Figure I-7: Approaches for the enrichment of the kinome and proteome. (A) Immobilized promiscuous kinase inhibitors (triangles) on Kinobeads selectively enrich protein kinases (rectangles) from complex protein mixtures (left). By pre-incubating the proteins with free inhibitor, targets bound by the inhibitor (violet rectangles) are enriched in lower abundance (right). (B) Metal ions such as Fe^{3+}, which are immobilized by IDA, are able to selectively coordinate phosphate groups present on peptides (with permission from [165]).

The most common and successful techniques for the enrichment of phosphorylated peptides include immunoaffinity purification with commercial antibodies, immobilized metal ion chromatography (IMAC) and enrichment using metal oxides [166]. While a multitude of protocols is utilized for the enrichment of phosphorylated peptides, Fe^{3+}-IMAC is one of the more commonly applied enrichment strategies, in batch [167] as well as HPLC format [168]. The idea of using IMAC for the enrichment of phosphorylated peptides was based on the observation that phosphorylated peptides and proteins can bind ferric ions [169]. Today, polymeric matrices are mainly functionalized with iminodiacetate (IDA) or nitrilotriacetic acid (NTA), which both can immobilize Fe^{3+} as well as other metal ions such as Ga^{3+} and Zr^{4+} ions (Figure I-7B). These multivalent metal ions are used for the enrichment of phosphorylated peptides as they provide a selective binding by coordinative bonds yet with different selectivities [170]. An optimized pH and acid concentration in the enrichment process have remarkably increased the selectivity over non-phosphorylated peptides with multiple acidic residues [171]. Combined enrichment strategies and extensive fractionation have enabled the coverage of up to 50,000 unique phosphorylated

peptides in the phosphoproteome of a single cell line [23]. Recent development has led to enhanced protocols that, for instance, require lower input amounts by exploiting automation systems [172] or improved the enrichment of phosphorylated tyrosine peptides that are normally underrepresented by recombinant SH2 domains [173].

3.2 Quantitative mass spectrometry

Enriched and fractionated peptides are subsequently subjected to mass spectrometric analysis. In general, mass spectrometers enable the determination of the mass of charged molecules in gas phase by applying electric and magnetic fields [174]. Consequently, mass-to-charge ratios (m/z ratio) of the analyzed peptides are uncovered. Resultant mass spectra consist of increasing m/z-values plotted against the intensity that has been determined for each analyte. The tandem mass spectrometry (MS/MS) approach to identify peptides basically starts with the ionization of peptides, which are transferred to mass analyzers enabling the acquisition of the peptide spectra (MS1 spectra). Afterwards, peptide ions are isolated from the peptide ion mixture and subsequently fragmented. Mass analysis of the peptide fragment ions results in peptide fragment spectra (MS2 spectra), which are the basis for deducing peptide sequences leading to the inference of proteins.

In order to further reduce peptide complexity, proteomic samples are commonly fractionated by ion-pair RP-HPLC at an acidic pH prior to ionization as the second dimension of chromatography [175]. This technique allows a direct coupling to the mass spectrometer due to solvent compatibility and achieves a superior peak capacity for peptide separation [149]. The principle of separation by RP is based on the interaction of peptides with the non-polar stationary phase (mostly octa-decyl alkane chains (C18)-based material) directly via hydrophobic residues and indirectly through polar residues, which is mediated by the amphiphilic ion-pairing reagent of the mobile phase [156]. Subsequent elution of bound peptides by a gradually increasing the concentration of a non-polar solvent, such as acetonitrile, leads to a separation of peptides according to their hydrophobicity.

While former rather harsh ionization techniques led to the physical destruction of biomolecules, the introduction of electrospray ionization (ESI) was a breakthrough in the field of mass spectrometry. ESI enables the generation of multiply charged species and transfer of, for instance, peptides into the gas phase [176]. The outmost importance of this development was already recognized by awarding the Nobel Prize in chemistry in 2002 to John Fenn. Directly coupled to the on-line HPLC system, a capillary under voltage leads to the formation of the so-called 'Taylor cone' of the exiting mobile phase. After leaving the capillary, the solvent evaporates from the droplets. This occurs until Coulomb forces exceed

the surface tension (Raleigh limit) resulting in coulomb explosions that generate multiply charged microdroplets carrying the peptides [176]. The final production of gas-phase ions is not completely understood so far, but might be either explained by the ion evaporation model (IEM) or the charge residue model (CRM) [177]. According to the IEM, as droplets reach a certain radius, the field strength at the surface of the droplets is large enough to induce the field desorption of solvated ions. In contrast, CRM suggests that electrospray droplets are subject to multiple evaporation and fission cycles, which lead to progeny droplets that contain on average one analyte ion or less. Afterwards, the remaining solvent evaporates and solely the analyte that carries all the charges of the droplet is left. Peptide ions are subsequently transferred by the ion optics to the mass analyzers.

Different mass analyzers have been developed that separate peptide ions according to their m/z and are embedded (also in combinations) in commercial mass spectrometers. The choice for utilizing a certain mass analyzer is based on the specific sample and research question and is mostly guided by multiple parameters such as the mass accuracy, mass resolution, m/z range, sensitivity, scan speed, and dynamic range of the analyzer [178-180]. Time of flight (TOF) mass analyzers, for instance, make use of the fact that ions with different m/z vary in flight times when accelerated from a source to a detector in a flight tube. Reflectrons within TOFs improve resolution by compensating for the different kinetic energies of peptides with the same m/z [181]. Quadrupole mass analyzers are built up of four rod electrodes that feature an inner axial space for ion transmission [182]. Oscillation-based trajectories along the inner axis of ions with a certain m/z are established when a radio frequency (RF) voltage is applied to the two opposing rods generating an electric field. Depending on the applied RF voltage and the m/z, ions move on stable trajectories or collide with the electrodes as well as exit the mass analyzer. In that way, quadrupoles are rather regarded as mass filters that can allow peptides with a certain m/z to be transferred to subsequent analysis. Similar to quadrupoles, ion traps maintain analyte ions on stable trajectories in an electric field defined by the applied voltages and m/z [183]. The latest development of a mass analyzer was the Orbitrap. This mass analyzer features a spindle-shaped central electrode, which is surrounded by a barrel-like outer electrode. Analyte ions that got injected from an additional ion storing unit (C-trap) rotate and oscillate along the central electrode with. The frequency of the oscillations depend on the m/z ratios of the ions and an instrument constant that changes proportionally with the voltage between the central and the outer electrodes [184].

While amino acid sequences of peptides and proteins were formerly only uncovered by Edman degradation [185], tandem mass spectrometry is today the most common method to define a peptide

according to its sequence. The approach is characterized by two separate acquisition modes that are divided by time or space and switched in-between by the mass spectrometer: determination of the MS1 spectra of single peptide (precursor) ions and MS2 spectra of fragmented precursor ions. The acquisition of tandem mass spectra is data-dependent when precursors are selected for fragmentation mostly based on their intensity [186]. Hence, the number of acquired mass spectra is limited by the speed of the mass spectrometer in data-dependent acquisition (DDA) experiments. The stochastic nature of precursor selection, which results in incomplete peptide identification and a constrained reproducibility of peptide identifications, therefore still constitutes a major disadvantage of the DDA approach [187]. Contrary, data-independent acquisition (DIA) features a grouping of fragment ions into m/z-dependent sections that are subsequently analyzed. This approach features a high reproducibility and quantification accuracy. The acquired MS2 spectra are then matched to a spectral library for identification [188]. Because multiple peptides in an m/z window are fragmented together, the resulting MS/MS spectra are highly complex, which requires advanced data processing. Another approach to overcome the issue of irreproducibility is the targeted analysis of peptides such as parallel reaction monitoring (PRM). Here, only precursors that were chosen prior to the measurement are fragmented according to their defined m/z and retention time [189]. While targeted approaches are particularly superior to DDA in reproducibility, they are not suitable for discovery-based research.

The basis for elucidating the peptide sequence by tandem mass spectrometry is the fragmentation of the peptide leading to an ideal fragmentation pattern of the peptide ions that differs each step by exactly one amino acid. In order to uniformly define the fragmentation of peptides, Roepstorff and Fohlman proposed a nomenclature that is commonly accepted [190]. Hereby, N-terminal peptide fragments are referred to as a, b or c-ions, while C-terminal fragments are called x, y or z-ions, depending on the position of the bond break within the peptide. Several methods exist that are utilized to perform the fragmentation of peptides. A widely used technique is collision-induced dissociation (CID), which lets peptide ions collide with neutral gas molecules such as helium, argon or nitrogen, mostly within an ion trap [191, 192]. Another approach is higher energy C-trap collisional dissociation (HCD). Here, ions are accelerated by current offsets and then collide with nitrogen or other gases in an octopole collision cell that is commonly referred to as HCD-cell. HCD generally generates higher kinetic energies than CID and is able to retain smaller fragment ions. Since the MS2 spectra acquisition for HCD is often performed in the Orbitrap, mass accuracy and resolution are improved compared to ion trap readout of CID, which especially enhances the detection of peptide modifications [193]. The fragmentation of peptides by CID and HCD mostly affects the peptide bond leading to the generation of mainly y- and b- ions. In contrast,

electron transfer dissociation (ETD) predominantly generates c- and z- ions. Here, electrons are transferred onto the peptides, which produces unstable positive radical ions leading to bond breakage [194]. With regard to the analysis of phosphorylated peptides, the higher rate of neutral loss ions produced by CID than HCD needs to be considered. Here, the loss of phosphoric acid ($-H_3PO_4$) from phosphorylated serine and threonine often dominates the spectra and compromises the identification of peptides [195]. The so-called multistage activation (MSA) approach can improve the spectra by applying a second resonance excitation of the generated neutral loss ion in the ion trap leading to increased identification rates for phosphorylated peptides [196].

Subsequently, the basic principles of the mass spectrometer mainly used in this work, the linear ion trap quadrupole (LTQ) Orbitrap mass spectrometer Fusion™ Lumos™, is explained in more detail. In addition to the ion trap and Orbitrap as mass analyzers, the Fusion™ Lumos™ features multiple fragmentation options, such as CID and HCD (if the instrument is additionally equipped, ETD and ultraviolet photodissociation (UVPD) as well), which allows versatile measurement setups (Figure I-8). The T-configuration of the machine enables the combination of different acquisition methods by reducing the distance between the ion source and each analyzer. MS1 spectra acquisition is generally performed in the Orbitrap providing high resolution and high mass accuracy of the precursor, while MS2 fragment spectra can be acquired either subsequently in the Orbitrap or simultaneously in the linear ion trap [197]. Consequently, parallelization and the acquisition rate can be largely improved.

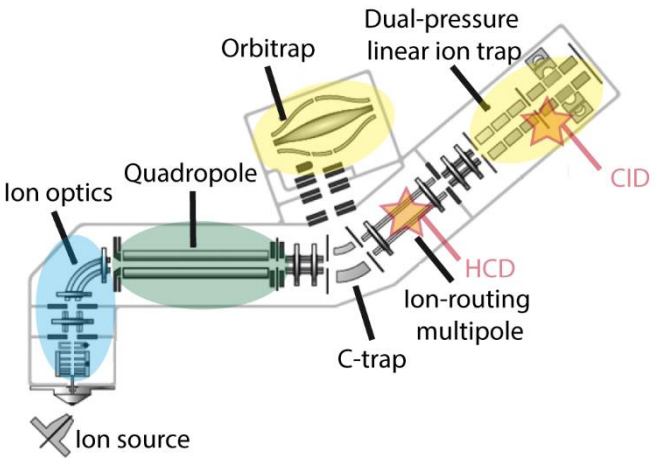

Figure I-8: Setup of the Fusion™ Lumos™ mass spectrometer. Peptide ions derived by ESI are transferred via the ion optics (blue) to the rear part of the machine. The quadrupole (green) serves as a mass filter. MS1 and MS2 analysis can be either performed in the dual-pressure linear ion-trap or in the Orbitrap mass analyzer (yellow). Multiple fragmentation options, such as CID and HCD (orange stars; performed in the ion trap and ion-routing multipole, respectively), are offered. This allows, in conjunction with the two mass analyzers, multiple analysis approaches (adapted and with permission from [197]).

3.3 Proteomic data analysis

After tandem spectrum acquisition, peptide sequences need to be extracted from the fragment spectra in conjunction with the calculated total mass of the peptide from the MS1 spectra. *De novo* sequencing yields the amino acid sequence directly from the fragmentation pattern of the MS2 without any other sources of sequence data [198]. However, due to imperfect recovery of peptide fragmentation data, *de novo* sequencing is highly challenging and not suitable for most research questions.The most common approaches for the identification of peptides make use of probability score-based search engines. Andromeda, which is implemented in the MaxQuant software suite [199], and Mascot [200] are the most frequently applied search engines for peptide identification. The basic principle behind these engines is the matching of observed fragment masses from MS2 spectra to a database of theoretical spectra that are generated by *in silico* digestion of known and putative protein sequences. In order to estimate whether a peptide spectrum match (PSM) is a random event, probabilities scores are computed. In addition to probability-based scoring, false discovery rates (FDRs) are often calculated to inspect the data for overall quality regarding potential random hits to theoretical spectra [201]. In particular, a decoy database that contains reversed or scrambled sequences is used for a second search of the experimental MS2 spectra. By definition, every hit in this database is false and also referred to as a decoy hit. Accordingly, a FDR can be estimated by taking the number of hits as well as of the decoys into account. By assuming that random (and also false) hits in the actual database occur on the same level as the decoy hits, a controllable number of false-positive identifications is allowed via a FDR cut-off. This arbitrary FDR cut-off is often set to 1 % [149]. Special caution needs to be taken in case of phosphorylated peptides, which often harbor several putative phosphorylated residues. While site determining ions that are adjoining to the phosphorylation site are indicatory of the modified residue, they might be missing or of very low abundance leading to an ambiguous localization. Different phosphorylation site localization tools exist that aim to estimate the probability of the localization, such as the Mascot Delta or PTM Score [202, 203]. Confidently localized phosphosites are frequently defined as class I sites that harbor a localization probability of > 0.75 on the corresponding phosphorylated peptide [204]. Furthermore, the inclusion of variable PTMs like phosphorylation of serines, threonines and tyrosines, vastly increases the search space, which may perturb the quality of peptide identification [205].

The quantification of identified peptides and proteins is the cornerstone to answer many research questions and is conducted by different approaches in proteomics (reviewed in [206]). While label-free quantification approaches derive peptide and protein abundance from spectral counting or peak

intensities, multiple labeling techniques exist that enable the multiplexing of proteomic samples and subsequent quantification. The most common metabolic labeling approach is stable isotope labeling by amino acids in cell culture (SILAC) [207]. Since labeling and multiplexing are performed prior to proteomic sample processing, experimental variation is covered by the labeling and accuracy is therefore enhanced compared to other quantification approaches. However, the use of SILAC is especially limited by the number of available isotopically labeled amino acids and a rather time-consuming labeling step.

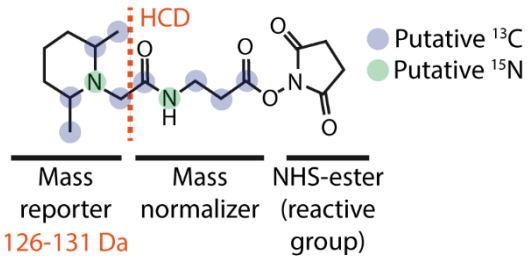

Figure I-9: Structural features of TMT10plex™ labels. The NHS-ester reacts with the N-terminus and -amino group of lysine residues forming a stable amide group. The mass reporter and the mass normalizer are isotopically labeled with ^{13}C (blue) and ^{15}N (green) on several positions. Due to the mass normalizer, the labels feature isobaric properties of the same peptide on LC and MS1 level. However, during HCD fragmentation on MS2/MS3 level, a unique mass reporter ion per label is released (126-131 Da) and its intensity is used for relative quantification.

Chemical labeling constitutes another renowned quantification approach, which takes advantage of small chemical tags such as N-hydroxysuccinimide (NHS) derivates targeting the peptidic N-terminus- and lysine residues. The most commonly used chemical moieties are isotope tags for relative and absolute quantification (iTRAQ) [208] and tandem mass tags (TMT) [209]. These tags contain, in addition to the reactive group for peptide labeling, a mass normalizer and a cleavable mass reporter, which both harbor different (but in total equal) numbers of ^{13}C and ^{15}N atoms among the tags (Figure I-9). Multiplexed peptides possess identical properties in LC and on MS1 level but can be distinguished on MS2 level by fragmentation into reporter ions and complementary ions. The intensities of the reporter ions are a readout for the relative abundance of the underlying peptide in the multiplexed samples. In the case of higher multiplexing tags such as the TMT10-plex set, the mass differences are additionally neutron-encoded leading to the subtle difference of ~ 6.3 mDa between reporter ions [210]. Here, the analysis of reporter ions needs to take place in the Orbitrap at high resolution to resolve neighboring reporter ions. Recent development of novel proline-based labels furthermore generated the possibility to multiplex up to sixteen conditions (TMTpro 16plex) [211]. In particular, the benefits of chemical labeling is the decreased MS measurement time, which does not come with the cost of increased MS1 complexity. However, fragmentation of co-isolated interfering peptide ions

quantification over isobaric chemical tags frequently causes ratio compression leading to drastically decreased accuracy of quantification [212, 213]. By applying a second fragmentation step to MS2 fragment ions, co-isolation of fragment ions that were derived from interfering peptides is decreased [214] and can be realized on a Fusion™ Lumos™ mass spectrometer. The MS3 scan is mostly performed on peptide fragments that underwent HCD at high energies to enable an efficient release of the reporter ions. The isolation of MS2 ions is furthermore executed by wave forms with multiple frequency notches (synchronous precursor selection, SPS). This multi notch MS3 method fosters the co-isolation and co-fragmentation of multiple MS2 fragment ions leading to a ten-fold increased number of reporter ions in the MS3 spectrum over a standard MS3 approach without SPS [215].

4 Objectives

Increasing counts of cancer diagnoses and deaths worldwide prompt efficacious therapy options to be available. Especially targeted cancer drugs that aim to perturb cancer-specific proteins in a certain subgroup of patients rise hope to battle the disease. Despite the overall clinical success of targeted cancer drugs, the exact actions on cellular signal transduction by these agents are in many cases not completely understood. This is well reflected by the frequently occurring low initial responses in groups of patients that technically should benefit from the respective drugs as well as undesired side effects that may even hamper clinical approval. Additionally, a better understanding of the effects on signaling networks could help in defining better molecular indications potentially leading to proposed combinations of drugs to overcome primary and acquired resistances.

Towards a better understanding of targeted cancer drugs, this thesis aimed to uncover the mode of actions of selected renowned clinical agents, including small molecule inhibitors as well as therapeutic antibodies, in different disease settings. As the analysis of drug action needs a global, and unbiased view on cellular signaling that is dominantly driven by protein phosphorylation, phosphoproteomics was chosen to serve as the ideal tool. In light of this, mass spectrometry-based phosphoproteomics has been applied to (a) study mechanisms behind low responses of PDAC cells towards radiation leading to the identification of small molecule inhibitors to putatively overcome the radioresistance (chapter II), (b) to elucidate the targets of selected AKT inhibitors and their influence on cellular signaling in HER2-overexpressing breast cancer cells also generating enhanced knowledge of AKT downstream signaling (chapter III) and (c) to discover the direct Fab-mediated effects of anti-HER2 and anti-CD20 therapeutic antibodies in appropriate cell line panels including the analysis of their potency and dynamic impact on signal transduction (chapter IV).

References

1. Consortium IHGS: Finishing the euchromatic sequence of the human genome. *Nature* 2004, 431(7011):931-945.
2. Jensen ON: Modification-specific proteomics: characterization of post-translational modifications by mass spectrometry. *Current opinion in chemical biology* 2004, 8(1):33-41.
3. Smith LM, Kelleher NL, Consortium for Top Down P: Proteoform: a single term describing protein complexity. *Nature methods* 2013, 10(3):186-187.
4. Deribe YL, Pawson T, Dikic I: Post-translational modifications in signal integration. *Nature Structural & Molecular Biology* 2010, 17(6):666-672.
5. Levene PA, Alsberg CL: THE CLEAVAGE PRODUCTS OF VITELLIN. *Journal of Biological Chemistry* 1906, 2(1):127-133.
6. Fischer EH, Krebs EG: CONVERSION OF PHOSPHORYLASE b TO PHOSPHORYLASE a IN MUSCLE EXTRACTS. *Journal of Biological Chemistry* 1955, 216(1):121-132.
7. Burnett G, Kennedy EP: THE ENZYMATIC PHOSPHORYLATION OF PROTEINS. *Journal of Biological Chemistry* 1954, 211(2):969-980.
8. Hunter T: Why nature chose phosphate to modify proteins. *Philosophical transactions of the Royal Society of London Series B, Biological sciences* 2012, 367(1602):2513-2516.
9. Walsh DA, Perkins JP, Krebs EG: An Adenosine 3',5'-Monophosphate-dependant Protein Kinase from Rabbit Skeletal Muscle. *Journal of Biological Chemistry* 1968, 243(13):3763-3765.
10. Manning G, Whyte DB, Martinez R, Hunter T, Sudarsanam S: The Protein Kinase Complement of the Human Genome. *Science* 2002, 298(5600):1912.
11. Kanev GK, de Graaf C, de Esch IJP, Leurs R, Würdinger T, Westerman BA, Kooistra AJ: The Landscape of Atypical and Eukaryotic Protein Kinases. *Trends in Pharmacological Sciences* 2019, 40(11):818-832.
12. Johnson LN, Lowe ED, Noble MEM, Owen DJ: The structural basis for substrate recognition and control by protein kinases. *FEBS Letters* 1998, 430(1):1-11.
13. Roskoski R, Jr.: Classification of small molecule protein kinase inhibitors based upon the structures of their drug-enzyme complexes. *Pharmacological research* 2016, 103:26-48.
14. Johnson LN, Lewis RJ: Structural Basis for Control by Phosphorylation. *Chemical Reviews* 2001, 101(8):2209-2242.
15. Needham EJ, Parker BL, Burykin T, James DE, Humphrey SJ: Illuminating the dark phosphoproteome. *Science Signaling* 2019, 12(565):eaau8645.
16. Hunter T: Signaling - 2000 and Beyond. *Cell* 2000, 100(1):113-127.
17. Murray AW: Recycling the cell cycle: cyclins revisited. *Cell* 2004, 116(2):221-234.
18. Ptacek J, Devgan G, Michaud G, Zhu H, Zhu X, Fasolo J, Guo H, Jona G, Breitkreutz A, Sopko R *et al*: Global analysis of protein phosphorylation in yeast. *Nature* 2005, 438(7068):679-684.
19. Echols N, Harrison P, Balasubramanian S, Luscombe NM, Bertone P, Zhang Z, Gerstein M: Comprehensive analysis of amino acid and nucleotide composition in eukaryotic genomes, comparing genes and pseudogenes. *Nucleic Acids Res* 2002, 30(11):2515-2523.
20. Ubersax JA, Ferrell Jr JE: Mechanisms of specificity in protein phosphorylation. *Nature Reviews Molecular Cell Biology* 2007, 8(7):530-541.
21. Sacco F, Perfetto L, Castagnoli L, Cesareni G: The human phosphatase interactome: An intricate family portrait. *FEBS letters* 2012, 586(17):2732-2739.
22. Cohen PT: Protein phosphatase 1--targeted in many directions. *Journal of cell science* 2002, 115(Pt 2):241-256.

23. Sharma K, D'Souza Rochelle CJ, Tyanova S, Schaab C, Wiśniewski Jacek R, Cox J, Mann M: Ultradeep Human Phosphoproteome Reveals a Distinct Regulatory Nature of Tyr and Ser/Thr-Based Signaling. *Cell Reports* 2014, 8(5):1583-1594.
24. Hunter T: Tyrosine phosphorylation: thirty years and counting. *Current opinion in cell biology* 2009, 21(2):140-146.
25. Tan CSH: Sequence, Structure, and Network Evolution of Protein Phosphorylation. *Science Signaling* 2011, 4(182):mr6-mr6.
26. Pearlman SM, Serber Z, Ferrell JE, Jr.: A mechanism for the evolution of phosphorylation sites. *Cell* 2011, 147(4):934-946.
27. Mandell DJ, Chorny I, Groban ES, Wong SE, Levine E, Rapp CS, Jacobson MP: Strengths of hydrogen bonds involving phosphorylated amino acid side chains. *J Am Chem Soc* 2007, 129(4):820-827.
28. Yaffe MB: Phosphotyrosine-binding domains in signal transduction. *Nature reviews Molecular cell biology* 2002, 3(3):177-186.
29. Reinhardt HC, Yaffe MB: Phospho-Ser/Thr-binding domains: navigating the cell cycle and DNA damage response. *Nature reviews Molecular cell biology* 2013, 14(9):563-580.
30. Pawson T, Scott JD: Protein phosphorylation in signaling; 50 years and counting. *Trends in Biochemical Sciences* 2005, 30(6):286-290.
31. Cohen P: The origins of protein phosphorylation. *Nature cell biology* 2002, 4(5):E127-E130.
32. Manning BD, Toker A: AKT/PKB Signaling: Navigating the Network. *Cell* 2017, 169(3):381-405.
33. Dajani R, Fraser E, Roe SM, Young N, Good V, Dale TC, Pearl LH: Crystal structure of glycogen synthase kinase 3 beta: structural basis for phosphate-primed substrate specificity and autoinhibition. *Cell* 2001, 105(6):721-732.
34. Maurer U, Charvet C, Wagman AS, Dejardin E, Green DR: Glycogen synthase kinase-3 regulates mitochondrial outer membrane permeabilization and apoptosis by destabilization of MCL-1. *Mol Cell* 2006, 21(6):749-760.
35. Sears R, Nuckolls F, Haura E, Taya Y, Tamai K, Nevins JR: Multiple Ras-dependent phosphorylation pathways regulate Myc protein stability. *Genes & development* 2000, 14(19):2501-2514.
36. Brunet A, Bonni A, Zigmond MJ, Lin MZ, Juo P, Hu LS, Anderson MJ, Arden KC, Blenis J, Greenberg ME: Akt promotes cell survival by phosphorylating and inhibiting a Forkhead transcription factor. *Cell* 1999, 96(6):857-868.
37. van der Vos KE, Coffer PJ: The extending network of FOXO transcriptional target genes. *Antioxidants & redox signaling* 2011, 14(4):579-592.
38. Hanahan D, Weinberg RA: Hallmarks of cancer: the next generation. *Cell* 2011, 144(5):646-674.
39. Weinstein IB, Joe A: Oncogene addiction. *Cancer Res* 2008, 68(9):3077-3080; discussion 3080.
40. Collett MS, Erikson RL: Protein kinase activity associated with the avian sarcoma virus src gene product. *Proceedings of the National Academy of Sciences of the United States of America* 1978, 75(4):2021-2024.
41. Solimini NL, Luo J, Elledge SJ: Non-oncogene addiction and the stress phenotype of cancer cells. *Cell* 2007, 130(6):986-988.
42. Hjaltelin JX, Izarzugaza JMG, Jensen LJ, Russo F, Westergaard D, Brunak S: Identification of hyper-rewired genomic stress non-oncogene addiction genes across 15 cancer types. *npj Systems Biology and Applications* 2019, 5(1):27.
43. Lahiry P, Torkamani A, Schork NJ, Hegele RA: Kinase mutations in human disease: interpreting genotype–phenotype relationships. *Nature Reviews Genetics* 2010, 11(1):60-74.

44. Vogelstein B, Papadopoulos N, Velculescu VE, Zhou S, Diaz LA, Jr., Kinzler KW: Cancer genome landscapes. *Science* 2013, 339(6127):1546-1558.
45. Jiang BH, Liu LZ: PI3K/PTEN signaling in angiogenesis and tumorigenesis. *Advances in cancer research* 2009, 102:19-65.
46. Davies MA, Samuels Y: Analysis of the genome to personalize therapy for melanoma. *Oncogene* 2010, 29(41):5545-5555.
47. Landrum MJ, Lee JM, Riley GR, Jang W, Rubinstein WS, Church DM, Maglott DR: ClinVar: public archive of relationships among sequence variation and human phenotype. *Nucleic Acids Res* 2014, 42(Database issue):D980-985.
48. Hornbeck PV, Kornhauser JM, Tkachev S, Zhang B, Skrzypek E, Murray B, Latham V, Sullivan M: PhosphoSitePlus: a comprehensive resource for investigating the structure and function of experimentally determined post-translational modifications in man and mouse. *Nucleic Acids Res* 2012, 40(Database issue):D261-270.
49. Wong S, Witte ON: The BCR-ABL story: bench to bedside and back. *Annual review of immunology* 2004, 22:247-306.
50. Wang Y, Wu N, Liu D, Jin Y: Recurrent Fusion Genes in Leukemia: An Attractive Target for Diagnosis and Treatment. *Current genomics* 2017, 18(5):378-384.
51. Tomlins SA, Rhodes DR, Perner S, Dhanasekaran SM, Mehra R, Sun XW, Varambally S, Cao X, Tchinda J, Kuefer R *et al*: Recurrent fusion of TMPRSS2 and ETS transcription factor genes in prostate cancer. *Science* 2005, 310(5748):644-648.
52. Dupain C, Gracia C, Harttrampf AC, Rivière J, Geoerger B, Massaad-Massade L: Newly identified LMO3-BORCS5 fusion oncogene in Ewing sarcoma at relapse is a driver of tumor progression. *Oncogene* 2019, 38(47):7200-7215.
53. Santarius T, Shipley J, Brewer D, Stratton MR, Cooper CS: A census of amplified and overexpressed human cancer genes. *Nature Reviews Cancer* 2010, 10(1):59-64.
54. Oh D-Y, Bang Y-J: HER2-targeted therapies — a role beyond breast cancer. *Nature Reviews Clinical Oncology* 2019.
55. Organization WH: Global Health Estimates 2016: Deaths by Cause, Age, Sex, by Country and by Region, 2000-2016. Geneva. 2018.
56. Gersten O, Wilmoth JR: The Cancer Transition in Japan since 1951. *Demographic Research* 2002, 7(5):271-306.
57. Bray F, Ferlay J, Soerjomataram I, Siegel RL, Torre LA, Jemal A: Global cancer statistics 2018: GLOBOCAN estimates of incidence and mortality worldwide for 36 cancers in 185 countries. *CA Cancer J Clin* 2018, 68(6):394-424.
58. Sakaguchi T, Satoi S, Yamamoto T, Yamaki S, Sekimoto M: The past, present, and future status of multimodality treatment for resectable/borderline resectable pancreatic ductal adenocarcinoma. *Surgery today* 2020, 50(4):335-343.
59. Chabner BA, Roberts TG: Chemotherapy and the war on cancer. *Nature Reviews Cancer* 2005, 5(1):65-72.
60. Curtis RE, Boice JD, Jr., Stovall M, Bernstein L, Greenberg RS, Flannery JT, Schwartz AG, Weyer P, Moloney WC, Hoover RN: Risk of leukemia after chemotherapy and radiation treatment for breast cancer. *N Engl J Med* 1992, 326(26):1745-1751.
61. Morgan G, Ward R, Barton M: The contribution of cytotoxic chemotherapy to 5-year survival in adult malignancies. *Clinical oncology (Royal College of Radiologists (Great Britain))* 2004, 16(8):549-560.

62. Yard BD, Adams DJ, Chie EK, Tamayo P, Battaglia JS, Gopal P, Rogacki K, Pearson BE, Phillips J, Raymond DP *et al*: A genetic basis for the variation in the vulnerability of cancer to DNA damage. *Nature communications* 2016, 7:11428-11428.
63. Minniti G, Amelio D, Amichetti M, Salvati M, Muni R, Bozzao A, Lanzetta G, Scarpino S, Arcella A, Enrici RM: Patterns of failure and comparison of different target volume delineations in patients with glioblastoma treated with conformal radiotherapy plus concomitant and adjuvant temozolomide. *Radiotherapy and oncology : journal of the European Society for Therapeutic Radiology and Oncology* 2010, 97(3):377-381.
64. Aupérin A, Le Péchoux C, Pignon JP, Koning C, Jeremic B, Clamon G, Einhorn L, Ball D, Trovo MG, Groen HJ *et al*: Concomitant radio-chemotherapy based on platin compounds in patients with locally advanced non-small cell lung cancer (NSCLC): a meta-analysis of individual data from 1764 patients. *Annals of oncology : official journal of the European Society for Medical Oncology* 2006, 17(3):473-483.
65. Ottmann OG, Druker BJ, Sawyers CL, Goldman JM, Reiffers J, Silver RT, Tura S, Fischer T, Deininger MW, Schiffer CA *et al*: A phase 2 study of imatinib in patients with relapsed or refractory Philadelphia chromosome-positive acute lymphoid leukemias. *Blood* 2002, 100(6):1965-1971.
66. Rosell R, Carcereny E, Gervais R, Vergnenegre A, Massuti B, Felip E, Palmero R, Garcia-Gomez R, Pallares C, Sanchez JM *et al*: Erlotinib versus standard chemotherapy as first-line treatment for European patients with advanced EGFR mutation-positive non-small-cell lung cancer (EURTAC): a multicentre, open-label, randomised phase 3 trial. *The Lancet Oncology* 2012, 13(3):239-246.
67. Fukuoka M, Wu YL, Thongprasert S, Sunpaweravong P, Leong SS, Sriuranpong V, Chao TY, Nakagawa K, Chu DT, Saijo N *et al*: Biomarker analyses and final overall survival results from a phase III, randomized, open-label, first-line study of gefitinib versus carboplatin/paclitaxel in clinically selected patients with advanced non-small-cell lung cancer in Asia (IPASS). *J Clin Oncol* 2011, 29(21):2866-2874.
68. Hauschild A, Grob JJ, Demidov LV, Jouary T, Gutzmer R, Millward M, Rutkowski P, Blank CU, Miller WH, Jr., Kaempgen E *et al*: Dabrafenib in BRAF-mutated metastatic melanoma: a multicentre, open-label, phase 3 randomised controlled trial. *Lancet* 2012, 380(9839):358-365.
69. Hyman DM, Puzanov I, Subbiah V, Faris JE, Chau I, Blay J-Y, Wolf J, Raje NS, Diamond EL, Hollebecque A *et al*: Vemurafenib in Multiple Nonmelanoma Cancers with BRAF V600 Mutations. *New England Journal of Medicine* 2015, 373(8):726-736.
70. Carles F, Bourg S, Meyer C, Bonnet P: PKIDB: A Curated, Annotated and Updated Database of Protein Kinase Inhibitors in Clinical Trials. *Molecules (Basel, Switzerland)* 2018, 23(4).
71. Zuccotto F, Ardini E, Casale E, Angiolini M: Through the "Gatekeeper Door": Exploiting the Active Kinase Conformation. *Journal of medicinal chemistry* 2010, 53(7):2681-2694.
72. Nolen B, Taylor S, Ghosh G: Regulation of protein kinases; controlling activity through activation segment conformation. *Mol Cell* 2004, 15(5):661-675.
73. Zhao Z, Wu H, Wang L, Liu Y, Knapp S, Liu Q, Gray NS: Exploration of Type II Binding Mode: A Privileged Approach for Kinase Inhibitor Focused Drug Discovery? *ACS Chemical Biology* 2014, 9(6):1230-1241.
74. Hodous BL, Geuns-Meyer SD, Hughes PE, Albrecht BK, Bellon S, Bready J, Caenepeel S, Cee VJ, Chaffee SC, Coxon A *et al*: Evolution of a Highly Selective and Potent 2-(Pyridin-2-yl)-1,3,5-triazine Tie-2 Kinase Inhibitor. *Journal of medicinal chemistry* 2007, 50(4):611-626.
75. Klaeger S, Heinzlmeir S, Wilhelm M, Polzer H, Vick B, Koenig P-A, Reinecke M, Ruprecht B, Petzoldt S, Meng C *et al*: The target landscape of clinical kinase drugs. *Science* 2017, 358(6367).

76. Yueh C, Rettenmaier J, Xia B, Hall DR, Alekseenko A, Porter KA, Barkovich K, Keseru G, Whitty A, Wells JA *et al*: Kinase Atlas: Druggability Analysis of Potential Allosteric Sites in Kinases. *Journal of medicinal chemistry* 2019, 62(14):6512-6524.
77. Roskoski R, Jr.: Allosteric MEK1/2 inhibitors including cobimetanib and trametinib in the treatment of cutaneous melanomas. *Pharmacological research* 2017, 117:20-31.
78. Cohen MS, Zhang C, Shokat KM, Taunton J: Structural bioinformatics-based design of selective, irreversible kinase inhibitors. *Science (New York, NY)* 2005, 308(5726):1318-1321.
79. Kwak EL, Sordella R, Bell DW, Godin-Heymann N, Okimoto RA, Brannigan BW, Harris PL, Driscoll DR, Fidias P, Lynch TJ *et al*: Irreversible inhibitors of the EGF receptor may circumvent acquired resistance to gefitinib. *Proceedings of the National Academy of Sciences of the United States of America* 2005, 102(21):7665-7670.
80. Klaeger S, Heinzlmeir S, Wilhelm M, Polzer H, Vick B, Koenig PA, Reinecke M, Ruprecht B, Petzoldt S, Meng C *et al*: The target landscape of clinical kinase drugs. *Science* 2017, 358(6367).
81. Klaeger S, Gohlke B, Perrin J, Gupta V, Heinzlmeir S, Helm D, Qiao H, Bergamini G, Handa H, Savitski MM *et al*: Chemical Proteomics Reveals Ferrochelatase as a Common Off-target of Kinase Inhibitors. *ACS Chemical Biology* 2016, 11(5):1245-1254.
82. Savitski MM, Reinhard FB, Franken H, Werner T, Savitski MF, Eberhard D, Martinez Molina D, Jafari R, Dovega RB, Klaeger S *et al*: Tracking cancer drugs in living cells by thermal profiling of the proteome. *Science* 2014, 346(6205):1255784.
83. Shapiro P: A promiscuous kinase inhibitor reveals secrets to cancer cell survival. *J Biol Chem* 2019, 294(21):8674-8675.
84. Troutman S, Moleirinho S, Kota S, Nettles K, Fallahi M, Johnson GL, Kissil JL: Crizotinib inhibits NF2-associated schwannoma through inhibition of focal adhesion kinase 1. *Oncotarget* 2016, 7(34):54515-54525.
85. Blanke CD, Demetri GD, von Mehren M, Heinrich MC, Eisenberg B, Fletcher JA, Corless CL, Fletcher CD, Roberts PJ, Heinz D *et al*: Long-term results from a randomized phase II trial of standard- versus higher-dose imatinib mesylate for patients with unresectable or metastatic gastrointestinal stromal tumors expressing KIT. *J Clin Oncol* 2008, 26(4):620-625.
86. Williams AF, Barclay AN: The immunoglobulin superfamily--domains for cell surface recognition. *Annual review of immunology* 1988, 6:381-405.
87. Köhler G, Milstein C: Continuous cultures of fused cells secreting antibody of predefined specificity. *Nature* 1975, 256(5517):495-497.
88. Strebhardt K, Ullrich A: Paul Ehrlich's magic bullet concept: 100 years of progress. *Nat Rev Cancer* 2008, 8(6):473-480.
89. Scott AM, Wolchok JD, Old LJ: Antibody therapy of cancer. *Nat Rev Cancer* 2012, 12(4):278-287.
90. Van den Eynde BJ, Scott AM: Tumor Antigens. In: *Encyclopedia of Immunology (Second Edition)*. edn. Edited by Delves PJ. Oxford: Elsevier; 1998: 2424-2431.
91. Rudnick SI, Adams GP: Affinity and avidity in antibody-based tumor targeting. *Cancer biotherapy & radiopharmaceuticals* 2009, 24(2):155-161.
92. Viti F, Tarli L, Giovannoni L, Zardi L, Neri D: Increased binding affinity and valence of recombinant antibody fragments lead to improved targeting of tumoral angiogenesis. *Cancer Res* 1999, 59(2):347-352.
93. Adams GP, Schier R, McCall AM, Simmons HH, Horak EM, Alpaugh RK, Marks JD, Weiner LM: High affinity restricts the localization and tumor penetration of single-chain fv antibody molecules. *Cancer Res* 2001, 61(12):4750-4755.

94. Rudnick SI, Lou J, Shaller CC, Tang Y, Klein-Szanto AJ, Weiner LM, Marks JD, Adams GP: Influence of affinity and antigen internalization on the uptake and penetration of Anti-HER2 antibodies in solid tumors. *Cancer Res* 2011, 71(6):2250-2259.
95. Fujimori K, Covell DG, Fletcher JE, Weinstein JN: A modeling analysis of monoclonal antibody percolation through tumors: a binding-site barrier. *Journal of nuclear medicine : official publication, Society of Nuclear Medicine* 1990, 31(7):1191-1198.
96. Muhsin M, Graham J, Kirkpatrick P: Bevacizumab. *Nature Reviews Drug Discovery* 2004, 3(12):995-996.
97. Williams RO, Paleolog E, Feldmann M: Cytokine inhibitors in rheumatoid arthritis and other autoimmune diseases. *Current opinion in pharmacology* 2007, 7(4):412-417.
98. Shealy DJ, Cai A, Staquet K, Baker A, Lacy ER, Johns L, Vafa O, Gunn G, 3rd, Tam S, Sague S *et al*: Characterization of golimumab, a human monoclonal antibody specific for human tumor necrosis factor α. *MAbs* 2010, 2(4):428-439.
99. Pietras RJ, Fendly BM, Chazin VR, Pegram MD, Howell SB, Slamon DJ: Antibody to HER-2/neu receptor blocks DNA repair after cisplatin in human breast and ovarian cancer cells. *Oncogene* 1994, 9(7):1829-1838.
100. Izumi Y, Xu L, di Tomaso E, Fukumura D, Jain RK: Tumour biology: herceptin acts as an anti-angiogenic cocktail. *Nature* 2002, 416(6878):279-280.
101. Maier LA, Xu FJ, Hester S, Boyer CM, McKenzie S, Bruskin AM, Argon Y, Bast RC, Jr.: Requirements for the internalization of a murine monoclonal antibody directed against the HER-2/neu gene product c-erbB-2. *Cancer Res* 1991, 51(19):5361-5369.
102. Molina MA, Codony-Servat J, Albanell J, Rojo F, Arribas J, Baselga J: Trastuzumab (herceptin), a humanized anti-Her2 receptor monoclonal antibody, inhibits basal and activated Her2 ectodomain cleavage in breast cancer cells. *Cancer Res* 2001, 61(12):4744-4749.
103. Byrd JC, Kitada S, Flinn IW, Aron JL, Pearson M, Lucas D, Reed JC: The mechanism of tumor cell clearance by rituximab in vivo in patients with B-cell chronic lymphocytic leukemia: evidence of caspase activation and apoptosis induction. *Blood* 2002, 99(3):1038-1043.
104. Nimmerjahn F, Ravetch JV: Antibodies, Fc receptors and cancer. *Current Opinion in Immunology* 2007, 19(2):239-245.
105. Gul N, van Egmond M: Antibody-Dependent Phagocytosis of Tumor Cells by Macrophages: A Potent Effector Mechanism of Monoclonal Antibody Therapy of Cancer. *Cancer Res* 2015, 75(23):5008-5013.
106. Rogers LM, Veeramani S, Weiner GJ: Complement in monoclonal antibody therapy of cancer. *Immunologic research* 2014, 59(1-3):203-210.
107. Hughes B: Antibody-drug conjugates for cancer: poised to deliver? *Nature reviews Drug discovery* 2010, 9(9):665-667.
108. Dhillon S: Trastuzumab emtansine: a review of its use in patients with HER2-positive advanced breast cancer previously treated with trastuzumab-based therapy. *Drugs* 2014, 74(6):675-686.
109. Borrebaeck CA, Carlsson R: Human therapeutic antibodies. *Current opinion in pharmacology* 2001, 1(4):404-408.
110. Clynes RA, Towers TL, Presta LG, Ravetch JV: Inhibitory Fc receptors modulate in vivo cytotoxicity against tumor targets. *Nat Med* 2000, 6(4):443-446.
111. Harjunpaa A, Junnikkala S, Meri S: Rituximab (anti-CD20) therapy of B-cell lymphomas: direct complement killing is superior to cellular effector mechanisms. *Scandinavian journal of immunology* 2000, 51(6):634-641.
112. Beers SA, Cragg MS, Glennie MJ: Complement: help or hindrance? *Blood* 2009, 114(27):5567-5568; author reply 5568.

113. Unruh TL, Li H, Mutch CM, Shariat N, Grigoriou L, Sanyal R, Brown CB, Deans JP: Cholesterol depletion inhibits src family kinase-dependent calcium mobilization and apoptosis induced by rituximab crosslinking. *Immunology* 2005, 116(2):223-232.
114. Chan HT, Hughes D, French RR, Tutt AL, Walshe CA, Teeling JL, Glennie MJ, Cragg MS: CD20-induced lymphoma cell death is independent of both caspases and its redistribution into triton X-100 insoluble membrane rafts. *Cancer Res* 2003, 63(17):5480-5489.
115. Cartron G, Dacheux L, Salles G, Solal-Celigny P, Bardos P, Colombat P, Watier H: Therapeutic activity of humanized anti-CD20 monoclonal antibody and polymorphism in IgG Fc receptor FcgammaRIIIa gene. *Blood* 2002, 99(3):754-758.
116. Ghielmini M, Rufibach K, Salles G, Leoncini-Franscini L, Léger-Falandry C, Cogliatti S, Fey M, Martinelli G, Stahel R, Lohri A *et al*: Single agent rituximab in patients with follicular or mantle cell lymphoma: clinical and biological factors that are predictive of response and event-free survival as well as the effect of rituximab on the immune system: a study of the Swiss Group for Clinical Cancer Research (SAKK). *Annals of oncology : official journal of the European Society for Medical Oncology* 2005, 16(10):1675-1682.
117. Váróczy L, Zilahi E, Gyetvai A, Kajtár B, Gergely L, Sipka S, Illés A: Fc-gamma-receptor IIIa polymorphism and gene expression profile do not predict the prognosis in diffuse large B-cell lymphoma treated with R-CHOP protocol. *Pathology oncology research : POR* 2012, 18(1):43-48.
118. FDA: In Vitro Companion Diagnostic Devices - Guidance for Industry and Food and Drug Administration Staff *https://wwwfdagov/media/81309/download* 2014.
119. Carter P, Presta L, Gorman CM, Ridgway JB, Henner D, Wong WL, Rowland AM, Kotts C, Carver ME, Shepard HM: Humanization of an anti-p185HER2 antibody for human cancer therapy. *Proc Natl Acad Sci U S A* 1992, 89(10):4285-4289.
120. Jørgensen J, Winther H: The Development of the HercepTest - From Bench to Bedside. In., edn.; 2010: 43-60.
121. Vogel CL, Cobleigh MA, Tripathy D, Gutheil JC, Harris LN, Fehrenbacher L, Slamon DJ, Murphy M, Novotny WF, Burchmore M *et al*: Efficacy and Safety of Trastuzumab as a Single Agent in First-Line Treatment of HER2-Overexpressing Metastatic Breast Cancer. *Journal of Clinical Oncology* 2002, 20(3):719-726.
122. Romond EH, Perez EA, Bryant J, Suman VJ, Geyer CE, Davidson NE, Tan-Chiu E, Martino S, Paik S, Kaufman PA *et al*: Trastuzumab plus Adjuvant Chemotherapy for Operable HER2-Positive Breast Cancer. *New England Journal of Medicine* 2005, 353(16):1673-1684.
123. Seidman AD, Berry D, Cirrincione C, Harris L, Muss H, Marcom PK, Gipson G, Burstein H, Lake D, Shapiro CL *et al*: Randomized Phase III Trial of Weekly Compared With Every-3-Weeks Paclitaxel for Metastatic Breast Cancer, With Trastuzumab for all HER-2 Overexpressors and Random Assignment to Trastuzumab or Not in HER-2 Nonoverexpressors: Final Results of Cancer and Leukemia Group B Protocol 9840. *Journal of Clinical Oncology* 2008, 26(10):1642-1649.
124. Nagata Y, Lan K-H, Zhou X, Tan M, Esteva FJ, Sahin AA, Klos KS, Li P, Monia BP, Nguyen NT *et al*: PTEN activation contributes to tumor inhibition by trastuzumab, and loss of PTEN predicts trastuzumab resistance in patients. *Cancer Cell* 2004, 6(2):117-127.
125. Berns K, Horlings HM, Hennessy BT, Madiredjo M, Hijmans EM, Beelen K, Linn SC, Gonzalez-Angulo AM, Stemke-Hale K, Hauptmann M *et al*: A Functional Genetic Approach Identifies the PI3K Pathway as a Major Determinant of Trastuzumab Resistance in Breast Cancer. *Cancer Cell* 2007, 12(4):395-402.

126. Scaltriti M, Rojo F, Ocaña A, Anido J, Guzman M, Cortes J, Di Cosimo S, Matias-Guiu X, Ramon y Cajal S, Arribas J *et al*: Expression of p95HER2, a Truncated Form of the HER2 Receptor, and Response to Anti-HER2 Therapies in Breast Cancer. *JNCI: Journal of the National Cancer Institute* 2007, 99(8):628-638.
127. Gerlinger M, Rowan AJ, Horswell S, Math M, Larkin J, Endesfelder D, Gronroos E, Martinez P, Matthews N, Stewart A *et al*: Intratumor heterogeneity and branched evolution revealed by multiregion sequencing. *N Engl J Med* 2012, 366(10):883-892.
128. Kwak EL, Ahronian LG, Siravegna G, Mussolin B, Borger DR, Godfrey JT, Jessop NA, Clark JW, Blaszkowsky LS, Ryan DP *et al*: Molecular Heterogeneity and Receptor Coamplification Drive Resistance to Targeted Therapy in MET-Amplified Esophagogastric Cancer. *Cancer Discov* 2015, 5(12):1271-1281.
129. Gainor JF, Dardaei L, Yoda S, Friboulet L, Leshchiner I, Katayama R, Dagogo-Jack I, Gadgeel S, Schultz K, Singh M *et al*: Molecular Mechanisms of Resistance to First- and Second-Generation ALK Inhibitors in ALK-Rearranged Lung Cancer. *Cancer Discov* 2016, 6(10):1118-1133.
130. Sequist LV, Waltman BA, Dias-Santagata D, Digumarthy S, Turke AB, Fidias P, Bergethon K, Shaw AT, Gettinger S, Cosper AK *et al*: Genotypic and histological evolution of lung cancers acquiring resistance to EGFR inhibitors. *Sci Transl Med* 2011, 3(75):75ra26.
131. Yu HA, Arcila ME, Rekhtman N, Sima CS, Zakowski MF, Pao W, Kris MG, Miller VA, Ladanyi M, Riely GJ: Analysis of tumor specimens at the time of acquired resistance to EGFR-TKI therapy in 155 patients with EGFR-mutant lung cancers. *Clin Cancer Res* 2013, 19(8):2240-2247.
132. Ritter CA, Perez-Torres M, Rinehart C, Guix M, Dugger T, Engelman JA, Arteaga CL: Human Breast Cancer Cells Selected for Resistance to Trastuzumab In vivo Overexpress Epidermal Growth Factor Receptor and ErbB Ligands and Remain Dependent on the ErbB Receptor Network. *Clinical Cancer Research* 2007, 13(16):4909-4919.
133. Nahta R, Yuan LXH, Zhang B, Kobayashi R, Esteva FJ: Insulin-like Growth Factor-I Receptor/Human Epidermal Growth Factor Receptor 2 Heterodimerization Contributes to Trastuzumab Resistance of Breast Cancer Cells. *Cancer Research* 2005, 65(23):11118-11128.
134. Shattuck DL, Miller JK, Carraway KL, Sweeney C: Met Receptor Contributes to Trastuzumab Resistance of Her2-Overexpressing Breast Cancer Cells. *Cancer Research* 2008, 68(5):1471-1477.
135. Yu HA, Arcila ME, Hellmann MD, Kris MG, Ladanyi M, Riely GJ: Poor response to erlotinib in patients with tumors containing baseline EGFR T790M mutations found by routine clinical molecular testing. *Annals of oncology : official journal of the European Society for Medical Oncology* 2014, 25(2):423-428.
136. Robert C, Karaszewska B, Schachter J, Rutkowski P, Mackiewicz A, Stroiakovski D, Lichinitser M, Dummer R, Grange F, Mortier L *et al*: Improved overall survival in melanoma with combined dabrafenib and trametinib. *N Engl J Med* 2015, 372(1):30-39.
137. Pirazzoli V, Ayeni D, Meador CB, Sanganahalli BG, Hyder F, de Stanchina E, Goldberg SB, Pao W, Politi K: Afatinib plus Cetuximab Delays Resistance Compared to Single-Agent Erlotinib or Afatinib in Mouse Models of TKI-Naïve EGFR L858R-Induced Lung Adenocarcinoma. *Clin Cancer Res* 2016, 22(2):426-435.
138. Tricker EM, Xu C, Uddin S, Capelletti M, Ercan D, Ogino A, Pratilas CA, Rosen N, Gray NS, Wong KK *et al*: Combined EGFR/MEK Inhibition Prevents the Emergence of Resistance in EGFR-Mutant Lung Cancer. *Cancer Discov* 2015, 5(9):960-971.
139. Tolcher AW, Peng W, Calvo E: Rational Approaches for Combination Therapy Strategies Targeting the MAP Kinase Pathway in Solid Tumors. *Molecular Cancer Therapeutics* 2018, 17(1):3-16.

140. Bhullar KS, Lagarón NO, McGowan EM, Parmar I, Jha A, Hubbard BP, Rupasinghe HPV: Kinase-targeted cancer therapies: progress, challenges and future directions. *Molecular Cancer* 2018, 17(1):48.
141. Taylor MH, Lee CH, Makker V, Rasco D, Dutcus CE, Wu J, Stepan DE, Shumaker RC, Motzer RJ: Phase IB/II Trial of Lenvatinib Plus Pembrolizumab in Patients With Advanced Renal Cell Carcinoma, Endometrial Cancer, and Other Selected Advanced Solid Tumors. *J Clin Oncol* 2020, 38(11):1154-1163.
142. Fukuoka S, Hara H, Takahashi N, Kojima T, Kawazoe A, Asayama M, Yoshii T, Kotani D, Tamura H, Mikamoto Y *et al*: Regorafenib Plus Nivolumab in Patients With Advanced Gastric or Colorectal Cancer: An Open-Label, Dose-Escalation, and Dose-Expansion Phase Ib Trial (REGONIVO, EPOC1603). *J Clin Oncol* 2020:Jco1903296.
143. Kirschner MW: The Meaning of Systems Biology. *Cell* 2005, 121(4):503-504.
144. Tyers M, Mann M: From genomics to proteomics. *Nature* 2003, 422(6928):193-197.
145. McLafferty FW: A Century of Progress in Molecular Mass Spectrometry. *Annual Review of Analytical Chemistry* 2011, 4(1):1-22.
146. Eliuk S, Makarov A: Evolution of Orbitrap Mass Spectrometry Instrumentation. *Annual Review of Analytical Chemistry* 2015, 8(1):61-80.
147. Wilhelm M, Schlegl J, Hahne H, Gholami AM, Lieberenz M, Savitski MM, Ziegler E, Butzmann L, Gessulat S, Marx H *et al*: Mass-spectrometry-based draft of the human proteome. *Nature* 2014, 509(7502):582-587.
148. Kim M-S, Pinto SM, Getnet D, Nirujogi RS, Manda SS, Chaerkady R, Madugundu AK, Kelkar DS, Isserlin R, Jain S *et al*: A draft map of the human proteome. *Nature* 2014, 509(7502):575-581.
149. Mallick P, Kuster B: Proteomics: a pragmatic perspective. *Nature biotechnology* 2010, 28(7):695-709.
150. Zhang Y, Fonslow BR, Shan B, Baek M-C, Yates JR: Protein Analysis by Shotgun/Bottom-up Proteomics. *Chemical Reviews* 2013, 113(4):2343-2394.
151. Shehadul Islam M, Aryasomayajula A, Selvaganapathy PR: A Review on Macroscale and Microscale Cell Lysis Methods. *Micromachines (Basel)* 2017, 8(3):83.
152. Sechi S, Chait BT: Modification of cysteine residues by alkylation. A tool in peptide mapping and protein identification. *Anal Chem* 1998, 70(24):5150-5158.
153. Steen H, Mann M: The abc's (and xyz's) of peptide sequencing. *Nature Reviews Molecular Cell Biology* 2004, 5(9):699-711.
154. Giansanti P, Aye TT, van den Toorn H, Peng M, van Breukelen B, Heck AJ: An Augmented Multiple-Protease-Based Human Phosphopeptide Atlas. *Cell Rep* 2015, 11(11):1834-1843.
155. Wang D, Eraslan B, Wieland T, Hallström B, Hopf T, Zolg DP, Zecha J, Asplund A, Li LH, Meng C *et al*: A deep proteome and transcriptome abundance atlas of 29 healthy human tissues. *Mol Syst Biol* 2019, 15(2):e8503.
156. Manadas B, Mendes VM, English J, Dunn MJ: Peptide fractionation in proteomics approaches. *Expert Rev Proteomics* 2010, 7(5):655-663.
157. Ducret A, Van Oostveen I, Eng JK, Yates JR, 3rd, Aebersold R: High throughput protein characterization by automated reverse-phase chromatography/electrospray tandem mass spectrometry. *Protein Sci* 1998, 7(3):706-719.
158. Ruprecht B, Wang D, Chiozzi RZ, Li L-H, Hahne H, Kuster B: Hydrophilic Strong Anion Exchange (hSAX) Chromatography Enables Deep Fractionation of Tissue Proteomes. In: *Proteomics: Methods and Protocols.* edn. Edited by Comai L, Katz JE, Mallick P. New York, NY: Springer New York; 2017: 69-82.

159. Yang F, Shen Y, Camp DG, 2nd, Smith RD: High-pH reversed-phase chromatography with fraction concatenation for 2D proteomic analysis. *Expert Rev Proteomics* 2012, 9(2):129-134.
160. Rappsilber J, Mann M, Ishihama Y: Protocol for micro-purification, enrichment, pre-fractionation and storage of peptides for proteomics using StageTips. *Nat Protoc* 2007, 2(8):1896-1906.
161. Bantscheff M, Eberhard D, Abraham Y, Bastuck S, Boesche M, Hobson S, Mathieson T, Perrin J, Raida M, Rau C *et al*: Quantitative chemical proteomics reveals mechanisms of action of clinical ABL kinase inhibitors. *Nature biotechnology* 2007, 25:1035.
162. Lemeer S, Heck AJR: The phosphoproteomics data explosion. *Current opinion in chemical biology* 2009, 13(4):414-420.
163. Medard G, Pachl F, Ruprecht B, Klaeger S, Heinzlmeir S, Helm D, Qiao H, Ku X, Wilhelm M, Kuehne T *et al*: Optimized chemical proteomics assay for kinase inhibitor profiling. *J Proteome Res* 2015, 14(3):1574-1586.
164. Reinecke M, Ruprecht B, Poser S, Wiechmann S, Wilhelm M, Heinzlmeir S, Kuster B, Medard G: Chemoproteomic Selectivity Profiling of PIKK and PI3K Kinase Inhibitors. *ACS Chem Biol* 2019.
165. Rogers LD, Foster LJ: Phosphoproteomics--finally fulfilling the promise? *Mol Biosyst* 2009, 5(10):1122-1129.
166. Macek B, Mann M, Olsen JV: Global and site-specific quantitative phosphoproteomics: principles and applications. *Annual review of pharmacology and toxicology* 2009, 49:199-221.
167. Mertins P, Tang LC, Krug K, Clark DJ, Gritsenko MA, Chen L, Clauser KR, Clauss TR, Shah P, Gillette MA *et al*: Reproducible workflow for multiplexed deep-scale proteome and phosphoproteome analysis of tumor tissues by liquid chromatography-mass spectrometry. *Nat Protoc* 2018, 13(7):1632-1661.
168. Ruprecht B, Koch H, Medard G, Mundt M, Kuster B, Lemeer S: Comprehensive and reproducible phosphopeptide enrichment using iron immobilized metal ion affinity chromatography (Fe-IMAC) columns. *Mol Cell Proteomics* 2015, 14(1):205-215.
169. Andersson L, Porath J: Isolation of phosphoproteins by immobilized metal (Fe3+) affinity chromatography. *Analytical Biochemistry* 1986, 154(1):250-254.
170. Posewitz MC, Tempst P: Immobilized Gallium(III) Affinity Chromatography of Phosphopeptides. *Analytical Chemistry* 1999, 71(14):2883-2892.
171. Tsai C-F, Wang Y-T, Chen Y-R, Lai C-Y, Lin P-Y, Pan K-T, Chen J-Y, Khoo K-H, Chen Y-J: Immobilized Metal Affinity Chromatography Revisited: pH/Acid Control toward High Selectivity in Phosphoproteomics. *Journal of Proteome Research* 2008, 7(9):4058-4069.
172. Post H, Penning R, Fitzpatrick MA, Garrigues LB, Wu W, MacGillavry HD, Hoogenraad CC, Heck AJ, Altelaar AF: Robust, Sensitive, and Automated Phosphopeptide Enrichment Optimized for Low Sample Amounts Applied to Primary Hippocampal Neurons. *J Proteome Res* 2017, 16(2):728-737.
173. Bian Y, Li L, Dong M, Liu X, Kaneko T, Cheng K, Liu H, Voss C, Cao X, Wang Y *et al*: Ultra-deep tyrosine phosphoproteomics enabled by a phosphotyrosine superbinder. *Nat Chem Biol* 2016.
174. Savaryn JP, Toby TK, Kelleher NL: A researcher's guide to mass spectrometry-based proteomics. *Proteomics* 2016.
175. Makarov A, Scigelova M: Coupling liquid chromatography to Orbitrap mass spectrometry. *Journal of chromatography A* 2010, 1217(25):3938-3945.
176. Fenn JB, Mann M, Meng CK, Wong SF, Whitehouse CM: Electrospray ionization for mass spectrometry of large biomolecules. *Science* 1989, 246(4926):64-71.

177. Kebarle P, Verkerk UH: Electrospray: From ions in solution to ions in the gas phase, what we know now. *Mass Spectrometry Reviews* 2009, 28(6):898-917.
178. Han X, Aslanian A, Yates JR, 3rd: Mass spectrometry for proteomics. *Current opinion in chemical biology* 2008, 12(5):483-490.
179. Yates JR, Ruse CI, Nakorchevsky A: Proteomics by mass spectrometry: approaches, advances, and applications. *Annual review of biomedical engineering* 2009, 11:49-79.
180. Guilhaus M: Special feature: Tutorial. Principles and instrumentation in time-of-flight mass spectrometry. Physical and instrumental concepts. *Journal of Mass Spectrometry* 1995, 30(11):1519-1532.
181. Mamyrin BA, Karataev VI, Shmikk DV, Zagulin VA: The mass-reflectron A new nonmagnetic time-of-flight high resolution mass-spectrometer. *Zhurnal Ehksperimental'noj i Teoreticheskoj Fiziki* 1973, 64(1):82-89.
182. Jonscher KR, Yates JR, 3rd: The quadrupole ion trap mass spectrometer--a small solution to a big challenge. *Anal Biochem* 1997, 244(1):1-15.
183. Douglas DJ, Frank AJ, Mao D: Linear ion traps in mass spectrometry. *Mass Spectrom Rev* 2005, 24(1):1-29.
184. Zubarev RA, Makarov A: Orbitrap Mass Spectrometry. *Analytical Chemistry* 2013, 85(11):5288-5296.
185. Edman P: Sequence determination. *Molecular biology, biochemistry, and biophysics* 1970, 8:211-255.
186. Nesvizhskii AI, Vitek O, Aebersold R: Analysis and validation of proteomic data generated by tandem mass spectrometry. *Nat Methods* 2007, 4(10):787-797.
187. Michalski A, Cox J, Mann M: More than 100,000 detectable peptide species elute in single shotgun proteomics runs but the majority is inaccessible to data-dependent LC-MS/MS. *J Proteome Res* 2011, 10(4):1785-1793.
188. Chapman JD, Goodlett DR, Masselon CD: Multiplexed and data-independent tandem mass spectrometry for global proteome profiling. *Mass Spectrom Rev* 2014, 33(6):452-470.
189. Peterson AC, Russell JD, Bailey DJ, Westphall MS, Coon JJ: Parallel Reaction Monitoring for High Resolution and High Mass Accuracy Quantitative, Targeted Proteomics. *Molecular & Cellular Proteomics* 2012, 11(11):1475-1488.
190. Roepstorff P, Fohlman J: Proposal for a common nomenclature for sequence ions in mass spectra of peptides. *Biomedical mass spectrometry* 1984, 11(11):601.
191. Hunt DF, Yates JR, Shabanowitz J, Winston S, Hauer CR: Protein sequencing by tandem mass spectrometry. *Proceedings of the National Academy of Sciences* 1986, 83(17):6233-6237.
192. Biemann K, Scoble HA: Characterization by tandem mass spectrometry of structural modifications in proteins. *Science* 1987, 237(4818):992-998.
193. Olsen JV, Macek B, Lange O, Makarov A, Horning S, Mann M: Higher-energy C-trap dissociation for peptide modification analysis. *Nat Methods* 2007, 4(9):709-712.
194. Syka JEP, Coon JJ, Schroeder MJ, Shabanowitz J, Hunt DF: Peptide and protein sequence analysis by electron transfer dissociation mass spectrometry. *Proceedings of the National Academy of Sciences of the United States of America* 2004, 101(26):9528-9533.
195. Boersema PJ, Mohammed S, Heck AJ: Phosphopeptide fragmentation and analysis by mass spectrometry. *Journal of mass spectrometry : JMS* 2009, 44(6):861-878.
196. Schroeder MJ, Shabanowitz J, Schwartz JC, Hunt DF, Coon JJ: A neutral loss activation method for improved phosphopeptide sequence analysis by quadrupole ion trap mass spectrometry. *Anal Chem* 2004, 76(13):3590-3598.

197. Senko MW, Remes PM, Canterbury JD, Mathur R, Song Q, Eliuk SM, Mullen C, Earley L, Hardman M, Blethrow JD *et al*: Novel Parallelized Quadrupole/Linear Ion Trap/Orbitrap Tribrid Mass Spectrometer Improving Proteome Coverage and Peptide Identification Rates. *Analytical Chemistry* 2013, 85(24):11710-11714.
198. Seidler J, Zinn N, Boehm ME, Lehmann WD: De novo sequencing of peptides by MS/MS. *Proteomics* 2010, 10(4):634-649.
199. Cox J, Neuhauser N, Michalski A, Scheltema RA, Olsen JV, Mann M: Andromeda: a peptide search engine integrated into the MaxQuant environment. *J Proteome Res* 2011, 10(4):1794-1805.
200. Perkins DN, Pappin DJ, Creasy DM, Cottrell JS: Probability-based protein identification by searching sequence databases using mass spectrometry data. *Electrophoresis* 1999, 20(18):3551-3567.
201. Hoopmann MR, Moritz RL: Current algorithmic solutions for peptide-based proteomics data generation and identification. *Current opinion in biotechnology* 2013, 24(1):31-38.
202. Savitski MM, Lemeer S, Boesche M, Lang M, Mathieson T, Bantscheff M, Kuster B: Confident Phosphorylation Site Localization Using the Mascot Delta Score. *Molecular & Cellular Proteomics* 2011, 10(2):M110.003830.
203. Olsen JV, Blagoev B, Gnad F, Macek B, Kumar C, Mortensen P, Mann M: Global, In Vivo, and Site-Specific Phosphorylation Dynamics in Signaling Networks. *Cell* 2006, 127(3):635-648.
204. Olsen JV, Vermeulen M, Santamaria A, Kumar C, Miller ML, Jensen LJ, Gnad F, Cox J, Jensen TS, Nigg EA *et al*: Quantitative Phosphoproteomics Reveals Widespread Full Phosphorylation Site Occupancy During Mitosis. *Science Signaling* 2010, 3(104):ra3-ra3.
205. Savitski MM, Wilhelm M, Hahne H, Kuster B, Bantscheff M: A Scalable Approach for Protein False Discovery Rate Estimation in Large Proteomic Data Sets. *Mol Cell Proteomics* 2015, 14(9):2394-2404.
206. Bantscheff M, Schirle M, Sweetman G, Rick J, Kuster B: Quantitative mass spectrometry in proteomics: a critical review. *Analytical and Bioanalytical Chemistry* 2007, 389(4):1017-1031.
207. Ong S-E, Blagoev B, Kratchmarova I, Kristensen DB, Steen H, Pandey A, Mann M: Stable Isotope Labeling by Amino Acids in Cell Culture, SILAC, as a Simple and Accurate Approach to Expression Proteomics. *Molecular & Cellular Proteomics* 2002, 1(5):376-386.
208. Ross PL, Huang YN, Marchese JN, Williamson B, Parker K, Hattan S, Khainovski N, Pillai S, Dey S, Daniels S *et al*: Multiplexed Protein Quantitation in Saccharomyces cerevisiae Using Amine-reactive Isobaric Tagging Reagents. *Molecular & Cellular Proteomics* 2004, 3(12):1154-1169.
209. Thompson A, Schäfer J, Kuhn K, Kienle S, Schwarz J, Schmidt G, Neumann T, Johnstone R, Mohammed AK, Hamon C: Tandem mass tags: a novel quantification strategy for comparative analysis of complex protein mixtures by MS/MS. *Anal Chem* 2003, 75(8):1895-1904.
210. McAlister GC, Huttlin EL, Haas W, Ting L, Jedrychowski MP, Rogers JC, Kuhn K, Pike I, Grothe RA, Blethrow JD *et al*: Increasing the Multiplexing Capacity of TMTs Using Reporter Ion Isotopologues with Isobaric Masses. *Analytical Chemistry* 2012, 84(17):7469-7478.
211. Thompson A, Wölmer N, Koncarevic S, Selzer S, Böhm G, Legner H, Schmid P, Kienle S, Penning P, Höhle C *et al*: TMTpro: Design, Synthesis, and Initial Evaluation of a Proline-Based Isobaric 16-Plex Tandem Mass Tag Reagent Set. *Analytical Chemistry* 2019, 91(24):15941-15950.
212. Karp NA, Huber W, Sadowski PG, Charles PD, Hester SV, Lilley KS: Addressing Accuracy and Precision Issues in iTRAQ Quantitation. *Molecular & Cellular Proteomics* 2010, 9(9):1885-1897.

213. Savitski MM, Mathieson T, Zinn N, Sweetman G, Doce C, Becher I, Pachl F, Kuster B, Bantscheff M: Measuring and Managing Ratio Compression for Accurate iTRAQ/TMT Quantification. *Journal of Proteome Research* 2013, 12(8):3586-3598.
214. Ting L, Rad R, Gygi SP, Haas W: MS3 eliminates ratio distortion in isobaric multiplexed quantitative proteomics. *Nat Methods* 2011, 8(11):937-940.
215. McAlister GC, Nusinow DP, Jedrychowski MP, Wühr M, Huttlin EL, Erickson BK, Rad R, Haas W, Gygi SP: MultiNotch MS3 Enables Accurate, Sensitive, and Multiplexed Detection of Differential Expression across Cancer Cell Line Proteomes. *Analytical Chemistry* 2014, 86(14):7150-7158

Abbreviations

ADCC	Antibody-dependent, cell-mediated cytotoxicity
ADCP	Antibody-dependent cellular phagocytosis
ATP	Adenosine triphosphate
bRP	Basic reversed-phase
CD	Cluster of differentiation
CDC	Complement-dependent cytotoxicity
CDR	Complementarity-determining regions
CDx	Companion diagnostics
CID	Collision-induced dissociation
CML	Chronic myeloid leukemia
CRM	Charge residue model
DDA	Data-dependent acquisition
DFG (motif)	Aspartic acid, phenylalanine and glycine (motif)
DIA	Data-independent acquisition
ESI	Electrospray ionization
ETD	Electron transfer dissociation
FDR	False discovery rate
HCD	Higher energy collision-induced dissociation
HPLC	High-performance liquid chromatography
IEM	Ion evaporation model
Ig	Immunoglobulin
IMAC	Immobilized metal ion chromatography
mAb	Monoclonal antibody
MS/MS	Tandem mass spectrometry
NK cells	Natural killer cells
NSCLC	Non-small cell lung cancer
PDAC	Pancreatic ductal adenomacarcinoma
PRM	Parallel reaction monitoring
PTM	Post-translational modification
RF	Radio frequency
RP	Reversed-phase
RTK	Receptor tyrosine kinase

SAX	Strong anionic chromatography
SILAC	Stable isotope labeling in cell culture
SPS	Synchronous precursor selection
STAGE	Stop-and-go-extraction
TOF	Time-of-flight
UVPD	Ultra violet photodissociation

List of figures

II Towards radiosensitization by targeted drugs in pancreatic cancer

Table of contents

Summary

Pancreatic ductal adenocarcinoma is one of the most aggressive cancer types and is well-known for its general low intrinsic radiosensitivity. In order to resolve mechanisms of how PDAC cells carry out radioresistance, a combination of proteomics and phosphoproteomics of two radiosensitive as well as radioresistant murine PDAC cell lines upon exposition to radiation was performed. A high depth of (phospho)proteomic identifications with > 13,000 confidently identified phosphorylation sites and > 7800 identified proteins was achieved. Measuring the response of the phosphoproteome upon radiation revealed > 700 phosphorylation sites on > 400 proteins, which were regulated in all four cell lines independently of the sensitivity status. This analysis validated already known radiomarkers, but also uncovered novel members of the radiation-dependent signaling network in PDAC cells that were shown to be exclusively based on protein phosphorylation but not protein expression level. Among those radioresponsive phosphoproteins were ten novel ATM substrates, which were validated by *in vitro* kinase assays. Comparison of radiosensitive and -resistant cells revealed a complex regulation of apoptotic processes, while changes in expression of DNA repair proteins did not seem to play a pivotal role for the mechanism of radioresistance. Especially increased expression of NQO1 was found to be a potential mechanism enabling resistance by clearing harmful reactive oxygen species from the PDAC cells. Further analysis of the radioresistance-associated-phosphoproteome, which was especially enriched in phosphoproteins with cytoskeleton organizational function, revealed increased Actin dynamics and FAK activity in radioresistant cells. Both likely lead to increased survival, migrational capacity and perturbations in chromatin condensation, which could oppose radiation. Based on these displayed adaptions in cellular protein expression and signaling in resistant PDAC cells, pharmacological inhibition of NQO1 and FAK are putative new avenues towards radiosensitization.

1 Introduction

Radiation therapy persists, along with chemotherapy, immunotherapy, hormonal therapy and surgery, to be one of the major pillars of modern cancer treatment, whose ultimate intention is the uncomplicated local tumor control without harming surrounding healthy cells. Approximately half of all cancer patients worldwide currently receive radiation therapy as a treatment modality [1]. The underlying mode of action of radiation therapy with e.g. gamma radiation by X-rays is based on the establishment of DNA lesions by mainly double-strand breaks (DSB). Irradiated cells subsequently react to this perturbation by initiating a defined molecular process known as DNA damage response (DDR), which is tightly controlled by the activity of different kinases as well as downstream signaling cascades. This process finally leads in a dose-dependent manner to survival or cell death such as apoptosis, from which the latter will be the anticipated result of a radiation therapy (as reviewed in [2]). Common to other cancer treatments as well, radiation therapy faces both intrinsic and acquired resistance. Mechanisms of how tumors evade the lethal effect of radiation are manifold and include the presence of cancer stem cells (CSC), increased DNA repair capacities, increased pro-survival pathway activation, infection by the human papillomavirus (HPV), hypoxia (as reviewed in [3]) and immune-evasion [4].

In comparison to other cancer types, pancreatic ductal adenocarcinoma (PDAC) is considered to be a rather radioresistant entity [5]. Along with an additional general resistance towards chemotherapy, low resectability and late diagnosis, the low radioresponsiveness contributes to 5-year relative survival rates of only 9 %. The low progress in diagnosis and efficient therapy options during the last decades is well depicted by similar survival rates for PDAC patients of 4 % in 1975 [6]. Even with the current treatment options in resectable PDAC, which consist of surgery, adjuvant chemotherapy and radiotherapy, local failure rates are high and range between 47–63 % [7-9]. The molecular hallmarks of PDAC include desmoplasia, which is characterized by a dense extracellular matrix and may contribute to both radiation- and chemoresistance [10, 11]. Hypoxia is another feature of PDAC [12], which can cause its general low response to radiation therapy [13]. PDAC establishment and progression are furthermore driven by a large number of genetic mutations, which activate oncogenic pathways and inhibit tumor suppressor pathways, including alterations in the KRAS, TP53, SMAD4, and CDKN2A genes [14]. Whereas the mutational landscape increases the heterogeneity in PDAC, these mutational adaptions of individual tumors may generally enable targeted therapy and radiosensitization by engaging affected pathways.

While the low resection rate and currently limited treatment efficacy generate an urgent need for radiosensitization in PDAC, targeted sensitizing treatment options towards the establishment of radio-responsiveness have not been approved for clinical use yet. So far, clinical studies (mostly in phase I and II) concentrate on the pharmacological inhibition of DDR-responsive (PARP, cell cycle checkpoints) and proliferation-inducing signaling pathways (EGFR) as well as more general immune checkpoints (as reviewed in [15]). In order to reveal cellular processes of intrinsic radioresistance on a comprehensive level and to propose novel targeted strategies to overcome radioresistance, a combined proteomic and phosphoproteomic approach to compare protein expression and cellular signaling in radiosensitive and radioresistant murine PDAC cell lines was performed.

2 Material and methods

Sample preparation for the (phospho)proteomic experiment

F5461, 53704PPT, 53578PPT and 5748PPT cells were seeded and 24 h later irradiated with either 0 Gy or 8 Gy. Each experiment was performed three times.1 h after irradiation, cells were washed twice with PBS and lysed in 40 mM Tris(hydroxymethyl)aminomethane (Tris)-HCl pH 7.6, 8 M urea, ethylenediaminetetraacetic acid (EDTA)-free protease inhibitor (Roche) and phosphatase inhibitors (Roche). Lysate was centrifuged for 1 h at 21,000 x g und the supernatant was subjected to sample preparation (all steps performed by Sophie Dobiasch, Department of Radiation Oncology, Technical University of Munich). The protein concentration in cell lysate was determined using the Coomassie Plus Bradford assay (Thermo Fisher Scientific) and all steps were performed according to the protocol of the manufacturer. Lysate of either 0 Gy (mix1) or 8 Gy (mix2) treated cells was in part pooled in a 1:1:1:1 ratio and processed along the individual lysates for each replicate.

200 µg protein of cell lysate was reduced with 10 mM dithiothreitol (DTT) for 40 min at 56 °C and alkylated with 55 mM chloroacetamide (CAA) at room temperature in the dark for 20 min. After dilution of the urea concentration from 6 M to 1.5 M with 40 mM Tris-HCl pH 7.6, the proteins were digested in a 1:50 trypsin/substrate weight ratio overnight at 37 °C and 700 rpm. In brief, desalting of the tryptic peptides was performed on Sep-Pak C18 50 mg columns (Waters) in 0.07 % trifluoroacetic acid (TFA) in 50 % acetonitrile (ACN). Afterwards labeling of the desalted peptides was performed with tandem mass tags 10 (TMT10)-plex (Thermo Fisher Scientific) at a final concentration of 6.67 mM TMT according to instructions provided by the manufacturer except for a 1:2 TMT/peptide ratio. One TMT channel was used for each cell line and treatment condition (126 = 53578PPT-0 Gy, 127N = 53578PPT-8 Gy, 127C = 53704PPT-0 Gy, 128N = 53704PPT-8 Gy, 128C = F5461-0 Gy, 129N = F5461-8 Gy, 129C = 5748PPT-0 Gy, 130N = 5748PPT-8 Gy, 130C = mix-0 Gy, 131 = mix-8 Gy). Pooled phosphopeptides were enriched from the pooled samples using Fe- immobilized metal ion affinity chromatography (IMAC) as previously described [10]. Subsequently, phosphopeptides were separated into six fractions using basic reversed-phase (bRP) chromatography in a micro-column format (five discs, Ø 1.5 mm, C18 material, 3M Empore per micro-column were used) in 25 mM NH_4COOH (pH 10). Peptides were fractionated with increasing ACN concentrations (5 %, 7.5 %, 10 %, 12.5 %, 15 %, 17.5 % and 50 % ACN). The desalted flow-through was combined with the 17.5 % fraction and the 50 % fraction with the 5 % fraction to give a total of six fractions. Non-phosphorylated peptides (flow through of the Fe-IMAC) were fractionated into 32 fractions by trimodal mixed mode chromatography, which uses reversed-

phase, weak anion exchange, and strong cation exchange, as recently published [11]. After drying in a centrifugal evaporator, the samples were stored at -20 °C until LC-MS^n analysis.

In vitro kinase assay

Peptides were designed as 15-mers (if not stated otherwise) with Serine or Alanine in the central position for wildtype or mutant, respectively. The synthesis was performed under an Fmoc-based solid-phase synthesis strategy as described previously [16] by JPT Peptide Technologies GmbH (Germany). Peptide pools were added individually to 50 mM HEPES-KOH pH 7.4, 150 mM NaCl, 6 mM $MgCl_2$, 4 mM $MnCl_2$, 1 mM DTT and 2 mM ATP to reach an end concentration of each peptide of 3 µM (pool 1) and 4.6 µM (pool 2) in the reaction mix. The reaction was started by supplementing 300 ng recombinant active ATM (Sigma-Aldrich, #14-933-M) (ATM samples) or vehicle (control samples) and was incubated at 30 °C for 1 h. Each reaction was performed in triplicate (if not stated otherwise). The reaction was quenched by adding an equal volume of 1 % FA in ACN. After drying in a centrifugal evaporator, the samples were stored at -20 °C until LC-MS/MS analysis.

LC-MS^n analysis of the (phospho)proteome

Nano-flow liquid chromatography tandem mass spectrometry (LC-MS^n) measurement of TMT-labeled non-phosphorylated and phosphorylated peptides was performed using a Dionex Ultimate3000 nano high performance liquid chromatography (HPLC) (Thermo Fisher Scientific) coupled to an Orbitrap Fusion Lumos mass spectrometer (Thermo Fisher Scientific). The fractions of phosphorylated peptides were injected twice. Peptides were desalted on a trap column (100 µm × 2 cm, packed in-house with Reprosil-Pur C18-AQ 5 µm resin; Dr. Maisch) in 0.1 % formic acid (FA) at 5 µl/min and separated on an analytical column (75 µm × 40 cm, packed in-house with Reprosil-Pur C18-AQ, 3 µm resin; Dr. Maisch) using a 50 min linear gradient from 8-34 % (full proteome) or 80 min linear gradient from 4-32 % (phosphoproteome) solvent B (0.1 % FA, 5 % dimethylsulfoxide (DMSO) in ACN) in solvent A (0. 1% FA, 5 % DMSO in water) at a flow rate of 300 nL/min. The Fusion Lumos was operated in data dependent acquisition and positive ionization mode. Full scan MS1 spectra were acquired over a range of 360-1300 m/z at a resolution of 60,000 (automatic gain control (AGC) target value $4e^5$, maximal injection time 10 ms). For LC-MS^2 analysis of the full proteome, up to 20 peptide precursors were selected for fragmentation by higher energy collision-induced dissociation (HCD; 1.2 m/z isolation window, AGC value of $2e^5$, maximum injection time of 50 ms) using 38 % normalized collision energy (NCE) and analyzed at a resolution of 30,000 in the Orbitrap. For LC-MS^3 analysis of the phosphoproteome, up to 10 peptide precursors were selected for MS2 fragmentation by collision-

induced dissociation (CID; 0.7 m/z isolation window, AGC value of $5e^4$, maximum injection time of 60 ms) using 35 % collision energy and analyzed at a resolution of 30,000 in the Orbitrap. An additional MS3 spectrum was acquired in the orbitrap over an m/z range of 100-1000 at 50,000 resolution for each peptide precursor. For this, fragment ions were selected by multi-notch isolation, allowing a maximum of 10 notches and an ion trap isolation width of 2 Da, and subsequently fragmented by HCD at 55 % NCE (AGC target value $1.2e^5$, maximal injection time 120 ms).

LC-MS/MS analysis of the kinase assay

Nano-flow LC-MS/MS measurement of peptides deriving from the *in vitro* kinase assay was performed using a Dionex Ultimate3000 nano HPLC (Thermo Fisher Scientific) coupled to an orbitrap Fusion Lumos mass spectrometer (Thermo Fisher Scientific). Peptides were desalted on a trap column (100 µm × 2 cm, packed in-house with Reprosil-Pur C18-AQ 5 µm resin; Dr. Maisch) in 0.1 % FA and separated on an analytical column (75 µm × 40 cm, packed in-house with Reprosil-Pur C18-AQ, 3 µm resin; Dr. Maisch) using a 51 min two-step gradient from 4-15-27 % B (0.1 % FA, 5 % DMSO in 100 % ACN) in solution A (0.1 % FA, 5 % DMSO in water). The Fusion Lumos was operated in data dependent acquisition and positive ionization mode. Full scan MS1 spectra were acquired over a range of 360-1300 m/z at a resolution of 60,000 (AGC target value $4x10^5$, maximal injection time 50 ms). Fragmentation was performed using HCD at 30 % NCE (AGC target value $5x10^4$, maximal injection time 120 ms) in the orbitrap at 30,000 resolution.

Peptide and protein identification and quantification of the (phospho)proteome

Protein and peptide identification and quantification were performed using MaxQuant [12] (version 1.5.6.5) by searching the tandem MS data against all mouse canonical sequences as annotated in the Swissprot reference database (16889 entries, downloaded 27.06.2017) using the embedded search engine Andromeda [13]. Carbamidomethylated cysteine was set as fixed modification and oxidation of methionine and N-terminal protein acetylation as variable modification. In addition, phosphorylation of serine, threonine and tyrosine was set as variable modification for the phosphoproteome. Trypsin/P was specified as the proteolytic enzyme and up to two missed cleavage sites were allowed. Precursor tolerance was set to 4.5 ppm and fragment ion tolerance to 20 ppm. The minimum peptide length was set to seven and all data were adjusted to 1 % peptide-spectrum match (PSM) and 1 % protein false discovery rate (FDR). A minimum score for modified peptides was set to 40. MS2- (full proteome) and MS3-based (phosphoproteome) TMT quantification was enabled, taking TMT correction factors as supplied by the manufacturer into account. Subsequent data analysis was performed on identified and

quantified protein groups (full proteome; as provided in the proteinGroups.txt) and phosphorylation sites (phosphoproteome; as provided in the Phospho (STY)Sites.txt).

Peptide and protein identification and quantification of the kinase assay

Peptide identification and quantification were performed by searching the MS data using MaxQuant [17] (version 1.6.0.1) against a database containing only sequences of the screened peptides. Phosphorylation of serine and threonine, oxidation of methionine, and N-terminal protein acetylation were set as variable modifications. Precursor and fragment ion tolerances were 4.5 ppm and 20 ppm, respectively. Subsequent data analysis was performed on identified and quantified protein groups phosphorylation sites (as provided in the Phospho (STY)Sites.txt).

Data analysis

The Perseus software suite [14] (version 1.5.5.3) was used for the (phospho)proteomic dataset to filter out contaminants, reverse hits and protein groups (in case of the full proteome dataset), which were only identified by site. Furthermore, only phosphorylation sites and protein groups that were detected in at least two out of the three replicates were considered for further analysis. Multiplicities of phosphorylation were added to the phosphorylation sites. Log2 fold changes for 8 Gy against 0 Gy control and resistance against sensitivity samples were calculated per phosphorylation site and protein group and tested for significance using a t-test (FDR = 1 % or 5 %, s0 = 0.1). Protein-protein interactions were analyzed using the String database [15] (version 11.0) (combined score > 0.4) and visualized in Cytoscape (version 3.4.0). The PANTHER Classification System was used for gene ontology (GO) enrichment analysis [16]. Identified and quantified phosphorylation sites of the synthetic peptides deriving from the *in vitro* kinase assay were only considered as ATM substrates in case of missing identification and quantification of the phosphorylated peptide in the control samples and missing identification and quantification of the respective phosphorylated mutant peptide.

Western Blotting

Protein lysates were generated by harvesting cells in 0.8 % NP40, 50 mM Tris-HCl pH 7.5, 5 % glycerol, 1.5 mM $MgCl_2$, 150 mM NaCl, 1 mM Na_3VO_4, 25 mM NaF, 1 mM DTT, protease inhibitors (SigmaFast, Sigma) and phosphatase inhibitors. Proteins were separated by sodiumdodecylsulfate polyacrylamide gel electrophoresis (SDS-PAGE) and electro-transferred onto PVDF membranes. Blots were stored in Tris-buffered saline (TBS), supplemented with 0.05 % Tween (TBS-T) and 2 % bovine serum albumin (BSA) for 1 h at room temperature and then incubated with primary antibody (diluted in TBS-T, 5 % BSA) overnight at 4 °C. The following primary antibodies were used: alpha-tubulin (1:1000, Santa Cruz

Biotechnology, #sc-5286), Phospho-FAK (Tyr576/577) (1:500, Cell Signaling Technology, #3281), FAK (1:1000, Cell Signaling Technology, #3285). Subsequently, blots were washed in TBS-T and probed with the corresponding fluorophore-conjugated secondary antibody for 30 min at room temperature. The immuno-reactive signals were detected directly by excitation of the respective fluorophore. Acquisition and quantification of the band intensities were carried out with the Odyssey (Licor) imaging system and respective software. Intensities of proteins were normalized to input housekeeping proteins and phosphorylated proteins were normalized to the intensity of the respective total protein.

3 Results and discussion

3.1 Phosphoproteomic analysis reveals common radiation-induced signaling changes

To identify the underlying mechanisms for intrinsic radioresistance in PDAC, a combined proteomic and phosphoproteomic analysis of two murine radiosensitive (53548 and 5748) and two radioresistant (F54561 and 53704) PDAC cell lines in response to radiation with X-rays (in triplicate; 8 Gy) was performed. Sensitivity of the cell lines towards radiation was previously determined within a screen on a total of 38 murine cell lines, from which the four cell lines indicated above were chosen as representatives for each sensitivity status (data not shown; experiments performed by Sophie Dobiasch, Department of Radiation Oncology, Technical University of Munich). Stable isotope labeling by TMT was used [18] to enable the comparison of both the sensitivity status as well as the response to radiation on the proteomes in parallel (Figure II-1).

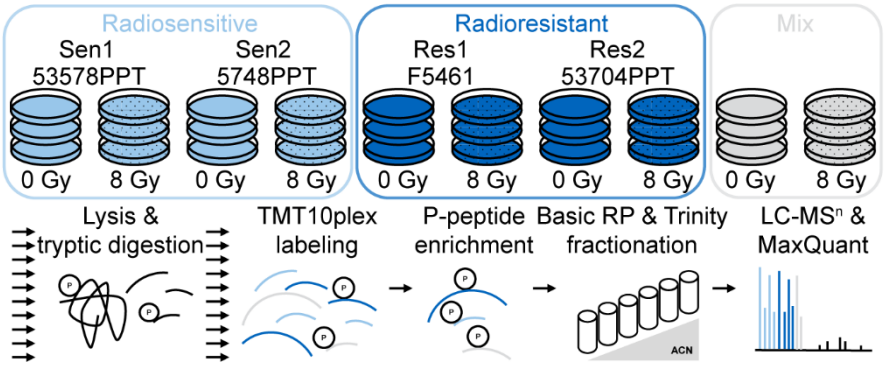

Figure II-1: (Phospho-)Proteomic workflow. Overview of the experimental design and the underlying sample processing steps of the (phospho-)proteomic workflow.

In order to be stringent, further analysis was restricted to those phosphorylation sites (p-sites) and proteins, which were identified in at least two out of three replicates. The workflow led to a deep phosphoproteome with 13,000 identified and quantified p-sites on > 3200 p-proteins, which was supplemented with > 7800 proteins in the full proteome (Figure II-2). A high correlation between replicates as exemplified by pooled control and treated samples (mix1 and mix2) (Figure II-3A) as well as general low coefficient of correlation (CV) between replicates (here for mix1) of 0.12 indicated a high data reproducibility (Figure II-3B). The even lower CV of 0.02 of the full proteome dataset might be explained by a general lower variance on protein level due to more spectral events being utilized for protein than for p-site quantification. Furthermore, quantification of the proteins on MS2-level might have been more prone to ratio compression in comparison to MS3-quantified p-sites. The

phosphoproteomic dataset drastically outperformed so far published phosphoproteomic studies between 2010 and 2017 about the effects of radiation on cellular signaling (Figure II-3C) [19-23] indicating a rich source for unwinding responses to radiation in general and resolving radioresistance mechanisms.

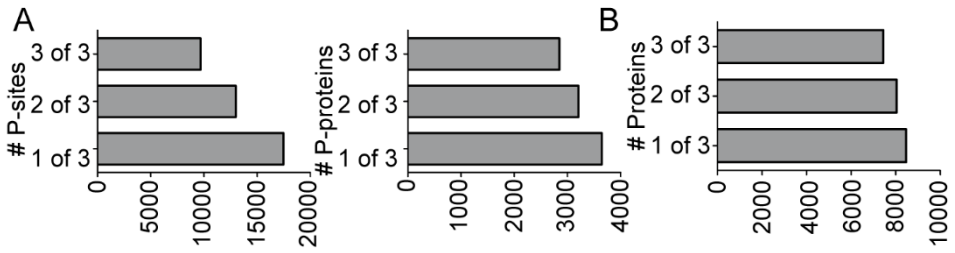

Figure II-2: Depth of the (Phospho)proteome. (A) Number of identified and quantified p-sites (left) and p-proteins (right). (B) Number of identified and quantified proteins. Data represent N = 2-3 biologically independent experiments.

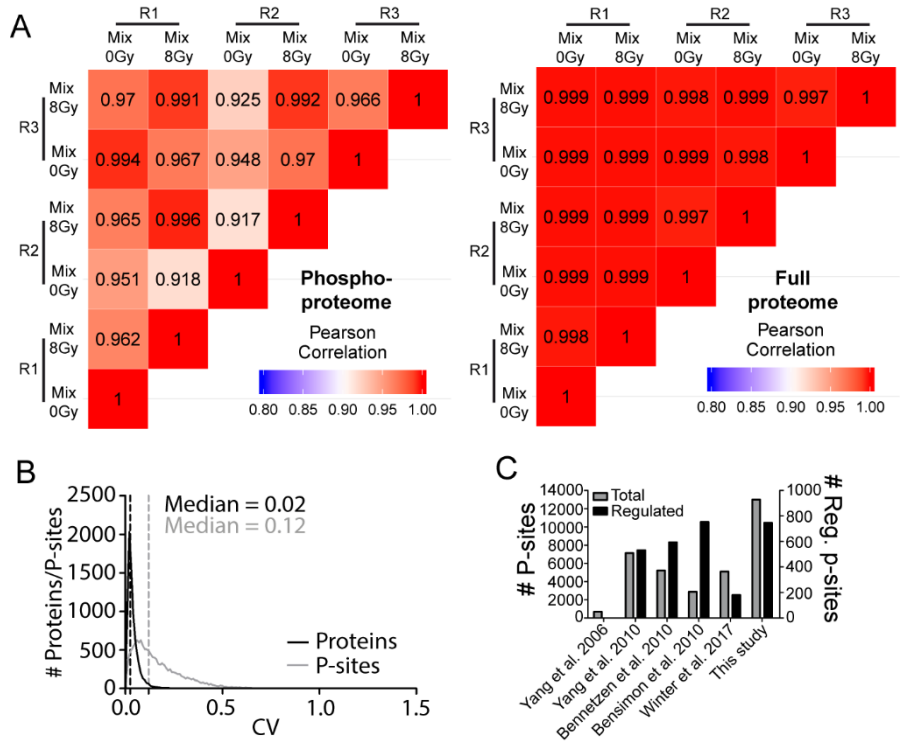

Figure II-3: Quality metrics of the datasets. (A) Matrices indicating the Pearson correlation of mix1 and mix2 samples between replicates R1-R3 for the phospho- (left) and full proteome (right). (B) Histogram of the CV of mix1 between replicates on protein (black line) and p-site (grey line) level. The median CV of both datasets is highlighted. (C) Comparison of identified and quantified as well as regulated p-sites of this dataset to recent phosphoproteomic studies about effects of radiation on cellular signaling.

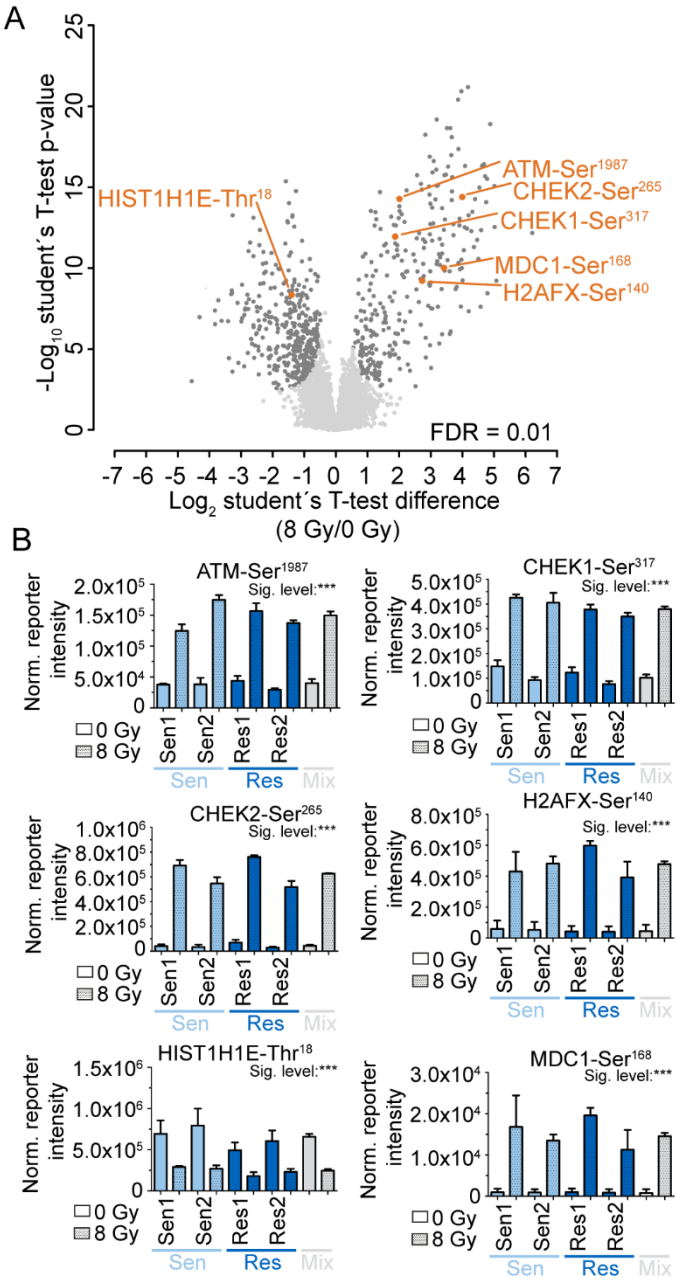

Figure II-4: The common radio-responsive phosphoproteome in both sensitivity states. (A) Volcano plot of the regulation of p-site intensities upon radiation of all four cell lines. Significantly regulated p-sites are marked in dark grey. Renowned DDR markers ATM-Ser^{1987}, CHEK1-Ser^{317}, CHEK2-Ser^{265} H2AFX-Ser^{140}, HIST1H1E-Thr^{18} and MDC1-Ser^{168} are highlighted in orange. (B) LC-MS^3 quantification of DDR marker ATM-Ser^{1987}, CHEK1-Ser^{317} (top, from left to right), CHEK2-Ser^{265}, H2AFX-Ser^{140}(middle, from left to right), Hist1h1e-Thr^{18} and MDC1-Ser^{168} (bottom, left to right) p-site intensity upon radiation in all four cell lines. Statistical analyses were performed by t-tests (FDR = 0.01, s0 = 0.1). Error bars represent SD. Significance levels (Sig. level): ns P > 0.05, * P ≤ 0.05, ** P ≤ 0.01, *** P ≤ 0.001. Data represent N = 2-3 biologically independent experiments.

In order to define the radiation-responsive phosphoproteome irrespective of the sensitivity state of the cells, significantly regulated p-sites between untreated and treated cells were determined (FDR of 1 %, Figure II-4A). This analysis led to a total of 747 p-sites, which reside on 409 proteins, including several well-known DDR markers, from which a few were exemplified in the following. Increased phosphorylation at ATM-Ser^{1987} (an autophosphorylation event, which is under debate to increase ATM activity in response to DNA DSB [24, 25]), at direct ATM substrate H2AFX-Ser^{140} [26], indirect ATM substrate CHEK-Ser^{265} and ATR substrate CHEK1-Ser^{317} [27] indicated the initiation of DDR in response to DNA DSB by radiation in all cell lines (Figure II-4B). Further recruitment and subsequent phosphorylation of H2AFX-Ser^{140}-reader MDC1 [28] was proven by increased phosphorylation at MDC1-Ser^{168}. In addition, phosphorylation at Hist1h1e-Thr^{18}, a renowned ATM-dependent histone marker [29], was significantly decreased upon radiation.

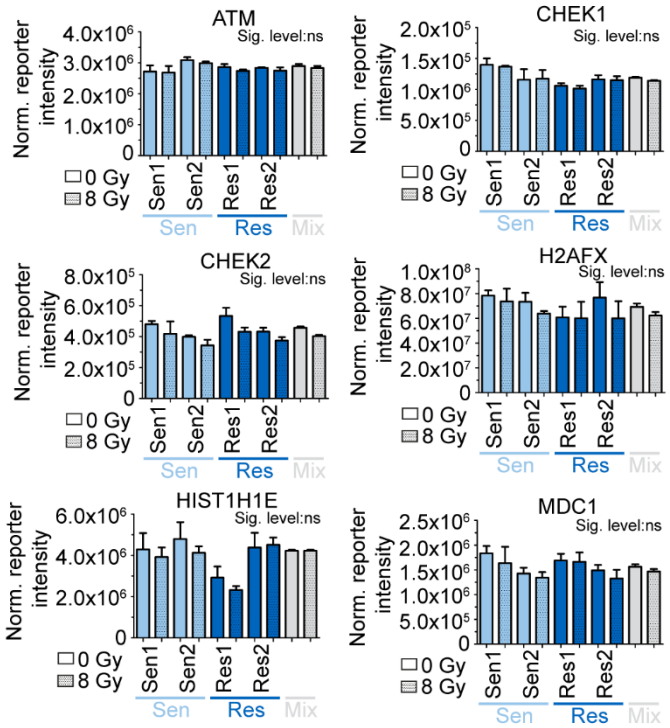

Figure II-5: Protein expression levels of DDR markers. LC-MS^2 quantification of ATM, CHEK1 (top, from left to right), CHEK2, H2AFX (middle, from left to right), HIST1H1E and MDC1 (bottom, left to right) protein intensity upon radiation in all four cell lines. Statistical analyses were performed by t-tests (FDR = 0.01, s0 = 0.1). Error bars represent SD. Significance levels (Sig. level): ns $P > 0.05$, * $P \leq 0.05$, ** $P \leq 0.01$, *** $P \leq 0.001$. Data represent N = 2-3 biologically independent experiments.

All elaborated examples as well as the remaining radiation-dependent regulations are based on altered protein phosphorylation but not protein expression (Figure II-5), which illustrates the need of phosphoproteomics for the global analysis of the immediate cellular response towards radiation. Enrichment analysis of GO terms of all regulated phosphoproteins (p-proteins) has highlighted an

accumulation of proteins which regulate DNA stability and dynamics (Figure II-6) demonstrating again the responsiveness of the p-proteome towards radiation by activating the DDR.

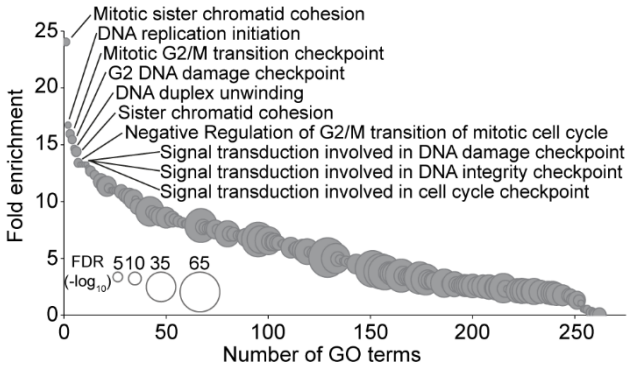

Figure II-6: Enrichment of GO terms in the radiationresponsive phosphoproteome. Fold enrichment for all significantly enriched GO terms from the radioresponsive phosphoproteome. The log10 FDR is depicted by the bubble size.

3.2 *In vitro* kinase assays validate novel ATM substrates

Initiation of DDR upon radiation in all four cell lines was additionally underscored by 136 p-sites on 105 proteins with pSer/pThr-Gln consensus sequence motif of DDR-initiating kinases ATM and ATR [30] (likewise DNA-PK [31]) in the set of the 747 significantly regulated p-sites (18 %; Figure II-7A). The well-established ATM autophosphorylation site ATM-Ser^{1987} and substrate CHEK1-Ser^{317} (Figure II-4B), for instance, were among these. The majority of the p-sites were significantly increased in phosphorylation upon radiation (Figure II-7B), which is in line with increased ATM activity that was assumed. An enrichment of the motif in the radio-responsive p-proteome was evident through the comparison with the fraction of the motif in the complete p-proteome, which was substantially decreased (3 %; not shown). Protein-protein interaction analysis revealed both various proteins of a high interconnectivity and proteins without any known protein-protein interaction to the rest of the network of the ATM-motif p-sites (Figure II-7B). The latter might indicate potential novel substrates that have not been linked to ATM signaling or DDR in general so far.

In order to validate novel substrates biochemically, *in vitro* ATM assays were executed for all 136 ATM motif-containing p-sites using synthetic peptides, recombinant ATM and LC-MS/MS for identification and quantification. Motif-specificity was assessed by analyzing the ability of ATM to phosphorylate Ser/Thr to Ala-mutants of the respective peptides and was the prerequisite to define a substrate. The five reported targets BID-Ser^{78} [32], Mcm3-Ser^{732} [33], RSF1-Ser^{364} [34], SF3B2-Ser^{272} [35] and SMC3-Ser^{1065} [36] were determined to be specifically phosphorylated by ATM, demonstrating the general feasibility of identifying candidate peptides as direct substrates of ATM by this assay (Figure II-7C). Among the

ten novel ATM substrates was, for example, FAM175a-Ser^{48} (or ABRAXAS1-Ser^{48}), which complements the reported phosphorylation on Ser$^{404/406}$ by ATM on yet another position and strengthens the protein's role in DNA damage resistance, DNA repair, and cell cycle checkpoint control [37]. ATF7IP (MCAF1), on the other hand, has not been attributed to the function of ATM and its phosphorylation on Ser^{509} might shed light on how its action as both transcription activator and repressor can be modulated [38]. Phosphorylation on NOL4L-Ser^{295} by ATM could generally functionalize the protein, whose function is so far not known, by putting it into the context of radiation-responsive DNA damage response. SCAF11-Ser^{704}, SLTM-Ser^{139}, SRRM2-Ser^{1209}, TATDN2-Ser^{310}, UBXN7-Ser^{288}, WBSCR22-Ser^{49} and ZC3H11A-Ser^{108} were moreover identified as novel ATM substrates, which is expanding the ever-growing number of ATM substrates. Beyond the *in vitro* identification of the substrates, a similar magnitude of phosphorylation by ATM could be deduced by fold changes upon radiation, which were in the same ranges for both known and novel ATM substrates in the phosphoproteomic experiment in cells (Figure II-7C, blue circles).

While the validation of the known and novel ATM substrates was performed by using recombinant kinase and synthetic peptides ex cellulo, further experiments would be necessary to finally proof prove direct kinase-substrate relationships on substrate protein-level as well as in a cellular environment. Still, the linearity of the ATM substrate motif underscores the chance of using peptidic substrates in such an assay.

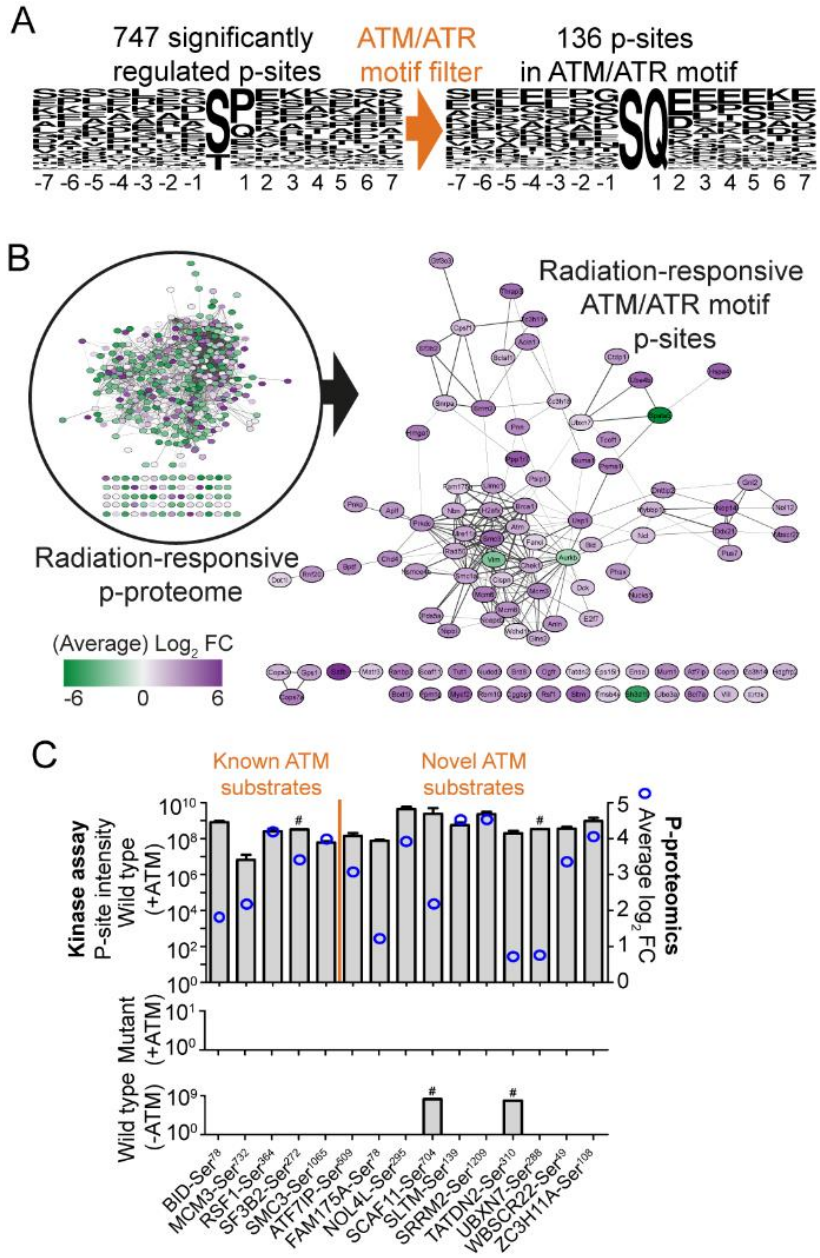

Figure II-7: Enrichment of the ATM/ATR motif in the radio-responsive phosphoproteome. (A) Frequency sequence logos showing amino acid distribution around the 747 radio-responsive p-sites in the (left) and 136 p-sites bearing the ATM/ATR motif (right) ± seven residues. (B) Protein-protein interaction-based networks (available from www.string-db.org) of p-proteins, which were significantly regulated upon radiation (small network in circle, left), and of p-proteins, whose regulated p-sites harbored the ATM/ATR motif (right). Edges are confidence-weighted. The log_2 FC in p-site intensity was averaged on each p-protein and over all five inhibitors. Increased phosphorylation intensity is visualized via a violet and decreased phosphorylation intensity by a green node. The thickness of the node lines demonstrates the standard deviation of averaged log_2 FC per p-protein, with broader lines indicating a higher standard deviation. (C) P-site intensity of identified known and novel substrates in the *in vitro* ATM assay (top). The average log2 FC for each p-site upon radiation is additionally highlighted via blue circles. P-site intensities of respective mutant peptides (middle) and wild type peptides without ATM (control; bottom) are shown as well. Error bars represent SD. Data represent N = 2-3 biologically independent experiments.

3.3 Increased NQO1 expression is associated with radioresistance in PDAC

Responses to radiation have demonstrated that DDR, at least in its initial stages, is realized through the same cellular signaling changes in both radiosensitivity states. However, other so far unknown signaling events need to fine tune the balance between cell survival and apoptosis upon radiation, leading to a divergence into radiosensitivity and radioresistance. In the interest of revealing radioresistance-associated proteomic adaptations, proteins with significantly different intensity between radiosensitive and radioresistant cell lines were detected by t-testing (FDR = 0.05, s0 = 0.1). Their association with major molecular events following the initiated DDR according to GO terms – non-homologous end joining (NHEJ) (GO:0006303), homologous recombination (HR) (GO:0000724) and apoptosis (GO:0006915) - were furthermore determined (Figure II-8). While no association with NHEJ was found among the proteins, three proteins responsible or associated with DSB repair by HR were detected. Interestingly, XRCC3, which is a major component of HR, is less expressed in radioresistant than in radiosensitive cells. This observation stands in strong contrast to reports suggesting elevated XRCC3 expression to be associated with radioresistance leading to increased DNA repair and less cell death [39]. Decreased XRCC3 expression observed in this dataset therefore might not be a potential resistance mechanism. This leads to the general assumption that dys-regulated DNA repair mechanisms may not cause radioresistance in the cell lines analyzed.

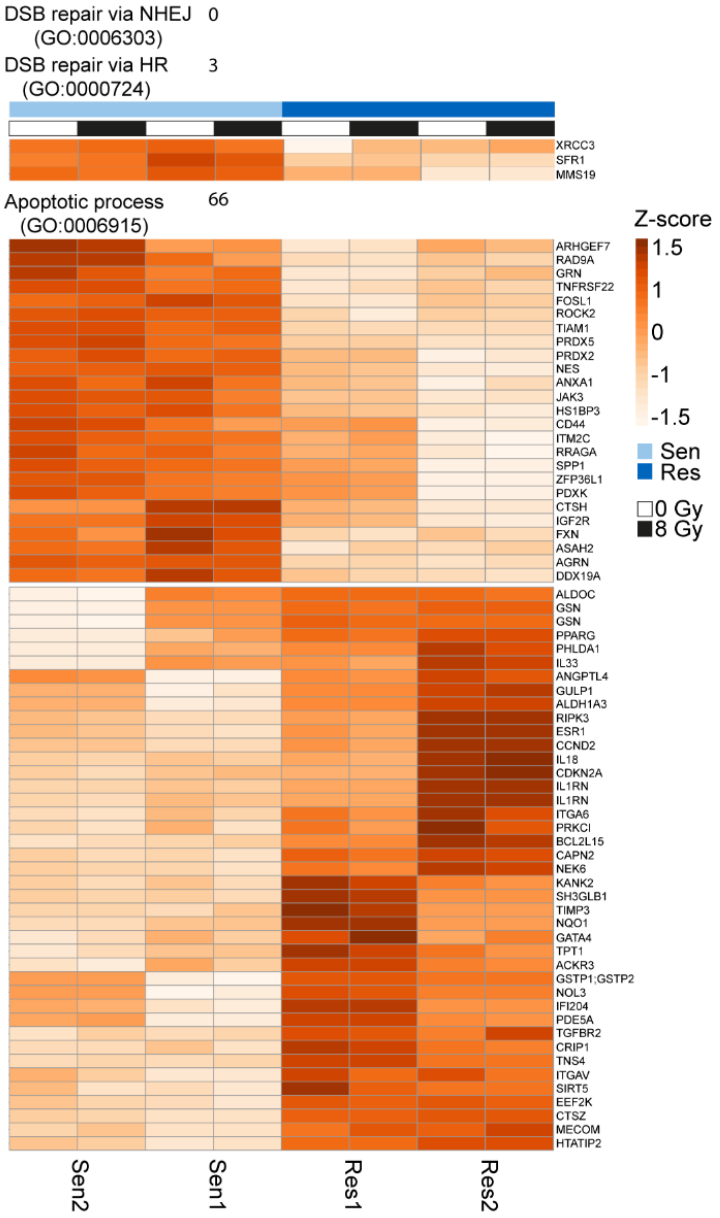

Figure II-8: Radioresistance-associated proteins. Heatmap of Z-scored intensities of significantly regulated proteins between radiosensitive and radioresistant cell lines that were categorized by the following GO terms (if applicable): DSB repair via NHEJ (GO:0006303), DSB repair via HR (GO:0000724) and apoptotic process (GO:0006915) (left). Statistical analyses were performed by t-tests (FDR = 0.05, s0 = 0.1). Data represent N = 2-3 biologically independent experiments.

Besides, 66 proteins were associated with the process of apoptosis, which implies a potential regulation of the strength of this type of cell death in the radioresistant cells. Among these proteins, NAD(P)H quinone oxidoreductase 1 (NQO1) harbored increased expression in the radioresistant cells and will be discussed in greater detail (Figure II-9A). Downstream of NRF2, NQO1 both stabilizes proteins from 20S proteasomal degradation in a non-catalytic mechanism and clears reactive oxygen species (ROS) from cells, particularly upon stress stimuli [40]. The latter is especially of interest since it has been

reported that increased ROS scavenger activity results in low ROS levels and subsequently to radioresistance [41]. Furthermore, decreased NRF2 expression has been shown to increase ROS levels and decrease NQO1 expression in irradiated cells.[42]. Taken together, increased NQO1 expression in the analyzed PDAC cell lines may contribute to their ability to overcome the radiation burden by eliminating high ROS levels. A recent report has analyzed the correlation between gene expression profiles and radioresistance of 533 tumor cell lines representing 26 cancer types, including PDAC and confirmed NQO1 expression as a putative driver of resistance [5]. Despite transcriptome and proteome levels of proteins are often difficult to compare, this highlighted the role for oxidative stress response in radiation resistance, even as a general mechanism in many different cancer types. Analysis of the correlation values found by Yard et al. for all the significantly expressed proteins of the proteomic dataset moreover uncovered additional proteins with both positive (or negative) correlation and positive (or negative) log2 FC, such as apoptosis-related proteins GSN, NOL3, CTSZ and FXN (Figure II-9B). This lends support for the hypothesis that also several other significantly expressed proteins indeed could contribute to the resistance mechanism. The finding that a high expression of NQO1 seems to be associated with PDAC progression and could serve as a prognostic biomarker in PDAC [43] further stresses the point of NQO1 being relevant in patients. Several small molecule inhibitors of NQO1, such as dicoumarol, were already reported [44] and have proven growth inhibitory effects in human pancreatic cell lines [45]. Interestingly, dicoumarol has been used as an anticoagulant drug for decades but has not been under review in clinical studies for cancer treatment so far. However, pharmacological NQO1 inhibition could be tested in future experiments to sensitize resistant cancer cells towards radiation.

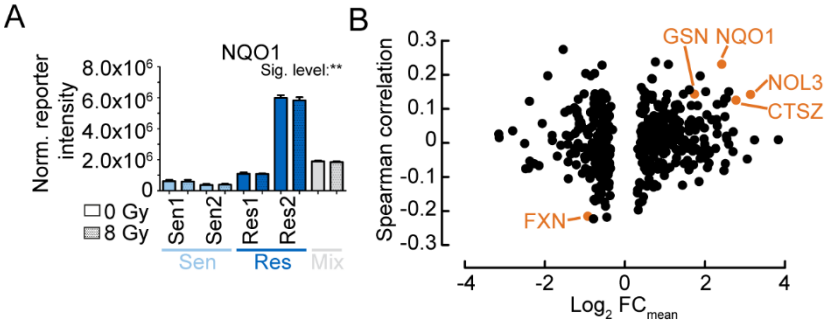

Figure II-9: NQO1 as radioresistance-associated protein in PDAC. (A) LC-MS² quantification of NQO1 in all four cell lines. (B) Spearman correlation of radioresistance-associated proteins of this dataset according to Yard et al. [5] and their Log_2 FC_{mean} within this dataset. NQO1 and additional apoptosis-related proteins are highlighted in orange. Statistical analyses were performed by t-tests (FDR = 0.05, s0 = 0.1). Error bars represent SD. Significance levels (Sig. level): ns $P > 0.05$, * $P \leq 0.05$, ** $P \leq 0.01$, *** $P \leq 0.001$. Data represent N = 2-3 biologically independent experiments.

3.4 Radioresistant cells feature increased actin dynamics and FAK activity

To analyze potential resistance mechanisms on an additional subproteomic level, significantly increased and decreased p-site intensities between both sensitivity states were determined, which resulted in a total of 361 p-sites on 192 proteins (FDR = 5 %, s0 = 0.1; Figure II-10). More significantly regulated p-sites upon radiation compared to the basal state of the cell lines were detected highlighting potential radiation-dependent resistance mechanisms in addition to radiation-independent processes. Further GO term analysis on significantly regulated p-proteins revealed the enrichment of proteins with cytoskeleton organizational functions especially in actin dynamics (Figure II-11A). As an example, significant changes of phosphorylation intensity on proteins responsible for actin dynamics such as actin filament bundler LIMA1 [46] on Ser^{360} and actin nucleation factor SPIRE1 [47] on Ser^{159}, which was in both cases in line with increased protein expression, were detected (Figure II-11B).

Significantly increased phosphorylation of focal adhesion kinase (FAK) furthermore highlighted the engagement of the cytoskeleton in radioresistant cells. FAK is a non-receptor tyrosine kinase that controls various cellular signaling pathways such as cell invasion [48], epithelial-mesenchymal transition [49] and cell survival [50, 51] by kinase-dependent and kinase-independent mechanisms. Elevated phosphorylation on domain activation loop Tyr^{576}, which indicates the formation of an activated FAK–SRC complex [52], on another activating FAK-p-site Tyr^{861} [53] (Figure II-12A), as well as on FAK substrate paxilin (PXN)-Tyr^{118} (Figure II-12B) in the resistant cell lines illustrated increased FAK activity. Elevated levels of phosphorylated FAK in the radioresistant cell lines were also demonstrated by Western Blotting (Figure II-13A) resulting in a considerable correlation to the phosphoproteomic experiment (Figure II-13B). The observed increased FAK activity can be speculated to increase cell survival in radioresistant cells, shifting the outcome of activated DDR upon radiation away from apoptosis to cell survival. Elevated expression of FAK has been already proposed to act as a driver of radioresistance in head and neck cancer [54]. This observation can be extended to elevated FAK activity presented by FAK phosphorylation as a radioresistance marker in PDAC, which does not have to be based on an increased expression. The latter point is also stressed by the fact that in the aforementioned study by Yard et al. [5] FAK expression has not shown any notable correlation with radioresistance.

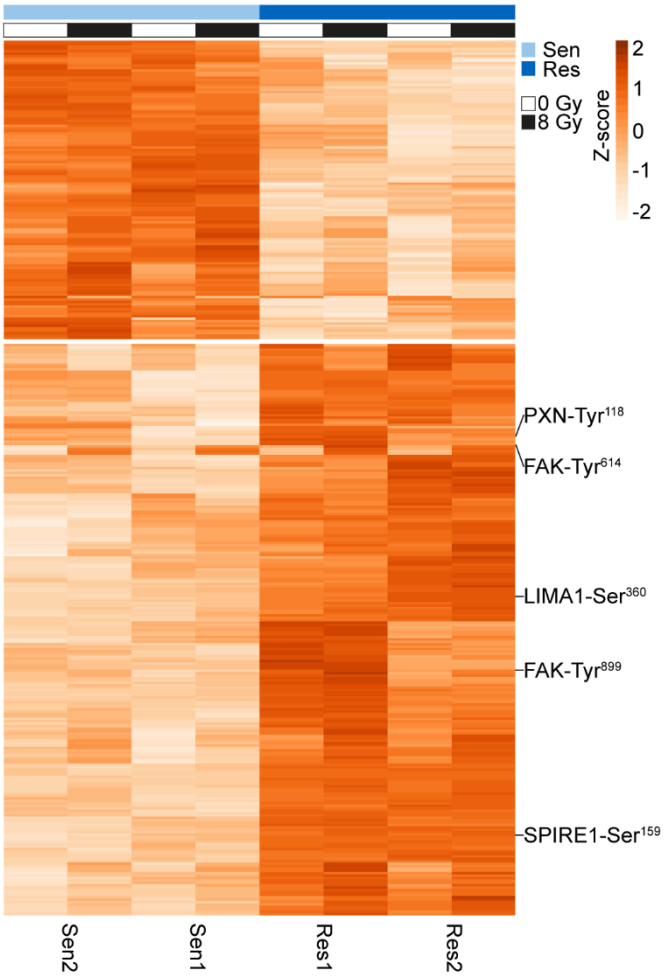

Figure II-10: Radioresistance-associated phosphoproteome. Heatmap of Z-scored intensities of significantly regulated p-sites between radiosensitive and radioresistant cell lines. Exemplary up-regulated p-sites are highlighted. Data represent N = 2-3 biologically independent experiments.

Actin dynamics plays a pivotal role in cell movement and cell protrusion and is linked to FAK-associated proteins, which directly bind to actin upon FAK activation by integrins [48, 55, 56]. Furthermore, a plethora of research has provided evidence for FAK signaling to impact the distribution of the nuclear scaffold protein lamin A/C, which further influences the chromatin organization and condensation as well as the ratio of hetero- to euchromatin. Especially the latter has been reported to enable cancer cells to establish radioresistance [57]. These observations suggest an additive or even synergistic effect on cytoskeleton organization in the radioresistant cells by both increased FAK activity as well as increased actin dynamics by a higher expression and activity of Actin-associated proteins.

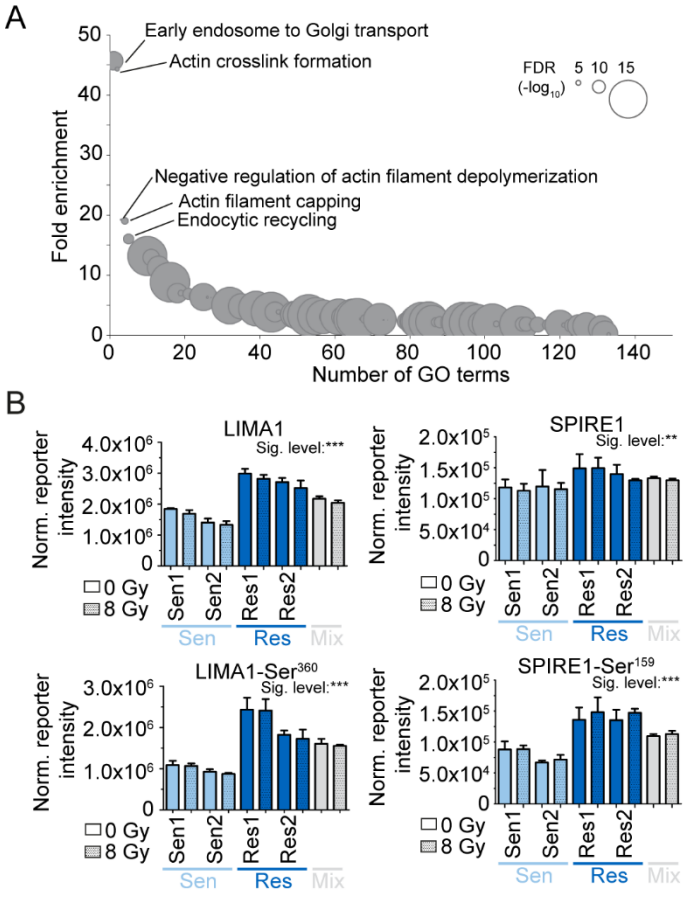

Figure II-11: Enrichment of cytoskeleton-associated proteins. (A) Fold enrichment for all significantly enriched GO terms from the radioresistance-associated phosphoproteome. (B) LC-MS^n quantification of total LIMA1 (left) and SPIRE1 (right) with each having a significantly regulated p-site in all four cell lines. Statistical analyses were performed by t-tests (FDR = 0.01, s0 = 0.1). Error bars represent SD. Significance levels (Sig. level): ns $P > 0.05$, * $P \leq 0.05$, ** $P \leq 0.01$, *** $P \leq 0.001$. Data represent N = 2-3 biologically independent experiments.

Pharmacological inhibition of FAK by defactinib has sensitized the two resistant cell lines towards radiation in subsequent experiments (data not shown; experiments performed by Sophie Dobiasch, Department of Radiation Oncology, Technical University of Munich). This stands in line with previous reports showing siRNA silenced FAK activity to radiosensitize human PDAC cell lines [58]. The high selectivity of defactinib for FAK, as previously determined by Kinobead screening [59], excludes the influence of off-target engagement and underlines the dependence of FAK activity for the radioresistance. Current studies of defactinib in clinical trials of up to phase II, for example in PDAC patients in combination with immune checkpoint inhibition, (as reviewed in [60]), furthermore indicate the safe usage in humans and may pave the way to initiate the analysis of FAK inhibition as a radiosensitizer in PDAC patients.

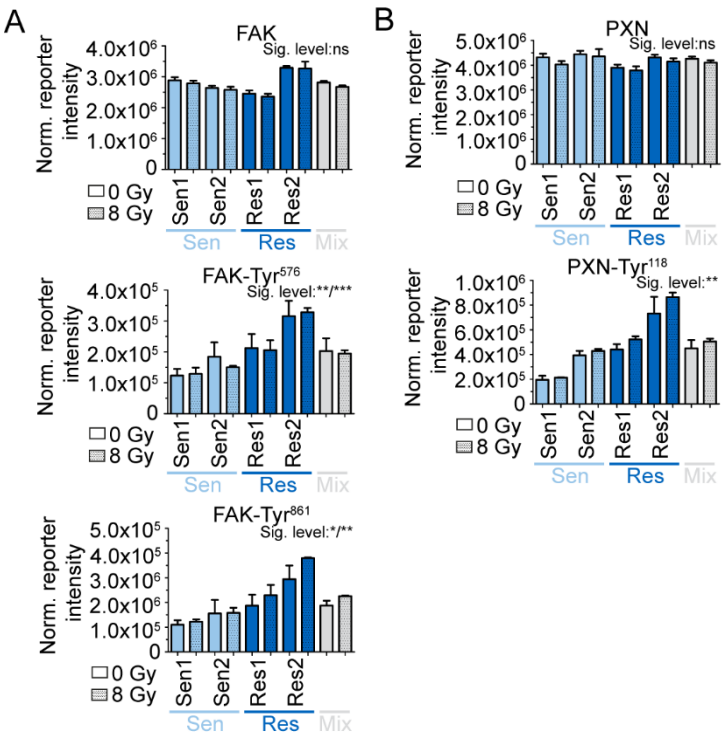

Figure II-12: Increased level of activated FAK in radioresistant cell lines. LC-MS^n quantification of total FAK (top), FAK-Tyr^{576} (middle) and FAK-Tyr^{861} (bottom) in all four cell lines. (B) LC-MS^n quantification of total PXN (top) and PXN-Tyr^{118} (bottom) in all four cell lines. Statistical analyses were performed by t-tests (FDR = 0.01, s0 = 0.1). Error bars represent SD. Significance levels (Sig. level): ns $P > 0.05$, * $P \leq 0.05$, ** $P \leq 0.01$, *** $P \leq 0.001$. If Sig. levels differ between radiation status 0Gy/8Gy, both levels will be indicated. Data represent N = 2-3 biologically independent experiments.

In summary, this study illustrates the high potential of not only proteomics but especially phosphoproteomics to uncover putative radioresistance markers on a global level. In combination with the knowledge about the mode of action of targeted drugs, novel specific radiosensitizers might be revealed leading to clinical evaluation. In light of this, the discussed examples of radioresistance-associated protein expression and phosphorylation levels do not claim completeness. The underlying data can rather be regarded to serve as a resource for further exploitation.

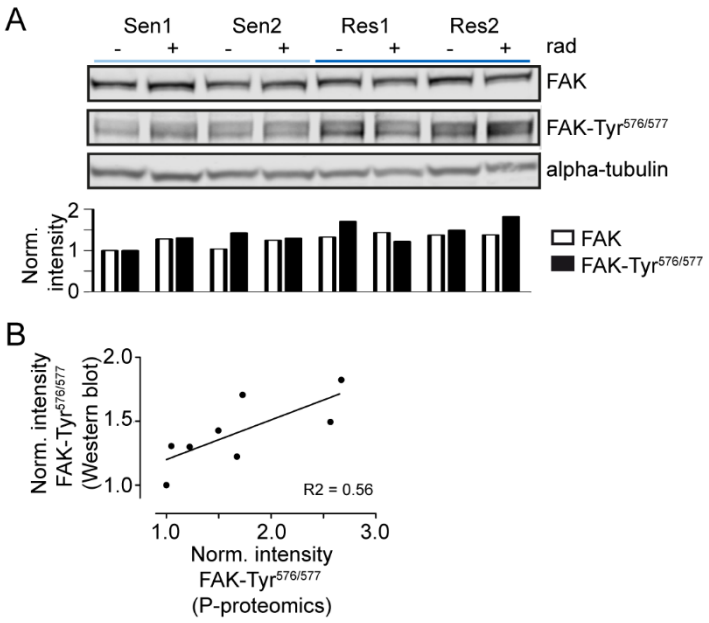

Figure II-13: Validation of increased FAK phosphorylation levels via Western blot. A) Western blot of FAK, FAK-Tyr$^{576/577}$ and alpha-tubulin in all four cell lines. Quantified band intensities are displayed below. (B) Correlation of FAK-Tyr$^{576/577}$ intensities derived from the phosphoproteomic experiment and the Western blot.

Acknowledgements

I would like to thank Dr. Sophie Dobiasch and Prof. Dr. Stephanie Combs (Department of Radiation Oncology, Technical University of Munich) as well as PD Dr. Günter Schneider (Klinikum rechts der Isar, Klinik und Poliklinik für Innere Medizin II: Gastroenterologie, Technical University of Munich) for fruitful collaborative work including the resistance screen, lysate preparation for the proteomic experiment and sensitization assays. Furthermore I highly appreciate the support in proteomic sample preparation and Western Blotting by Andrea Hubauer and Nicolas Goldbach.

References

1. Atun R, Jaffray DA, Barton MB, Bray F, Baumann M, Vikram B, Hanna TP, Knaul FM, Lievens Y, Lui TYM *et al*: Expanding global access to radiotherapy. *The Lancet Oncology* 2015, 16(10):1153-1186.
2. Roos WP, Thomas AD, Kaina B: DNA damage and the balance between survival and death in cancer biology. *Nat Rev Cancer* 2016, 16(1):20-33.
3. Baumann M, Krause M, Overgaard J, Debus J, Bentzen SM, Daartz J, Richter C, Zips D, Bortfeld T: Radiation oncology in the era of precision medicine. *Nature reviews Cancer* 2016, 16(4):234-249.
4. Yamamoto K, Venida A, Yano J, Biancur DE, Kakiuchi M, Gupta S, Sohn ASW, Mukhopadhyay S, Lin EY, Parker SJ *et al*: Autophagy promotes immune evasion of pancreatic cancer by degrading MHC-I. *Nature* 2020.
5. Yard BD, Adams DJ, Chie EK, Tamayo P, Battaglia JS, Gopal P, Rogacki K, Pearson BE, Phillips J, Raymond DP *et al*: A genetic basis for the variation in the vulnerability of cancer to DNA damage. *Nat Commun* 2016, 7:11428.
6. Siegel RL, Miller KD, Jemal A: Cancer statistics, 2019. *CA Cancer J Clin* 2019, 69(1):7-34.
7. Neoptolemos JP, Dunn JA, Stocken DD, Almond J, Link K, Beger H, Bassi C, Falconi M, Pederzoli P, Dervenis C *et al*: Adjuvant chemoradiotherapy and chemotherapy in resectable pancreatic cancer: a randomised controlled trial. *Lancet* 2001, 358(9293):1576-1585.
8. Further evidence of effective adjuvant combined radiation and chemotherapy following curative resection of pancreatic cancer. Gastrointestinal Tumor Study Group. *Cancer* 1987, 59(12):2006-2010.
9. Neoptolemos JP, Stocken DD, Friess H, Bassi C, Dunn JA, Hickey H, Beger H, Fernandez-Cruz L, Dervenis C, Lacaine F *et al*: A randomized trial of chemoradiotherapy and chemotherapy after resection of pancreatic cancer. *The New England journal of medicine* 2004, 350(12):1200-1210.
10. Whatcott CJ, Han H, Posner RG, Hostetter G, Von Hoff DD: Targeting the tumor microenvironment in cancer: why hyaluronidase deserves a second look. *Cancer Discov* 2011, 1(4):291-296.
11. Armstrong T, Packham G, Murphy LB, Bateman AC, Conti JA, Fine DR, Johnson CD, Benyon RC, Iredale JP: Type I collagen promotes the malignant phenotype of pancreatic ductal adenocarcinoma. *Clinical cancer research : an official journal of the American Association for Cancer Research* 2004, 10(21):7427-7437.
12. Koong AC, Mehta VK, Le QT, Fisher GA, Terris DJ, Brown JM, Bastidas AJ, Vierra M: Pancreatic tumors show high levels of hypoxia. *Int J Radiat Oncol Biol Phys* 2000, 48(4):919-922.
13. Rockwell S, Dobrucki IT, Kim EY, Marrison ST, Vu VT: Hypoxia and radiation therapy: past history, ongoing research, and future promise. *Curr Mol Med* 2009, 9(4):442-458.
14. Waddell N, Pajic M, Patch A-M, Chang DK, Kassahn KS, Bailey P, Johns AL, Miller D, Nones K, Quek K *et al*: Whole genomes redefine the mutational landscape of pancreatic cancer. *Nature* 2015, 518(7540):495-501.
15. Wolfe AR, Williams TM: Altering the response to radiation: radiosensitizers and targeted therapies in pancreatic ductal adenocarcinoma: preclinical and emerging clinical evidence. *Annals of Pancreatic Cancer* 2018, 1(8).
16. Zolg DP, Wilhelm M, Schnatbaum K, Zerweck J, Knaute T, Delanghe B, Bailey DJ, Gessulat S, Ehrlich H-C, Weininger M *et al*: Building ProteomeTools based on a complete synthetic human proteome. *Nature Methods* 2017, 14(3):259-262.

17. Cox J, Mann M: MaxQuant enables high peptide identification rates, individualized p.p.b.-range mass accuracies and proteome-wide protein quantification. *Nature biotechnology* 2008, 26:1367.
18. Thompson A, Schäfer J, Kuhn K, Kienle S, Schwarz J, Schmidt G, Neumann T, Hamon C: Tandem Mass Tags: A Novel Quantification Strategy for Comparative Analysis of Complex Protein Mixtures by MS/MS. *Analytical Chemistry* 2003, 75(8):1895-1904.
19. Yang F, Stenoien DL, Strittmatter EF, Wang J, Ding L, Lipton MS, Monroe ME, Nicora CD, Gristenko MA, Tang K *et al*: Phosphoproteome profiling of human skin fibroblast cells in response to low- and high-dose irradiation. *J Proteome Res* 2006, 5(5):1252-1260.
20. Yang F, Waters KM, Miller JH, Gritsenko MA, Zhao R, Du X, Livesay EA, Purvine SO, Monroe ME, Wang Y *et al*: Phosphoproteomics profiling of human skin fibroblast cells reveals pathways and proteins affected by low doses of ionizing radiation. *PLoS One* 2010, 5(11):e14152.
21. Bennetzen MV, Larsen DH, Bunkenborg J, Bartek J, Lukas J, Andersen JS: Site-specific Phosphorylation Dynamics of the Nuclear Proteome during the DNA Damage Response. *Molecular & Cellular Proteomics* 2010, 9(6):1314-1323.
22. Bensimon A, Schmidt A, Ziv Y, Elkon R, Wang SY, Chen DJ, Aebersold R, Shiloh Y: ATM-dependent and -independent dynamics of the nuclear phosphoproteome after DNA damage. *Sci Signal* 2010, 3(151):rs3.
23. Winter M, Dokic I, Schlegel J, Warnken U, Debus J, Abdollahi A, Schnölzer M: Deciphering the acute cellular phosphoproteome response to irradiation with X-rays, protons and carbon ions. *Molecular & Cellular Proteomics* 2017.
24. Bakkenist CJ, Kastan MB: DNA damage activates ATM through intermolecular autophosphorylation and dimer dissociation. *Nature* 2003, 421(6922):499-506.
25. Dupré A, Boyer-Chatenet L, Gautier J: Two-step activation of ATM by DNA and the Mre11–Rad50–Nbs1 complex. *Nature Structural & Molecular Biology* 2006, 13(5):451-457.
26. Redon CE, Dickey JS, Bonner WM, Sedelnikova OA: gamma-H2AX as a biomarker of DNA damage induced by ionizing radiation in human peripheral blood lymphocytes and artificial skin. *Advances in space research : the official journal of the Committee on Space Research (COSPAR)* 2009, 43(8):1171-1178.
27. Zhao H, Piwnica-Worms H: ATR-mediated checkpoint pathways regulate phosphorylation and activation of human Chk1. *Mol Cell Biol* 2001, 21(13):4129-4139.
28. Stucki M, Clapperton JA, Mohammad D, Yaffe MB, Smerdon SJ, Jackson SP: MDC1 Directly Binds Phosphorylated Histone H2AX to Regulate Cellular Responses to DNA Double-Strand Breaks. *Cell* 2005, 123(7):1213-1226.
29. Guo CY, Wang Y, Brautigan DL, Larner JM: Histone H1 dephosphorylation is mediated through a radiation-induced signal transduction pathway dependent on ATM. *J Biol Chem* 1999, 274(26):18715-18720.
30. Kim ST, Lim DS, Canman CE, Kastan MB: Substrate specificities and identification of putative substrates of ATM kinase family members. *J Biol Chem* 1999, 274(53):37538-37543.
31. Bannister AJ, Gottlieb TM, Kouzarides T, Jackson SP: c-Jun is phosphorylated by the DNA-dependent protein kinase in vitro; definition of the minimal kinase recognition motif. *Nucleic Acids Research* 1993, 21(5):1289-1295.
32. Kamer I, Sarig R, Zaltsman Y, Niv H, Oberkovitz G, Regev L, Haimovich G, Lerenthal Y, Marcellus RC, Gross A: Proapoptotic BID Is an ATM Effector in the DNA-Damage Response. *Cell* 2005, 122(4):593-603.
33. Shi Y, Dodson GE, Mukhopadhyay PS, Shanware NP, Trinh AT, Tibbetts RS: Identification of Carboxyl-terminal MCM3 Phosphorylation Sites Using Polyreactive Phosphospecific Antibodies. *Journal of Biological Chemistry* 2007, 282(12):9236-9243.

34. Min S, Choi YW, Yun H, Jo S, Ji J-H, Cho H: Post-Translational Regulation of the RSF1 Chromatin Remodeler under DNA Damage. *Mol Cells* 2018, 41(2):127-133.
35. Prados-Carvajal R, López-Saavedra A, Cepeda-García C, Jimeno S, Huertas P: Multiple roles of the splicing complex SF3B in DNA end resection and homologous recombination. *DNA Repair* 2018, 66-67:11-23.
36. Matsuoka S, Ballif BA, Smogorzewska A, McDonald ER, Hurov KE, Luo J, Bakalarski CE, Zhao Z, Solimini N, Lerenthal Y *et al*: ATM and ATR Substrate Analysis Reveals Extensive Protein Networks Responsive to DNA Damage. *Science* 2007, 316(5828):1160-1166.
37. Wu Q, Paul A, Su D, Mehmood S, Foo TK, Ochi T, Bunting EL, Xia B, Robinson CV, Wang B *et al*: Structure of BRCA1-BRCT/Abraxas Complex Reveals Phosphorylation-Dependent BRCT Dimerization at DNA Damage Sites. *Mol Cell* 2016, 61(3):434-448.
38. Liu L, Ishihara K, Ichimura T, Fujita N, Hino S, Tomita S, Watanabe S, Saitoh N, Ito T, Nakao M: MCAF1/AM is involved in Sp1-mediated maintenance of cancer-associated telomerase activity. *The Journal of biological chemistry* 2009, 284(8):5165-5174.
39. Yanagisawa T, Urade M, Yamamoto Y, Furuyama J: Increased expression of human DNA repair genes, XRCC1, XRCC3 and RAD51, in radioresistant human KB carcinoma cell line N10. *Oral Oncol* 1998, 34(6):524-528.
40. Dinkova-Kostova AT, Talalay P: NAD(P)H:quinone acceptor oxidoreductase 1 (NQO1), a multifunctional antioxidant enzyme and exceptionally versatile cytoprotector. *Archives of biochemistry and biophysics* 2010, 501(1):116-123.
41. Diehn M, Cho RW, Lobo NA, Kalisky T, Dorie MJ, Kulp AN, Qian D, Lam JS, Ailles LE, Wong M *et al*: Association of reactive oxygen species levels and radioresistance in cancer stem cells. *Nature* 2009, 458(7239):780-783.
42. Zhao Q, Mao A, Yan J, Sun C, Di C, Zhou X, Li H, Guo R, Zhang H: Downregulation of Nrf2 promotes radiation-induced apoptosis through Nrf2 mediated Notch signaling in non-small cell lung cancer cells. *International journal of oncology* 2016, 48(2):765-773.
43. Ji M, Jin A, Sun J, Cui X, Yang Y, Chen L, Lin Z: Clinicopathological implications of NQO1 overexpression in the prognosis of pancreatic adenocarcinoma. *Oncology letters* 2017, 13(5):2996-3002.
44. Scott KA, Barnes J, Whitehead RC, Stratford IJ, Nolan KA: Inhibitors of NQO1: identification of compounds more potent than dicoumarol without associated off-target effects. *Biochem Pharmacol* 2011, 81(3):355-363.
45. Cullen JJ, Hinkhouse MM, Grady M, Gaut AW, Liu J, Zhang YP, Darby Weydert CJ, Domann FE, Oberley LW: Dicumarol Inhibition of NADPH:Quinone Oxidoreductase Induces Growth Inhibition of Pancreatic Cancer via a Superoxide-mediated Mechanism. *Cancer Research* 2003, 63(17):5513.
46. Song Y, Maul RS, Gerbin CS, Chang DD: Inhibition of anchorage-independent growth of transformed NIH3T3 cells by epithelial protein lost in neoplasm (EPLIN) requires localization of EPLIN to actin cytoskeleton. *Mol Biol Cell* 2002, 13(4):1408-1416.
47. Bosch M, Le KH, Bugyi B, Correia JJ, Renault L, Carlier MF: Analysis of the function of Spire in actin assembly and its synergy with formin and profilin. *Mol Cell* 2007, 28(4):555-568.
48. Hauck CR, Hsia DA, Ilic D, Schlaepfer DD: v-Src SH3-enhanced interaction with focal adhesion kinase at beta 1 integrin-containing invadopodia promotes cell invasion. *J Biol Chem* 2002, 277(15):12487-12490.
49. Fan H, Zhao X, Sun S, Luo M, Guan JL: Function of focal adhesion kinase scaffolding to mediate endophilin A2 phosphorylation promotes epithelial-mesenchymal transition and mammary cancer stem cell activities in vivo. *J Biol Chem* 2013, 288(5):3322-3333.

50. Lim ST, Chen XL, Lim Y, Hanson DA, Vo TT, Howerton K, Larocque N, Fisher SJ, Schlaepfer DD, Ilic D: Nuclear FAK promotes cell proliferation and survival through FERM-enhanced p53 degradation. *Mol Cell* 2008, 29(1):9-22.
51. Kurenova E, Xu L-H, Yang X, Baldwin AS, Craven RJ, Hanks SK, Liu Z-g, Cance WG: Focal Adhesion Kinase Suppresses Apoptosis by Binding to the Death Domain of Receptor-Interacting Protein. *Molecular and Cellular Biology* 2004, 24(10):4361-4371.
52. Owen JD, Ruest PJ, Fry DW, Hanks SK: Induced focal adhesion kinase (FAK) expression in FAK-null cells enhances cell spreading and migration requiring both auto- and activation loop phosphorylation sites and inhibits adhesion-dependent tyrosine phosphorylation of Pyk2. *Mol Cell Biol* 1999, 19(7):4806-4818.
53. Sawhney RS, Cookson MM, Omar Y, Hauser J, Brattain MG: Integrin alpha2-mediated ERK and calpain activation play a critical role in cell adhesion and motility via focal adhesion kinase signaling: identification of a novel signaling pathway. *J Biol Chem* 2006, 281(13):8497-8510.
54. Skinner HD, Giri U, Yang L, Woo SH, Story MD, Pickering CR, Byers LA, Williams MD, El-Naggar A, Wang J *et al*: Proteomic Profiling Identifies PTK2/FAK as a Driver of Radioresistance in HPV-negative Head and Neck Cancer. *Clinical Cancer Research* 2016, 22(18):4643.
55. Brami-Cherrier K, Gervasi N, Arsenieva D, Walkiewicz K, Boutterin MC, Ortega A, Leonard PG, Seantier B, Gasmi L, Bouceba T *et al*: FAK dimerization controls its kinase-dependent functions at focal adhesions. *Embo j* 2014, 33(4):356-370.
56. Tomar A, Lawson C, Ghassemian M, Schlaepfer DD: Cortactin as a target for FAK in the regulation of focal adhesion dynamics. *PLoS One* 2012, 7(8):e44041.
57. Storch K, Cordes N: Focal adhesion-chromatin linkage controls tumor cell resistance to radio- and chemotherapy. *Chemother Res Pract* 2012, 2012:319287-319287.
58. Cordes N, Frick S, Brunner TB, Pilarsky C, Grutzmann R, Sipos B, Kloppel G, McKenna WG, Bernhard EJ: Human pancreatic tumor cells are sensitized to ionizing radiation by knockdown of caveolin-1. *Oncogene* 2007, 26(48):6851-6862.
59. Klaeger S, Heinzlmeir S, Wilhelm M, Polzer H, Vick B, Koenig PA, Reinecke M, Ruprecht B, Petzoldt S, Meng C *et al*: The target landscape of clinical kinase drugs. *Science* 2017, 358(6367).
60. Nevala-Plagemann C, Hidalgo M, Garrido-Laguna I: From state-of-the-art treatments to novel therapies for advanced-stage pancreatic cancer. *Nature Reviews Clinical Oncology* 2019.

Abbreviations

5-FU	5-fluorouracil
ACN	Acetonitrile
AGC	Automatic gain control
bRP	Basic reversed-phase
BSA	Bovine serum albumin
CAA	Chloroacetamide
CID	Collision-induced dissociation
CSC	Cancer stem cells
CV	Coefficient of correlation
DDR	DNA damage response
DMSO	Dimethylsulfoxide
DNA	Desoxyribonucleic acid
DSB	Double-strand break
DTT	Dithiothreitol
EDTA	Ethylenediaminetetraacetic acid
FDR	False discovery rate
GO	Gene ontology
HCD	Higher energy collision-induced dissociation
HPLC	High performance liquid chromatography
HPV	Human papillomavirus
HR	Homologous recombination
IMAC	Immobilized metal ion affinity chromatography
LC-MS^n	Liquid chromatography tandem mass spectrometry (MS2 or MS3)
MS1	Mass spectrum of intact peptides
MS2	Fragment mass spectrum of MS1 precursor
MS3	Fragment mass spectrum of MS2 precursor
NCE	Normalized collision energy
NHEJ	Non-homologous end joining
PDAC	Pancreatic ductal adenocarcinoma
P-protein	Phosphoprotein
P-site	Phosphorylation site
PSM	Peptide-spectrum match
ROS	Reactive oxygen species
RP	Reversed-phase
SDS-PAGE	Sodiumdodecylsulfate polyacrylamide gel electrophoresis
TBS	Tris-buffered saline
TFA	Trifluoroacetic acid
TMT	Tandem mass tag
Tris	Tris(hydroxymethyl)aminomethane

List of figures

III Mode of action of AKT inhibitors

Table of contents

Summary

Several small molecule inhibitors of AGC kinase AKT are currently under clinical investigation due to its pivotal role in cellular signaling in cancer. In order to elucidate how these potential drugs exert their effects on cancer cells, a combination of chemical proteomics and phosphoproteomics was employed on the five designated AKT inhibitors AZD5363, GSK2110183, GSK690693, Ipatasertib and MK-2206 in BT-474 breast cancer cells. Target affinity screening in form of the kinobeads technology led to the identification of between four and 29 nanomolar targets for each inhibitor. Subsequently, phosphoproteomic perturbation analysis revealed 1700 regulated phosphorylation sites upon treatment with the inhibitors. 276 phosphorylation sites were addressed by all five inhibitors, which could be traced back to the overlapping target spectrum of the inhibitors of solely AKT1 and AKT2, indicating a comprehensive view on the AKT signaling network. 41 regulated phosphorylation sites of this network harbored the AKT motif and 15 of these were validated as novel AKT substrates by a recombinant kinase assay. Hence, new roles of AKT as well as the AKT inhibitors in the regulation of these proteins can be suggested. Furthermore, secretome analysis identified STC2 as a response marker in the cell culture model, which could be translated to plasma samples of patients.

1 Introduction

Downstream of activated receptor tyrosine kinases (RTKs) and lipid kinases (PI3Ks) [1-3], AGC kinase AKT binds to PI3K lipid products PIP3 and PI3,4PS over its Pleckstrin homology (PH) domain [4] and is subject to phosphorylation on its activation sites at Thr^{308} and Ser^{473} [5]. Fully activated AKT subsequently phosphorylates proteins on serine and threonine residues, which provokes either activation or inhibition of the substrates reasoning in altered cell metabolism, growth control, proliferation and survival. More than 100 AKT substrates have been identified so far, which led to the definition of the minimal consensus substrate recognition motif P/R-X-R-X-X-S/T- φ (in which X denotes any amino acid and φ a large hydrophobic residue) [6]. Although all three AKT paralogs AKT1, AKT2 and AKT3, highly share their substrate repertoire to a large degree, gene-specific substrate engagement can occur on the basis of differential subcellular localization and activating mutations [7].

Due to its regulation of manifold signaling pathways, aberrations in AKT signaling can result in different types of cellular dysregulation including overgrowth syndromes [8], atherosclerosis [9], insulin resistance and diabetes [10], neurological diseases such as the tuberus sclerosis complex (TSC) disorder [11] and cancer [12]. ATP competitive as well as allosteric inhibitors have been developed, which target the ATP pocket of the kinase domain or the PH domain, preventing the kinase to anchor at the plasma membrane. This is the cellular localization where activation through upstream kinases occurs. In this way, AKT is locked in the inactive form. The most advanced compounds of these are currently in clinical phase III for different cancer types including HER2-positive breast cancer and exert nanomolar affinity towards AKT. Due to the highly similar ATP-binding pockets among kinases of the AGC kinase family and others, the selectivity of ATP-competitive AKT inhibitors is, however, generally low [13]. Clinical efficacy of the compounds as single agents is furthermore often limited. This might be the consequence of suboptimal patient stratification [14], increased receptor tyrosine kinase activity upon AKT inhibition [15] and on-target adverse effects (e.g. hyperglycaemia), which account for dose-limiting toxicities [16].

Although a few inhibitors of AKT are at the edge of approval for clinical use, a comprehensive mode of action analysis including the analysis of targets as well as the molecular consequences of target inhibition on cellular signaling has been not been executed so far. Hence, the knowledge of the many cellular actions of AKT inhibitors seems to e.g. predict efficacy in patients with different molecular backgrounds or to anticipate on-target and off-target effects as well as to reveal underlying mechanisms of low response. Therefore, a combined chemical and phosphoproteomic approach to analyze the target

spectrum and cellular mode of action of the five clinical AKT inhibitors GSK690693 (21) (phase I), AZD5363 (22), GSK2110183 (23), MK-2206 (24) (all phase II), and Ipatasertib (25) (phase III) in HER2-overexpressing BT-474 breast cancer cells was undertaken.

2 Material and methods

AKT modulators

AKT modulators VIII (#14870) and SC79 (#14972) were purchased from Cayman Chemical. PHT-427 (#P3076) was obtained from LKT Laboratories. AZD5363 (#S8019), GSK2110183 (#S7521), GSK690693 (#S1113), Ipatasertib (#2808), MK-2206 (#S1078), Perifosine (#S1037) and Miransertib (#S8339) were bought from Selleckchem. Uprosertib (#A-1504) was purchased from Active Biochem.

Cell culture and kinase inhibitor treatment

BT-474 cells were cultured in Dulbecco's modified Eagle's medium (DMEM)/Hams F-12 (1:1) with 10 % fetal bovine serum (FBS) and 1 % antibiotic and antimycotic solution (Biochrom) at 37 °C and 5 % CO_2 according to standard cell culture methods. Cell line authentication was accomplished by short tandem repeat (STR) profiling (Multiplexion, Heidelberg, Germany) [17]. For kinase inhibitor treatments, BT-474 cells were grown until a 70 % confluency was reached. 1 h prior to the treatment, the medium was exchanged. Subsequently, fresh medium supplemented with kinase inhibitor at the indicated concentration was added to the cells, which were further incubated at 37 °C for the indicated times.

Cell viability assay with alamarBlue reagent

2 x 10^4 cells of BT-474 cells were seeded into a 96-well microtiter plate in quadruplicate for each inhibitor and incubated at 37 °C and 5 % CO_2. After 24 h, dilutions of the kinase inhibitors (10 µM, 3 µM, 1 µM, 300 nM, 100 nM, 30 nM, 10 nM, 3 nM, 1 nM) in medium were added to the cells. After a 72 h treatment, alamarBlue reagent (Thermo Fisher Scientific) was added 1:10 to each well. The fluorescence was quantified at $\lambda_{excitation}$ = 544 nm and $\lambda_{emission}$ = 584 nm on the microplate reader FluoStar Omega (BMG Labtech).

Protein concentration assay

The protein concentration in cell lysate was determined using the Coomassie Plus Bradford (Thermo Fisher Scientific) assay according to the protocol of the manufacturer.

Sample preparation for kinase selectivity profiling

For the analysis of kinase inhibitor targets in BT-474 cells, Kinobead γ-pulldowns were performed as previously described [18]. Briefly, cells were lysed in 0.8 % NP40, 50 mM Tris-HCl pH 7.5, 5 % glycerol, 1.5 mM $MgCl_2$, 150 mM NaCl, 1 mM Na_3VO_4, 25 mM NaF, 1 mM dithiothreitol (DTT), protease inhibitors (SigmaFast, Sigma) and phosphatase inhibitors (Roche). Designated AKT inhibitors were spiked into 1 mL of lysate, which was adjusted to 5 mg/mL protein, with increasing concentrations

(dimethylsulfoxid (DMSO) control, 3 nM, 10 nM, 30 nM, 100nM, 300nM, 1 µM, 3 µM, 10 µM and 30 µM) and incubated for 45 min at 4°C. Afterwards, incubation with 35 µL settled kinobeads took place for 30 min at 4 °C. In order to enable the determination of a correction factor for each protein and to calculate apparent dissociation constants, a second kinobead pulldown (with fresh beads) was performed on the unbound fraction of the DMSO control. Proteins bound to kinobeads were eluted with LDS sample buffer (NuPAGE, Thermo Fisher Scientific) containing 50 mM DTT and alkylated with 55 mM chloroacetamide (CAA). Kinobead pulldown eluates were purified by short sodiumdodecylsulfate polyacrylamide gel electrophoresis (SDS-PAGE) (ca. 1 cm; Thermo Fisher Scientific) and were subsequently subjected to in-gel tryptic digestion according to standard procedures. After drying in a centrifugal evaporator, the samples were stored at -20 °C until LC-MS/MS analysis.

Sample preparation for TMT-DDA phosphoproteomic analysis and PRM assay

After treatment with designated AKT inhibitors, BT-474 cells were washed twice with phosphate-buffered saline (PBS) and lysed in 40 mM Tris-HCl pH 7.6, 8 M urea, ethylenediaminetetraacetic acid (EDTA)-free protease inhibitor (Roche) and phosphatase inhibitors (Roche). Lysate was centrifuged for 1 h at 21,000 x g and the supernatant was subjected to further processing. 2 mg protein of BT-474 lysate was reduced with 10 mM DTT for 40 min at 56 °C and alkylated with 25 mM CAA at room temperature in the dark for 20 min. After dilution of the urea concentration from 6 M to 1.5 M with 40 mM tris(hydroxymethyl)aminomethane (Tris)-HCl pH 7.6, the proteins were digested in a 1:100 trypsin/substrate weight ratio for 4 h at 37 °C and 700 rpm. The second digestion step was performed overnight again in a 1:100 trypsin/substrate weight ratio in presence of 1 mM $CaCl_2$. Desalting of tryptic peptides was performed on Sep-Pak C18 50 mg columns (Waters) in 0.07 % trifluoroacetic acid (TFA) in 50 % acetonitrile (ACN). P-peptides were enriched using Fe-immobilized metal affinity chromatography (IMAC) as previously described [19]. P-peptides were further desalted by using 0.07 % TFA in 50 % ACN in the micro-column format (three discs, Ø 1.5 mm, C18 material, 3M Empore per micro-column were used) as described [20]. After adding an equivalent of 500 fmol Pierce Retention Time Calibration Mixture (Thermo Fisher Scientific) for each MS injection to each parallel reaction monitoring (PRM) sample, sample preparation for label-free PRM assays was completed at this point. P-peptides for TMT-data dependent acquisition (DDA) analysis were labeled using tandem mass tages (TMT) 6-plex at a final concentration of 6.67 mM according to instructions provided by the manufacturer. One TMT channel was used for each treatment condition (126 = control, 127 = AZD5363, 128 = GSK2110183, 129 = GSK690693, 130 = ipatasertib, 131 = MK-2206). Subsequently, peptides were separated into six fractions using basic reversed-phase fractionation in micro-column format (five discs,

Ø 1.5 mm, C18 material, 3M Empore per micro-column were used) in 25 mM NH4COOH (pH 10). Peptides were fractionated with increasing ACN concentrations (5 %, 7.5 %, 10 %, 12.5 %, 15 %, 17.5 % and 50 % ACN). The desalted flow-through was combined with the 17.5 % fraction and the 50 % fraction with the 5 % fraction to give a total of six fractions. After drying in a centrifugal evaporator, the samples were stored at -20 °C until LC-MS^3 analysis.

Peptide synthesis

Peptides were designed as 15-mers (11-mer for Crosstide) with Serine or Alanine in the central position for wildtype or mutant, respectively, with a free N–terminal amino group and a C–terminal amide group. The synthesis was performed by an automated peptide synthesizer (Intavis Bioanalytical Instruments AG) in 2 µmol-scale by applying Fmoc chemistry. Purity was analyzed by MALDI–TOF–MS on an UltrafleXtreme (Bruker).

In vitro AKT2 assay

Peptide pools were added to 20 mM 4-(2-hydroxyethyl)-1-piperazineethanesulfonic acid (HEPES)-KOH pH 7.4, 5 mM $MgCl_2$, 1 mM DTT and 2 mM adenosine triphosphate (ATP) to reach an end concentration of 6 µM. The reaction was started by supplementing 12.5 ng/µl recombinant active AKT2 (Jena Bioscience, #PR-333,) and was incubated at 30 °C for different times (0, 5, 10, 30, 60, 120, 180 min). The reaction was quenched by adding an equal volume of 1 % FA in ACN. After drying in a centrifugal evaporator, the samples were stored at -20 °C until LC-MS/MS analysis.

Enrichment and subsequent processing of secreted proteins

Secreted proteins from AKT inhibitor-treated BT-474 cells were enriched, digested and further processed as previously described [21]. In short, BT-474 cells were first incubated in depletion medium (DMEM without methionine, 10 % dialyzed FBS, 0.2 mM L-cystine, 2.5 mM L-alanyl-L-glutamine, 0.5 mM sodium pyruvate) for 30 min and afterwards for 24 h in azidohomoalanine (AHA) labeling medium (depletion medium supplemented with 0.1 mM azidohomoalanine). In parallel to the metabolic labeling, kinase inhibitor treatment took place. Conditioned medium was supplemented with EDTA-free protease inhibitors (Roche) and phosphatase inhibitors (Roche) and was concentrated via centrifugal filters (3kDa cut-off, Amicon) at 4 °C. For the enrichment and digestion of AHA-labeled proteins, the Click-iT® Protein Enrichment Kit (Thermo Fisher Scientific) was applied according to the instructions of the supplier, despite that only half of the suggested volumes were used. Resulting peptides were further desalted by using 0.1 % FA in 50 % ACN in the micro-column format (three discs, Ø 1.5 mm, C18 material, 3M Empore per micro-column were used) as described [20] and labeled using

TMT 6-plex (Thermo Fisher Scientific) at a final concentration of 6.67 mM according to instructions provided by the manufacturer. TMT6-labeled peptides were separated into four fractions using basic reversed-phase fractionation in micro-column format (five discs, Ø 1.5 mm, C18 material, 3M Empore per micro-column were used) in 25 mM NH_4COOH (pH 10). Peptides were fractionated with increasing ACN concentrations (5 %, 10 %, 15 %, 17.5 % and 50 % ACN). The desalted flow-through was combined with the 17.5 % fraction and the 50 % fraction with the 5 % fraction to give a total of four fractions. After drying in a centrifugal evaporator, the samples were stored at -20 °C until LC-MS^3 analysis.

LC-MSn measurements

Kinome

Nano-flow LC-MS/MS measurement of peptides in Kinobead eluates was performed using a nanoLC-Ultra 1D+ (Eksigent) coupled to a linear trap quadrupole (LTQ) Orbitrap Elite mass spectrometer (Thermo Fisher Scientific). Peptides were desalted on a trap column (100 µm × 2 cm, packed in-house with Reprosil-Pur C18-AQ 5 µm resin; Dr. Maisch) in 0.1 % FA at 5 µl/min and separated on an analytical column (75 µm × 40 cm, packed in-house with Reprosil-Pur C18-AQ, 3 µm resin; Dr. Maisch) using a 100 min linear gradient from 4-32 % solvent B (0.1 % formic acid (FA), 5 % DMSO in ACN) in solvent A1 (0.1 % FA, 5 % DMSO in water) at a flow rate of 300 nL/min. The mass spectrometer was operated in data dependent acquisition and positive ionization mode. MS1 spectra were acquired over a range of 360-1300 m/z at a resolution of 30,000 (at m/z 400) in the orbitrap and an automatic gain control (AGC) target value of 1 x 10^5. Up to 15 peptide precursors were selected for fragmentation by higher energy collision-induced dissociation (HCD; isolation width of 2 Th, maximum injection time of 100 ms, AGC value of 2 x 10^5) using 30 % normalized collision energy (NCE) and analyzed in the orbitrap (7,500 resolution).

TMT6 phosphoproteome

Nano-flow LC-MS^3 measurement of TMT-labeled p-peptides was performed using a Dionex Ultimate3000 nano high performance liquid chromatography (HPLC) (Thermo Fisher Scientific) coupled to an orbitrap Fusion mass spectrometer (Thermo Fisher Scientific). Peptides were desalted on a trap column (Acclaim C18 PepMap100, 75 µm i.d. ×2 cm; Thermo Fisher Scientific) in 0.1 % FA and separated on an analytical column (Acclaim C18 PepMap RSLC, 75 µM i.d. ×15 cm; Thermo Fisher Scientific) using a 120 min gradient from 3-25 % solvent B (0.1 % FA, 5 % DMSO in 100 % ACN) in solution solvent A (0.1 % FA, 5 % DMSO in water). The Fusion was operated in data dependent acquisition and positive ionization mode. Full scan MS1 spectra were acquired over a range of 300-

1700 m/z at a resolution of 60,000 (AGC target value 4 x 10^5, maximal injection time 50 ms). Fragmentation was performed using collision-induced dissociation (CID) at 40 % NCE and MS2 spectra acquisition (AGC target value 4 x 10^4, maximal injection time 60 ms) took place in the ion trap. For TMT quantification an additional MS3 spectrum was acquired in the orbitrap over an m/z range of 100-500 at 60,000 resolution for each peptide precursor. For this, fragment ions were selected by multi-notch isolation, allowing a maximum of 10 notches and an ion trap isolation width of 2 Da, and subsequently fragmented by HCD at 55 % NCE (AGC target value 1 x 10^5, maximal injection time 120 ms).

In vitro kinase assay

Nano-flow LC-MS/MS measurement of peptides deriving from the *in vitro* kinase assay was performed using a Dionex Ultimate3000 nano HPLC (Thermo Fisher Scientific) coupled to an orbitrap Fusion Lumos mass spectrometer (Thermo Fisher Scientific). Peptides were desalted on a trap column (100 µm × 2 cm, packed in-house with Reprosil-Pur C18-AQ 5 µm resin; Dr. Maisch) in 0.1 % FA and separated on an analytical column (75 µm × 40 cm, packed in-house with Reprosil-Pur C18-AQ, 3 µm resin; Dr. Maisch) using a 51 min two-step gradient from 4-15-27 % solvent B (0.1 % FA, 5 % DMSO in 100 % ACN) in solution solvent A (0.1 % FA, 5 % DMSO in water). The Fusion Lumos was operated in data dependent acquisition and positive ionization mode. Full scan MS1 spectra were acquired over a range of 360-1300 m/z at a resolution of 60,000 (AGC target value 5 x 10^4, maximal injection time 50 ms). Fragmentation was performed using HCD at 30 % NCE (AGC target value 5 x 10^4, maximal injection time 120 ms) in the orbitrap at 30,000 resolution.

PRM assay

Nano-flow LC-MS/MS measurement of peptides for generating a spectral library and the PRM assay was performed using a Dionex Ultimate3000 nano HPLC (Thermo Fisher Scientific) coupled to an orbitrap Fusion Lumos mass spectrometer (Thermo Fisher Scientific). Peptides were desalted and separated as described for *in vitro* kinase assay samples, except for a longer gradient of 110 min for the spectral library generation. The Fusion Lumos was operated in data dependent acquisition and positive ionization mode. For generating the spectral library, full scan MS1 spectra were acquired over a range of 360-1300 m/z at a resolution of 60,000 (AGC target value 4 x 10^5, maximal injection time 50 ms). Targeted MS2 scans were acquired over a range of 120-2000 m/z and fragmentation was performed using HCD at 30 % NCE (AGC target value 1 x 10^5, maximal injection time 50 ms) in the orbitrap at 15,000 resolution by taking into account the mass list of p-peptides. For the PRM assay, full scan MS1 spectra were acquired over a range of 360-1300 m/z at a resolution of 15,000 (AGC target value 4 x 10^5,

maximal injection time 50 ms). Targeted MS2 scans were acquired over a range of 120-2000 m/z and fragmentation was performed using HCD at 30 % NCE (AGC target value 2 x 10^5, maximal injection time 100 ms) in the Orbitrap at 15,000 resolution by taking into account the final mass list of p-peptides.

TMT6 secretome

Nano-flow LC-MS^3 measurement of TMT-labeled peptides from enriched secretomes was performed using a Dionex Ultimate3000 nano HPLC (Thermo Fisher Scientific) coupled to an orbitrap Fusion Lumos mass spectrometer (Thermo Fisher Scientific). Peptides were desalted on a trap column (100 µm × 2 cm, packed in-house with Reprosil-Pur C18-AQ 5 µm resin; Dr. Maisch) in 0.1 % FA and separated on an analytical column (75 µm × 40 cm, packed in-house with Reprosil-Pur C18-AQ, 3 µm resin; Dr. Maisch) using a 80 min gradient from 6-34 % solvent B (0.1 % FA, 5 % DMSO in 100 % ACN) in solution solvent A (0.1 % FA, 5 % DMSO in water). The Fusion Lumos was operated in data dependent acquisition and positive ionization mode. Full scan MS1 spectra were acquired over a range of 360-1300 m/z at a resolution of 60,000 (AGC target value 4 x 10^5, maximal injection time 20 ms). Fragmentation was performed using CID at 35 % NCE and MS2 spectra acquisition (AGC target value 2 x 10^4, maximal injection time 60 ms) took place in the ion trap. For TMT quantification an additional MS3 spectrum was acquired in the orbitrap over an m/z range of 100-1000 at 15,000 resolution for each peptide precursor. For this, fragment ions were selected by multi-notch isolation, allowing a maximum of 10 notches and subsequently fragmented by HCD at 55 % NCE (AGC target value 5 x 10^4, maximal injection time 22 ms).

Database searching and data analysis

Protein and peptide identification and quantification was performed using MaxQuant (79) (version 1.5.6.5). If not stated otherwise, the MS data was searched against all human canonical and isoform protein sequences as annotated in the Swissprot reference database (42,095 entries, downloaded 14.11.2016) using the embedded search engine Andromeda (80).

Kinome

Carbamidomethylated cysteine was set as fixed modification; and phosphorylation of serine, threonine, and tyrosine, oxidation of methionine, and N-terminal protein acetylation were variable modifications. Trypsin/P was specified as the proteolytic enzyme and up to two missed cleavage sites were allowed. Precursor and fragment ion tolerances were 4.5 parts per million (ppm) and 20 ppm, respectively. Label-free quantification [22] and match-between-runs were enabled within MaxQuant. Protein intensities were normalized to the respective DMSO control. Half maximal inhibitory concentration (IC50) and

half maximal effective concentration (EC50) values were calculated by a four-parameter log-logistic regression using an internal pipeline that utilizes the 'drc' [23] package in R. A K_d^{app} was computed by multiplying the estimated EC50 with a protein-dependent correction factor that was limited to a maximum value of 1. The correction factor for a protein is defined as the ratio of the amount of protein captured from two consecutive pulldowns of the same DMSO control lysate [18] and was set to the average of correction factors across all experiments using the same lysate and beads.

TMT6 phosphoproteome

Carbamidomethylated cysteine was set as a fixed modification; and phosphorylation of serine, threonine, and tyrosine, oxidation of methionine, and N-terminal protein acetylation were variable modifications. Trypsin/P was specified as the proteolytic enzyme and up to two missed cleavage sites were allowed. Precursor and fragment ion tolerances were 10 ppm and 4.5 ppm, respectively. MS3-based TMT quantification was enabled, taking TMT correction factors as supplied by the manufacturer into account. Within one replicate, the sum of p-site intensities per TMT channel were normalized to the average sum of intensities of all TMT channels. Subsequently, the average intensities for each phosphorylation site per replicate was normalized to the average intensity of the same phosphorylation site across all replicates. Data was further analyzed by Perseus (version 1.5.5.3) [24]. Only p-sites that were identified and quantified in at least three out of four replicates were considered for further analysis. Log_2 fold-changes (FC) for each inhibitor against the vehicle control were calculated per phosphorylation site and tested for significance using a t-test (false discovery rate (FDR) = 5 %, s0 = 0.1). Protein-protein interactions were analyzed using the String database [25] (version 11.0) (combined score > 0.4) and visualized in Cytoscape (version 3.4.0). Frequency sequence logos were generated using WebLogo [26] (available from http://weblogo.berkeley.edu/).

In vitro kinase assay

Peptide identification and quantification was performed by searching the MS data against a database containing only sequences of the screened peptides. Phosphorylation of serine and threonine, oxidation of methionine, and N-terminal protein acetylation were set as variable modifications. Precursor and fragment ion tolerances were 4.5 ppm and 20 ppm, respectively. Peptide-spectrum-match intensities for each peptide were summed, with the prerequisite that the peptide was identified in at least two out of three replicates. Only those PSMs of p-peptides with a higher localization probability of the intended p-site than another p-site were considered for summing up peptide intensity. The intensity of each peptide across experiments was further normalized to the total peptide intensity in each experiment.

PRM assay

In order to obtain the spectral library, respective raw files were searched in MaxQuant with carbamidomethylated cysteine as a fixed modification; and phosphorylation of serine, threonine, and tyrosine, oxidation of methionine, and N-terminal protein acetylation as variable modifications. Trypsin/P was specified as the proteolytic enzyme and up to two missed cleavage sites were allowed. Precursor and fragment ion tolerances were 10 ppm and 4.5 ppm, respectively. The PRM raw data files were imported into the Skyline software package (version 4.1.0.11714) [27]. Confident p-peptide identification was carried out based on iRT information using spiked-in retention time peptides, matching relative transition intensities between the PRM peak and the library MS2 spectrum (if available) and requiring site determining ions for each phosphorylation site. For accurate p-peptide quantification, low-quality or interfered transitions were discarded manually. Peaks were integrated using the automatic peak finding function followed by the manual curation of all peak boundaries. By calculating the sums of all transition areas associated with the p-peptide, quantification of each p-peptide was accomplished. Peak areas were normalized based on the total MS1 intensity across the experiments. Log_2 FC values for each inhibitor against the vehicle control were calculated per p-peptide. The median log_2 FC of the 13 quantified p-peptides for each inhibitor was computed to obtain a simple AKT perturbation score.

TMT6 secretome

Carbamidomethylated cysteine was set as a fixed modification; oxidation of methionine, N-terminal protein acetylation and AHA instead of methionine were variable modifications. Trypsin/P was specified as the proteolytic enzyme and up to two missed cleavage sites were allowed. Precursor and fragment ion tolerances were 10 ppm and 4.5 ppm, respectively. MS3-based TMT quantification was enabled, taking TMT correction factors as supplied by the manufacturer into account. Within one replicate, the sum protein intensities per TMT channel were normalized to the average sum of intensities of all TMT channels. Subsequently, the average intensities for each protein per replicate was normalized to the average intensity of the same protein across all replicates. Data was further analyzed by Perseus (version 1.5.5.3) [24]. Only proteins that have been identified and quantified in at least two out of three replicates were considered for further analysis. Log_2 FC for each inhibitor against the vehicle control were calculated per protein and tested for significance using a t-test (FDR = 5 %, s0 = 0.09). Prediction of secretion of identified proteins was performed by using the Human Protein Atlas [28] (available from www.proteinatlas.org) and Uniprot [29] (available from www.uniprot.org).

Western Blots

Protein lysates were generated by either harvesting cells in urea (40 mM Tris-HCl pH 7.6, 8 M urea) or RIPA lysis buffer (150 mM NaCl, 1 % IGEPAL CA-630, 0.5 % Sodium deoxycholate, 0.1 % SDS in 50 mM Tris (pH 8.0)), supplemented with protease inhibitor (Merck Millipore or Sigma) and phosphatase inhibitor cocktail (Roche). Proteins were separated by SDS-PAGE and electro-transferred onto PVDF membranes. Blots were stored in Tris-buffered saline, supplemented with 0.05 % Tween (TBS-T) and 5 % non-fat milk or 2 % BSA for 1 h at room temperature and then incubated with primary antibody (diluted in TBS/0.05 % Tween, 5 % non-fat milk or BSA) overnight at 4 °C. The following primary antibodies were used: β-Actin (1:1000, Santa Cruz Biotechnology, #sc-47778), GAPDH (1:1000, Cell Signaling Technology, #5174), Phospho-AKT (Thr308) (1:1000, Cell Signaling Technology, #13038), Phospho-AKT (Ser473) (1:1000, Cell Signaling Technology, #4060), AKT (1:1000, Cell Signaling Technology, #9272). Subsequently, blots were washed in TBS-T and probed with the corresponding fluorophore-conjugated secondary antibody for 30 min at room temperature. The immuno-reactive signals were detected directly by excitation of the respective fluorophore. Acquisition and quantification of the band intensities were carried out with the Odyssey (Licor) imaging system and respective software. Intensities of proteins were normalized to input ACTB and phosphorylated proteins were normalized to the intensity of the respective total protein.

3 Results and Discussion

3.1 Kinobeads reveales the target spectrum of five clinical AKT inhibitors

Kinase affinity profiling was performed on the four ATP-competitive ATK inhibitors (AZD5363, GSK2110183, GSK690693 and Ipatasertib) and one allosteric AKT inhibitor (MK-2206) using the kinobead approach [18, 30] in order to determine the targets including apparent affinity constants (K_D^{app}). BT-474 cells were chosen as a breast cancer model because of their elevated AKT activity due to HER2-overexpression. The constraint of these cells is that AKT3 expression is low compared to AKT1 and AKT2, which has been determined by the kinobead assay as well as a deep proteome profile [31]. Since the substrate specificity is mostly similar among all three AKT isoforms, the reduced AKT3 expression should play a minor role for determining molecular actions of the inhibitors. Cellular sensitivity in the nanomolar range towards the five AKT inhibitors investigated here was ascertained by metabolic Alamar Blue assays (Figure III-1).

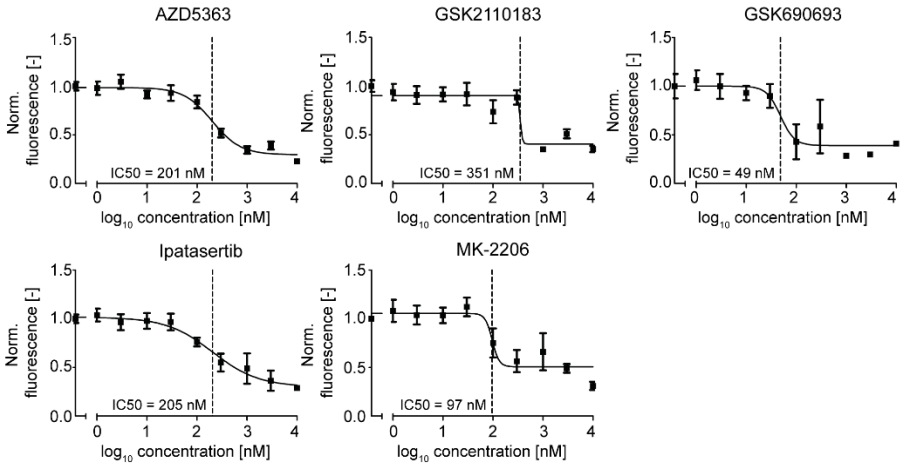

Figure III-1: Cellular metabolic assays of AKT inhibitors in BT-474 cells. Inhibition curves for AKT inhibitors AZD5363, GSK2110183, GSK690693, Ipatasertib and MK-2206 on BT-474 breast cancer cells. The relative IC50 is highlighted. Error bars represent standard deviation (SD). Data represent N = 3 biologically independent experiments.

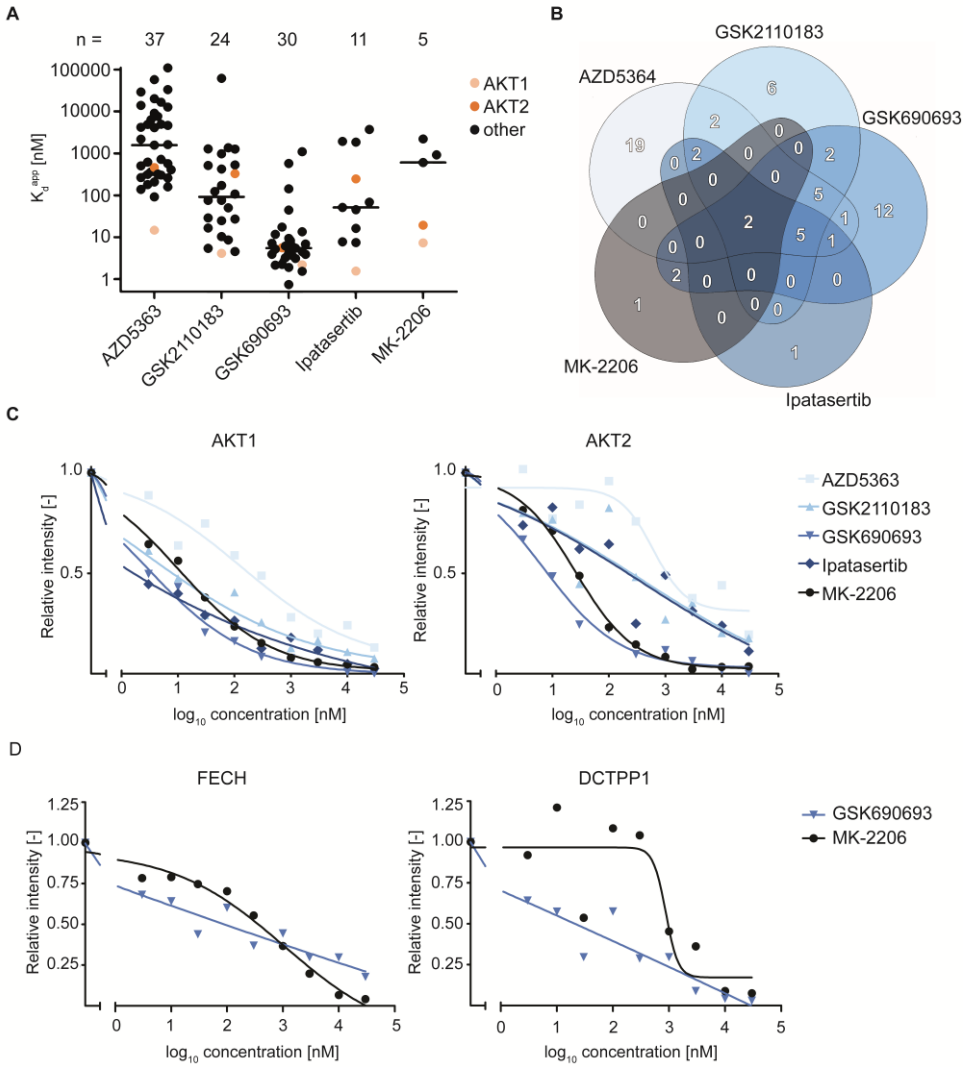

Figure III-2: Chemical proteomic kinobead assay for target profiling of AZD5363, GSK2110183, GSK690693, Ipatasertib and MK-2206. (A) Overview of the number of targeted kinases as well as non-kinase proteins and corresponding apparent binding affinities of each inhibitor. AKT1 and AKT2 are highlighted in orange. (B) Overlap of the target space between AKT inhibitors. AKT1 and AKT2 are the targets shared by all five inhibitors. (C) Binding curves of all inhibitors to AKT1 (left) and AKT2 (right). (D) Binding curves of GSK690693 and MK-2206 to FECH (left) and DCTPP (right). Data represent N = 10 concentration-based, independent experiments.

Allosteric MK-2206, which only targeted a total of five proteins in the kinobead assay, was the most selective inhibitor in the screen. The ATP-competitive compounds AZD5363, GSK2110183, GSK690693 and Ipatasertib possessed a wider target spectrum ranging from 11 to 37 targets with K_d^{app} values from low nM to mid µM (Figure III-2A), covering notably other kinases from the AGC family. Drug-specific off-targets were observed especially for GSK690693, which may help explaining the dose-limiting toxicities (hyperglycemia, skin rashes) that caused the clinical development of this compound to end [16, 32]. AKT1 and AKT2 were the only kinases bound by all five inhibitors (Figure III-2B). Clear differences in affinity between both AKT isoforms AKT1 and AKT2 were determined for AZD5363

(K_d^{app} AKT1=92 nM, K_d^{app} AKT2=457 nM), GSK2110183 (K_d^{app} AKT1=4 nM, K_d^{app} AKT2=328 nM) and Ipatasertib (K_d^{app} AKT1=2 nM, K_d^{app} AKT2=246 nM). Contrarily, GSK690693 (K_d^{app} AKT1=2 nM, K_d^{app} AKT2=6 nM) and MK-2206 (K_d^{app} AKT1=7 nM, K_d^{app} AKT2=19 nM) showed similar affinities for both AKT1 and AKT2 (Figure III-2C). Similar affinities for AKT1 and AKT2 were determined by recombinant kinase assays for GSK690693 and MK-2206 [33, 34], while lower IC50's for AKT2 in the case of AZD5363, GSK2110183 and Ipatasertib were declared [35-37]. Disagreement between different types of binding assays are reported and can arise from accessibilities to molecular factors such as interaction partners or metabolites that interfere with cellular kinase action [38, 39].

Kinase inhibitors might also bind to proteins other than kinases as it has been shown before in different cell lines [40]. Here, ferrochelatase (FECH) and dCTP pyrophosphatase 1 (DCTPP1) were identified as sub-micromolar non-kinase targets of GSK-690693 and MK-2206 (Figure III-2D). This finding confirms recent data, which has shown FECH- and DCTPP1-binding by GSK690693 and MK-2206 in different cell lines [38]. FECH inhibition is described to cause phototoxicity in patients [40, 41] and could be an actual potential adverse effect with intracellular and plasma concentrations of MK-2206 in the high nM to low μM range [42]. Oppositely, inhibition of DCTPP1 might be advantageous in breast cancer patients since it has been reported that high DCTPP1 activity bears strong association with tumor progression and poor prognosis [43]. Although the affinity matrix used in the kinobead approach limits the proteins that can be specifically enriched and in spite of affinity constants determined in cell lysates, which may differ from the situation *in cellulo* [38], this data (again) encourages kinome- or proteome-wide affinity profiling of small molecules at an early stage of development in order to identify and manage potential adverse off-target effects.

3.2 Phosphoproteomics illuminates broad common cellular perturbation by AKT inhibitors

In order to identify the consequences of AKT inhibitor action onto cellular signaling, a phosphoproteomic analysis was performed on BT-474 cells in response to the five AKT inhibitors. Stable isotope labeling by TMT [44] enabled the direct side-by-side comparison of the effects of the five drugs (including a DMSO control) (Figure III 3A). In total, 19,330 p-sites on 5069 proteins were identified and quantified in total (Figure III 3B). Further analysis was restricted to only those 10,900 p-sites, which were identified and quantified in at least three out of four replicates. The median coefficient of variation over all p-site intensities between the control replicates was 10%, which indicated a high reproducibility of the biochemical workflow and LC-MS^3 analysis.

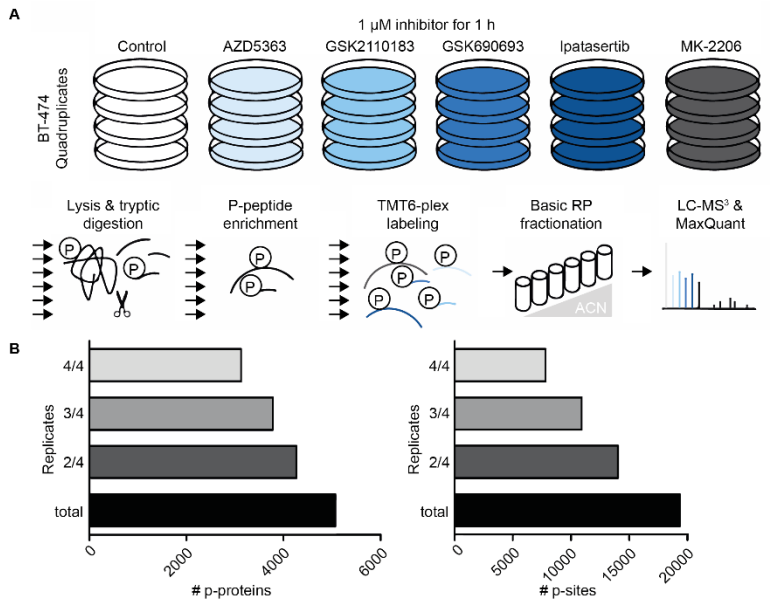

Figure III-3: Phosphoproteomic workflow and the number of identifications. (A) The schematic setup of the phosphoproteomic workflow is presented. (B) The number of identified and quantified p-proteins (left) and p-sites (right) depending on the occurrence in at least one (total), two (2/4), three (3/4) or four (4/4) biological replicates.

Drug engagement of AKT in BT-474 cells was demonstrated using Western blotting (Figure III-4A), which indicated complete abrogation of Thr^{308} and Ser^{473} phosphorylation upon allosteric compound MK-2206 treatment. MK-2206 stabilizes the PH-in conformation and thereby prevents localization of AKT to the plasma membrane and subsequent phosphorylation by PDK1/mTOR. In contrast, the ATP-competitive inhibitors increased phosphorylation at these p-sites by induced translocation of AKT to the plasma membrane shifting the balance between cytosolic and membrane-tethered AKT. The phosphoproteomic data furthermore revealed Ser^{458} phosphorylation on AKT2 to be significantly decreased by MK-2206 but not by the other compounds (Figure III-4B). Phosphorylation on the nearby Thr^{451} was not regulated by any of the inhibitors. Phosphorylation of AKT2-Ser^{458} has not been functionally annotated and, in addition, structural information on this part of the protein has not been reported so far. However, one may speculate that phosphorylation of Ser^{458} could be used as a molecular marker for the PH-in conformation of AKT2, which is favored when engaged by allosteric inhibitors [44, 45].

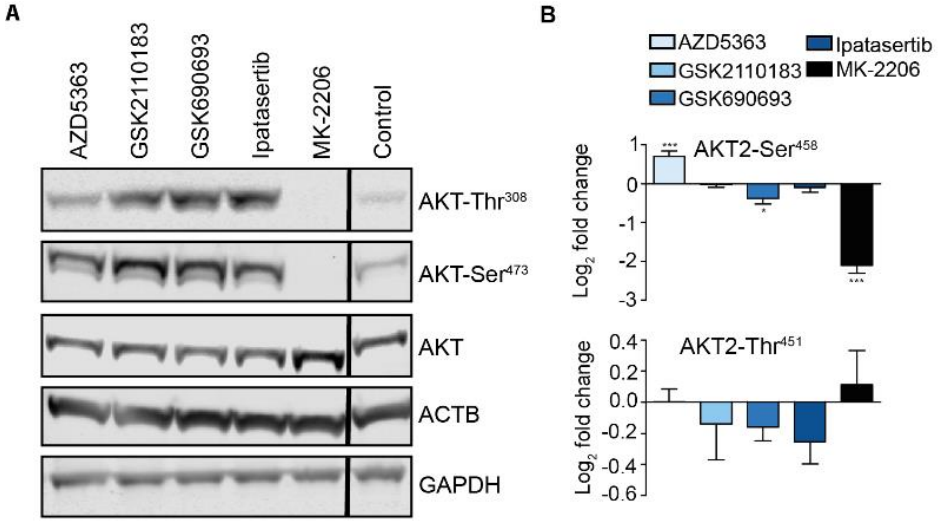

Figure III-4: Engagement of AKT by the AKT inhibitors. (A) Immunoblots showing phosphorylated AKT-Thr^{308} and AKT-Ser^{473}, AKT, ACTB and GAPDH intensity in response to AKT inhibitor treatment. (B) LC-MS^3 quantification of AKT2-Ser^{458} (top) and AKT2-Thr^{451} (bottom) p-site intensity upon AKT inhibitor treatment. Data represent N = 1 (A) and N = 4 (B) biologically independent experiments. Statistical analyses were performed by t-tests (FDR = 0.05, s0 = 0.1). Error bars represent SD. * P ≤ 0.05, ** P ≤ 0.01, *** P ≤ 0.001.

P-site intensities between untreated and treated cells were compared in order to reveal the part of the phosphoproteome that was significantly regulated by the compounds (log_2 fold change (log_2 FC), false discovery rate (FDR) of 5 %; as exemplified for AZD5363 in Figure III-5A). This analysis led to a total of 1730 drug-perturbed p-sites. As expected, the number of regulated p-sites mostly followed the number of targets of the drugs (Figure III-5B). Even the most selective drug (MK-2206) regulated > 500 p-sites showing that AKT activity impacts a large number of proteins. The finding in the kinobeads assay that the five drugs only have the two targets AKT1 and AKT2 in common provided an opportunity to specifically attribute the many drug-induced changes in protein phosphorylation to AKT inhibition. Therefore, the following analysis was confined to those 276 p-sites (on 185 proteins) that were significantly regulated by all five compounds. This strict focus on common regulated p-sites may eliminate substantial effects, which are inhibitor-specific. However, this granted the chance to more comprehensively study the consequences of AKT pathway inhibition. AKT inhibition, in addition to the AKT engagement found by Western Blotting, was shown by decreased phosphorylation intensity of direct substrates of AKT (e.g. GSK3B-Ser^9, log_2 FC_{av}= -0.7; FOXO3-Ser^{253}, log_2 FC_{av}= -0.5 and AKT1S1-Thr^{246}, log_2 FC_{av}= -2.2), and indirect downstream targets (e. g. RICTOR-Thr^{1135}, log_2 FC_{av}= -1.5; IRS1-Ser^{270}, log_2 FC_{av}= -1.4; Figure III-5C).

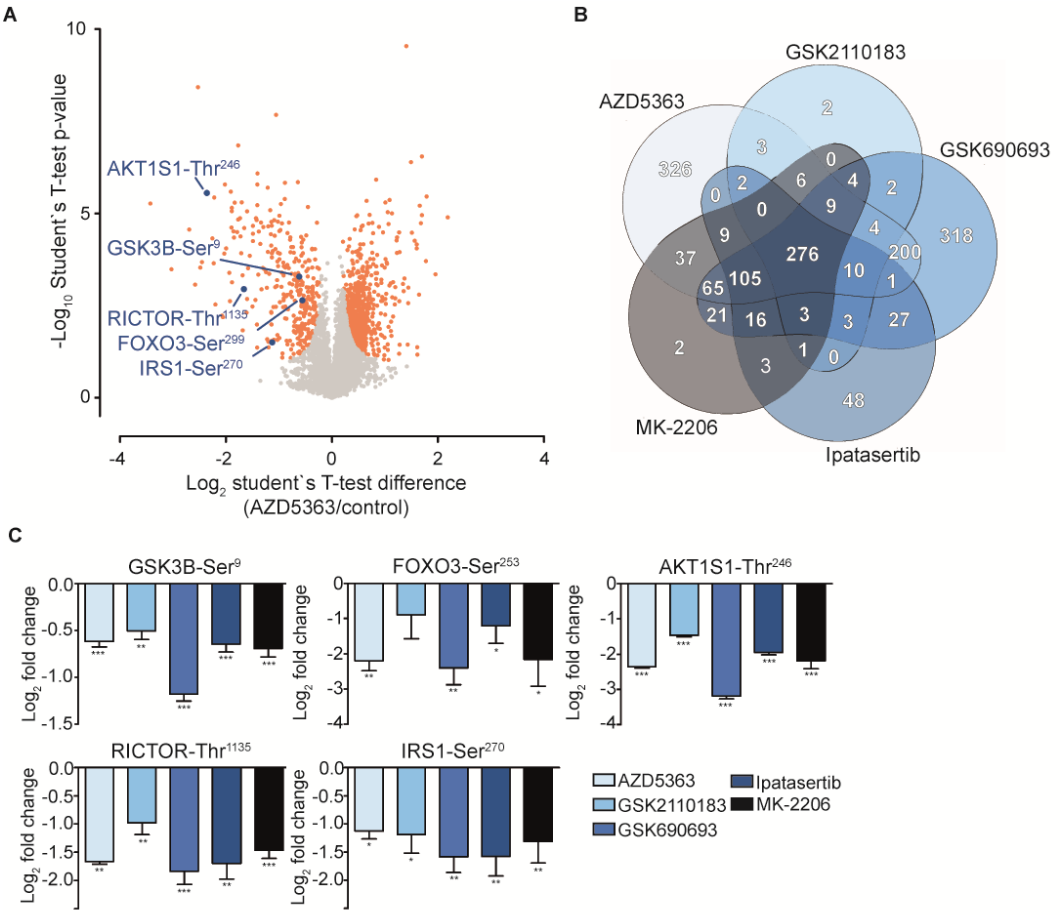

Figure III-5: Deep AKT-inhibitor-perturbed phosphoproteome of BT-474 cells. (A) Volcano plot of the regulation of p-site intensities by AZD5363. Significantly regulated p-sites are marked in orange. Known phosphorylated AKT pathway members GSK3B-Ser^{9}, FOXO3-Ser^{253}, AKT1S1-Thr^{246}, RICTOR-Thr^{1135} and IRS1-Ser^{270} are highlighted in blue. (B) Venn diagram of overlapping significantly regulated phosphosites between the AKT inhibitors. Data represent N = 3-4 biologically independent experiments. (C) LC-MS^{3} quantification of known AKT pathway member GSK3B-Ser^{9}, FOXO3-Ser^{253}, AKT1S1-Thr^{246} (top, from left to right), RICTOR-Thr^{1135} and IRS1-Ser^{270} (bottom, left to right) p-site intensity upon AKT inhibitor treatment. Statistical analyses were performed by t-tests (FDR = 0.05, s0 = 0.1). Error bars represent SD. * P ≤ 0.05, ** P ≤ 0.01, *** P ≤ 0.001.

The 185 proteins commonly regulated by all five AKT inhibitors may be part of a common AKT signaling network. Surveying the scientific literature (Pubmed) as well as the STRING protein interaction database [25] (www.string-db.org) classified 67 of these phosphoproteins as known AKT network members (Figure III-6). The phosphoproteomic analysis also assigned 118 proteins to potential novel functions or regulatory networks as exemplified by centrosomal protein CEP170, FAM83H and C6ORF132. CEP170 plays a pivotal role in the organization of microtubules [46] and showed significant regulation of p-site intensity on several residues. FAM83H is part of the keratin cytoskeleton formation [47] and its p-site intensity on Ser^{1025} was significantly decreased by all drugs. Providing such functional contexts is particularly useful for proteins that have no ascribed function so far. This is illustrated by the

protein product of the C6ORF32 gene, for which several p-sites were significantly regulated by AKT inhibitors.

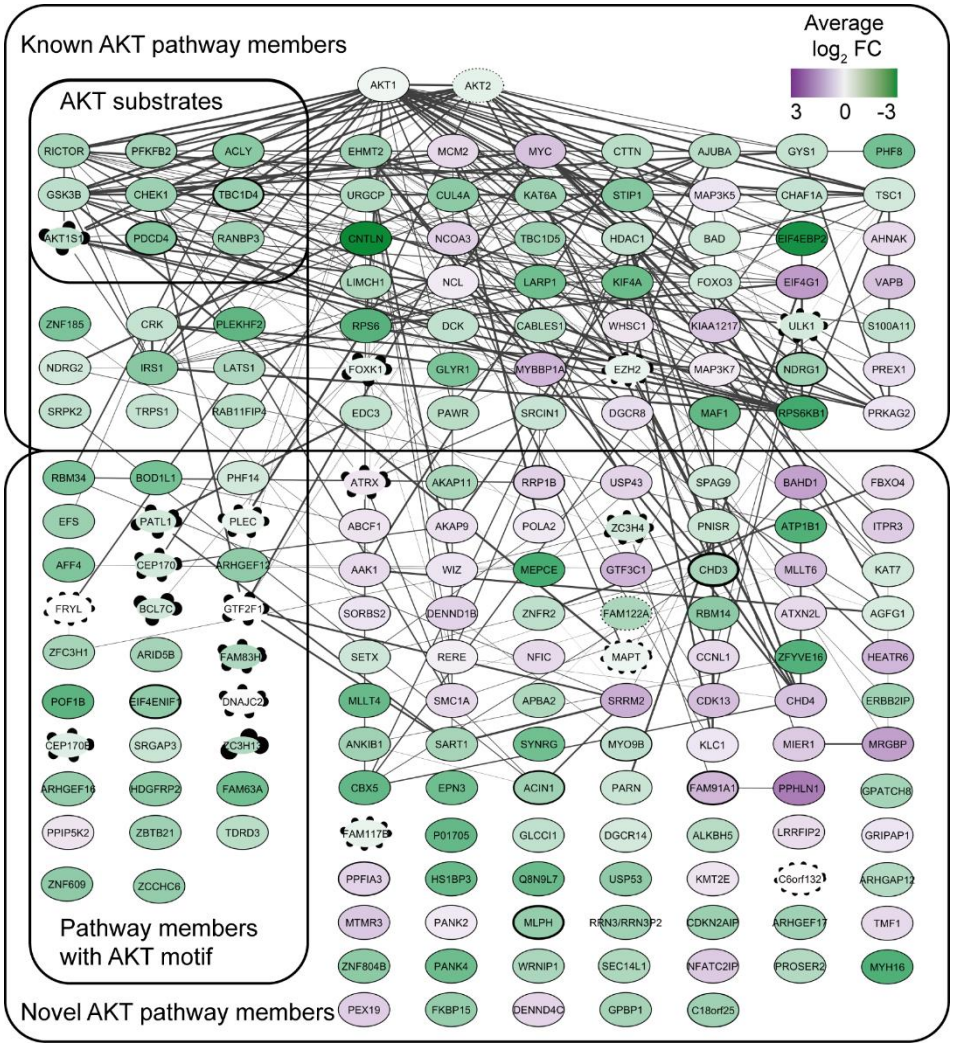

Figure III-6: Extended AKT signaling network. Protein-protein interaction-based network (available from www.string-db.org) of p-proteins, which were significantly regulated by all five AKT inhibitors and represent the extended AKT pathway. Edges are confidence-weighted. The log2 FC in p-site intensity was averaged on each p-protein and over all five inhibitors. The averaged log2 FC is color-coded such that an increased phosphorylation is indicated by a violet and decreased phosphorylation intensity by a green node. Differential p-site intensity regulation on one phosphoprotein is indicated by a dotted node line. Its standard deviation is indicated by the thickness of the node line with broader lines indicating a higher standard deviation. Known AKT substrates and p-proteins bearing an AKT motif are highlighted. P-proteins were further divided into known and novel AKT pathway members according to literature research via PubMed (available from www.ncbi.nlm.nih.gov/pubmed). Data represent N = 3-4 biologically independent experiments.

3.3 PRM assay confirms AKT network regulation

Due to the lack of antibodies for most of the p-sites identified in the phosphoproteome, a quantitative mass spectrometry-based assay called PRM was used in order to validate several p-sites as novel AKT

network members. In addition to the validation of the findings above, the panel of screened drugs was expanded to include the ATP competitor Uprosertib [48], the allosteric AKT inhibitors VIII [49], Miransertib [50], Perifosine [51] and PHT-427 [52] as well as the AKT activator SC-79 [53] to further demonstrate that the regulation of p-site intensities of the novel AKT network members is AKT-specific. In parallel, Western blot analysis was performed for AKT Thr^{308} and Ser^{473} phosphorylation (Figure III-7) to analyze AKT engagement. While the ATP competitor Uprosertib showed an increase in AKT phosphorylation similar to the other ATP competitive drugs analyzed above, the results of the allosteric inhibitors were heterogeneous. PHT-427 and AKT inhibitor VIII showed complete abrogation of AKT Thr^{308} and Ser^{473} phosphorylation, which was in line with preventing the translocation of AKT to the plasma membrane. However, the increase in phosphorylation following Miransertib and Perifosine treatment was inconsistent with expected effects of allosteric inhibitors. AKT activator SC-79, on the other hand, did not show any appreciable effect on the phosphorylation status of AKT.

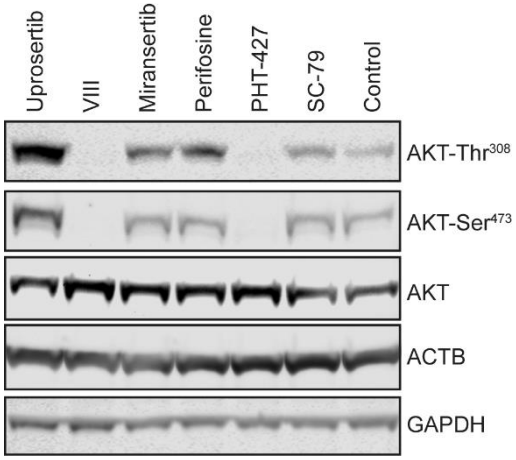

Figure III-7: Engagement of AKT by additional AKT inhibitors. Immunoblots showing phosphorylated AKT-Ser^{308} and AKT-Ser^{473}, AKT, ACTB and GAPDH intensity in response to AKT modulator treatment. Data represent N = 1 (D) biologically independent experiments.

The PRM assay covered three known direct substrates (AKT1S1, TSC2, FOXO3), one feedback loop pathway member (RICTOR), as well as seven novel network members (CEP170, CEP170B, FAM63A, FAM83H, MLPH, ZBTB21, ZCCHC6) (Figure III-8A). The intensities of all PRM signals for a given p-site were summed into a total intensity for each phosphopeptide (p-peptide) (as exemplified for FAM83H in Figure III-8B). Subsequently, a simple AKT perturbation score was calculated for each inhibitor by computing the median $\log_2$ FC of the intensities of the 13 p-peptides (Figure III-8C). The PRM assay confirmed the results of the initial phosphoproteomic experiment (TMT-DDA) for AZD5363, GSK2110183, GSK690693, Ipatasertib and MK-2206 (Figure III-8D).

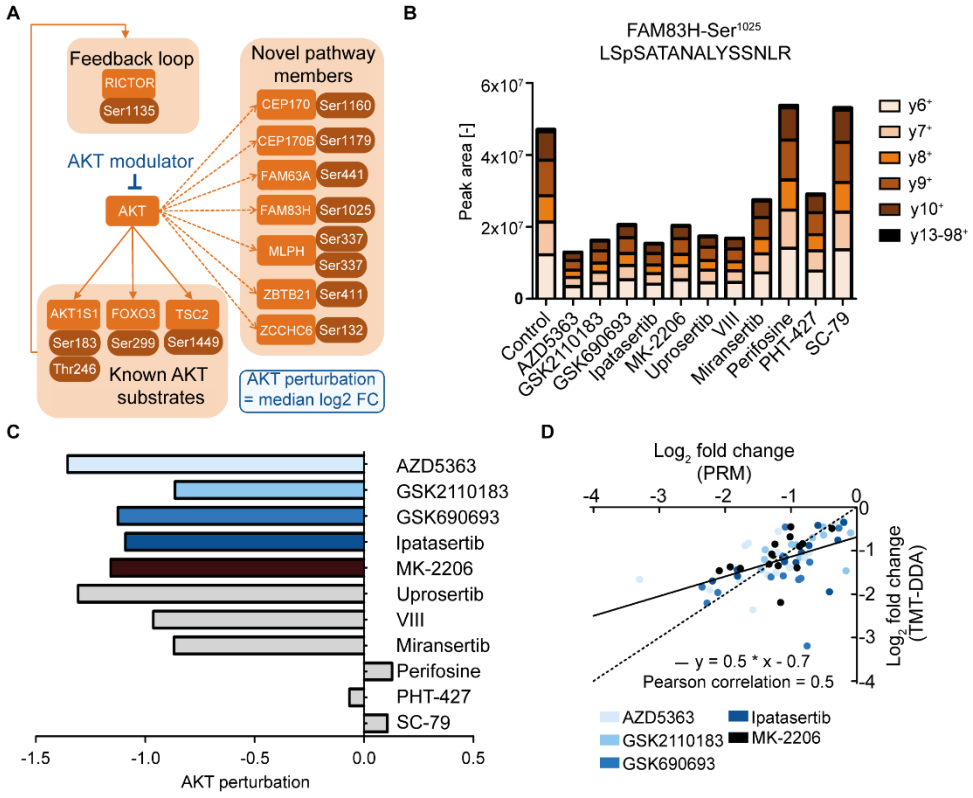

Figure III-8: Phospho-PRM assay to validate action of AKT modulators. (A) Covered 13 p-peptides representing known and novel AKT pathway members are presented in a schematic overview. (B) Summed intensities of selected precursor ions, exemplified here for FAM83H-Ser^{1025}, upon treatment with AKT modulators AZD5363, GSK2110183, GSK690693, Ipatasertib, MK-2206, Uprosertib, VIII, Miransertib, Perifosine, PHT-427 and SC-79. (C) AKT perturbation score for each AKT modulator. (D) Scatter plot of log2 FC of the 13 p-peptides, which were covered both in the TMT-DDA and PRM dataset, upon AKT inhibitor treatment. The nodes are colored according to the AKT inhibitor. Linear regression is indicated by a solid line and the Pearson correlation coefficient is highlighted. The identity line is shown with a dotted line. Data represent N = 3-4 biologically independent experiments.

The discrepancy between the PRM and DDA-TMT phosphorylation intensity can be explained by the potential influence of ratio compression on the quantification of p-peptide intensity in the DDA-TMT experiment, which may be hinted by overall higher $\log_2$ FCs in the PRM assay. Uprosertib, VIII and Miransertib showed comparable perturbation scores of -1, akin to the first five compounds, or below but PHT-427, Perifosine and SC-79 had no perceptible effect on the phosphorylation status on the p-peptides in this assay. The missing effect of Perifosine on target engagement as well as action on downstream signaling is contradicting earlier reports [54] and may be only explained by so far not known differences in the molecular setup of the compound used in this experiment. SC-79, on the other hand, might not have shown effects due to an already complete activation of AKT signaling through HER2 overexpression in BT-474 cells. Surprisingly, allosteric Miransertib and PHT-427 have shown

controversial results by demonstrating either action on AKT in the Western Blot but not on AKT pathway members in the PRM assay or vice versa. This might be explained by a different mode of AKT binding by the compounds, which influences the AKT phosphorylation status. Especially the latter result stresses the point to employ an assay, which not only covers markers for target engagement but takes (several) downstream signaling events into account to comprehensively understand the action of a certain compound on a biological system. While Western Blotting is limited by the sheer number of markers to include as well as the availability of notably phospho-antibodies to fulfill this task, a PRM assay as presented here may be the superior technique.

3.4 Novel AKT substrates are among AKT network members

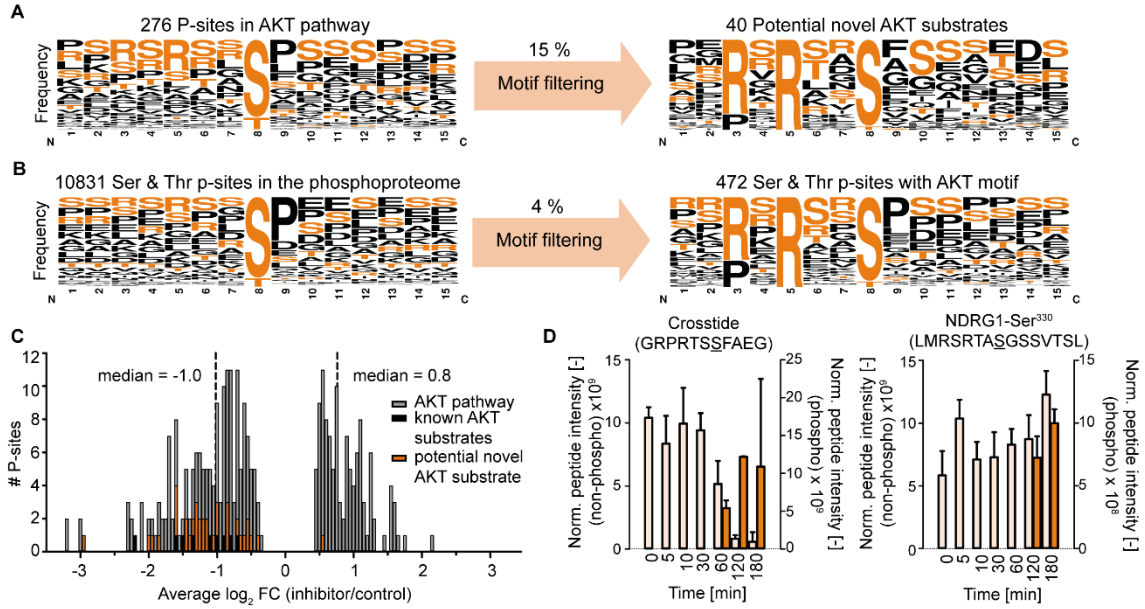

Figure III-9: In-vitro kinase assay to confirm novel AKT2 substrates. (A) Frequency sequence logos showing amino acid distribution around the 276 AKT pathway p-sites (left) and 40 potential novel AKT substrates harboring the AKT motif (right) ± seven residues. (B) Frequency sequence logos showing amino acid distribution around all quantified Ser and Thr p-sites (left) and Ser and Thr p-sites harboring the AKT motif (right) ± seven residues. (C) Histogram of averaged log_2 FC among all 276 AKT pathway p-sites. Known AKT substrates (black) and potential novel AKT substrates (orange) are highlighted. Median averaged log_2 FCs are indicated. (D) Normalized peptide intensities of non-phosphorylated and phosphorylated Crosstide (left) and NDRG1-Ser^{330} (right) after 0, 5, 10, 30, 60, 120 or 180 min incubation in the AKT2 kinase assay. Data represent *N* = 3-4 (A-C) and *N* = 3 (D) independent experiments. Error bars represent SD.

50 of the 276 commonly regulated p-sites in the AKT network harbored the AKT substrate motif (18%), from which nine were reported and 40 potentially novel AKT substrates (Figure III-9A). Compared to the complete phosphoproteomic dataset, in which 472 of the 10,831 total Ser and Thr p-sites harbored the AKT motif (4 %; Figure III-9B), the AKT network revealed an enrichment for the AKT substrate

motif. Treatment with the five AKT inhibitors led to reduced phosphorylation intensity of all known and novel but one novel AKT substrate p-sites (Figure III-9C), which highlights the potential to find novel substrates in the dataset.

In order to validate novel substrates biochemically, a kinetic *in vitro* AKT assay was executed for all 40 potential novel AKT substrate p-sites using synthetic peptides (15-mers) containing the candidate p-site and using LC-MS/MS for quantification. Since the substrate specificity among the 3 AKT isoforms is similar, AKT2 was chosen to be used in the assay to represent all AKT isoforms. Crosstide, which resembles GSK3B-Ser^{9}, and metastasis suppressor and autophagy inhibitor NDRG1-Ser^{330} [55, 56] were used as positive controls and were robustly phosphorylated in this assay (Figure III-9D). The rather slow kinetics of the phosphorylation could be explained by the pool of peptides, in which the peptides competed each other for phosphorylation by AKT2.

15 peptide candidates were verified to be phosphorylated by AKT2, uncovering regulatory functions for AKT in novel cellular contexts. Motif-specificity was assessed by analyzing the ability of AKT2 to phosphorylate Ser/Thr to Ala-mutants of the respective peptides. None of these mutants were phosphorylated by AKT2 on another Ser or Thr residue within the novel substrate candidates. For example, CEP170-Ser^{1160} and FAM83H-Ser^{1025} were among the 15 novel AKT substrates (Figure III-10), which could display a direct regulatory role of AKT in centrosomal and cytoskeletal organization, respectively. CEP170 is a fundamental part of the centrosome during mitosis and perturbed mitosis by altered CEP170 function could be fatal for cancerous as well as healthy cells [57]. The potential kinase-substrate relationship between AKT and CEP170 could complement earlier literature showing that AKT is localized to centrosomes during mitosis and is involved in the regulation of centrosome migration and spindle orientation [58, 59]. AKT-regulated FAM83H activity, on the other hand, may interfere with the organization of the keratin cytoskeleton, which is necessary for cell migration [47]. Both CEP170 and FAM83H have been reported to be negative prognostic markers in several cancer types [60, 61] (Human Protein Atlas available from www.proteinatlas.org). Further experiments would be necessary to explore the consequences of phosphorylation by AKT on these proteins. However, one could speculate that this finding, in case of an activation of the proteins by AKT phosphorylation, may provide a rational for AKT inhibition in patients with elevated CEP170 and FAM83H expression levels.

Due to the fact that the validation of the novel AKT substrates was performed by using a recombinant kinase and synthetic peptides ex cellulo, further experiments would be necessary to finally proof direct kinase-substrate relationships on substrate protein-level as well as in a cellular environment. Still, the

linearity of the AKT substrate motif underscores the chance of using peptidic substrates in an AKT assay. In general, the strong enrichment for the AKT motif and the validation of novel AKT substrates by AKT2 assays reinforced the definition of an extended AKT pathway. Moreover, the general potential of deciphering kinase-substrate relationships from drug-perturbed phosphoproteomes treated with inhibitors harboring a common target spectrum has been underlined.

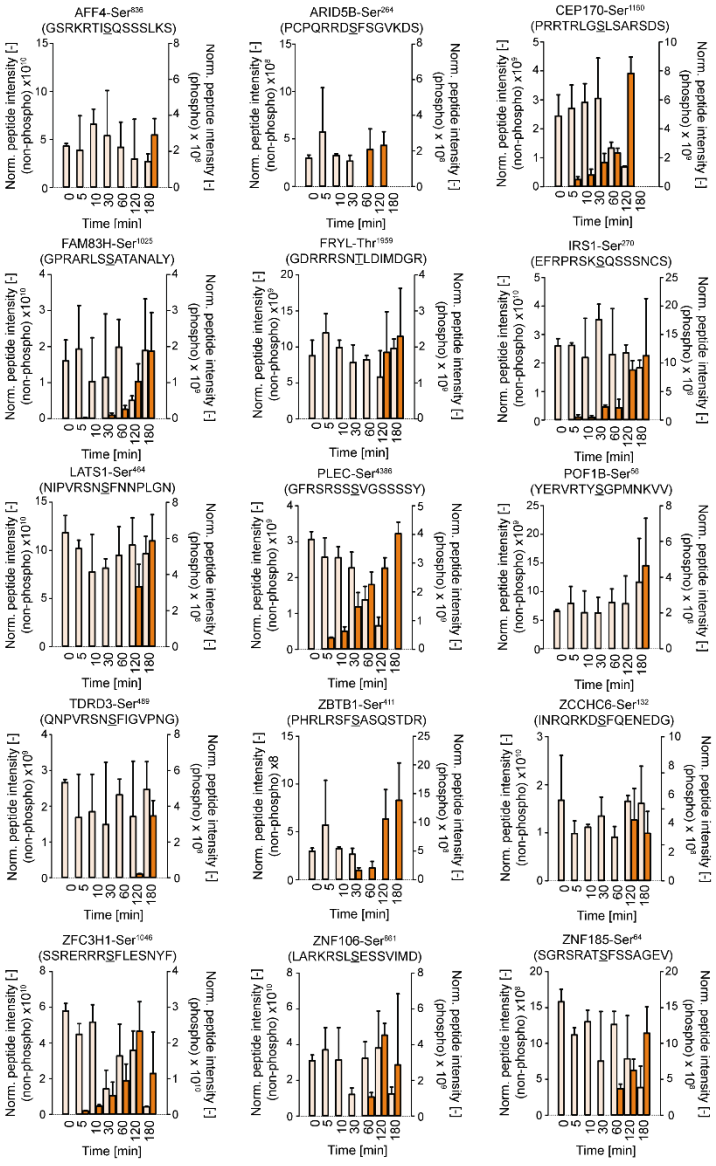

Figure III-10: Confirmed novel AKT2 substrates by *in vitro* kinase assays. Normalized peptide intensities of non-phosphorylated and phosphorylated AFF4-Ser^{836}, AIRD5B-Ser^{264}, FRYL-Thr^{1959} (first row, left to right), IRS1-Ser^{270}, LATS1-Ser^{464}, PLEC-Ser^{4272} (second row, left to right), POF1B-Ser^{56}, TDRD3-Ser^{489}, ZBTB1-Ser^{411} (third row, left to right), ZCCHC6-Ser^{132}, ZFC3H1-Ser^{1046}, ZNF106-Ser^{861} (fourth row, left to right) and ZNF185-Ser^{64} (last row) peptides after 0, 5, 10, 30, 60, 120 or 180 min incubation in the AKT2 kinase assay. Data represent *N* = 3 independent experiments. Error bars represent SD.

3.5 Secreted STC2 is a potential treatment marker for AKT inhibition

The phosphoproteomic data indicated the regulation of autophagy by AKT inhibition, which has been already reported to be based on both direct and indirect mechanisms [62]. Phosphorylation of initiator of autophagosome biogenesis ULK1 [63, 64] was regulated by AKT inhibition on several residues. Ser^{623}, Ser^{638} (phosphorylated by AMPK and mTOR) and Thr^{660} have shown a decrease in phosphorylation upon treatment with most AKT inhibitors. Ser^{341} (log_2 FC_{av}= 0.5) and Ser^{450} (log_2 FC_{av}= -1.0) were regulated by all drugs but neither of these p-sites have been functionally annotated, yet (Figure III-11A). On the contrary, phosphorylation of Ser^{465}, Ser^{467} (phosphorylated by AMPK) and Ser^{469} were not changed upon AKT inhibition. Indeed, experiments which have been carried out by Nils Gassen (University of Bonn) have demonstrated an increased autophagic flux upon treating BT-474 cells with MK-2206 (data not shown) proving an increase in ULK1 activity, which may be reflected by its phosphorylation status. Furthermore, ULK1 and 46 further (out of the 185 known and novel) AKT pathway members with perturbed p-sites upon AKT inhibition, are associated with autophagy according to the current literature. This indicated a more comprehensive direct and indirect regulation of the autophagy machinery by AKT activity than anticipated so far [62]. Reports are conflicting about whether ULK1 activity is a favorable [65] or an unfavorable prognostic marker in cancer [66]. This raises the question whether a substantial increase of functional autophagy in response to AKT inhibition as observed in this study would represent a benefit for patients or an on-target treatment liability.

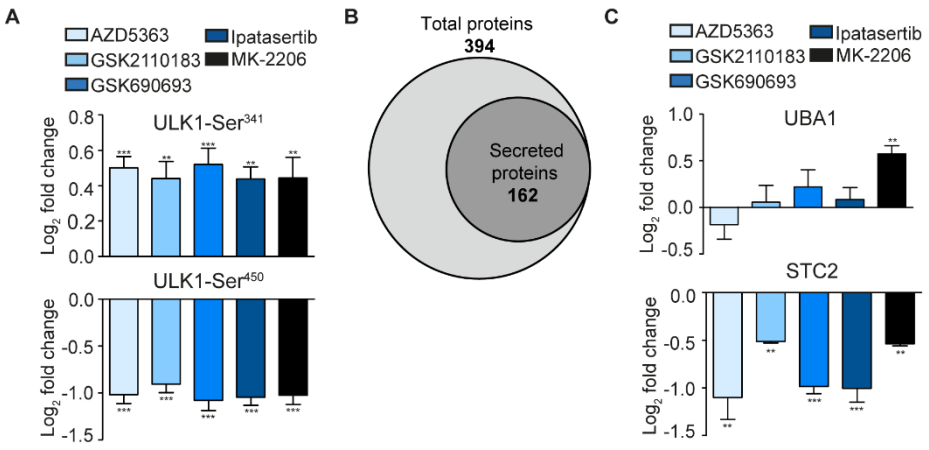

Figure III-11: Influence of the AKT inhibitors on autophagy and the secretome. (A) LC-MS^3 quantification of ULK1-Ser^{341} (top) and ULK1-Ser^{450} (bottom) p-site intensity upon AKT inhibitor treatment. (F) LC-MS^3 quantification of UBA1 intensity. Venn diagram of identified proteins in the secretome dataset and predicted secreted proteins thereof. (F) LC-MS^3 quantification of STC1 intensity upon AKT inhibitor treatment. Data represent *N* = 3 (A, D-F) and *N* = 4 (C) biologically independent experiments. Statistical analyses were performed by t-tests (FDR = 0.05, s = 0.1 or s = 0.09). Error bars represent SD. * P ≤ 0.05, ** P ≤ 0.01, *** P ≤ 0.001.

Reports have been suggesting that AKT influences lysosomal activity, especially during autophagy [67, 68] and that lysosomal damage shifts disruptive autophagy to secretion [69]. In order to study the potential influence of AKT inhibition on secreted proteins, deriving from autophagy or conventional mechanism, a mass spectrometry-based secretome analysis was carried out. Instead of facilitating the secretome analysis by serum starvation, a metabolic labeling strategy using AHA in a click chemistry-based approach to enrich secreted proteins from conditioned medium [21] in the presence or absence of the five AKT drugs was employed to avoid any further perturbation of cell signaling. 394 proteins were identified and quantified, of which 41 % were predicted to be secreted (according to the Human Protein Atlas [70], www.proteinatlas.org) or annotated to be secreted in Uniprot [29] (Figure III-11B). 19 proteins of the latter have been reported to be secreted by an autophagy-mediated process [71]. Here, however, only UBA1 showed significantly increased secretion in response to MK-2206 ($\log_2 FC_{av} = 0.57$) but no other AKT inhibitor (Figure III-11C top). A significant decrease in protein secretion upon drug treatment (four compounds) was found for one single protein, Stanniocalcin-2 STC2 [72-74] ($\log_2 FC_{av} = -0.83$) (Figure III-11C bottom). These results suggest that AKT inhibition drugs do not generally lead to altered protein secretion. However, the decrease in STC2 level after AKT inhibitor treatment might be of interest since the protein has been suggested to serve as an unfavorable prognostic marker for several cancers including hepatocellular and ovarian carcinomas [75, 76]. Furthermore, STC2 has been already detected in the plasma of breast cancer patients [74]. STC2 therefore could putatively serve as a plasma-accessible treatment response marker in patients undergoing AKT inhibitory therapy.

Acknowledgements

I would like to thank Dr. Benjamin Ruprecht for initializing the project, Andreas Klaus for in-gel digestion of kinobead eluates, Andrea Hubauer for establishing AKT Western Blots, Dr. Runsheng Zheng for assisting with peptide synthesis, Dr. Martin Frejno for helping with correlation analyses, and Dr. Daniel Zolg and Dr. Tina Ludwig for training on PRM assays and Skyline. I am indebted to Theresa Siekmann for performing the secretome experiments during her M.Sc. thesis under my supervision. I also gratefully acknowledge Dr. Elena Kunold and Prof. Dr. Stephan Sieber (Department of Organic Chemistry II, Technical University of Munich) for the LC-MS^3 measurement of the TMT-phospho samples, and Dr. Nils Gassen and Kathrin Hafner (Max Planck Institute of Psychiatry, Munich) for the fruitful collaboration including the autophagy experiments and all related discussions.

References

1. Burgering BM, Coffer PJ: Protein kinase B (c-Akt) in phosphatidylinositol-3-OH kinase signal transduction. *Nature* 1995, 376(6541):599-602.
2. Franke TF, Yang S-I, Chan TO, Datta K, Kazlauskas A, Morrison DK, Kaplan DR, Tsichlis PN: The protein kinase encoded by the Akt proto-oncogene is a target of the PDGF-activated phosphatidylinositol 3-kinase. *Cell* 1995, 81(5):727-736.
3. Kohn AD, Kovacina KS, Roth RA: Insulin stimulates the kinase activity of RAC-PK, a pleckstrin homology domain containing ser/thr kinase. *The EMBO Journal* 1995, 14(17):4288-4295.
4. James SR, Downes CP, Gigg R, Grove SJ, Holmes AB, Alessi DR: Specific binding of the Akt-1 protein kinase to phosphatidylinositol 3,4,5-trisphosphate without subsequent activation. *Biochemical Journal* 1996, 315(Pt 3):709-713.
5. Alessi DR, Andjelkovic M, Caudwell B, Cron P, Morrice N, Cohen P, Hemmings BA: Mechanism of activation of protein kinase B by insulin and IGF-1. *Embo j* 1996, 15(23):6541-6551.
6. Alessi DR, Caudwell FB, Andjelkovic M, Hemmings BA, Cohen P: Molecular basis for the substrate specificity of protein kinase B; comparison with MAPKAP kinase-1 and p70 S6 kinase. *FEBS Lett* 1996, 399(3):333-338.
7. Lien EC, Lyssiotis CA, Juvekar A, Hu H, Asara JM, Cantley LC, Toker A: Glutathione biosynthesis is a metabolic vulnerability in PI(3)K/Akt-driven breast cancer. *Nature cell biology* 2016, 18(5):572-578.
8. Lindhurst MJ, Sapp JC, Teer JK, Johnston JJ, Finn EM, Peters K, Turner J, Cannons JL, Bick D, Blakemore L *et al*: A mosaic activating mutation in AKT1 associated with the Proteus syndrome. *N Engl J Med* 2011, 365(7):611-619.
9. Fernandez-Hernando C, Ackah E, Yu J, Suarez Y, Murata T, Iwakiri Y, Prendergast J, Miao RQ, Birnbaum MJ, Sessa WC: Loss of Akt1 leads to severe atherosclerosis and occlusive coronary artery disease. *Cell metabolism* 2007, 6(6):446-457.
10. George S, Rochford JJ, Wolfrum C, Gray SL, Schinner S, Wilson JC, Soos MA, Murgatroyd PR, Williams RM, Acerini CL *et al*: A family with severe insulin resistance and diabetes due to a mutation in AKT2. *Science* 2004, 304(5675):1325-1328.
11. Crino PB, Nathanson KL, Henske EP: The tuberous sclerosis complex. *N Engl J Med* 2006, 355(13):1345-1356.
12. Zhang Y, Kwok-Shing Ng P, Kucherlapati M, Chen F, Liu Y, Tsang YH, de Velasco G, Jeong KJ, Akbani R, Hadjipanayis A *et al*: A Pan-Cancer Proteogenomic Atlas of PI3K/AKT/mTOR Pathway Alterations. *Cancer Cell* 2017, 31(6):820-832.e823.
13. Yang J, Cron P, Good VM, Thompson V, Hemmings BA, Barford D: Crystal structure of an activated Akt/protein kinase B ternary complex with GSK3-peptide and AMP-PNP. *Nature structural biology* 2002, 9(12):940-944.
14. Davies BR, Greenwood H, Dudley P, Crafter C, Yu D-H, Zhang J, Li J, Gao B, Ji Q, Maynard J *et al*: Preclinical Pharmacology of AZD5363, an Inhibitor of AKT: Pharmacodynamics, Antitumor Activity, and Correlation of Monotherapy Activity with Genetic Background. *Molecular Cancer Therapeutics* 2012, 11(4):873.
15. Chandarlapaty S, Sawai A, Scaltriti M, Rodrik-Outmezguine V, Grbovic-Huezo O, Serra V, Majumder PK, Baselga J, Rosen N: AKT inhibition relieves feedback suppression of receptor tyrosine kinase expression and activity. *Cancer Cell* 2011, 19(1):58-71.

16. Crouthamel MC, Kahana JA, Korenchuk S, Zhang SY, Sundaresan G, Eberwein DJ, Brown KK, Kumar R: Mechanism and management of AKT inhibitor-induced hyperglycemia. *Clin Cancer Res* 2009, 15(1):217-225.
17. Castro F, Dirks WG, Fahnrich S, Hotz-Wagenblatt A, Pawlita M, Schmitt M: High-throughput SNP-based authentication of human cell lines. *Int J Cancer* 2013, 132(2):308-314.
18. Medard G, Pachl F, Ruprecht B, Klaeger S, Heinzlmeir S, Helm D, Qiao H, Ku X, Wilhelm M, Kuehne T *et al*: Optimized chemical proteomics assay for kinase inhibitor profiling. *J Proteome Res* 2015, 14(3):1574-1586.
19. Ruprecht B, Koch H, Medard G, Mundt M, Kuster B, Lemeer S: Comprehensive and reproducible phosphopeptide enrichment using iron immobilized metal ion affinity chromatography (Fe-IMAC) columns. *Mol Cell Proteomics* 2015, 14(1):205-215.
20. Rappsilber J, Mann M, Ishihama Y: Protocol for micro-purification, enrichment, pre-fractionation and storage of peptides for proteomics using StageTips. *Nat Protoc* 2007, 2(8):1896-1906.
21. Eichelbaum K, Winter M, Diaz MB, Herzig S, Krijgsveld J: Selective enrichment of newly synthesized proteins for quantitative secretome analysis. *Nat Biotech* 2012, 30(10):984-990.
22. Cox J, Hein MY, Luber CA, Paron I, Nagaraj N, Mann M: Accurate proteome-wide label-free quantification by delayed normalization and maximal peptide ratio extraction, termed MaxLFQ. *Mol Cell Proteomics* 2014, 13(9):2513-2526.
23. Ritz C, Baty F, Streibig JC, Gerhard D: Dose-Response Analysis Using R. *PLoS One* 2015, 10(12):e0146021.
24. Tyanova S, Temu T, Sinitcyn P, Carlson A, Hein MY, Geiger T, Mann M, Cox J: The Perseus computational platform for comprehensive analysis of (prote)omics data. *Nat Meth* 2016, 13(9):731-740.
25. Szklarczyk D, Morris JH, Cook H, Kuhn M, Wyder S, Simonovic M, Santos A, Doncheva NT, Roth A, Bork P *et al*: The STRING database in 2017: quality-controlled protein-protein association networks, made broadly accessible. *Nucleic Acids Res* 2017, 45(D1):D362-d368.
26. Crooks GE, Hon G, Chandonia JM, Brenner SE: WebLogo: a sequence logo generator. *Genome research* 2004, 14(6):1188-1190.
27. MacLean B, Tomazela DM, Shulman N, Chambers M, Finney GL, Frewen B, Kern R, Tabb DL, Liebler DC, MacCoss MJ: Skyline: an open source document editor for creating and analyzing targeted proteomics experiments. *Bioinformatics (Oxford, England)* 2010, 26(7):966-968.
28. Uhlén M, Fagerberg L, Hallström BM, Lindskog C, Oksvold P, Mardinoglu A, Sivertsson Å, Kampf C, Sjöstedt E, Asplund A *et al*: Tissue-based map of the human proteome. *Science* 2015, 347(6220).
29. The UniProt Consortium: UniProt: the universal protein knowledgebase. *Nucleic Acids Research* 2017, 45(D1):D158-D169.
30. Klaeger S, Heinzlmeir S, Wilhelm M, Polzer H, Vick B, Koenig PA, Reinecke M, Ruprecht B, Petzoldt S, Meng C *et al*: The target landscape of clinical kinase drugs. *Science* 2017, 358(6367).
31. Ruprecht B, Zaal EA, Zecha J, Wu W, Berkers CR, Kuster B, Lemeer S: Lapatinib Resistance in Breast Cancer Cells Is Accompanied by Phosphorylation-Mediated Reprogramming of Glycolysis. *Cancer Research* 2017, 77(8):1842-1853.
32. LoRusso P, Hurwitz H, Chiorean E, Jewell R, Lampkin T, Bachman K, Kumar R, Lebowitz P, Weber B: AKT inhibitor GSK690693: Preliminary results from the first time in human study. *Cancer Research* 2008, 68(9 Supplement):LB-68-LB-68.
33. Heerding DA, Rhodes N, Leber JD, Clark TJ, Keenan RM, Lafrance LV, Li M, Safonov IG, Takata DT, Venslavsky JW *et al*: Identification of 4-(2-(4-amino-1,2,5-oxadiazol-3-yl)-1-ethyl-

7-{[(3S)-3-piperidinylmethyl]oxy}-1H- imidazo[4,5-c]pyridin-4-yl)-2-methyl-3-butyn-2-ol (GSK690693), a novel inhibitor of AKT kinase. *Journal of medicinal chemistry* 2008, 51(18):5663-5679.

34. Hirai H, Sootome H, Nakatsuru Y, Miyama K, Taguchi S, Tsujioka K, Ueno Y, Hatch H, Majumder PK, Pan B-S *et al*: MK-2206, an Allosteric Akt Inhibitor, Enhances Antitumor Efficacy by Standard Chemotherapeutic Agents or Molecular Targeted Drugs In vitro and In vivo. *Molecular Cancer Therapeutics* 2010, 9(7):1956.
35. Addie M, Ballard P, Buttar D, Crafter C, Currie G, Davies BR, Debreczeni J, Dry H, Dudley P, Greenwood R *et al*: Discovery of 4-amino-N-[(1S)-1-(4-chlorophenyl)-3-hydroxypropyl]-1-(7H-pyrrolo[2,3-d]pyrimidin -4-yl)piperidine-4-carboxamide (AZD5363), an orally bioavailable, potent inhibitor of Akt kinases. *Journal of medicinal chemistry* 2013, 56(5):2059-2073.
36. Dumble M, Crouthamel M-C, Zhang S-Y, Schaber M, Levy D, Robell K, Liu Q, Figueroa DJ, Minthorn EA, Seefeld MA *et al*: Discovery of Novel AKT Inhibitors with Enhanced Anti-Tumor Effects in Combination with the MEK Inhibitor. *PLoS ONE* 2014, 9(6):e100880.
37. Blake JF, Xu R, Bencsik JR, Xiao D, Kallan NC, Schlachter S, Mitchell IS, Spencer KL, Banka AL, Wallace EM *et al*: Discovery and Preclinical Pharmacology of a Selective ATP-Competitive Akt Inhibitor (GDC-0068) for the Treatment of Human Tumors. *Journal of medicinal chemistry* 2012, 55(18):8110-8127.
38. Klaeger S, Heinzlmeir S, Wilhelm M, Polzer H, Vick B, Koenig P-A, Reinecke M, Ruprecht B, Petzoldt S, Meng C *et al*: The target landscape of clinical kinase drugs. *Science* 2017, 358(6367).
39. Reinecke M, Ruprecht B, Poser S, Wiechmann S, Wilhelm M, Heinzlmeir S, Kuster B, Medard G: Chemoproteomic Selectivity Profiling of PIKK and PI3K Kinase Inhibitors. *ACS Chem Biol* 2019.
40. Klaeger S, Gohlke B, Perrin J, Gupta V, Heinzlmeir S, Helm D, Qiao H, Bergamini G, Handa H, Savitski MM *et al*: Chemical Proteomics Reveals Ferrochelatase as a Common Off-target of Kinase Inhibitors. *ACS Chemical Biology* 2016, 11(5):1245-1254.
41. Savitski MM, Reinhard FB, Franken H, Werner T, Savitski MF, Eberhard D, Martinez Molina D, Jafari R, Dovega RB, Klaeger S *et al*: Tracking cancer drugs in living cells by thermal profiling of the proteome. *Science* 2014, 346(6205):1255784.
42. Doi T, Tamura K, Tanabe Y, Yonemori K, Yoshino T, Fuse N, Kodaira M, Bando H, Noguchi K, Shimamoto T *et al*: Phase 1 pharmacokinetic study of the oral pan-AKT inhibitor MK-2206 in Japanese patients with advanced solid tumors. *Cancer chemotherapy and pharmacology* 2015, 76(2):409-416.
43. Song Ff, Xia Ll, Ji P, Tang Yb, Huang Zm, Zhu L, Zhang J, Wang Jq, Zhao Gp, Ge Hl *et al*: Human dCTP pyrophosphatase 1 promotes breast cancer cell growth and stemness through the modulation on 5-methyl-dCTP metabolism and global hypomethylation. *Oncogenesis* 2015, 4:e159.
44. Barnett Stanley F, Defeo-Jones D, Fu S, Hancock Paula J, Haskell Kathleen M, Jones Raymond E, Kahana Jason A, Kral Astrid M, Leander K, Lee Ling L *et al*: Identification and characterization of pleckstrin-homology-domain-dependent and isoenzyme-specific Akt inhibitors. *Biochemical Journal* 2005, 385(2):399.
45. Calleja V, Laguerre M, Parker PJ, Larijani B: Role of a Novel PH-Kinase Domain Interface in PKB/Akt Regulation: Structural Mechanism for Allosteric Inhibition. *PLoS Biology* 2009, 7(1):e1000017.

46. Guarguaglini G, Duncan PI, Stierhof YD, Holmström T, Duensing S, Nigg EA: The Forkhead-associated Domain Protein Cep170 Interacts with Polo-like Kinase 1 and Serves as a Marker for Mature Centrioles. *Molecular Biology of the Cell* 2005, 16(3):1095-1107.
47. Kuga T, Kume H, Kawasaki N, Sato M, Adachi J, Shiromizu T, Hoshino I, Nishimori T, Matsubara H, Tomonaga T: A novel mechanism of keratin cytoskeleton organization through casein kinase Ialpha and FAM83H in colorectal cancer. *Journal of cell science* 2013, 126(Pt 20):4721-4731.
48. Dumble M, Crouthamel MC, Zhang SY, Schaber M, Levy D, Robell K, Liu Q, Figueroa DJ, Minthorn EA, Seefeld MA *et al*: Discovery of novel AKT inhibitors with enhanced anti-tumor effects in combination with the MEK inhibitor. *PLoS One* 2014, 9(6):e100880.
49. Zhao Z, Leister WH, Robinson RG, Barnett SF, Defeo-Jones D, Jones RE, Hartman GD, Huff JR, Huber HE, Duggan ME *et al*: Discovery of 2,3,5-trisubstituted pyridine derivatives as potent Akt1 and Akt2 dual inhibitors. *Bioorganic & medicinal chemistry letters* 2005, 15(4):905-909.
50. Yu Y, Savage RE, Eathiraj S, Meade J, Wick MJ, Hall T, Abbadessa G, Schwartz B: Targeting AKT1-E17K and the PI3K/AKT Pathway with an Allosteric AKT Inhibitor, ARQ 092. *PLoS ONE* 2015, 10(10):e0140479.
51. Hilgard P, Klenner T, Stekar J, Nössner G, Kutscher B, Engel J: D-21266, a new heterocyclic alkylphospholipid with antitumour activity. *European Journal of Cancer* 1997, 33(3):442-446.
52. Moses SA, Ali MA, Zuohe S, Du-Cuny L, Zhou LL, Lemos R, Ihle N, Skillman AG, Zhang S, Mash EA *et al*: In vitro and in vivo activity of novel small-molecule inhibitors targeting the pleckstrin homology domain of protein kinase B/AKT. *Cancer Res* 2009, 69(12):5073-5081.
53. Jo H, Mondal S, Tan D, Nagata E, Takizawa S, Sharma AK, Hou Q, Shanmugasundaram K, Prasad A, Tung JK *et al*: Small molecule-induced cytosolic activation of protein kinase Akt rescues ischemia-elicited neuronal death. *Proceedings of the National Academy of Sciences of the United States of America* 2012, 109(26):10581-10586.
54. Hennessy BT, Lu Y, Poradosu E, Yu Q, Yu S, Hall H, Carey MS, Ravoori M, Gonzalez-Angulo AM, Birch R *et al*: Pharmacodynamic Markers of Perifosine Efficacy. *Clinical Cancer Research* 2007, 13(24):7421-7431.
55. Sahni S, Bae DH, Lane DJ, Kovacevic Z, Kalinowski DS, Jansson PJ, Richardson DR: The metastasis suppressor, N-myc downstream-regulated gene 1 (NDRG1), inhibits stress-induced autophagy in cancer cells. *J Biol Chem* 2014, 289(14):9692-9709.
56. Murray JT, Campbell DG, Morrice N, Auld GC, Shpiro N, Marquez R, Peggie M, Bain J, Bloomberg GB, Grahammer F *et al*: Exploitation of KESTREL to identify NDRG family members as physiological substrates for SGK1 and GSK3. *The Biochemical journal* 2004, 384(Pt 3):477-488.
57. Guarguaglini G, Duncan PI, Stierhof YD, Holmstrom T, Duensing S, Nigg EA: The forkhead-associated domain protein Cep170 interacts with Polo-like kinase 1 and serves as a marker for mature centrioles. *Mol Biol Cell* 2005, 16(3):1095-1107.
58. Wakefield J, Stephens D, Tavaré J: A role for glycogen synthase kinase-3 in mitotic spindle dynamics and chromosome alignment, vol. 116; 2003.
59. Buttrick GJ, Beaumont LM, Leitch J, Yau C, Hughes JR, Wakefield JG: Akt regulates centrosome migration and spindle orientation in the early Drosophila melanogaster embryo. *The Journal of cell biology* 2008, 180(3):537-548.
60. Kim KM, Park SH, Bae JS, Noh SJ, Tao GZ, Kim JR, Kwon KS, Park HS, Park BH, Lee H *et al*: FAM83H is involved in the progression of hepatocellular carcinoma and is regulated by MYC. *Sci Rep* 2017, 7(1):3274.

61. Uhlen M, Zhang C, Lee S, Sjöstedt E, Fagerberg L, Bidkhori G, Benfeitas R, Arif M, Liu Z, Edfors F *et al*: A pathology atlas of the human cancer transcriptome. *Science* 2017, 357(6352):eaan2507.
62. Wang RC, Wei Y, An Z, Zou Z, Xiao G, Bhagat G, White M, Reichelt J, Levine B: Akt-mediated regulation of autophagy and tumorigenesis through Beclin 1 phosphorylation. *Science* 2012, 338(6109):956-959.
63. Chan EYW, Kir S, Tooze SA: siRNA Screening of the Kinome Identifies ULK1 as a Multidomain Modulator of Autophagy. *Journal of Biological Chemistry* 2007, 282(35):25464-25474.
64. Matsuura A, Tsukada M, Wada Y, Ohsumi Y: Apg1p, a novel protein kinase required for the autophagic process in Saccharomyces cerevisiae. *Gene* 1997, 192(2):245-250.
65. Zhang L, Fu L, Zhang S, Zhang J, Zhao Y, Zheng Y, He G, Yang S, Ouyang L, Liu B: Discovery of a small molecule targeting ULK1-modulated cell death of triple negative breast cancer in vitro and in vivo. *Chemical science* 2017, 8(4):2687-2701.
66. Zhang HY, Ma YD, Zhang Y, Cui J, Wang ZM: Elevated levels of autophagy-related marker ULK1 and mitochondrion-associated autophagy inhibitor LRPPRC are associated with biochemical progression and overall survival after androgen deprivation therapy in patients with metastatic prostate cancer. *Journal of clinical pathology* 2017, 70(5):383-389.
67. Hirata N, Suizu F, Matsuda-Lennikov M, Tanaka T, Edamura T, Ishigaki S, Donia T, Lithanatudom P, Obuse C, Iwanaga T *et al*: Functional characterization of lysosomal interaction of Akt with VRK2. *Oncogene* 2018, 37(40):5367-5386.
68. Palmieri M, Pal R, Nelvagal HR, Lotfi P, Stinnett GR, Seymour ML, Chaudhury A, Bajaj L, Bondar VV, Bremner L *et al*: mTORC1-independent TFEB activation via Akt inhibition promotes cellular clearance in neurodegenerative storage diseases. *Nat Commun* 2017, 8:14338.
69. Kimura T, Jia J, Claude-Taupin A, Kumar S, Choi SW, Gu Y, Mudd M, Dupont N, Jiang S, Peters R *et al*: Cellular and molecular mechanism for secretory autophagy. *Autophagy* 2017, 13(6):1084-1085.
70. Thul PJ, Akesson L, Wiking M, Mahdessian D, Geladaki A, Ait Blal H, Alm T, Asplund A, Bjork L, Breckels LM *et al*: A subcellular map of the human proteome. *Science* 2017, 356(6340).
71. Kimura T, Jia J, Kumar S, Choi SW, Gu Y, Mudd M, Dupont N, Jiang S, Peters R, Farzam F *et al*: Dedicated SNAREs and specialized TRIM cargo receptors mediate secretory autophagy. *Embo j* 2017, 36(1):42-60.
72. Jellinek DA, Chang AC, Larsen MR, Wang X, Robinson PJ, Reddel RR: Stanniocalcin 1 and 2 are secreted as phosphoproteins from human fibrosarcoma cells. *The Biochemical journal* 2000, 350 Pt 2:453-461.
73. Wagner GF, Jaworski EM, Haddad M: Stanniocalcin in the seawater salmon: structure, function, and regulation. *The American journal of physiology* 1998, 274(4 Pt 2):R1177-1185.
74. Zawadzka AM, Schilling B, Cusack MP, Sahu AK, Drake P, Fisher SJ, Benz CC, Gibson BW: Phosphoprotein Secretome of Tumor Cells as a Source of Candidates for Breast Cancer Biomarkers in Plasma. *Molecular & Cellular Proteomics* 2014, 13(4):1034-1049.
75. Wang H, Wu K, Sun Y, Li Y, Wu M, Qiao Q, Wei Y, Han Z-G, Cai B: STC2 is upregulated in hepatocellular carcinoma and promotes cell proliferation and migration in vitro. *BMB Reports* 2012, 45(11):629-634.
76. Wu J, Lai M, Shao C, Wang J, Wei JJ: STC2 overexpression mediated by HMGA2 is a biomarker for aggressiveness of high-grade serous ovarian cancer. *Oncology reports* 2015, 34(3):1494-1502.

Abbreviations

ACN	Acetonitrile
AGC	Automatic gain control
AHA	Azidohomoalanine
ATP	Adenosine triphosphate
CAA	Chloroacetamide
CID	Collision-induced dissociation
DDA	Data-dependent acquisition
DMEM	Dulbecco's modified Eagle's medium
DMSO	Dimethylsulfoxide
EC50	Half maximal effective concentration
EDTA	Ethylenediaminetetraacetic acid
FA	Formic acid
FBS	Fetal bovine serum
FC	Fold change
FDR	False discovery rate
HCD	Higher energy collision-induced dissociation
HEPES	4-(2-hydroxyethyl)-1-piperazineethanesulfonic acid
HPLC	High performance liquid chromatography
IC50	Half maximal inhibitory concentration
IMAC	Immobilized metal ion affinity chromatography
Kdapp	Apparent affinity constant
LC-MS/MS	Liquid chromatography tandem mass spectrometry
LTQ	Linear trap quadropole
MS1	Mass spectrum of intact peptides
MS2	Fragment mass spectrum of MS1 precursor
MS3	Fragment mass spectrum of MS2 precursor
nanoLC	Nano flow liquid chromatography
NCE	Normalized collision energy
PBS	Phosphate-buffered saline
PH	Pleckstrin homology
P-peptide	Phosphorylated peptide
PPM	Parts per million
P-proteins	Phosphorylated protein
P-site	Phosphorylation site
RTK	Receptor tyrosine kinase
SD	Standard deviation
SDS-PAGE	Sodiumdodecylsulfate polyacrylamide gel electrophoresis
STR	Short tandem repeat
TFA	Trifluoroacetic acid
TMT	Tandem mass tags
Tris	Tris(hydroxymethyl)aminomethane

List of figures

IV Mode of action of anti-HER2 and anti-CD20 antibodies

Table of contents

Summary

The general lack of a comprehensive understanding of the direct mode of action of many approved therapeutic antibodies as well as high prevalence of low responses and relapses motivated to perform phosphoproteomic analyses of two selected classes of therapeutic antibodies - anti-HER2 antibodies pertuzumab and trastuzumab as well as anti-CD20 antibody rituximab. Cell line panels consisted of breast cancer cell lines BT-474, SK-BR-3 and MDA-MB-175, and B-cell lymphoma and lymphoblastoid cell lines SU-DHL-4, Ramos and ARH-77. These enabled a diverse platform to robustly study both common effects and resistance mechanisms of the drugs. In addition, concentration- and time-dependent drug application facilitated the characterization of responding phosphorylation events by their potency and temporal dynamics. A phosphoproteomic TMT10-based multiplexing sample preparation and data analysis workflow resulted in deep drug-perturbed phosphoproteomes of more than 12,000 p-sites for a multiplexed set. Phosphoproteomic changes of anti-HER2 drugs were mainly driven by lapatinib, which highlighted by > 2000 regulated p-sites. In contrast, the breast cancer phosphoproteomes have been only sparsely responsive towards anti-HER2 therapeutic antibodies. MAPK and MTOR signaling pathways were enriched in the drug-regulated phosphoproteomes and have validated responsiveness towards lapatinib but neither trastuzumab nor pertuzumab. Contrarily, sensitive B-cell lymphoma cells were comprehensively and increasingly perturbed over time in their phosphoproteomes by anti-CD20 mAb rituximab reaching several thousands of regulated p-sites. The observation that phosphorylated MAPK1/3 can serve as both rituximab-resistance and -treatment markers was additionally stressed by the sensitization of resistant cells towards rituximab by pharmacological inhibition of MAPK signaling pathway members. Further analyses highlighted the importance of MAPK1/3 activity for rituximab action by the localization of phosphorylated MAPK1/3 to the cell membrane. In addition, comprehensive pathway enrichment analysis has uncovered the importance of an early activation of calcium-dependent NFAT signaling. A cell cycle arrest by the phosphorylation-based regulation of the RB1/CDK/WEE1 axis among many other cell cycle proteins has been found to robustly take effect after several hours of treatment. In summary, the phosphoproteomic analysis revealed remarkably opposing capabilities of the therapeutic antibodies to exert direct actions on cancer cells and hint to novel response and resistance markers.

1 Introduction

Monoclonal antibodies (mAb´s) are heavily used in the therapy of many human diseases including hematological malignancies and solid cancer. They possess multiple mode of actions due to their multiple binding moieties. The recognition of the cancer cell is enabled by binding of the designated surface antigen by the Fab region. This commonly establishes a direct action on cellular signaling that drives the perturbation of cancer growth and survival. Engagement of effector cells and the complement system over the Fc terminus can further induce complement-dependent cytotoxicity (CDC), antibody-dependent cellular cytotoxicity (ADCC) and antibody-dependent cellular phagocytosis (ADCP) [1].

A renowned target of therapeutic mAbs is human epidermal growth factor receptor 2 (HER2), which promotes the progress of further signaling pathways (e.g. PI3K-AKT-MTOR and MAPK signaling) upon activation by dimerization. HER2 gene amplification and protein overexpression strongly correlate with tumor aggressiveness and decreased patient survival and is characteristic for~22 % of breast cancer tumors [2, 3]. The clinically approved antibodies pertuzumab and trastuzumab target different epitopes of HER2 [4, 5] and bear differing modes of actions. These include, apart from effector functions, distinct direct actions on the cancer cells [6, 7]. Trastuzumab inhibits mainly ligand-independent receptor dimerization and subsequent signaling by binding to the juxtamembrane region of the extracellular domain (ECD) of HER2 (subdomain IV). Contrarily, pertuzumab binds to HER2 domain II, the dimerization moiety, thereby mainly inhibiting ligand-dependent dimerization. While the therapy with trastuzumab demands HER2 overexpression, pertuzumab can be applied against tumors with a lower HER2 level. Due to its disruption of ligand-driven signaling, it shows efficacy in tumors that are driven by heregulin-stimulated HER2/HER3 dimerization. Trastuzumab is since its approval in 1998 standard-of-care first-line therapy for HER2-positive breast cancer tumors in an adjuvant as well as metastatic setting. A combination with chemotherapy (such as taxane agents) is often favored in the clinic [8]. Trastuzumab has also been showing efficacy in other HER2-positive cancer types such as gastric cancer [9]. The addition of pertuzumab to the combination of trastuzumab and docetaxel has furthermore improved clinical outcomes and is approved since 2012 as first-line treatment in HER2-positive metastatic breast cancer [10]. Still, an overall response rate of merely 40 % has been described for this treatment regimen [11]. The portfolio of anti-HER2 drugs furthermore comprises antibody conjugate trastuzumab emtansine and the two small molecule dual EGFR/HER2 inhibitor lapatinib and triple EGFR/HER2/HER3 inhibitor neratinib, which are all approved for breast cancer

therapy as well [12-14]. In addition, novel antibody–drug conjugates and bispecific antibodies targeting HER2 are also under investigation in clinical trials.

Another clinically successful class of therapeutic antibodies are anti-cluster of differentiation 20 (CD20) mAbs. CD20 is a non-glycosylated surface protein with four transmembrane domains assembling into homo-tetramers on the cell surface of, almost exclusively, B-cells [15]. CD20 is expressed in high levels during the B-cell development. However, it is not expressed in B-cell progenitors and no longer present in mature plasma cells [16]. The depletion of CD20 positive B-cells is less likely to cause permanent side effects since B-cells can be repopulated from immature naïve B-cells [17]. Furthermore, the humoral response against encountered pathogens remains functional [18]. Despite the fact that CD20 is involved in B cell receptor activation-dependent calcium intake, it is unclear whether CD20 itself is a calcium ion channel [19, 20]. Chimaric rituximab, which targets and depletes B-cells by binding CD20, was the first monoclonal antibody to receive clinical approval in 1997. It has since been used to treat various B-cell malignancies such as non-Hodgkin lymphoma (NHL) [21, 22] either as monotherapy or, more frequently, together with cyclophosphamide, doxorubicin, vincristine, and prednisone (R-CHOP) or kinase inhibitor ibrutinib [21, 23]. After its approval for rheumatoid arthritis in 2006, rituximab has been applied to lower the adaptive immune response in even further autoimmune diseases like multiple sclerosis and chronic graft-versus-host disease [24]. The described effects of rituximab include ADCC [25] and CDC [26, 27] alongside direct effects leading to compartmentalization of CD20 into lipid rafts and finally caspase-dependent and -independent apoptosis [28-30]. While R-CHOP is the standard-of-care therapy in NHL, low response rates are a difficulty seen in up to 20 % (primary) and 30 % (acquired resistance) of the patients [31]. Several novel anti-CD20 mAbs, which try to overcome some of rituximab´s shortcomings, are either already approved (ofatumumab, obinutuzumab and ocrelizumab) or are in development and possess alternative features such as an alternate binding epitope, humanization or altered glycosylation [32-34].

Albeit the clinical relevance of mAbs is undoubtedly immense, the detailed mode of actions are in many cases unknown. Particularly, the parallel actions of the Fab and the Fc terminus of the mAbs cause a complex impact on tumors *in vivo*, which complicates the study of their actions. Furthermore, the share of individual effects in the total mode of action is difficult to decipher. For instance, this is demonstrated by contradictory studies about the importance of ADCC in the actions of rituximab [35-37]. In order to contribute to an enhanced knowledge about the actions of mAbs, the hereinafter discussed experiments aimed to uncover molecular consequences of direct antigen engagement on a global scale. The ultimate

goal would be to suggest response markers that could be relevant *in vivo* and to understand underlying resistance mechanisms that are driven by the tumor itself. Therefore, a concentration- and time-dependent phosphoproteomic workflow was applied to gain insights into the action of two classes of therapeutic mAbs of pivotal importance in the treatment of solid and hematopoietic cancers, respectively: anti-HER2 pertuzumab and trastuzumab as well as anti-CD20 rituximab.

2 Material and methods

Therapeutic antibodies and small molecule inhibitors

Therapeutic antibodies trastuzumab (Herceptin, Roche) and rituximab (mabThera, Roche and Rixathon, Sandoz) were provided by the group of Tumorimmunology and Translational Immuntherapy of the Technical University of Munich. Pertuzumab (A2008), lapatinib (#S1028), dabrafenib (#2807), ibrutinib (#S2680), BMS-387032 (#S1145), rabusertib (#S2626), R-406 (#S2194), fostamatinib (#S2625), ulixertinib (#S7854), PH-797804 (#S2726) and trametinib (#S2673) were purchased from Selleckchem. ONO4059 (#HY-15771A) was obtained from MedChemExpress and MK-1775 (#A-1117) from Active Biochem.

Cell culture

BT-474, MDA-MB-175 and SK-BR-3 cells were cultured in Dulbecco's modified Eagle's medium (DMEM)/Hams F-12 (1:1) with 10 % fetal bovine serum (FBS), while SU-DHL-4, Ramos and ARH-77 cells were kept in RPMI 1640 with 10 % FBS. All cell lines were incubated at 37 °C and 5 % CO_2 and handled according to standard cell culture methods. Cell line authentication was accomplished by short tandem repeat (STR) profiling (Multiplexion, Heidelberg, Germany) [38]. For kinase inhibitor and mAb treatments, breast cancer cells were grown until a 70 % confluency was reached and the suspensions of the B cells were adjusted to 2.25 x 10^6 cells/mL. Subsequently, fresh medium supplemented with kinase inhibitor or mAb at the indicated concentration was added to the cells which were further incubated at 37 °C for the indicated times. Suspension cells were harvested by centrifuging for 1 min at 75 x g.

Metabolic cell assay with AlamarBlue

2 x 10^4 cells of the breast cancer cell lines and 5 x 10^3 cells of the B cell lines were seeded into a 96-well microtiter plate in triplicate or quadruplicate and incubated at 37 °C and 5 % CO_2. Directly afterwards (B cell lines) or after 24 h (breast cancer cell lines), dilutions of the kinase inhibitors or mAbs or combinations thereof in the indicated concentrations in medium were added to the cells. After a 72 h treatment, alamarBlue reagent (Thermo Fisher Scientific) was added 1:10 to each well. The fluorescence was quantified at λ_{ex} = 544 nm and λ_{em} = 584 nm on the microplate reader FluoStar Omega (BMG Labtech). Curve fitting was performed by using the non-linear least squares fit within GraphPad Prism (version 5.01).

Cytotoxic assay

2 x 10^4 BT-474 cells were seeded into a 96-well microtiter plate, distinct for this experiment in F-12K medium supplemented with 10% FBS, in quadruplicate and incubated at 37 °C and 5 % CO_2. After 24 h, IncuCyte Cytotox Green reagent (Essen Bioscience, #4633) was added to the medium in 1:5000 dilution. Live cell imaging was performed by capturing images every 2 hours with 10x magnification in the IncuCyte S3 System (EssenBioscience). Analysis of green fluorescence and confluency of cells was performed by using the integrated software (version 2018A). Curve fitting was performed by using the non-linear least squares fit within GraphPad Prism (version 5.01).

Protein concentration assay

The protein concentration in cell lysate was determined using the Coomassie Plus Bradford assay (Thermo Fisher Scientific) according to the protocol of the manufacturer.

Sample preparation for the (phospho)proteomic experiment

Immediately after the treatment, cells were lysed in 40 mM Tris(hydroxymethyl)aminomethane (Tris)-HCl pH 7.6, 8 M urea, ethylenediaminetetraacetic acid (EDTA)-free protease inhibitor (Roche) and phosphatase inhibitors (Roche). Lysate was centrifuged for 1 h at 21,000 x g und the supernatant was subjected to sample preparation. If not stated otherwise, 200 µg protein of cell lysate was reduced with 10 mM dithiothreitol (DTT) for 40 min at 56 °C and alkylated with 55 mM chloroacetamide (CAA) at room temperature in the dark for 20 min. After dilution of the urea concentration from 6 M to 1.5 M with 40 mM Tris-HCl pH 7.6, the proteins were digested in a 1:50 trypsin/substrate weight ratio overnight at 37 °C and 700 rpm. Desalting of the tryptic peptides was performed on Sep-Pak C18 50 mg columns or Sep-Pak tC18 100 mg plates (Waters) as described elsewhere in 0.07 % trifluoroacetic acid (TFA) in 50 % acetonitrile (ACN). If not stated otherwise, labeling of the desalted peptides was performed afterwards with tandem mass tags 10 (TMT10)-plex (Thermo Fisher Scientific) at a final concentration of 6.67 mM TMT according to instructions provided by the manufacturer except for a 1:2 TMT/peptide ratio. One TMT channel was used for each drug concentration (126 = vehicle control; from 127N = lowest drug concentration to 131 = highest drug concentration). Pooled phosphopeptides were enriched using Fe- immobilized metal ion affinity chromatography (IMAC) as previously described [39]. If applied, enriched phosphopeptides were subjected to phosphotyrosine immunoprecipitation enrichment by utilizing the PTMScan Phospho-Tyrosine Rabbit mAb (P-Tyr-1000) Kit (Cell Signaling Technology, #8803) according to the manufacturer´s protocol. Further purifying of phosphotyrosine peptides was performed in micro-column format (three discs, Ø 1.5 mm,

C18 material, 3M Empore per micro-column were used) either with C18 alone or biphasic as IMAC/C18 columns by addition of PHOS-Select Iron Affinity Gel-(Fe^{3+}-IMAC; Sigma Aldrich, #P9740) as described earlier [40]. Subsequently, phosphopeptides were separated into six fractions using basic reversed-phase (bRP) chromatography in micro-column format (five discs, Ø 1.5 mm, C18 material, 3M Empore per micro-column were used) in 25 mM NH_4COOH (pH 10). Peptides were fractionated with increasing ACN concentrations (5%, 7.5%, 10%, 12.5%, 15%, 17.5% and 50% ACN). The desalted flow-through was combined with the 17.5 % fraction and the 50 % fraction with the 5 % fraction to give a total of six fractions. If undertaken, non-phosphorylated peptides (flow through of the Fe-IMAC) were fractionated into 32 fractions by hydrophilic strong anionic exchange chromatography (hSAX) as described elsewhere [41] or measured as a single shot to enable total sum normalization of the phosphoproteome data. After drying in a centrifugal evaporator, the samples were stored at -20 °C until LC-MS^n analysis.

LC-MS^3 analysis of the (phospho)proteome

Nano-flow liquid chromatography tandem mass spectrometry (LC-MS^3) measurement of TMT-labeled non-phosphorylated and phosphorylated peptides was performed using a Dionex Ultimate3000 nano high performance liquid chromatography (HPLC) (Thermo Fisher Scientific) coupled to an Orbitrap Fusion Lumos mass spectrometer (Thermo Fisher Scientific). The fractions of phosphorylated peptides were injected twice. Peptides were desalted on a trap column (100 µm × 2 cm, packed in-house with Reprosil-Pur C18-AQ 5 µm resin; Dr. Maisch) in 0.1 % formic acid (FA) at 5 µl/min and separated on an analytical column (75 µm × 40 cm, packed in-house with Reprosil-Pur C18-AQ, 3 µm resin; Dr. Maisch) using a 50 min linear gradient from 8-34 % (full proteome) or 80 min linear gradient from 4-32 % (phosphoproteome) solvent B (0.1 % FA, 5 % dimethylsulfoxide (DMSO) in ACN) in solvent A (0. 1% FA, 5 % DMSO in water) at a flow rate of 300 nL/min. The Fusion Lumos was operated in data dependent acquisition and positive ionization mode. An overview of utilized parameters used for MS^3 analysis can be found in Table IV-1.

Table IV-1: Parameters used for MS3 analysis on the Fusion Lumos of both phosphoproteome and full proteome samples.

MS n	Parameter	Phosphoproteome HER2 mAbs	Phosphoproteome CD20 mAbs	Full proteome
1	Detector type	Orbitrap	Orbitrap	Orbitrap
	Resolution	60K	60K	60K
	Scan range [m/z]	360-1300	360-1300	360-1500
	Maximum injection time (maxIT) [ms]	50	50	50
	Automatic gain control (AGC) target	400K	400K	400K
2	Charge state	2-6	2-6	2-6
	Dynamic exclusion [s]	90	90	90
	Isolation window [m/z]	0.7	0.7	0.7
	First mass [m/z]	100	100	120
	Activation type	CID	CID	CID
	Activation Q	0.25	0.25	0.25
	Activation time [ms]	10	10	10
	Collision energy [%]	35	35	35
	Multistage activation	true	true	false
	Neutral loss	97.9763	97.9763	-
	Detector type	Orbitrap	Orbitrap	Ion trap (scan rate = rapid)
	Resolution	15K	15K	-
	maxIT [ms]	60	22	60
	AGC target	20K	50K	20K
3	Precursor selection mass range [m/z]	400-2000	400-2000	400-2000
	Isobaric tag exclusion	TMT	TMT	TMT
	Isolation window [m/z]	1.3;1.0;0.8;0.7	1.2;0.9;0.7;0.6	1.2;0.9;0.7;0.6
	MS2 isolation window [m/z]	3	3	2
	Multinotch activation	true	true	true
	Number of notches	10	10	10
	Activation type	HCD	HCD	HCD
	Collision energy [%]	55	55	55
	Detector type	Orbitrap	Orbitrap	Orbitrap
	Resolution	50K	50K	50K
	Scan range [m/z]	100-1000	100-1000	100-1000
	maxIT [ms]	120	120	120
	AGC target	120K	120K	120K

Peptide and protein identification and quantification

Protein and peptide identification and quantification was performed using MaxQuant [42] (version 1.6.0.16 or 1.6.3.3) by searching the tandem MS data against all human canonical and isoform sequences

as annotated in the Swissprot reference database (42355 entries, downloaded 06.06.2018) using the embedded search engine Andromeda [43]. Carbamidomethylated cysteine was set as a fixed modification and oxidation of methionine and N-terminal protein acetylation as variable modification. In addition, phosphorylation of serine, threonine and tyrosine was set as variable modification for the phosphoproteome. Trypsin/P was specified as the proteolytic enzyme and up to two missed cleavage sites were allowed. Precursor tolerance was set to 4.5 ppm and fragment ion tolerance to 20 ppm. The minimum peptide length was set to seven and all data were adjusted to 1 % peptide-spectrum match (PSM) and 1 % protein false discovery rate (FDR). A minimum score for modified peptides was set to 40. MS3-based TMT quantification was enabled, taking TMT correction factors as supplied by the manufacturer into account. Subsequent data analysis was performed on identified and quantified protein groups (full proteome; as provided in the proteinGroups.txt) and phosphorylation sites (phosphoproteome; as provided in the Phospho (STY)Sites.txt).

Data analysis

The Perseus software suite [44] (version 1.5.5.3) was used to filter out contaminants, reverse hits and protein groups, which were only identified by site (the latter in case of full proteome datasets). Multiplicities of phosphorylation sites were considered for further analysis. Protein and phosphorylation site intensities were normalized by a total sum normalization. Intensities were further normalized to the respective vehicle control. A four-parameter log-logistic regression using an internal pipeline that utilizes the 'drc' [45] package in R was applied to fit curves to the concentration-dependent phosphorylation site intensities in each TMT experiment. Phosphorylation sites were considered to be regulated for the a) the HER2 mAb dataset if i) the effect size (log2 fold change (FC), which considered the first and last two data points of the concentration series) was > 0.3 and ii) the R2 was > 0.75 and for b) the CD20 mAb dataset if i) the effect size was > 0.5, ii) the R2 was > 0.75 and iii) the EC50 was < 10 µg/ml. Enriched pathways among phosphorylated proteins were analyzed by using the Reactome knowledge base (available at https://reactome.org) [46] and by setting a maximum FDR of 0.1 for enriched pathways. Proteins of interest were mapped to signaling pathways by applying the KEGG database resource (release 91.0) [47].

Dot blotting and Western blotting

Protein lysates were generated by harvesting cells in 0.8 % NP40, 50 mM Tris-HCl pH 7.5, 5 % glycerol, 1.5 mM $MgCl_2$, 150 mM NaCl, 1 mM Na_3VO_4, 25 mM NaF, 1 mM DTT, protease inhibitors (SigmaFast, Sigma) and phosphatase inhibitors and heating the lysate for 10 min at 90 °C in 2 x NuPAGE LDS sample

buffer (Invitrogen, #NP0007), 100 mM DTT. For dot blotting, protein suspensions were carefully spotted onto PVDF membranes and dried for 15 min at room temperature. Samples for Western Blotting were separated by sodiumdodecylsulfate polyacrylamide gel electrophoresis (SDS) and electro-transferred onto PVDF membranes. Blots were stored in Tris-buffered saline (TBS), supplemented with 0.05 % Tween (TBS-T) and 2 % bovine serum albumin (BSA) for 1 h at room temperature and then incubated with primary antibody (diluted in TBS-T, 5 % BSA or 5 % non-fat dry milk) overnight at 4 °C. The following primary antibodies were used: β-Actin (1:1000, Santa Cruz Biotechnology, #sc-47778), AKT (1:1000, Cell Signaling Technology, #9272), CD20 (1:500, Abcam, #ab9475), GAPDH (1:1000, Santa Cruz Biotechnology, #SC-365062), Phospho-HER2 (Tyr1221/1222) (1:1000, Cell Signaling Technology, #2243), HER2 (1:1000, Cell Signaling Technology, #2165), Phospho-p44/42 MAPK (Erk1/2)(Thr202/Tyr204) (Cell Signaling Technology, #4370), p44/42 MAPK (Erk1/2) (Cell Signaling Technology, #4695), Phospho-p90RSK (Thr359/Ser363) (1:750, Cell Signaling Technology, #9344), RSK1/RSK2/RSK3 (1:500, Cell Signaling Technology, #9355), α-tubulin (1:200, Santa Cruz Biotechnology, #SC-12462-R). Subsequently, blots were washed in TBS-T and probed with the corresponding fluorophore-conjugated secondary antibody for 30 min at room temperature. The immuno-reactive signals were detected directly by excitation of the respective fluorophore. Acquisition and quantification of the band intensities were carried out with the Odyssey (Licor) imaging system and respective software. Intensities of proteins were normalized to input housekeeping proteins and phosphorylated proteins were normalized to the intensity of the respective total protein.

Immunofluorescence labeling and confocal laser scanning microscopy (CLSM)

The channels on the microscopy slide (µ-slides VI0.4, ibiTreat; Ibidi, #80606) were filled each with 30 µL of poly-L-lysine (0.1 mg/mL; Biochrom, #L7240) and incubated for one hour at room temperature for coating. After washing the channels five times with 30 µL PBS^+, 2.5 x 10^5 cells in 50 µL suspension were seeded per channel for Ramos and SU-DHL 4, while 5x10^6 cells were used for ARH-77. 100 µL medium was added to each channel after one hour of settlement. 16 hours post-seeding, the cells were washed twice with PBS^+ and subjected to the treatments as indicated. Thereafter, cells were washed twice with PBS^+ and fixated for 15 min at room temperature using 100 µl 4 % formaldehyde in PBS^+. After three subsequent washing steps, slides were incubated at room temperature for 60 min with 5 % BSA, 0.3 % Triton X-100 in PBS^+ for permeabilization and blocking. Slides were washed twice with 100 µL PBS^+ and incubated with the primary antibodies in 1 % BSA, 0.3 % Triton X-100 in PBS^+ overnight at 4 °C in a humid box: CD20 (Abcam, #ab9475), Phospho-p44/42 MAPK (Erk1/2)(Thr202/ Tyr204) (Cell Signaling Technology, #4370) and p44/42 MAPK (Erk1/2) (Cell Signaling Technology, #4695).

Following three washing steps (100 µL PBS^+ each), the secondary antibodies were applied which were incubated 30 min in the dark: donkey anti-Rabbit IgG H&L (Alexa Fluor 488) (Abcam, #ab150073) and goat anti-Mouse IgG H&L (Alexa Fluor 647) (Abcam, #ab150115). Cells were washed with 100 µL PBS^+ and 25 µL 0.1 µg/mL DAPI was applied. After four minutes incubation, cells were washed three times with 100 µL PBS^+. Finally, 30 µL mounting medium (Ibidi, #500001) was applied. Until readout, slides were kept in the dark at 4 °C in a humid box. Cells were imaged on an Olympus FLUOVIEW FV3000 confocal scanning microscope with an IX83 scanning unit using a UPLSAPO60XW lens (60x/NA1.2/WD 0.28, water immersion) and the laser wavelengths λ_{ex}=405/ λ_{em}=461 (DAPI), λ_{ex}=488/ λ_{em}=520 (Alexa Fluor 488) and λ_{ex}=633/ λ_{em}=647 (Alexa Fluor 647). Images were further processed with ImageJ (version 2.0.0-rc-69/1.52p) [48].

3 Results and discussion

3.1 Cell line panels for the study of therapeutic antibodies

In order to study the action of anti-HER2 trastuzumab and pertuzumab, and anti-CD20 rituximab by phosphoproteomics, suitable cell lines were chosen. Due to their high relevance for the treatment of breast cancer tumors and lymphomas, respectively, HER2-positive breast cancer and CD20-positive B-cell lymphoma cell lines were the basis for further experiments. Lapatinib, a dual HER2/EGFR small molecule inhibitor, was added to the panel of anti-HER2 mAbs. Thus, the comparison of the effects of both the intracellular HER2 engagement and the blocking of extracellular HER2 dimerization was enabled. In order to study the action of the drugs comprehensively, perturbations of the phosphoproteomes were performed in a concentration-dependent manner. An additional advantage of this approach was that information about the potency of drug action could be obtained. Consequently, also appropriate ranges of drug concentrations had to be defined that cover drug-induced changes in protein phosphorylation.

Appertain to the luminal B and HER2 breast cancer subtype [49], both BT-474 and SK-BR-3 cell lines are heavily utilized in research due to their elevated HER2 activity. Increased levels of HER2 expression and phosphorylation in comparison to triple negative breast cancer cell line MDA-MB-231 [50] were demonstrated by Western Blotting (Figure IV-1A). Metabolic activity assays with Alamar Blue have highlighted sensitivity towards lapatinib in both cell lines with similar sub-micromolar half-maximum inhibitory concentrations (IC50s) but lower effect size in SK-BR-3 cells (Figure IV-1B, top). In contrast, trastuzumab realized diminished effects of 25 % or less on the metabolic activity of both cell lines (Figure IV-1B, bottom). Pertuzumab has been reported to exert even lower effects than trastuzumab on the proliferation of BT-474 and SK-BR-3 cells [51, 52], but could be more efficacious by supplementing heregulin HRG, which drives ligand-dependent HER2 heterodimerization [53]. A similar trend of lower effects by trastuzumab compared to lapatinib was observed for the phosphorylation level of the two major autophosphorylation sites HER2-Tyr$^{1221/1222}$ by dot blot analysis (Figure IV-1C). These results are in agreement with reports that have illustrated rather low effect sizes of trastuzumab on the cellular proliferation and HER2 phosphorylation levels in breast cancer cell line panels. Still, BT-474 and SK-BR-3 cells were specified as trastuzumab-sensitive [50]. Cytotoxicity assays with the IncuCyte green cytotoxicity reagent have furthermore demonstrated a cytotoxic effect of lapatinib on BT-474 cells, which is missing during trastuzumab treatment (Figure IV-2). This led to the assumption that the direct

action of trastuzumab on breast cancer cells is cytostatic, which is again in line with previous reports [54, 55]. These initial results already point out a differential action of the anti-HER2 drugs on breast cancer cells.

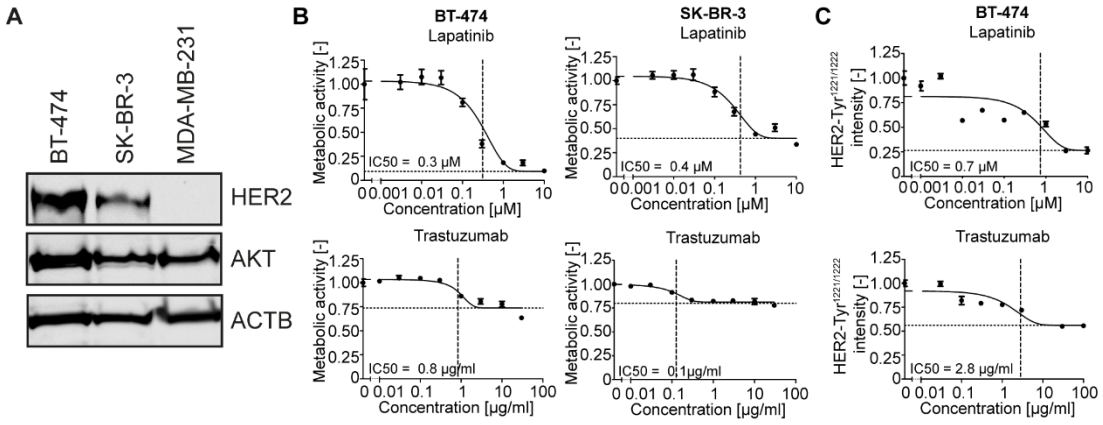

Figure IV-1: Breast cancer cell lines to study anti-HER2 drug action. (A) Immunoblots showing HER2, AKT and ACTB intensity in BT-474, SK-BR-3 and MDA-MB-231 breast cancer cells. (B) Metabolic activity of BT-474 (left) and SK-BR-3 (right) cells upon treatment with lapatinib (top) and trastuzumab (bottom) in an Alamar Blue assay. (C) Phosphorylation intensity on HER2-Tyr$^{1221/1222}$ in BT-474 cells upon treatment with lapatinib (top) and trastuzumab (bottom) as determined in a dot blot assay. The relative IC50 is highlighted by a dashed line and the bottom of the curve by a pointed line. Error bars represent standard deviation (SD). Data represent N = 1 (A and C) and N = 3 (B) biologically independent experiments.

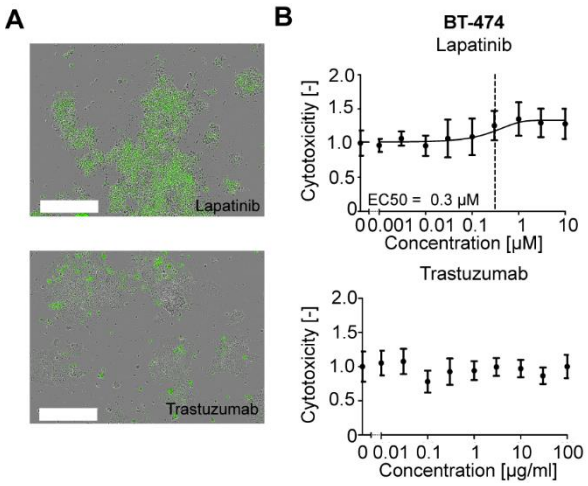

Figure IV-2: Cytotoxicity analysis of lapatinib and trastuzumab with an IncuCyte green cytotoxicity assay. (A) Example phase microscope pictures of lapatinib- (top) and trastuzumab-treated (bottom) BT-474 cells (10 µM / 100 µg/ml, 72 h) stained with the IncuCyte green cytotoxicity reagent. Bar length is 400 µm. (B) Analysis of the cytotoxicity of lapatinib (top) and trastuzumab (bottom) in BT-474 cells in an IncuCyte green cytotoxicity assay (readout after 72 h treatment). The relative half-maximum effective concentration (EC50) is highlighted by a dashed line, if applicable. Error bars represent the SD. Data represent N = 3 biologically independent experiments.

With regard to cover a broad range of breast cancer subtypes, the MDA-MB-175 cell line was furthermore added to the cell line panel to study HER2 inhibitor action. MDA-MB-175 cells belong to the luminal A breast cancer subtype, are trastuzumab-sensitive and bear enhanced levels of activated HER3, a dimerization partner of HER2 [50, 56].

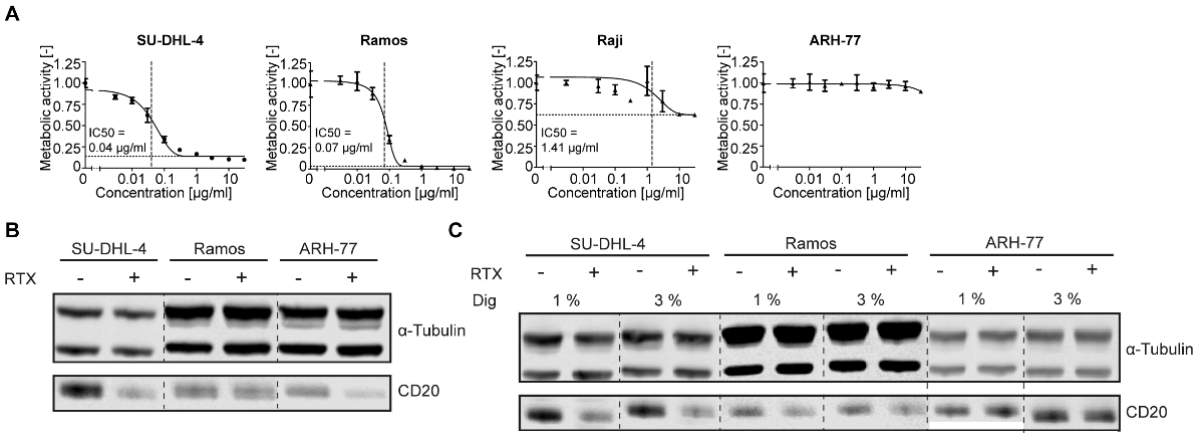

Figure IV-3: B cell lines to study the action of rituximab. (A) Metabolic activity of SU-DHL-4, Ramos, Raji and ARH-77 cells upon treatment with rituximab (from left to right) in an Alamar Blue assay. The relative IC50 is highlighted by a dashed line and the bottom of the curve by a pointed line. Error bars represent standard deviation (SD). (B) Immunoblots showing α-Tubulin and CD20 intensity in SU-DHL-4, Ramos and ARH-77 cells with or without 1h treatment with 30 µg/ml rituximab (RTX). (C) Immunoblots showing α-Tubulin and CD20 intensity in SU-DHL-4, Ramos and ARH-77 cells with or without 1h treatment with 30 µg/ml rituximab (RTX) after lysis with 1 % or 3 % digitonin (Dig). Data represent N = 3 (A) and N = 1 (B & C) biologically independent experiments.

Due to their clinical relevance, especially $CD20^+$ lymphoma cell lines are a prime model system to study the actions of rituximab. Sensitivity of SU-DHL-4 and Ramos cells towards rituximab treatment with IC50s < 100 ng/ml were displayed by metabolic assays. Contrarily, Raji and ARH-77 cells indicated partial and total intrinsic resistance (Figure IV-3A). The final cell line panel contained diffuse large cell B-cell lymphoma SU-DHL-4 [57], Burkitt lymphoma Ramos [58] and B-lymphoblastoid, formerly labeled as plasma cell leukemia [59], ARH-77 cells. Hence, different lymphoma types and sensitivities towards the drug were included, which offered the chance to study both common actions of rituximab and resistance mechanisms in ARH-77 cells. So far, reported mechanisms of low response in ARH-77 cells were attributed to a diminished rituximab-mediated CDC effect [60]. The phosphoproteomic study of this thesis therefore could reveal resistance mechanisms that are based on Fab-mediated actions of the drug.

Moreover, immunoblot analysis of the B-cell lines demonstrated basal CD20 expression, which was decreased upon 1h 30 µg/ml rituximab treatment in all three cell lines (Figure IV-3B). This indicated a

shift of CD20 molecules into lipid rafts by rituximab as it has been reported by literature [29]. Supplementing the NP-40-containing lysis buffer with 1 and 3 % digitonin, a renowned lipid raft-disrupting detergent [61], has enabled the solubilization of lipid rafts-standing CD20 in ARH-77 cells (Figure IV-3C). With these data one can exclude a down-regulation of CD20 expression as resistance mechanism in ARH-77 cells and conclude a different lipid raft compositions of the three cell lines. In line of this, reports showed that the level of ganglioside GM1, a major constituent of lipid rafts, correlates with the response of lymphomas to rituximab, which was independent of the CD20 expression level [62]. The analysis of the GM1 level in the cell line panel has not been executed so far. However, obtaining this data could give further insight into the involvement of lipid rafts and molecular actions of rituximab.

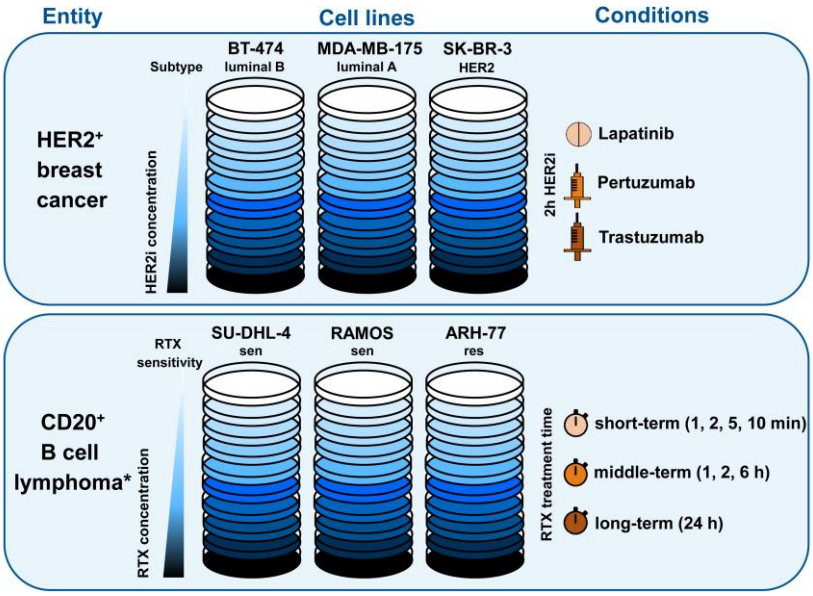

Figure IV-4: Final cell line panels for the phosphoproteomic analysis of anti-HER2 (top) and anti-CD20 mAbs (bottom). Experimental conditions regarding included drugs and treatment times are displayed as well. * ARH-77 is classified as B-lymphoblastoid cell line. sen = sensitive, res = resistant.

In summary, the final two cell line panels comprised each three cell lines, which were subjected to the drugs in ten different concentration (Figure IV-4). The concentration ranges used in the metabolic assays (lapatinib: 1 nM – 10 µM; trastuzumab: 10 ng/ml – 100 µg/ml; rituximab: 0 - 30 µg/ml) covered the IC50s and EC50s, which should allow to encompass effects in further phosphoproteomic analyses. Moreover, the concentration ranges comprised average plasma concentrations of the drugs in patients [63-65]. In addition to the treatment of the three B cell lines with ten concentrations of rituximab, a time component was introduced, which spanned a duration from short-term (1, 2, 5, 10 min), middle-term (1, 2, 6 h) and long-term (24 h) exposure of the cells to rituximab. Consequently, dynamics of signaling events following rituximab engagement might be revealed leading to the functional ranking of

phosphorylation events. This is especially of interest since most of the reports so far studied the effects of rituximab upon prolonged treatment of 24 h or longer [66, 67].

3.2 Optimization of the phosphoproteomic sample processing workflow

In prospect of a high number of samples to process, different sample preparation strategies were evaluated. The aim was to define a phosphoproteomic workflow that both enables comprehensive identifications and is suitable to process rather a large number of samples. In the regard of optimizing the sample processing workflow on a sample that recapitulates the intended phosphoproteomic experiments, BT-474 cells were treated for 1 h with ten concentrations of lapatinib. In this way, ten samples were processed and measured with a standard LC-MS^3 method. Four different sample preparation strategies were employed, which differed in i) the total protein input (equally distributed over the ten different samples), ii) the IMAC phosphopeptide enrichment step (performed either before or after TMT labeling and pooling of the ten samples), and iii) inclusion of phosphotyrosine peptide-immunoprecipitation (pY-IP) (Figure IV-5A). Strategy I and II differed by desalting pY-IP eluates either by standard C18 solid phase extraction (SPE) (I) or by using a two-step enrichment strategy by including Fe^{3+}-IMAC in addition to C18-SPE (II) as described earlier [40]. The highest number of identified and quantified phosphorylation sites (p-sites) was reached with strategy III, leading to > 10,700 p-sites. This number decreased when pY-IPs were added to the workflow (> 9800 p-sites; Figure IV-5B). The underlying reason might be that the additional processing steps of the pY-IP caused peptides to get lost for subsequent analysis. More additional steps in strategy II resulted in even lower number of identifications (> 8900 p-sites), which are similar to those of strategy IV. As expected, the addition of the pY-IP to the workflow raised the number of pY sites, resulting in 419/381 pY sites compared to 262 pY-sites. The number dropped again when only one tenth of total protein input was processed (IV, 155 pY-sites). In the interest of reducing sample processing steps and combining the ten samples as early as possible to cover the maximal amount of technical variance, strategy IV was chosen to be used for further experiments (Figure IV-6). Despite the fact that the number of p-site identifications has not been the highest, they were still in an acceptable order of magnitude.

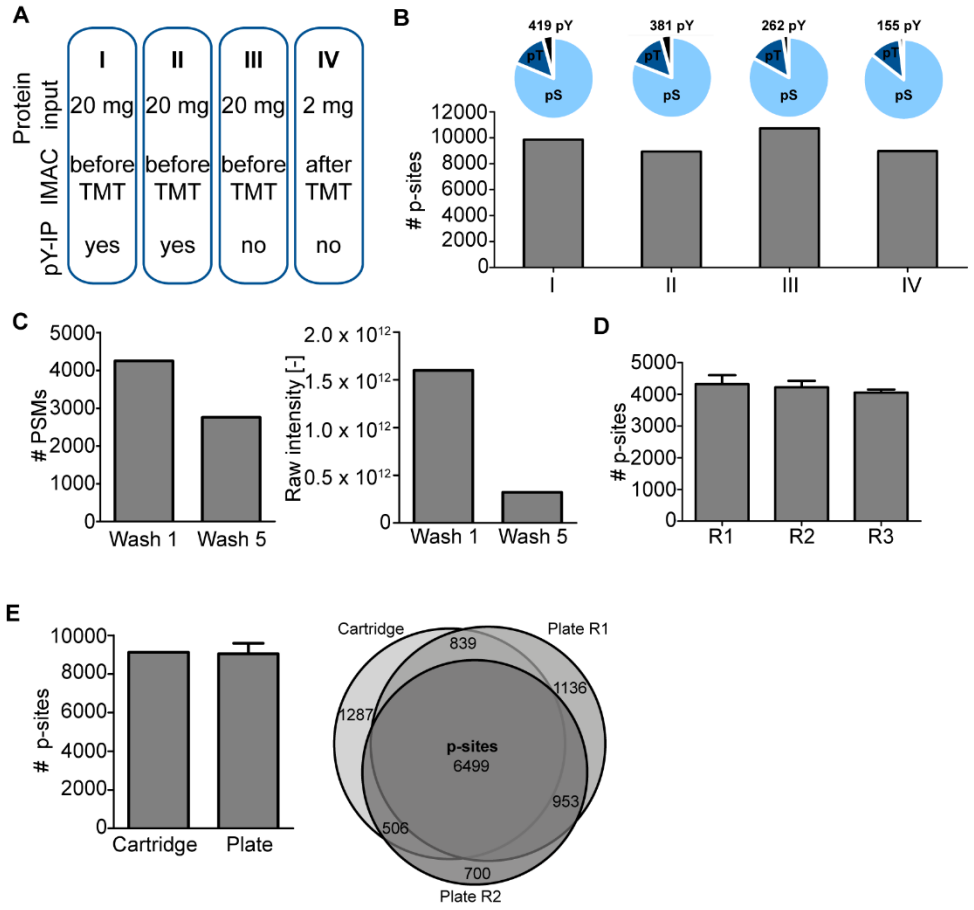

Figure IV-5: Evaluation of different phosphoproteomic sample preparation strategies. (A) Overview of the four analyzed sample preparation strategies. (B) Number of identified and quantified p-sites for each strategy. The ratios of pSer, pThr and pTyr sites are furthermore noted. (C) Number of PSM´s (left) and raw intensity (right) of the first and fifth wash step after plate-based desalting. (D) Number of p-sites after three consecutive re-uses of the same plate-based desalting moiety. (E) Number of p-sites (left) and overlap of p-sites (right) of cartridge- and plate-desalted samples. Error bars represent SD. Data represent N = 1 (A-C), N = 3 (D) and N = 1 or 2 (E) biologically independent experiments.

In order to increase the throughput in the sample processing pipeline, desalting of tryptic digests on 96-well plate-based C18 SPE was furthermore evaluated to replace C18 SPE (single-well) cartridges. Plate-based desalting of 200 µg BT-474 tryptic digest has demonstrated that five wash steps with 0.1 % FA and 50 % ACN were sufficient to reduce the number of remaining peptide-spectrum matches (PSMs) and peptide intensity in the washing fractions, which allows for multiple use of wells without the risk of sample carry-over (Figure IV-5C). In this regard, it has been illustrated that three subsequent usages of the same well to desalt 200 µg BT-474 tryptic digest did not diminish p-site identifications (Figure IV-5D). In addition, a direct comparison between plate- and cartridge-based desalting of ten 200 µg BT-474 tryptic digests, which was followed by the aforementioned strategy IV, resulted in a comparable number of identified p-sites with sufficient overlap between both desalting platforms. These results

prompted to include plate-based C18 SPE for the desalting of tryptic digests into the sample processing workflow.

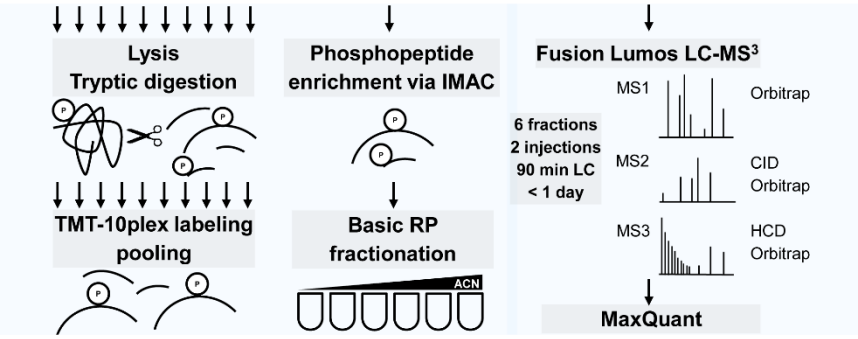

Figure IV-6: Final sample preparation workflow for the phosphoproteomic analysis.

3.3 Depth of drug-perturbed phosphoproteomes

The depth of the HER drug-perturbed phosphoproteomes was characterized by 8800 to 10,000 p-sites on average per breast cancer cell line (Figure IV-7A). As expected, the overlap between all three cell lines with > 6400 p-sites on > 2200 proteins overlap (Figure IV-7B) was moderate due to stochastic sampling of precursor ions for MS2 analysis and the different signaling network states in the cell lines. This was furthermore demonstrated by the finding that only 16 % of all p-sites (3098 p-sites) were identified in all nine datasets (Figure IV-7C).

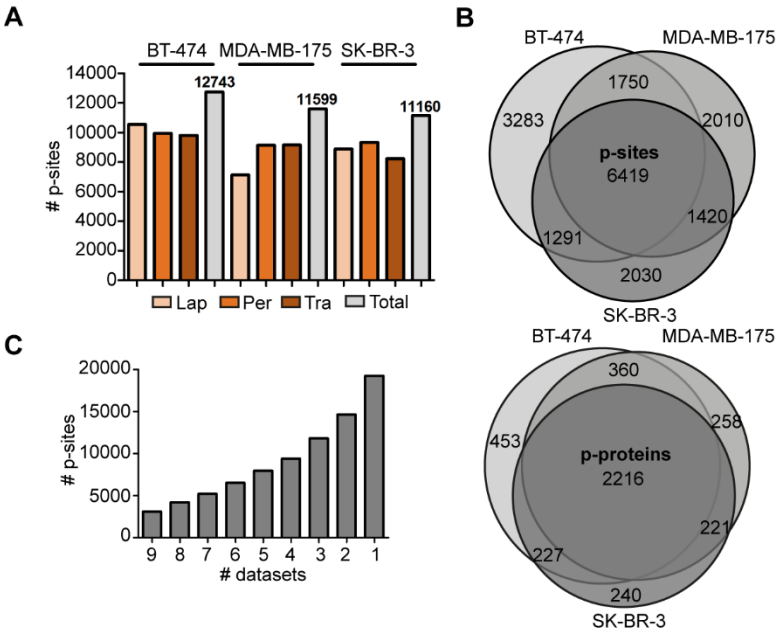

Figure IV-7: Phosphoproteomic identifications in HER2-inhibited breast cancer cell lines. (A) Number of identified and quantified p-sites in BT-474, MDA-MB-175 and SK-BR-3 cells after lapatinib (Lap), pertuzumab (Per) and trastuzumab (Tra) treatment and total number of all identified p-sites in each cell line. (B) Overlap of p-sites (top) and p-proteins (bottom) between the three cell lines. (C) Number of reproducible p-site identification in the total of 9 or less datasets.

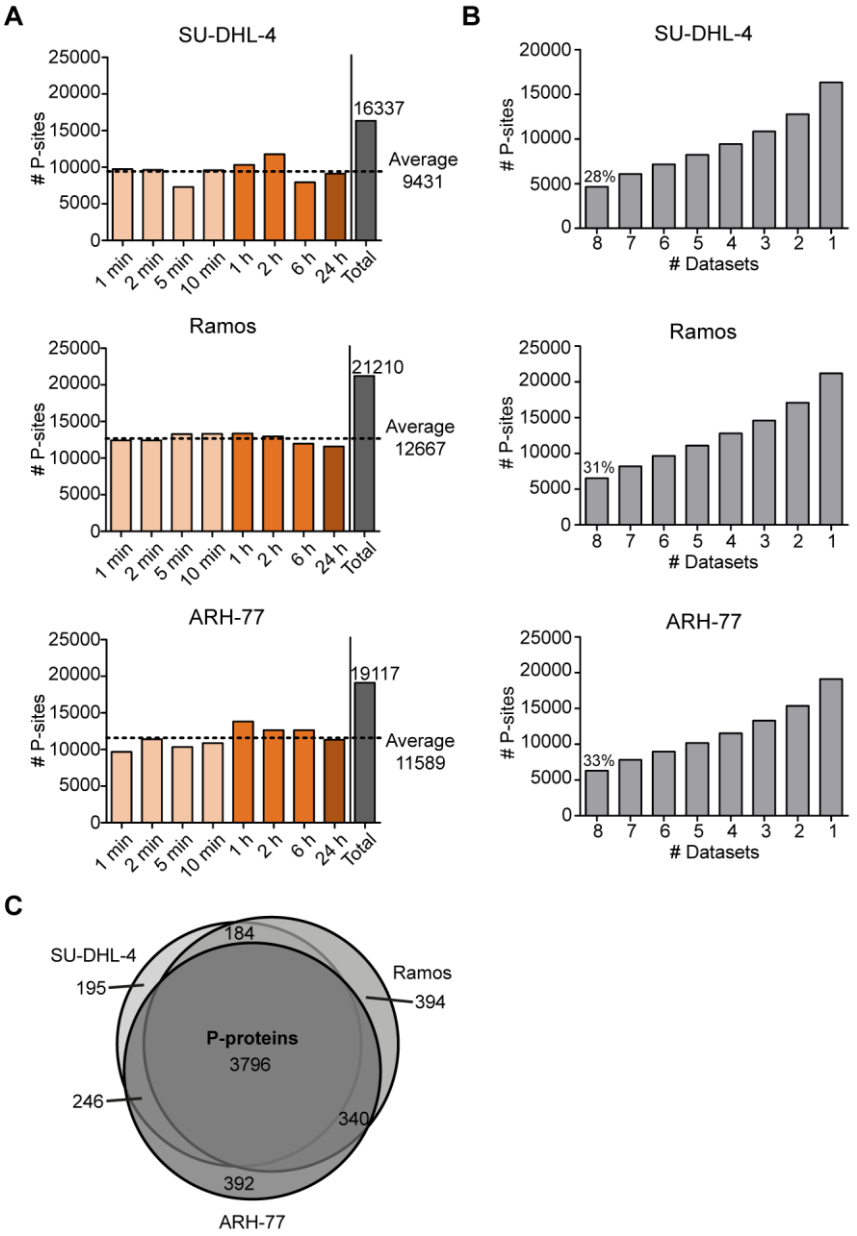

Figure IV-8: Phosphoproteomic identifications in rituximab-treated B-cell lines. (A) Number of identified and quantified p-sites over all eight time points and the total number in SU-DHL-4 (top), Ramos (middle) and ARH-77 cells (bottom). The average number of p-sites in each cell line is highlighted by a dashed line. (B) Number of reproducible p-site identifications in the total of 8 or less datasets in SU-DHL-4 (top), Ramos (middle) and ARH-77 cells (bottom). The percentage of p-sites, which were identified in all 8 datasets, is indicated. (C) Overlap of identified p-proteins between SU-DHL-4, Ramos and ARH-77 cells.

Similary, deep phosphoproteomes from > 9400 to > 12,600 identified and quantified p-sites on average for each of the three rituximab-treated B cell lines were captured (Figure IV-8A). The reproducible identification of p-sites over the eight datasets followed the same trend in the three cell lines and was characterized by on average 30 % of all p-sites that have been identified in all eight time-points in a cell line (Figure IV-8B). The number of p-proteins and its overlap of ~ 3800 identified p-proteins between

the three B-cell lines was considerably higher than for the three breast cancer cell lines due to overall higher p-site identifications (Figure IV-8C). The numbers of identifications greatly exceeded recently published rituximab-perturbed phosphoproteomes [66] and, therefore, highlighted the depth of the phosphoproteomic datasets in this thesis.

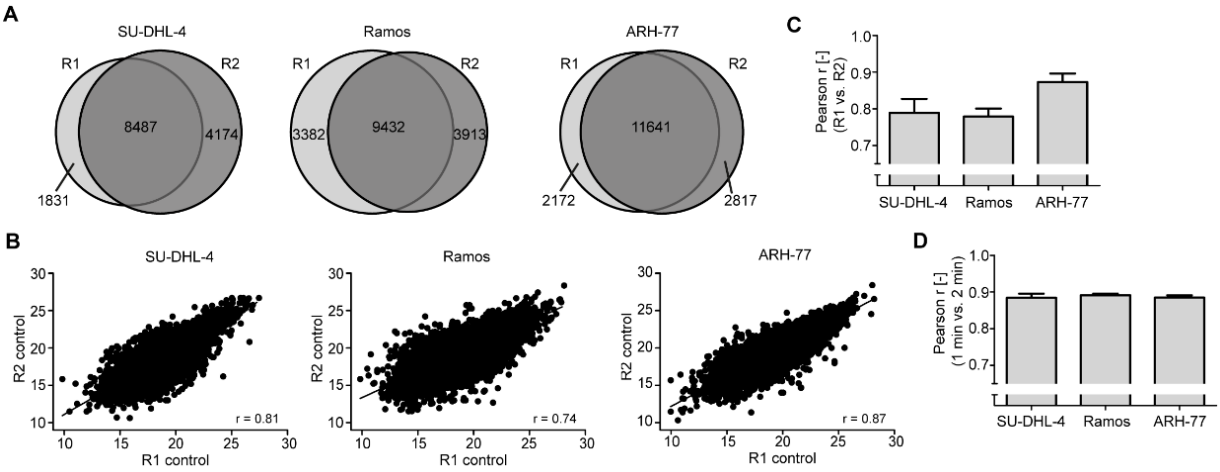

Figure IV-9: Correlation analysis of cell culture-based replicates of rituximab-treated cell lines. (A) Overlap of identified and quantified p-sites in the 1 h treatment replicate 1 (R1) and 2 (R2) in SU-DHL-4 (left), Ramos (middle) and ARH-77 cells (right). (B) Scatter plot of p-site intensities in R1 and R2 of the control (PBS). (C) Pearson correlation coefficient r between R1 and R2 in all ten concentrations. (D) Pearson correlation coefficient r between 1 min and 2 min treatment in all ten concentrations. Error bars represent standard deviation (SD).

The analysis of two cell culture-based replicates of a 1 h rituximab treatment has demonstrated a reasonable overlap of identified and quantified p-sites (Figure IV-9A) and correlation over all ten concentrations (Figure IV-9B+C). The lowest reproducibility of the Ramos replicates might have been caused by a several months long gap between sample preparation including LC-MS/MS analysis of the two replicates, in contrast to several weeks (SU-DHL-4) and days (ARH-77) of the other replicates. This hypothesis led to the assumption that cell line-specific data, which have been prepared and acquired subsequently, should harbor higher reproducibility. This is suggested by increased correlation coefficients of > 0.88 between the 1 and 2 min treatment phosphoproteomes indicating overall good data quality of the drug-perturbed phosphoproteomes (Figure IV-9D).

3.4 Drug-responsive phosphoproteomes

In order to define drug-responsive p-sites among the ten concentration-dependent phosphoproteomes, a data filtering workflow was established that was based on a four-parameter logistic curve fitting of the data (Figure IV-10A). After a two-step filtering, which took the effect size of the original data (log2 fold change (FC) that considered the first and last two data points of the concentration series) and the

coefficient of determination R2 of the curve fitting into account. The remaining p-sites were defined to be regulated by the applied drug treatment.

The number of regulated p-sites varied heavily among the different breast cancer phosphoproteomes. Lapatinib-treated cells demonstrated the highest responsiveness resulting in > 2000 regulated p-sites in BT-474 cells (Figure IV-10B). In contrast to lapatinib, the p-sites that were regulated by pertuzumab and trastuzumab were diminished and topped out at 578 and 175, respectively, in BT-474 cells. Median effect sizes revealed the highest degree of regulation indeed again to be caused by lapatinib, especially in BT-474 and MDA-MB-175 cells (> 0.8) (Figure IV-10C). Antibody-perturbed p-sites were characterized by median effect sizes of 0.4-0.5, with the exception for MDA-MB-175 cells treated with pertuzumab. Despite different time frames of the treatment, the median EC50 of p-site regulation in lapatinib-treated BT-474 cells was furthermore comparable –here 223 nM – with the IC50 and EC50 determined in the metabolic and cytotoxic assays, respectively (Figure IV-10D). A similar median effect size was determined for MDA-MB-175 cells, while regulated p-sites in SK-BR-3 cells showed a median effect size of > 20 μM. This might have been caused by the lower number of regulated p-sites and a subsequent higher chance of dealing with suboptimal curves. Due to the applied effect size filter of > 0.3 to define regulated p-sites, small effects on the phosphoproteomes of antibody-treated cells might have been filtered out rigorously, leading to the apparent diminished regulation of the phosphoproteomes. However, the analysis still prompted the assumption that the general perturbation of the phosphoproteomes, in terms of quantity and quality, is generally lower for the therapeutic antibodies than for lapatinib. This is in line with the aforementioned data obtained from the applied metabolic and cytototoxic assays.

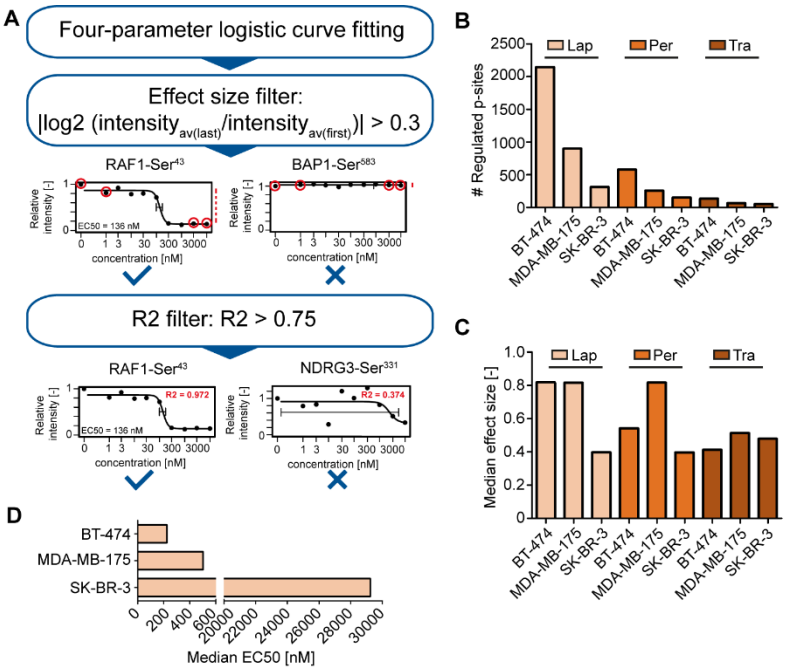

Figure IV-10: HER2 inhibitor-responsive phosphoproteomes. (A) Workflow for the filtering of the concentration-dependent phosphoproteomes to find regulated p-sites according to a four-parameter logistic curve fitting. (B) Number of p-sites, which have been regulated by lapatinib (Lap), pertuzumab (Per) and trastuzumab (Tra) in all three breast cancer cell lines. (C) Median effect sizes of regulated p-sites in all nine datasets. (D) Median EC50 of p-sites, which were found to be regulated by lapatinib in all three breast cancer cell lines.

In order to reduce the number of p-sites to perform the four-parameter logistic curve fitting on, the rituximab-treated phosphoproteome datasets were subjected to effect size filtering first (Figure IV-11A). After R2 filtering, an additional filtering of an EC50 > 10 µg/ml was executed to remove p-sites, which were regulated with low potency by rituximab.

In the two rituximab-sensitive cell lines SU-DHL-4 and Ramos the numbers of regulated p-sites have increased over treatment time starting with a few dozens and reaching up to > 2600 and > 5400 p-sites, respectively (Figure IV-11B). These numbers highlighted a comprehensive time-dependent perturbation by rituximab, whose early beginnings could be recapitulated by analyzing the regulations in the minute time points. The majority of regulated p-sites were found to be regulated in one to two time points, while a few dozens of them were regulated in up to six and seven time points. A reproducible regulation especially in adjacent time points strengthened the evidence for these regulations. Median effect sizes are in line with time-dependent regulation of the phosphoproteomes by increasing over time and peaking at 6 and 2 h in SU-DHL-4 and Ramos cells (Figure IV-11C). The decrease of effect sizes after 24 hours in both cell lines indicate potential feedback loops and/or beginning cell death, which could counteract the engagement of cellular signaling by rituximab. Overall higher effect sizes in SU-

DHL-4 cells might have been provoked by an actual increased effect due to rituximab treatment. However, this observation could be easily introduced by a technical bias such as a decreased ratio compression in the SU-DHL-4 datasets. The normalization for ratio compression is not trivial and could only be performed indirectly over standardized samples which are additionally multiplexed over TMT. Similar to the median effect sizes, the potency of rituximab on the phosphoproteome was increasing over time, which is indicated by lower median EC50 values in the hours than in the minute time points.

In contrast to SU-DHL-4 and Ramos cells, rituximab-resistant ARH-77 cells have been regulated only sparsely and without a time-dependence. A resistance mechanism, which drives cells to counteract actively against CD20 engagement by rituximab, might therefore be excluded.

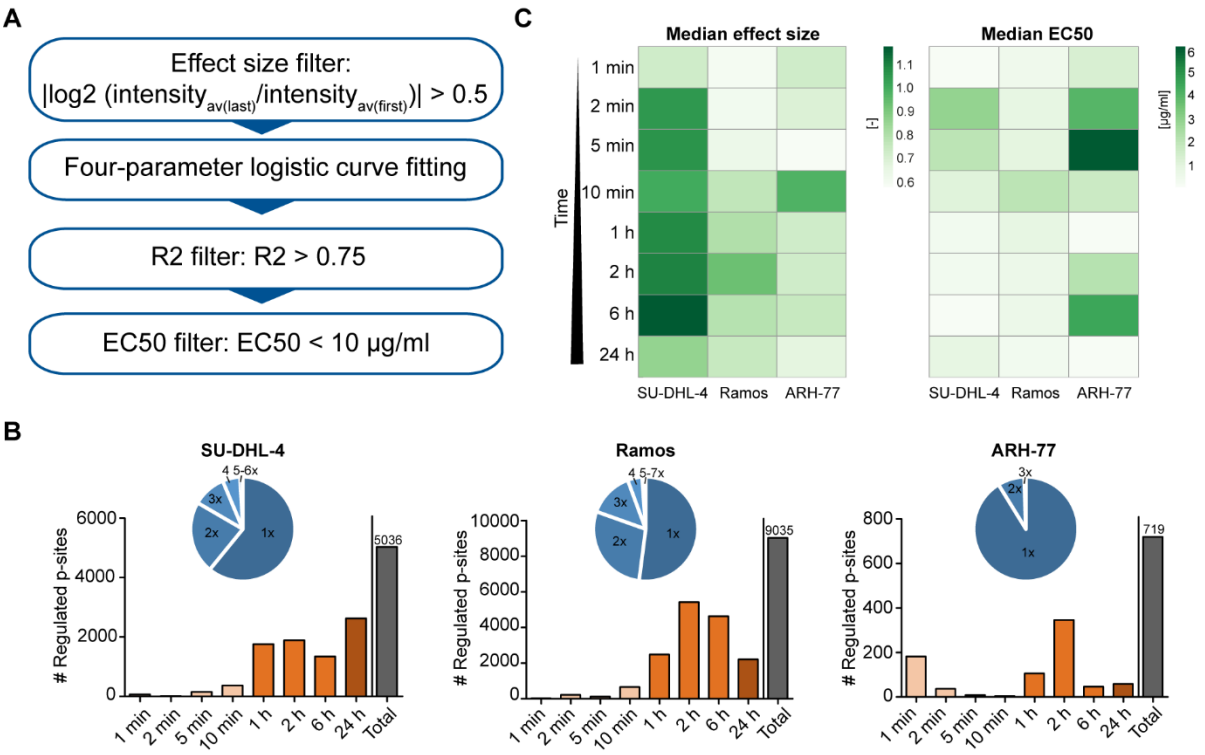

Figure IV-11: Rituximab-responsive phosphoproteomes. (A) Workflow for filtering regulated p-sites from rituximab-treated phosphoproteomes. (B) Number of regulated p-sites in each treatment time point in SU-DHL-4 (left), Ramos (middle) and ARH-77 cells (right). A blue pie chart indicates how many regulated p-sites were identified reproducibly in several time-datasets. (C) Heatmap of median effect sizes (left) and EC50 values (right) for each time point of all three cell lines.

3.5 Drug-induced phosphoproteomic changes differ greatly between lapatinib and anti-HER2 therapeutic antibodies

As for exploring the action of the three anti-HER2 drugs in more detail, further analysis concentrated on the regulated p-sites in BT-474 cells, which have been prone to the highest number of phosphoproteomic perturbations. The overlap of regulated p-sites was slight and highlighted again a

drug-specific action of lapatinib on BT-474 cells (Figure IV-12A). Reactome pathway enrichment of lapatinib-regulated p-proteins revealed a comprehensive engagement of cellular operations such as mRNA splicing, cell cycle, TP53 activity, apoptosis and signal transduction as exemplified by MTOR and MAPK signaling (Figure IV-12B).

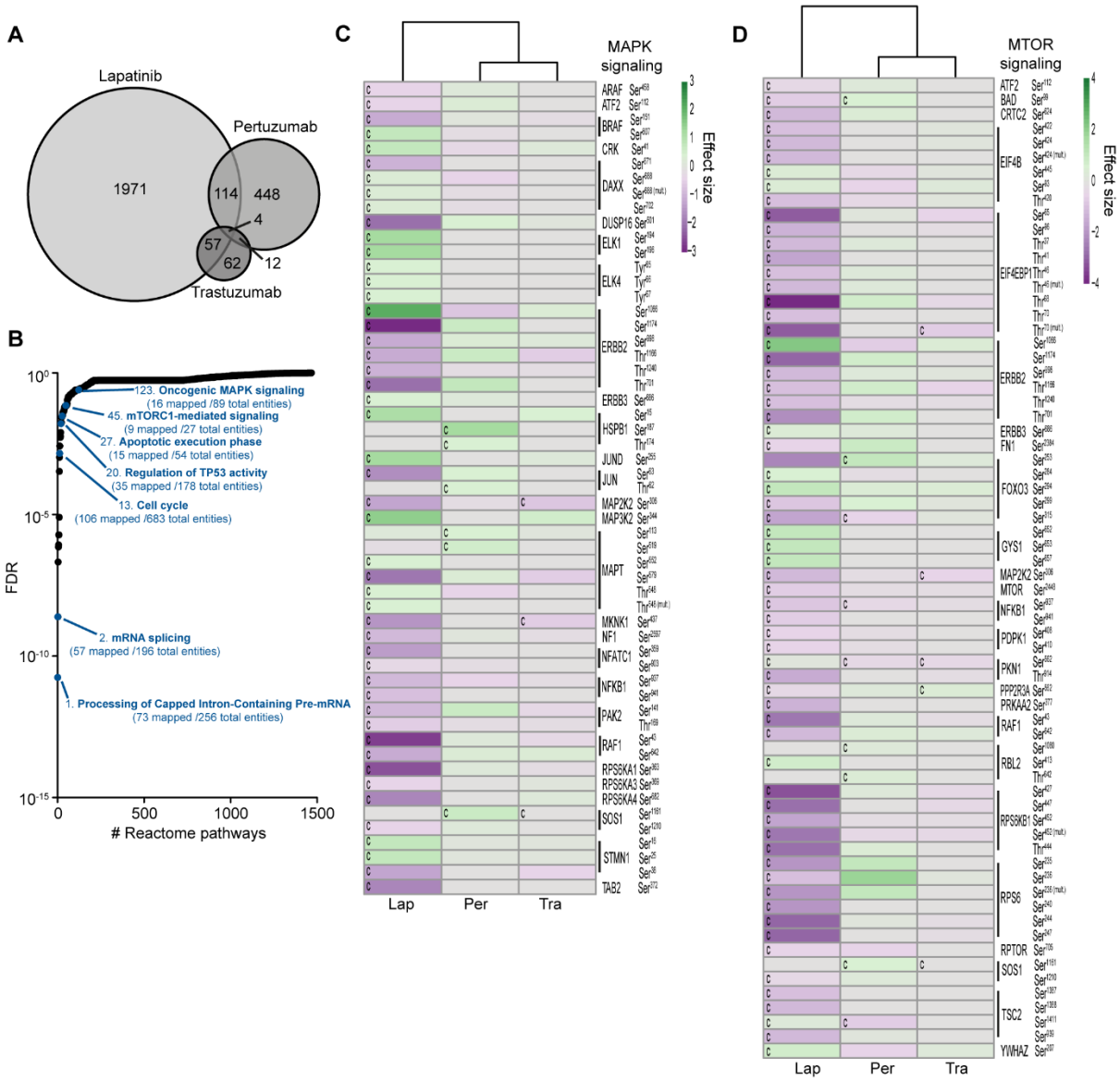

Figure IV-12: Comprehensive perturbation of MAPK and MTOR signaling by lapatinib but neither by trastuzumab nor pertuzumab in BT-474 cells. (A) Overlap of regulated p-sites between lapatinib-, pertuzumab- and trastuzumab-treated BT-474 cells. (B) Reactome pathway enrichment analysis of p-sites, which were regulated by lapatinib in BT-474 cells according to the FDR of Reactome pathways. Several pathways are highlighted in blue. (C) (D) Heatmap of KEGG-mapped p-proteins, whose p-sites were regulated by lapatinib (Lap), pertuzumab (Per) and trastuzumab (Tra) in BT-474, belonging to the MAPK signaling (C) or MTOR signaling pathway (D). The effect size of each p-site is indicated by a green-violet color code. Positive curve filtering for a p-site is indicated by a 'c'.

The latter two signaling pathways were comprehensively regulated by lapatinib distributed over a multitude of proteins. Contrarily, pertuzumab and trastuzumab have regulated only a few p-sites with generally lower effect sizes in these pathways (Figure IV-12C+D).

The phosphorylation of several renowned signaling members downstream of HER2 was differentially regulated, including SHC1, AKT1S1 and RAF1 [68]. As an example, phosphorylation of SHC-Tyr^{427} induces interaction with GRB2 leading to further activation of downstream signaling [69] and was reduced by lapatinib in all cell lines, but increased in SK-BR-3 cells by pertuzumab and trastuzumab (Figure IV-13). This observation indicates a blockade of signal transduction from membrane-spanning RTKs such as HER2 to cytosolic downstream partners by lapatinib, and, surprisingly, an activation by the therapeutic antibodies in SK-BR-3 cells. Phosphorylation of AKT1S1 Thr^{264}, a direct AKT substrate inhibiting its activity [70], was again comprehensively decreased by lapatinib and regulated neglectably with comparably high EC50 values by pertuzumab in BT-474 and MDA-MB-175 cells. In line with decreased signaling activation downstream of SHC1/GRB2, the data pinpoints decreased AKT activity by lapatinib but no or neglectable action of pertuzumab and trastuzumab. Phosphorylation on RAF1-Ser^{43}, which inhibits Raf1´s activity [71], was solely decreased by lapatinib in BT-474 cells illustrating not only a drug-specific action, but also a cell line-dependent regulation of the MAPK signaling pathway by lapatinib.

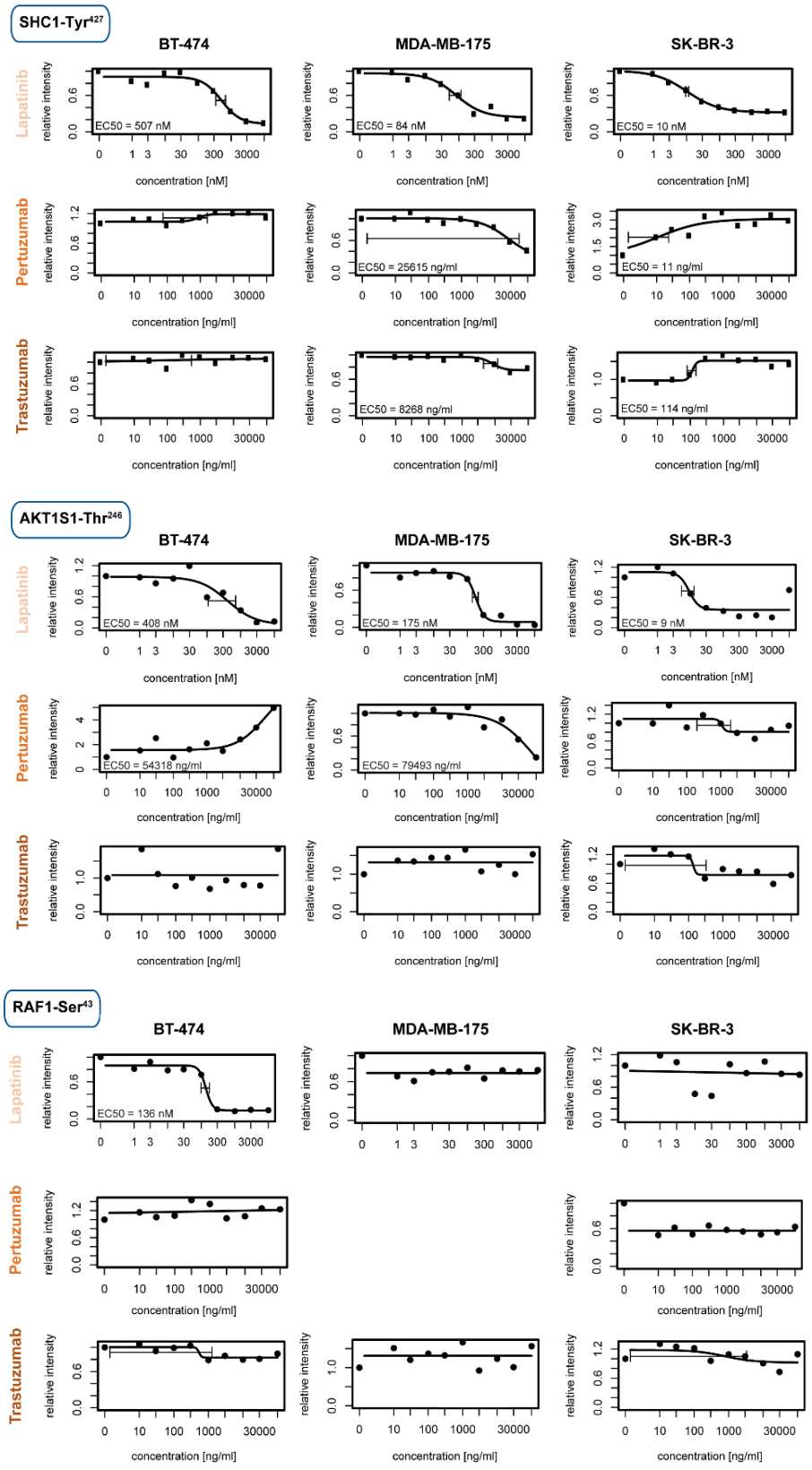

Figure IV-13: Drug-induced regulation of the phosphorylation of SHC1-Tyr^{427} (top), AKT1S1-Thr^{246} (middle), and RAF1-Ser^{43} (bottom) in all three breast cancer cell lines. The curve fit of each condition is displayed. If curve filtering was positive, the EC50 of the curve is additionally highlighted. A missing plot indicates the missing identification of the p-site in the respective phosphoproteome.

A closer look at the action of lapatinib on the classical MAPK signaling pathway in BT474 cells highlighted the ability to prioritize the effects of the drug on p-proteins and their p-sites not only by their effect sizes but also by their potencies as quantified by the EC50 (Figure IV-14).

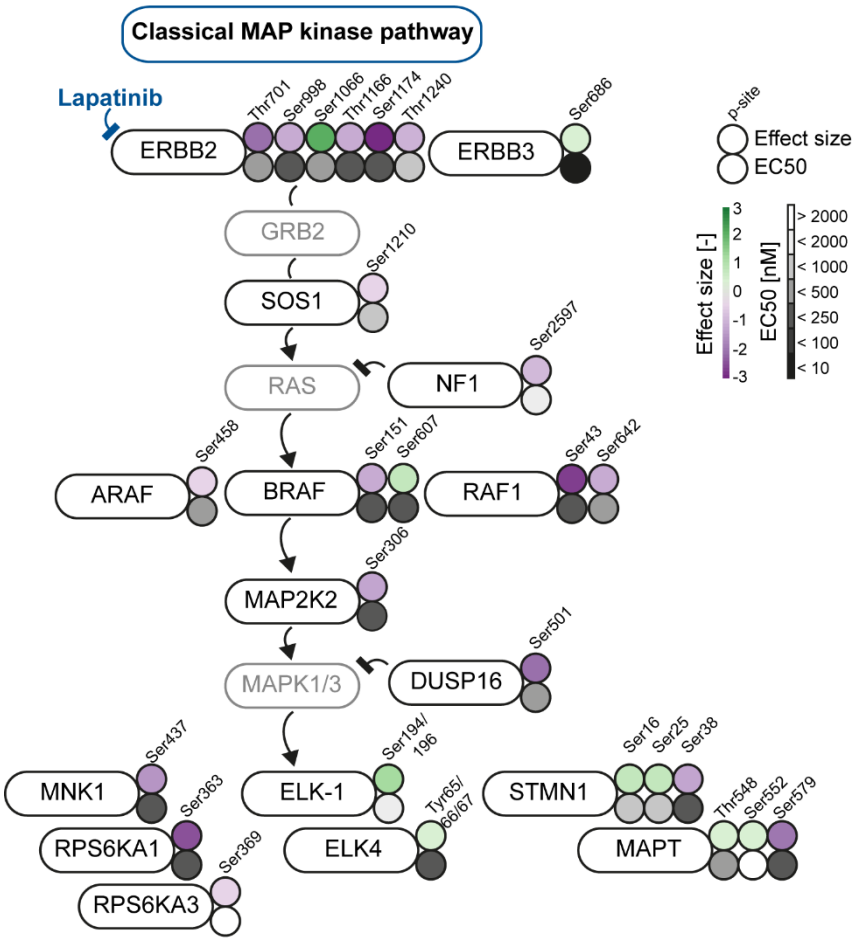

Figure IV-14: Phosphoproteomic perturbations of the classical MAP kinase pathway by lapatinib in BT-474 cells. Regulated p-sites of pathway members are highlighted and characterized by their effect size and EC50, which are color-coded. Arrows indicate a kinase-substrate relationship and blocked arrows a negative regulation such as a phosphatase-substrate relationship. Grey proteins are essential for the signaling pathway but have not been regulated or identified by corresponding p-sites.

As an example, the intended target of lapatinib HER2, was regulated on several p-sites, from which only Thr^{701} is functionally annotated as an ERK substrate [76] - its decreased phosphorylation indicated an inhibition of ERK activity. However, the reduction of phosphorylation of non-annotated p-sites Thr^{116}, Ser^{998} and Ser^{1174} harbored higher potencies, which suggests a higher priority in the lapatinib-response and therefore a need for functional annotation. Further downstream, all three regulated p-sites on STMN1 are activity-inhibiting for the protein [77], but especially phosphorylation on Ser^{38} is potently decreased by lapatinib. The reason for the differential potencies of regulation even on the same protein

may be the complexity of the signaling network itself, where several kinases and phosphatases can act on the same substrate. The analysis of concentration-dependent drug perturbations therefore enables to order the effects on the phosphoproteome by their potency. In general, one has to note that the effect size of phosphoproteomic perturbations is a necessity for mode of action analyses but the potency will add valuable information. This will especially be helpful if effect sizes are equal, but potencies still vary.

The response of cellular signaling in HER2-overexpressing cells towards HER2 inhibition is highly dependent on their 3D microenvironment [72], which could explain the conflicting results. However, studies with the same cell lines and treatment conditions have highlighted divergent effects of trastuzumab. These reports described suppressed AKT and increased ERK phosphorylation upon trastuzumab treatment [73, 74]. Based on the data of this thesis, however, therapeutic antibodies seem to exert only minor direct effects on the selected breast cancer cell lines in contrast to lapatinib. With the cytostatic action of trastuzumab in mind, long-term exposure, which have not been analyzed in this thesis, might be needed to potently inhibit HER2 downstream signaling by the antibodies. Still, effector functions might contribute more, if not the most, to the efficacy of the antibodies in patients. This could be demonstrated by a considerably complementary action of lapatinib and trastuzumab in patients, which is suggested by better clinical outcomes when a dual HER2 blockade through the small molecule and antibody is applied [75].

3.6 Rituximab-resistant ARH-77 cells are sensitized by inhibiting MAPK pathway members

In contrast to the anti-HER2 mAbs, several thousands of p-sites were responsive towards rituximab suggesting a pivotal share of direct action on the therapeutic effect of the anti-CD20 mAb.

The drivers of phosphorylation-based signaling, protein and lipid kinases, can be regulated in their activity by phosphorylation on their own. Therefore, direct action on signaling pathways could be deduced from responsive kinases. Regulated kinases, which were defined by a regulation of at least one p-site in any time point, were compared between the cell lines (Figure IV-15A). In agreement with the general aforementioned findings, the sensitive cell lines harbored the highest number of regulated kinases, with an overlap of 76 kinases. The regulated kinases were consistently distributed over protein and lipid kinase families (Figure IV-15B) indicating again a comprehensive regulation of the phosphorylation-based signaling network by rituximab in SU-DHL-4 and Ramos cells.

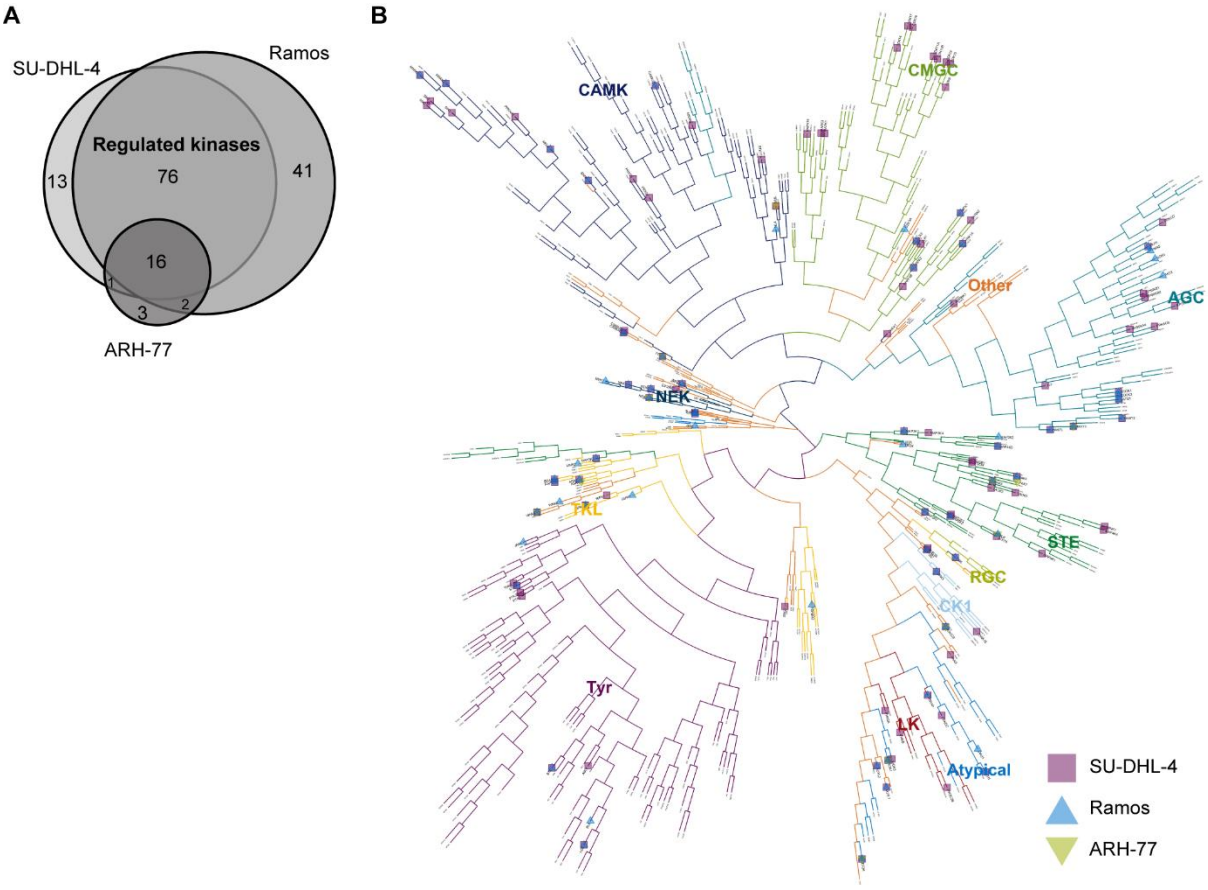

Figure IV-15: Phosphoproteomic regulation of protein and lipid kinases by rituximab. (A) Overlap of kinases, whose phosphorylation status has been regulated by rituximab. (B) Kinome tree of all human protein and lipid kinases. Kinase families are colored separately. Regulated kinases are highlighted by violet rectangles (SU-DHL-4), blue triangles (Ramos) and green triangles (ARH-77).

Particularly those regulated p-sites that were solely regulated in the sensitive cell lines and were annotated to control kinase activity could be used to infer direct engagement of signaling pathways by rituximab. For example, phosphorylation of MAPK1/3-Tyr$^{187/204}$ and MAPK14-Tyr^{182} indicates an induction of each kinase's activity [78][79] and was increased after middle- and long-term treatment with rituximab. This has also been found for SYK-Ser^{295}, illustrating increased SYK degradation [80] (Figure IV-16). Phosphorylation of BTK-Tyr^{223} is activity-inducing [81] and was reduced in the sensitive cell lines to a greater extent than in the resistant cell line. Decreased phosphorylation of MAP2K2-Ser^{306} and BRAF-Ser^{151} in the sensitive cell lines furthermore described a diminished MAP2K2 activity [82] and increased BRAF-RAS interaction[83].

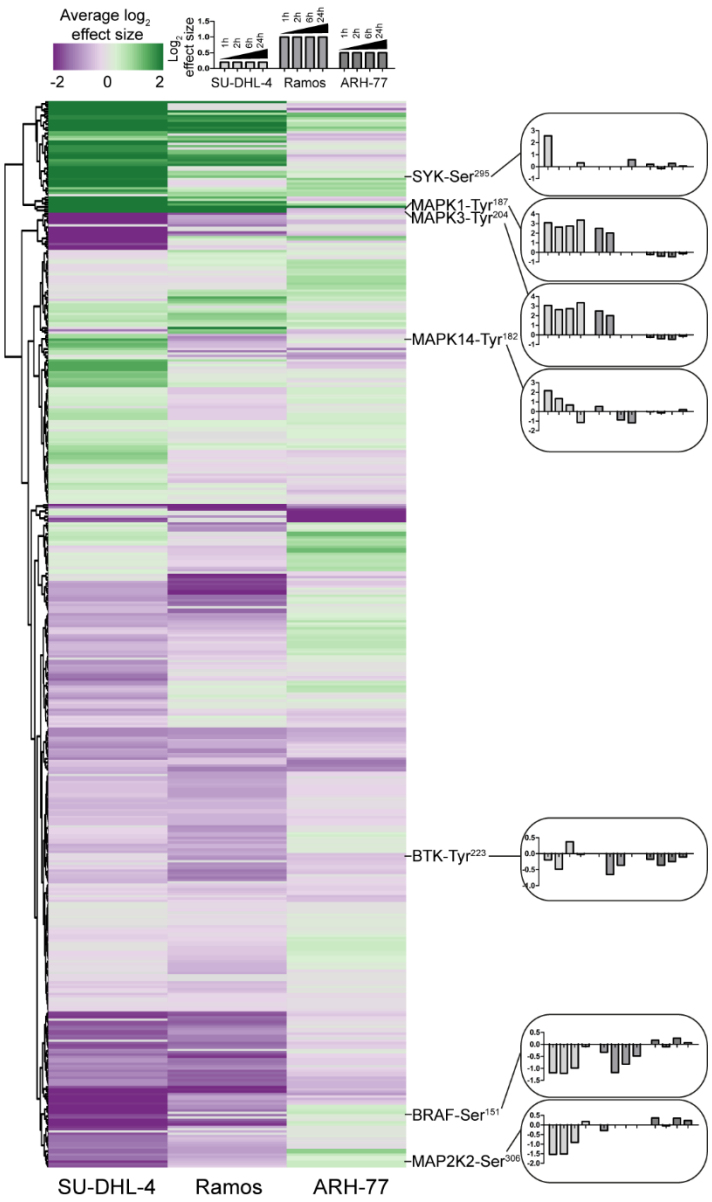

Figure IV-16: Heatmap of regulated kinase p-sites. The average effect size (based on 1, 2, 6 and 24 hours treatment) of each p-site is indicated by a green-violet color code. Additional bar charts highlight the effect sizes in each time point and cell line of selected kinase p-sites.

Table IV-2: Results of the sensitization experiments in ARH-77 cells with selected kinase inhibitors and rituximab. n.d. = not determined.

Kinase inhibitor	Target kinase	IC50 [nM]		Effect [-]		Sensitization
		Single	Combi	Single	Combi	
Dabrafenib	BRAF	157	n.d.	0.18	0.24	No (no effect)
ONO4059	BTK	n.d.	n.d.	0.29	0.33	
Ibrutinib	BTK	n.d.	n.d.	0.53	0.69	No (single treatment-sensitive)
BMS-387032	CDK	191	147	0.98	0.99	
Rabusertib	CHEK1	306	277	0.98	0.99	
R-406	SYK (active agent)	553	756	0.60	0.51	
Fostamatinib	SYK (pro-drug)	1090	1010	0.72	0.62	
MK-1775	WEE1	238	223	0.98	0.98	
Ulixertinib (BVD-523)	MAPK1/3	n.d.	n.d.	0.40	0.69	Yes
PH-797804	MAPK14	n.d.	n.d.	0.32	0.58	
Trametinib	MAP2K2	3464	n.d.	0.15	0.41	

Based on the presumed rituximab-induced kinase activity changes, 11 highly selective clinical inhibitors (as determined earlier [84]) of respective kinases were applied alone and in combination with 30 µg/ml rituximab on resistant ARH-77 cells (Table IV-2). Thereby, the aim was to identify sensitizing drugs and validate the importance of the respective kinase activity for rituximab-engaged signaling. While ARH-77 cells were resistant towards dabrafenib and ONO4059 as single as well as combination treatment (Figure IV-17A), ibrutinib, BMS-387032, rabusertib, R-406, fostamatinib, and MK-1775 have elucidated the same inhibitory effects alone and in combination with rituximab (Figure IV-17B). Ulixertinib (BVD-523), PH-797804, and trametinib, all MAPK signaling inhibitors, were the only screened drugs to sensitize ARH-77 cells towards rituximab treatment (Figure IV-17C).

Whilst the IC50 of trametinib in combination with rituximab is in sub-nanomolar range, picomolar concentrations of ulixertinib and PH-797804 in combination with 30 µg/ml rituximab executed inhibitory effects of up to 20 % (Figure IV-18). These effects highlighted a potent sensitization towards rituximab by MAPK inhibition.

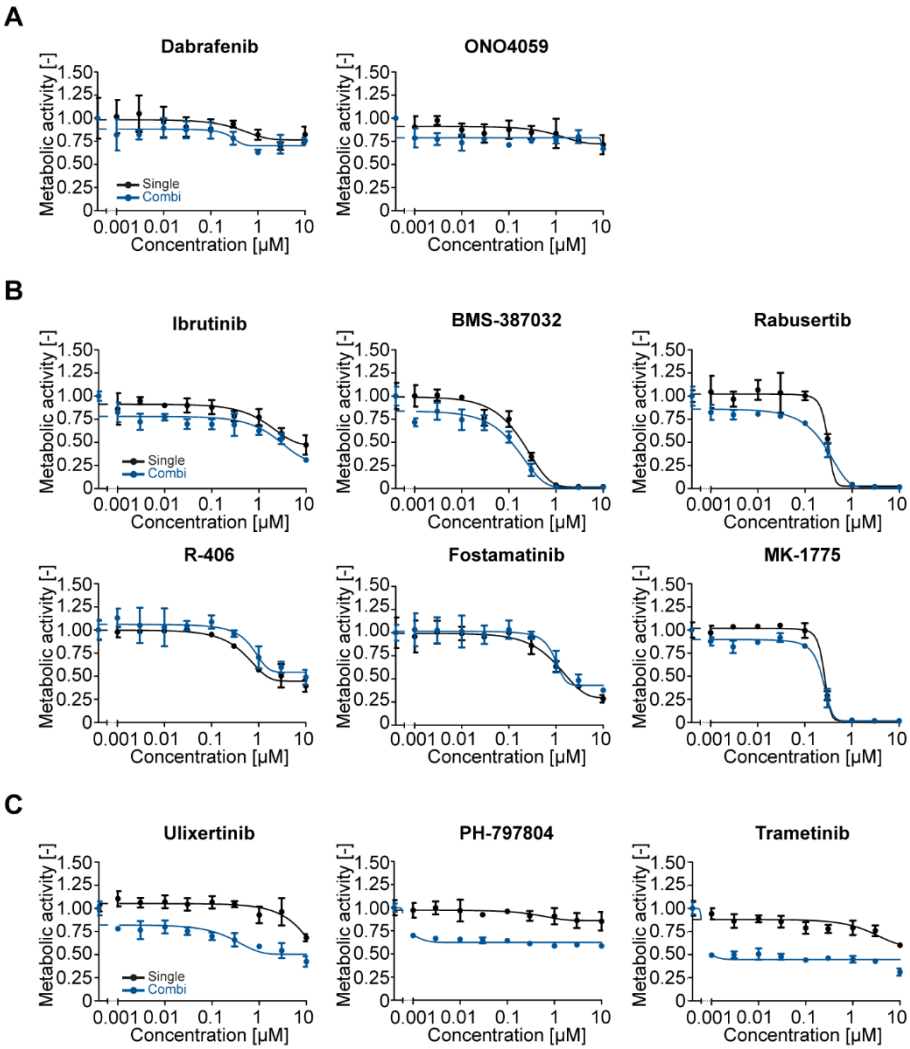

Figure IV-17: Sensitization of ARH-77 cells with selected kinase inhibitors. Metabolic activity of ARH-77 cells upon treatment with (A) dabrafenib, ONO4059, (B) ibrutinib, BMS-387032, rabusertib, R-406, fostamatinib, MK-1775, (C) ulixertinib, PH-797804 and tramitinib alone (Single) or with 30 µg/m rituximab (Combi) in an Alamar Blue assay. Error bars represent standard deviation (SD). Data represent N = 3 (A, B & C) biologically independent experiments.

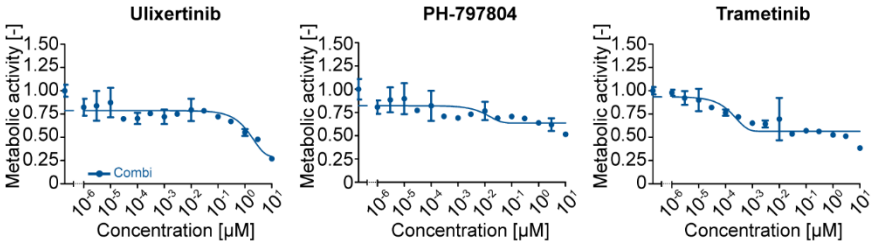

Figure IV-18: Sensitization of ARH-77 cells with MAPK signaling inhibitors in picomolar concentrations. Metabolic activity of ARH-77 cells upon treatment with ulixertinib, PH-797804 and trametinib with 30 µg/m rituximab (Combi) in an Alamar Blue assay. Error bars represent standard deviation (SD). Data represent N = 3 biologically independent experiments.

In contrast to the inhibition of MAPK1/3, MAPK14 and MAP2K2 in SU-DHL-4 cells, which has not changed rituximab sensitivity, pharmacological MAPK signaling inhibition has induced resistance in

former sensitive Ramos cells (Figure IV-19). This validated the significance of MAPK13 activity for the action of Rituximab, which was however cell-dependent.

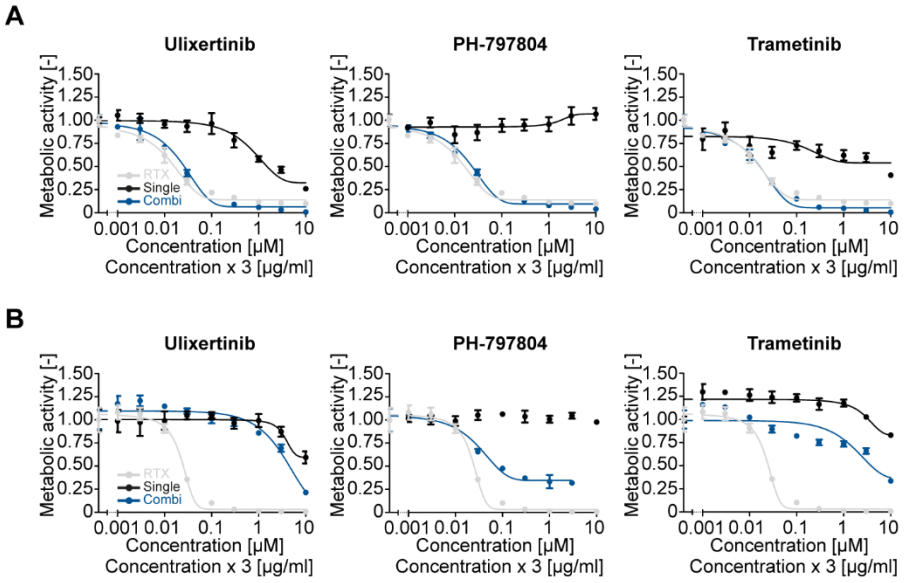

Figure IV-19: Differential effect of rituximab in combination with MAPK signaling inhibitors in SU-DHL-4 and Ramos cells. Metabolic activity of (A) SU-DHL-4 and (B) Ramos cells upon treatment with rituximab (RTX), ulixertinib, PH-797804 and trametinib alone (Single) or with 30 µg/ml rituximab (Combi) in an Alamar Blue assay. The concentration of RTX is x 3 [µg/ml]. Error bars represent standard deviation (SD). Data represent N = 3 biologically independent experiments.

3.7 Phosphorylated MAPK1/3 can serve as both rituximab-resistance and -treatment markers

Phosphoproteomic data indicated a regulation of MAPK signaling by rituximab. In particular, increased MAPK1/3 and MAPK14 as well as decreased MAP2K2 activity has been detected. Furthermore, chemical inhibition of MAPK signaling sensitized ARH-77 cells towards rituximab. Hence, further analysis focused on the function of MAPK1/3 for rituximab activity. Phosphorylation of MAPK1/3-Tyr$^{187/204}$ was increased upon engagement of rituximab points in the sensitive cell lines, starting as early as after 1 min rituximab treatment and increasing further in a time-dependent manner (Figure IV-20A). Contrarily, ARH-77 cells have not shown a concentration-dependent modulation of MAPK1/3-Tyr$^{187/204}$ phosphorylation in any time point. In addition, the phosphorylation level of MAPK1/3-Tyr$^{187/204}$ in the basal state of the three cell lines varied drastically – from highest levels in ARH-77 cells, medium levels in SU-DHL-4 and diminished levels in Ramos cells (Figure IV-20B). Western Blotting demonstrated increased MAPK1/3 activity after rituximab treatment as evident from increased phosphorylation of direct substrate RSK1/2/3-Thr^{159}/Ser^{363} in SU-DHL-4 and Ramos cells (Figure IV-20C). A missing

response of RSK1/2/3-Thr^{159}/Ser^{363} phosphorylation in ARH-77 to rituximab could be an artefact of the already increased MAPK1/3 activity in the basal state of the cells.

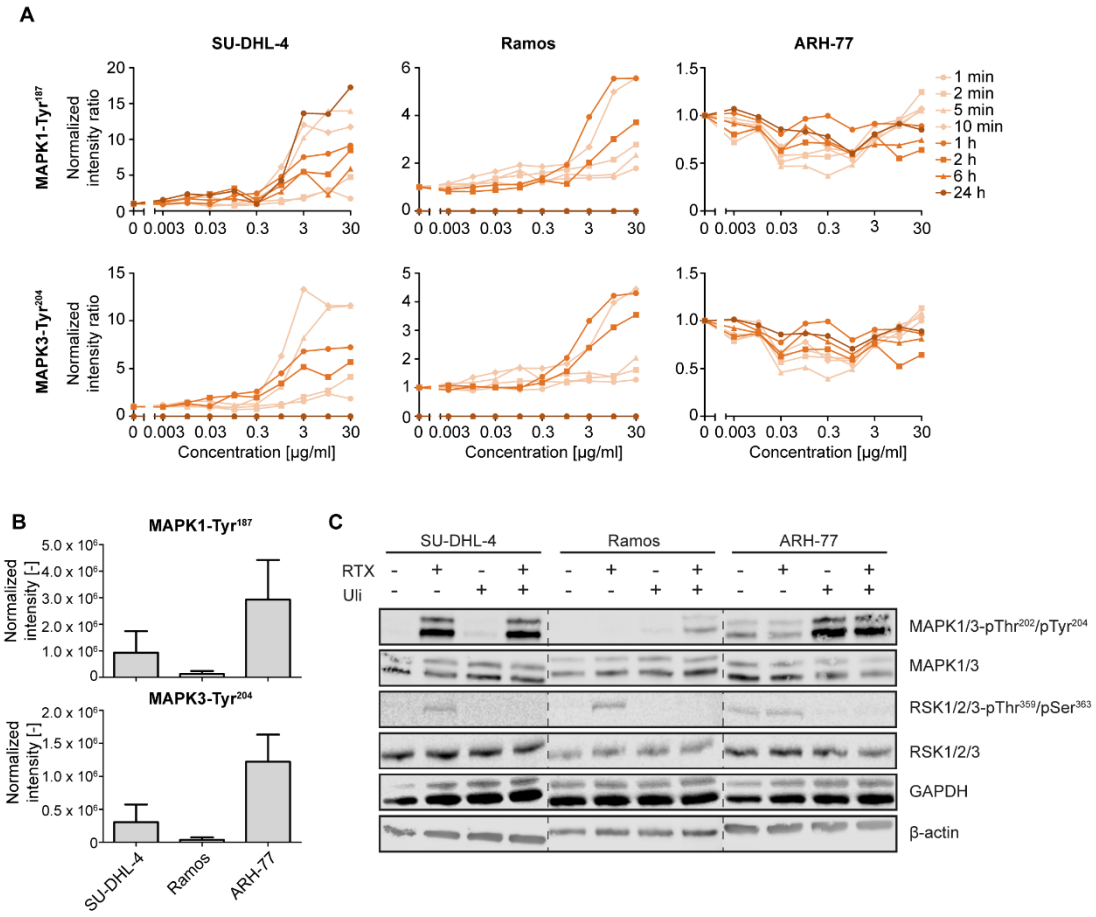

Figure IV-20: Increased intensity of phosphorylated MAPK1/3 upon rituximab treatment in sensitive cell lines. (A) Concentration-dependent normalized intensity ratios of phosphorylated MAPK1-Tyr^{187} (top) and MAPK3-Tyr^{204} (bottom) derived from the phosphoproteomic experiment in all three cell lines. (B) Basal normalized intensity of MAPK1/MAPK3-pTyr^{187}/pTyr^{204}, MAPK1/MAPK3, RSK1/2/3-pThr^{159}/pSer^{363}, RSK1/2/3, GAPDH and beta-actin in all three cell lines derived from the phosphoproteomic experiment. (C) Immunoblots showing in SU-DHL-4, Ramos and ARH-77 cells as control or after 1h single or combination treatment with 30 µg/ml rituximab (RTX) and 10 µM ulixertinib (Uli). Error bars represent standard deviation (SD). Data represent N = 1 (A & C) and N = 8 (B) biologically independent experiments.

Elevated MAPK1/3 activity after rituximab treatment in sensitive cells seems to be counterintuitive at first glance. Normally, it is regarded to cause increased cell proliferation. Reports about MAPK signaling upon rituximab engagement are conflicting suggesting either an activation [85] or inactivation of MAPK1/3 activity [86] and might not be in line with this data due to different cell lines, additional cross-linking of rituximab or generally dissimilar treatment parameters. While MAPK1/3 phosphorylation was only increased after combination treatment with ulixertinib in the sensitive cell lines, ARH-77 cells were showing increased phosphorylation upon both single and combination ulixertinib application. An

increase in MAPK1/3 phosphorylation by ulixertinib despite blocked downstream signaling, as seen here by completely abrogated RSK1/2/3 phosphorylation, has been already described in other cell lines [87]. Yet the lack of this behavior in the sensitive cell lines clearly demonstrates another aspect of differential MAPK signaling between the sensitive and resistant cell lines in this study.

MAPK1/3 is reported to be shuttled between nucleus and cytoplasm, whose balance tightly regulates the activity of the kinase [88]. A consistent coverage of both cellular compartments was confirmed in the basal state of the three cell lines (Figure IV-21, Figure IV-22, Figure IV-23). Upon rituximab application, in single and in combination treatment with ulixertinib, all the cell lines underwent a localization of phosphorylated MAPK1/3 to the cell membrane (overlapping with CD20 localization). A potential aftermath of the membrane localization might be a change in substrate availability of MAPK1/3. Still, since this observation was made for all three cell lines, a direct link to sensitivity or resistance cannot be drawn. So far, reports about this behavior are scarce but suggested a general increase of MAPK1/3 phosphorylation as well as a localization into lipid rafts upon rituximab treatment [85]. The data of this thesis can complement these reports by the remark that membrane localization of phosphorylated MAPK1/3 is independent of the cellular activity of rituximab. Nevertheless, the exact mechanism of de-localization and the cellular aftermath leading to the response to rituximab are still unknown.

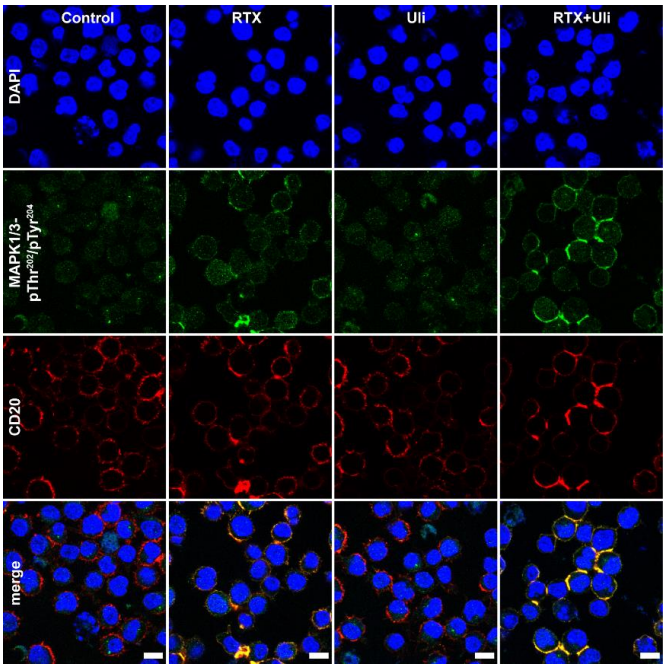

Figure IV-21: Membrane localization of phosphorylated MAPK1/3 upon rituximab treatment in SU-DHL-4 cells. Immunofluorescence pictures of SU-DHL-4 cells stained for the nuclei (DAPI), MAPK1/MAPK3-pTyr^{187}/pTyr^{204} and CD20 with or without 1h single or combination treatment with 30 µg/ml rituximab (RTX) and 10 µM ulixertinib (Uli). A merged picture of all stainings is added. Bar = 10 µm.

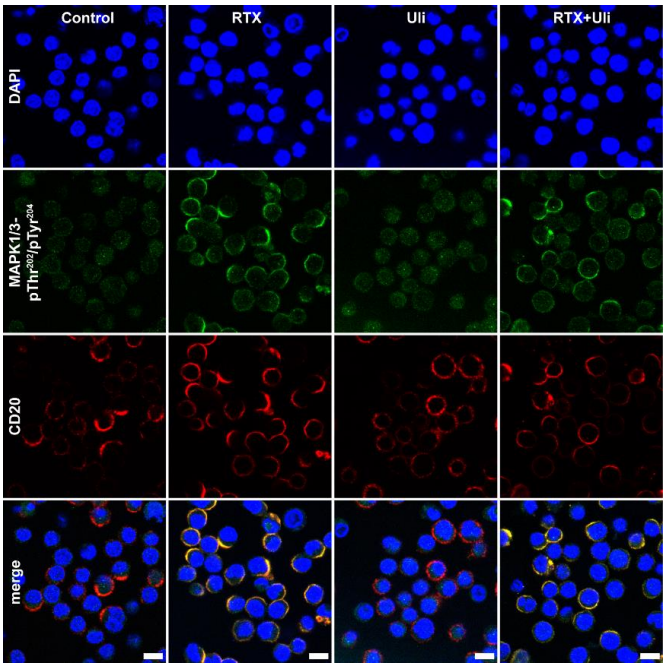

Figure IV-22: Membrane localization of phosphorylated MAPK1/3 upon rituximab treatment in Ramos cells. Immunofluorescence pictures of Ramos cells stained for the nuclei (DAPI), MAPK1/MAPK3-pTyr^{187}/pTyr^{204} and CD20 with or without 1h single or combination treatment with 30 µg/ml rituximab (RTX) and 10 µM ulixertinib (Uli). A merged picture of all stainings is added. Bar = 10 µm.

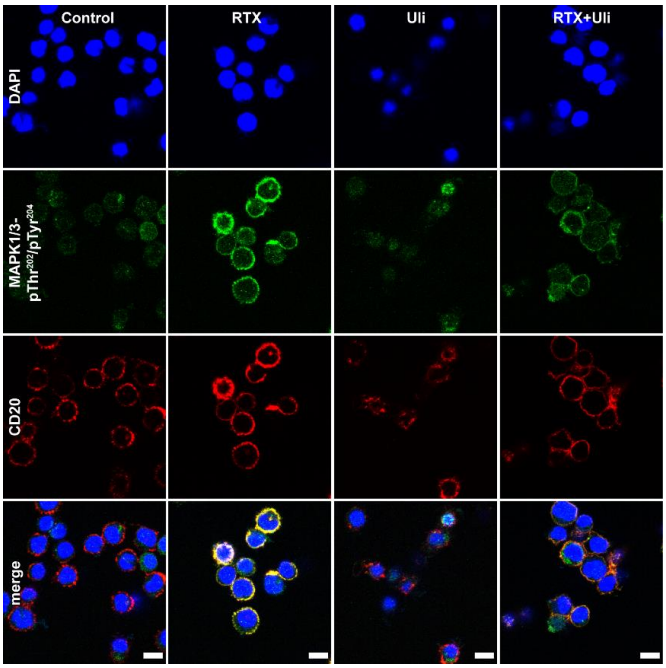

Figure IV-23: Membrane localization of phosphorylated MAPK1/3 upon rituximab treatment in ARH-77 cells. Immunofluorescence pictures of SU-DHL-4 cells stained for the nuclei (DAPI), MAPK1/MAPK3-pTyr^{187}/pTyr^{204} and CD20 with or without 1h single or combination treatment with 30 µg/ml rituximab (RTX) and 10 µM ulixertinib (Uli). A merged picture of all stainings is added. Bar = 10 µm.

In summary, the data indicate elevated levels of phosphorylated MAPK1/MAPK3-Tyr^{187}/Tyr^{204} to serve both as a resistance marker in the basal state and as a treatment marker upon rituximab application. However, the exact mechanism of how MAPK activity/phosphorylation can shape the response towards rituximab treatment is still not clear. Although the localization of phosphorylated MAPK1/3 to the cell membrane was sensitivity-independent, the (assumed) differential lipid raft composition of the cell lines might imply lipid-based factors to additionally contribute to MAPK-dependent rituximab resistance and sensitivity. The sensitizing effect of MAPK signaling inhibitors ulixertinib, PH-797804 and trametinib in rituximab-resistant cells could suggest clinical potential to fight rituximab resistance, especially since the drugs are already in later stages of clinical studies (ulixertinib and PH-797804: Phase II) or are even already approved (trametinib). However, the introduction of resistance by applying the three inhibitors in one of the two sensitive cells prompts high caution when inhibiting MAPK signaling in rituximab-sensitive cells.

3.8 Rituximab activates NFAT early and arrests the cell cycle later on

To comprehensively analyze cellular functions that are engaged by rituximab, a Reactome enrichment was performed on regulated p-proteins, here exemplified in Ramos cells. Enriched pathways were observed as early as after 1 min and, as expected, were found in increased numbers over time leading to > 180 pathways upon 24 h rituximab application (Figure IV-24A). The high number of enriched pathways reflect the immense number of regulated p-sites, which restricted the following analysis on selected cases. Examples for a very early response starting from 1 min rituximab treatment were two Reactome entities, which deal with NFAT activation (R-HSA-2025928: Calcineurin activates NFAT; R-HSA-5607763: CLEC7A (Dectin-1) induces NFAT activation). Contrary to NFAT activation, cell cycle-annotated pathway members (R-HSA-69278 Cell Cycle, Mitotic; R-HSA-1640170: Cell cycle) were enriched in later time points of up to 24 h. A reproducible enrichment of pathways in up to 6 time points was observed, which strengthened the consistency of the action of rituximab on these functionalities, such as the cell cycle-associated pathways (Figure IV-24B).

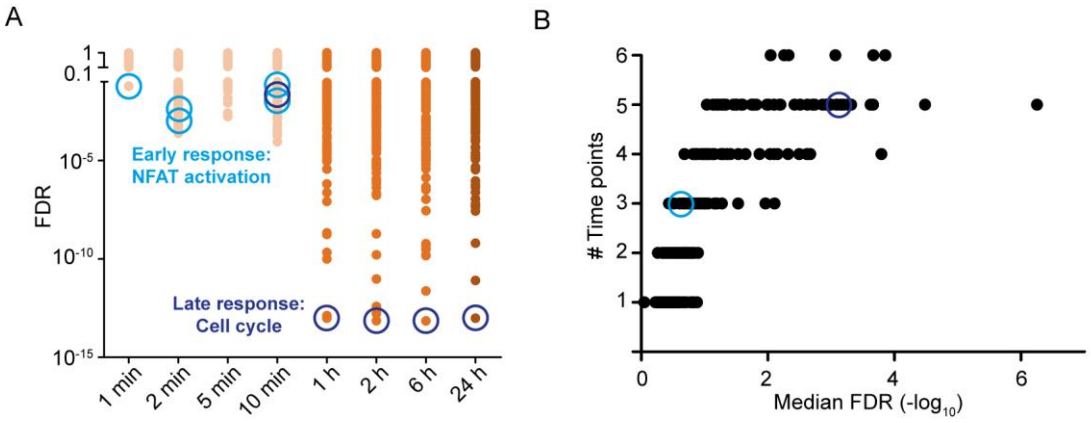

Figure IV-24: Enrichment of regulated pathways by rituximab in Ramos cells. (A) Time-resolved enrichment of Reactome pathways. Enriched pathways were filtered according to a FDR of 0.1. Enriched NFAT activation entities (R-HSA-2025928, R-HSA-5607763) are highlighted by light blue circles and cell cycle entities (R-HSA-69278, R-HSA-1640170) by dark blue circles. (B) Reactome pathways according to the number of time points, in which they are enriched. The median -log10 FDR is indicated.

NFATC1-4 (NFAT1-4) are renowned transcription factors, which are activated by a calcium influx-dependent dephosphorylation by calcineurin [89, 90]. Decreased phosphorylation upon rituximab treatment was observed for the majority of NFATC1-4 p-sites in Ramos cells (Figure IV-25A). Reported NFATC2 pSer-sites that are dephosphorylated by calcineurin upon ionomycin stimulation [91] harbored decreased intensity in this dataset. Consequently, a dephosphorylation by calcineurin and therefore an activation of NFATC2 can be deduced. The potencies of dephosphorylation of these p-sites by rituximab, ranging from 0.4 to 2.1 µg/ml, were in the same order of magnitude and therefore could highlight the same source of dephosphorylation. With this regard, the additionally identified p-sites on NFATC2 as well as on NFATC1, NFATC3, and NFATC4 that have been decreased in their phosphorylation intensity might be potential direct targets of calcineurin. A similar response on NFAT activation is observed in SU-DHL-4 cells. This is exemplified by an early decrease in phosphorylation of calcineurin target NFATC2-Ser^{268} and NFATC2-Ser^{110}, which is part of the SPRIEIT motif guiding calcineurin binding [92] (Figure IV-25B). Interestingly, phosphorylation intensity of NFATC2-Ser^{110} was decreased in ARH-77 cells, although to a lesser extent than in the two sensitive cell lines. In contrast, phosphorylation of NFATC2-Ser^{268} has not been regulated by rituximab in the resistant cells. The lack of NFAT activation by missing dephosphorylation through calcineurin in the resistant cell line might be additionally augmented by a generally low expression of all four NFATCs in ARH-77 cells as compared to the sensitive cell lines (Figure IV-25C). Expression of calcineurin subunits have not shown a general trend between sensitive and resistant cells.

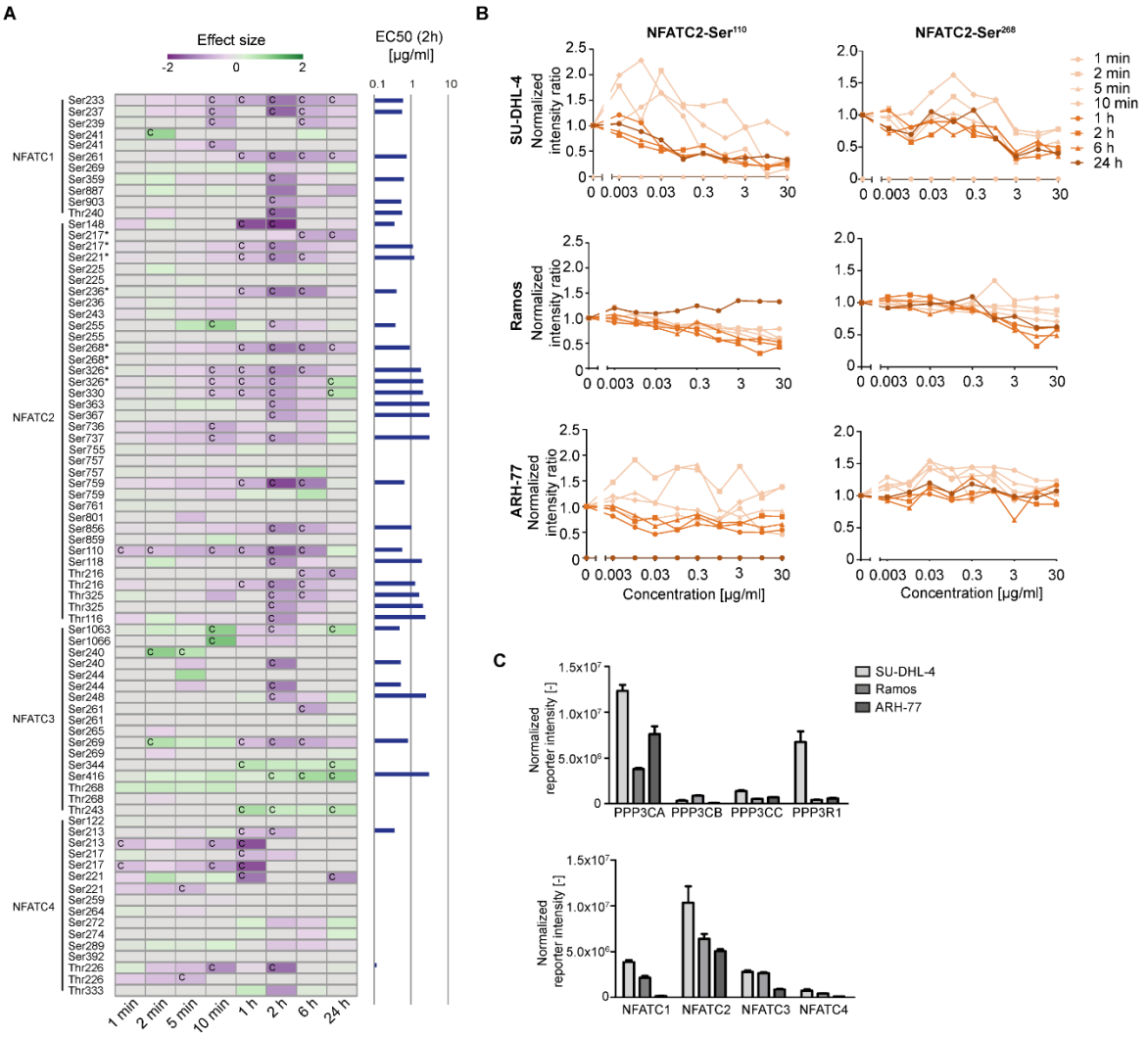

Figure IV-25: Rituximab prompts early NFATC dephosphorylation. (A) Heatmap of all identified and quantified p-sites of NFATC1-4. The effect size of each p-site is indicated by a green-violet color code for each time point. A 'c' highlights those p-sites, which were regulated by rituximab in the respective time point. Asterisks are marking p-sites, which are reported to be dephosphorylated upon ionomycin treatment [91]. Additional bar charts illustrate the EC50 of the respective p-site after the 2 h rituximab treatment. (B) Concentration-dependent normalized intensity ratios of phosphorylated NFATC2-Ser110 (left) and NFATC2-Ser268 (right) derived from the phosphoproteomic experiment in all three cell lines. (C) Normalized intensities of calcineurin subunits (PPP3CA, PPP3CB, PPP3CC and PPP3R1) and NFATC proteins (NFATC1, NFATC2, NFATC3 andNFATC4). Error bars represent standard deviation (SD). Data represent N = 10 concentration-dependent biologically independent experiments.

The regulation of NFATC1-4 p-sites was observed starting as early as 1 min after rituximab application and was missing in resistant cells and indicates a pivotal role of NFAT activation in the mode of action of the antibody. This observation can complement literature that have provided evidence for a calcium influx and cell death induced by the shift of CD20 into lipid rafts by rituximab [29, 93]. Furthermore, Syk engagement, as found in SU-DHL-4 and Ramos cells and discussed above, is in line with the known activation cascade of calcineurin [94, 95]. Several reports pointed towards a distinct role of NFAT

signaling in cancer cells. NFATC2 and NFATC3 seem to have a pro-apoptotic activity, whereas NFATC1 executes anti-apoptotic effects prompting the study of calcineurin inhibitors for certain cancers types [96, 97]. Consequently, increased expression levels of NFATC2, in comparison to NFATC1, NFATC3 and NFATC4, suggest a pro-apoptotic action that could complement rituximab-dependent NFAT signaling activation as a very early part of the mode of action of the antibody.

Contrary to NFAT activation, engagement of cell cycle proteins was enriched after prolonged rituximab treatment. Over 200 regulated p-proteins were mapped to the cell cycle by the Reactome pathway enrichment. Among those proteins, Retinoblastoma protein RB1, a well-studied tumor suppressor and one of the key regulators of cell cycle progression [98], has been regulated on several p-sites. The regulation has mostly started after 1 hour with increasing effect size until 6 hours of treatment suggesting a rather late response compared to e.g. NFAT activation (Figure IV-26A). As discussed earlier, the decrease in the effect size after an even longer treatment of 24 hours could hint to a counteracting activity of cellular signaling and beginning of cell death. The majority of identified RB1 p-sites have been dephosphorylated upon rituximab treatment. This indicates a blocked cell cycle progression from G1 to S phase, leading to modulated apoptosis, differentiation, and cell growth [99]. As an example, RB1-Ser^{249} is a known cyclin-dependent kinase (CDK) phosphorylation site [100] and its phosphorylation has decreased upon rituximab action (Figure IV-26B). Upstream kinases of RB1, CDK1/2/3 and WEE1, have been dephosphorylated on e.g. Tyr^{15} and Ser^{165}, respectively. Decreased phosphorylation intensity of CDK1/2/3-Tyr^{15}, a WEE1 p-site, suggests decreased enzymatic activity [101], which is in agreement with decreased RB1-Ser^{249} phosphorylation. The resistant cell line missed an effect on these signaling cascades as exemplified with a steady phosphorylation of RB1-Ser^{249} (Figure IV-26C).

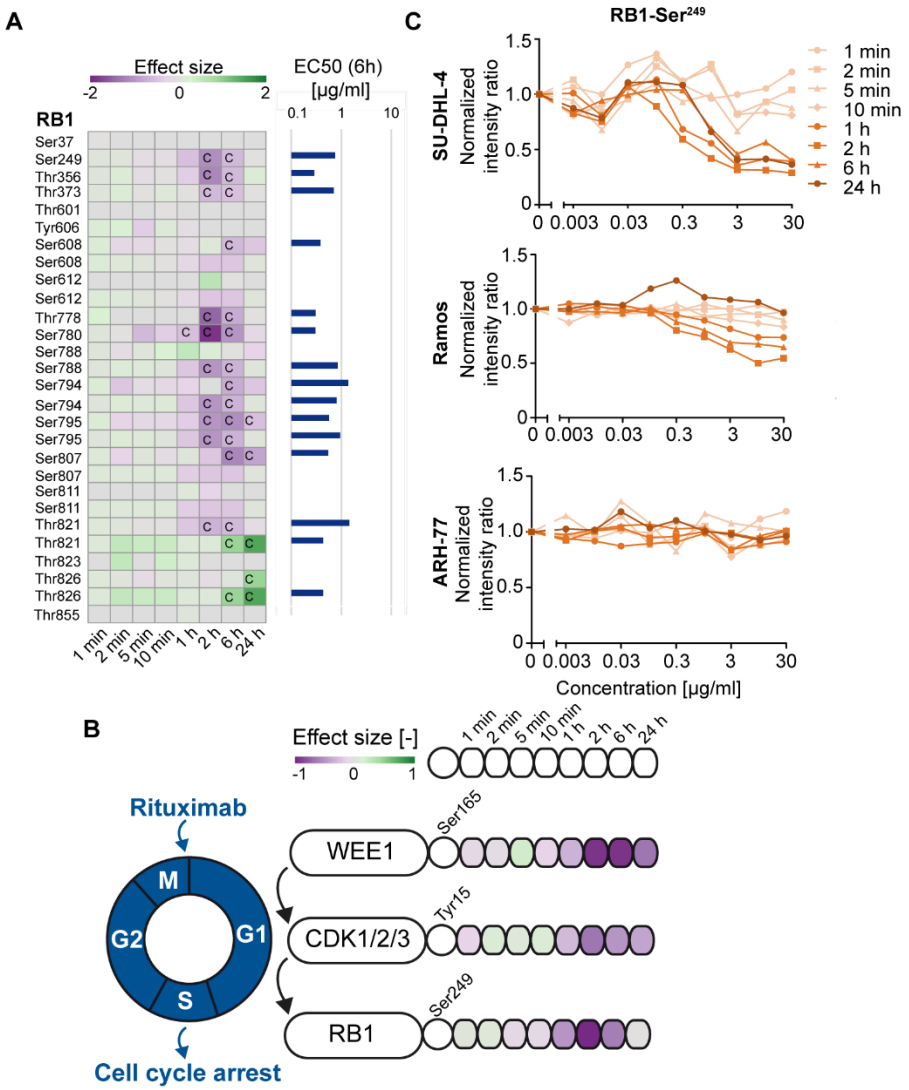

Figure IV-26: RB-1 dephosphorylation by rituximab leads to cell cycle arrest. (A) Heatmap of all identified and quantified p-sites of RB1 in Ramos cells. The effect size of each p-site is indicated by a green-violet color code for each time point. A "c" highlights those p-sites, which were regulated by rituximab in the respective time point. Additional bar charts illustrate the EC50 of the respective p-site after the 6 h rituximab treatment. (B) Selected p-sites of cell cycle members WEE1, CDK1/2/3 and RB1 are highlighted and characterized by their effect size in each time point in Ramos cells. Arrows indicate a kinase-substrate relationship. (C) Concentration-dependent normalized intensity ratios of phosphorylated RB1-Ser^{249} derived from the phosphoproteomic experiment in all three cell lines. Error bars represent standard deviation (SD). Data represent N = 10 concentration-dependent biologically independent experiments.

A cell cycle arrest at G1 phase upon anti-CD20 mAb application has already been reported [102]. The data of this thesis, however, illustrates in detail how a comprehensive protein phosphorylation-based engagement of the cell cycle machinery leads to cell cycle arrest in the sensitive cell lines. Due to its occurrence in the hours range, the cell cycle arrest can be regarded as a late response of rituximab

engagement. It displays a pivotal part of the mode of action of rituximab, which is additionally highlighted by the sheer amount of regulated affiliated proteins.

The fact that both examples of integral parts of the mode of action of rituximab could have been missed with a phosphoproteomic analysis of solely extended treatment times strengthens the importance of a time-dependent analysis of drug action. Especially short-term (minute range) treatments enable to uncover very early responses to a studied drug, which further activate perturbations of cellular signaling leading to the final fate of treated cells and could be counteracted by feedback actions after longer times. Still, time-dependent regulations of the phosphoproteome analyzed in this thesis should be validated by an additional dataset that makes use of a time-multiplexed sample processing, instead of the concentration-multiplexed samples analyzed in this thesis. In this regard, high correlations between the fold changes of p-site intensities in both datasets can prove the apparent temporal regulations between the separate datasets discussed here.

In summary, this study demonstrates that the systematic analysis of the direct action of therapeutic antibodies on cancer cells by phosphoproteomic is feasible and critical to understand signaling networks. The presented data suggests that the therapeutic action of anti-HER2 mAbs is rather driven by effector functions than by a direct perturbation of cancer cell signaling. In contrast, the share of the direct effects by anti-CD20 rituximab on the total drug action seems to be considerably high. These examples portray the complexity of antibody action and could motivate further studies. The established sample processing and data analysis workflow might be easily applied for future analyses of the mode of action in additional cell line panels and patient-derived cells as well as for other therapeutic mAbs and antibody constructs.

Acknowledgements

I am greatly thankful for the help of PD Dr. Karl Kramer with the cytotoxicity Incucyte assays and immunofluorescence experiments and Dr. Guillaume Médard for all kinase-related discussions and help with the kinome tree. I also want to thank my students, whom I supervised during their M.Sc. theses: Leonie Reichart for the concentration-dependent phosphoproteomic experiments, Mona Huygelen for the sensitization experiments, and Nicola Berner for Western Blotting, the immunofluorescence and time-dependent phosphoproteomic experiments. I especially want to thank Prof. Dr. Angela Krackhardt and her group (Tumorimmunology and Translational Immuntherapy, Technical University of Munich) for providing trastuzumab and rituximab, and therefore having enabled this project early on.

References

1. Scott AM, Wolchok JD, Old LJ: Antibody therapy of cancer. *Nat Rev Cancer* 2012, 12(4):278-287.
2. Ménard S, Fortis S, Castiglioni F, Agresti R, Balsari A: HER2 as a prognostic factor in breast cancer. *Oncology* 2001, 61 Suppl 2:67-72.
3. Ross JS, Slodkowska EA, Symmans WF, Pusztai L, Ravdin PM, Hortobagyi GN: The HER-2 receptor and breast cancer: ten years of targeted anti-HER-2 therapy and personalized medicine. *The oncologist* 2009, 14(4):320-368.
4. Franklin MC, Carey KD, Vajdos FF, Leahy DJ, de Vos AM, Sliwkowski MX: Insights into ErbB signaling from the structure of the ErbB2-pertuzumab complex. *Cancer Cell* 2004, 5(4):317-328.
5. Carter P, Presta L, Gorman CM, Ridgway JB, Henner D, Wong WL, Rowland AM, Kotts C, Carver ME, Shepard HM: Humanization of an anti-p185HER2 antibody for human cancer therapy. *Proc Natl Acad Sci U S A* 1992, 89(10):4285-4289.
6. Spector NL, Blackwell KL: Understanding the mechanisms behind trastuzumab therapy for human epidermal growth factor receptor 2-positive breast cancer. *J Clin Oncol* 2009, 27(34):5838-5847.
7. Agus DB, Akita RW, Fox WD, Lewis GD, Higgins B, Pisacane PI, Lofgren JA, Tindell C, Evans DP, Maiese K *et al*: Targeting ligand-activated ErbB2 signaling inhibits breast and prostate tumor growth. *Cancer Cell* 2002, 2(2):127-137.
8. Perez EA, Romond EH, Suman VJ, Jeong JH, Sledge G, Geyer CE, Jr., Martino S, Rastogi P, Gralow J, Swain SM *et al*: Trastuzumab plus adjuvant chemotherapy for human epidermal growth factor receptor 2-positive breast cancer: planned joint analysis of overall survival from NSABP B-31 and NCCTG N9831. *J Clin Oncol* 2014, 32(33):3744-3752.
9. Oh D-Y, Bang Y-J: HER2-targeted therapies — a role beyond breast cancer. *Nature Reviews Clinical Oncology* 2020, 17(1):33-48.
10. von Minckwitz G, Procter M, de Azambuja E, Zardavas D, Benyunes M, Viale G, Suter T, Arahmani A, Rouchet N, Clark E *et al*: Adjuvant Pertuzumab and Trastuzumab in Early HER2-Positive Breast Cancer. *New England Journal of Medicine* 2017, 377(2):122-131.
11. Swain SM, Kim SB, Cortés J, Ro J, Semiglazov V, Campone M, Ciruelos E, Ferrero JM, Schneeweiss A, Knott A *et al*: Pertuzumab, trastuzumab, and docetaxel for HER2-positive metastatic breast cancer (CLEOPATRA study): overall survival results from a randomised, double-blind, placebo-controlled, phase 3 study. *The Lancet Oncology* 2013, 14(6):461-471.
12. Lambert JM, Chari RV: Ado-trastuzumab Emtansine (T-DM1): an antibody-drug conjugate (ADC) for HER2-positive breast cancer. *Journal of medicinal chemistry* 2014, 57(16):6949-6964.
13. Martin M, Holmes FA, Ejlertsen B, Delaloge S, Moy B, Iwata H, von Minckwitz G, Chia SKL, Mansi J, Barrios CH *et al*: Neratinib after trastuzumab-based adjuvant therapy in HER2-positive breast cancer (ExteNET): 5-year analysis of a randomised, double-blind, placebo-controlled, phase 3 trial. *The Lancet Oncology* 2017, 18(12):1688-1700.
14. Geyer CE, Forster J, Lindquist D, Chan S, Romieu CG, Pienkowski T, Jagiello-Gruszfeld A, Crown J, Chan A, Kaufman B *et al*: Lapatinib plus Capecitabine for HER2-Positive Advanced Breast Cancer. *New England Journal of Medicine* 2006, 355(26):2733-2743.
15. Beers SA, Chan CH, French RR, Cragg MS, Glennie MJ: CD20 as a target for therapeutic type I and II monoclonal antibodies. *Semin Hematol* 2010, 47(2):107-114.
16. Edwards JCW, Cambridge G: B-cell targeting in rheumatoid arthritis and other autoimmune diseases. *Nature Reviews Immunology* 2006, 6:394.

17. Abulayha AM, Tabal SA, Shawesh EI, Elbasir MA, Elbanani AS, Lamami YM, Bredan A: Depletion of peripheral blood B cells with Rituximab and phenotype characterization of the recovering population in a patient with follicular lymphoma. *Leukemia research* 2010, 34(3):307-311.
18. Cragg MS, Walshe CA, Ivanov AO, Glennie MJ: The biology of CD20 and its potential as a target for mAb therapy. *Current directions in autoimmunity* 2005, 8:140-174.
19. Li H, Ayer LM, Lytton J, Deans JP: Store-operated cation entry mediated by CD20 in membrane rafts. *J Biol Chem* 2003, 278(43):42427-42434.
20. Walshe CA, Beers SA, French RR, Chan CHT, Johnson PW, Packham GK, Glennie MJ, Cragg MS: Induction of Cytosolic Calcium Flux by CD20 Is Dependent upon B Cell Antigen Receptor Signaling. *Journal of Biological Chemistry* 2008, 283(25):16971-16984.
21. Pierpont TM, Limper CB, Richards KL: Past, Present, and Future of Rituximab—The World's First Oncology Monoclonal Antibody Therapy. *Frontiers in Oncology* 2018, 8(163).
22. Maloney DG, Liles TM, Czerwinski DK, Waldichuk C, Rosenberg J, Grillo-Lopez A, Levy R: Phase I clinical trial using escalating single-dose infusion of chimeric anti-CD20 monoclonal antibody (IDEC-C2B8) in patients with recurrent B-cell lymphoma. *Blood* 1994, 84(8):2457-2466.
23. Shanafelt TD, Wang XV, Kay NE, Hanson CA, O'Brien S, Barrientos J, Jelinek DF, Braggio E, Leis JF, Zhang CC *et al*: Ibrutinib–Rituximab or Chemoimmunotherapy for Chronic Lymphocytic Leukemia. *New England Journal of Medicine* 2019, 381(5):432-443.
24. Kasi PM, Tawbi HA, Oddis CV, Kulkarni HS: Clinical review: Serious adverse events associated with the use of rituximab - a critical care perspective. *Critical care (London, England)* 2012, 16(4):231.
25. Clynes RA, Towers TL, Presta LG, Ravetch JV: Inhibitory Fc receptors modulate in vivo cytotoxicity against tumor targets. *Nat Med* 2000, 6(4):443-446.
26. Harjunpaa A, Junnikkala S, Meri S: Rituximab (anti-CD20) therapy of B-cell lymphomas: direct complement killing is superior to cellular effector mechanisms. *Scandinavian journal of immunology* 2000, 51(6):634-641.
27. Beers SA, Cragg MS, Glennie MJ: Complement: help or hindrance? *Blood* 2009, 114(27):5567-5568; author reply 5568.
28. Byrd JC, Kitada S, Flinn IW, Aron JL, Pearson M, Lucas D, Reed JC: The mechanism of tumor cell clearance by rituximab in vivo in patients with B-cell chronic lymphocytic leukemia: evidence of caspase activation and apoptosis induction. *Blood* 2002, 99(3):1038-1043.
29. Unruh TL, Li H, Mutch CM, Shariat N, Grigoriou L, Sanyal R, Brown CB, Deans JP: Cholesterol depletion inhibits src family kinase-dependent calcium mobilization and apoptosis induced by rituximab crosslinking. *Immunology* 2005, 116(2):223-232.
30. Chan HT, Hughes D, French RR, Tutt AL, Walshe CA, Teeling JL, Glennie MJ, Cragg MS: CD20-induced lymphoma cell death is independent of both caspases and its redistribution into triton X-100 insoluble membrane rafts. *Cancer Res* 2003, 63(17):5480-5489.
31. Coiffier B, Sarkozy C: Diffuse large B-cell lymphoma: R-CHOP failure-what to do? *Hematology American Society of Hematology Education Program* 2016, 2016(1):366-378.
32. Bello C, Veliz M, Pinilla-Ibarz J: Ofatumumab in the treatment of low-grade non-Hodgkin's lymphomas and chronic lymphocytic leukemia. *Expert review of clinical immunology* 2011, 7(3):295-300.
33. Lee HZ, Miller BW, Kwitkowski VE, Ricci S, DelValle P, Saber H, Grillo J, Bullock J, Florian J, Mehrotra N *et al*: U.S. Food and drug administration approval: obinutuzumab in combination

with chlorambucil for the treatment of previously untreated chronic lymphocytic leukemia. *Clin Cancer Res* 2014, 20(15):3902-3907.
34. Syed YY: Ocrelizumab: A Review in Multiple Sclerosis. *CNS drugs* 2018, 32(9):883-890.
35. Cartron G, Dacheux L, Salles G, Solal-Celigny P, Bardos P, Colombat P, Watier H: Therapeutic activity of humanized anti-CD20 monoclonal antibody and polymorphism in IgG Fc receptor FcgammaRIIIa gene. *Blood* 2002, 99(3):754-758.
36. Ghielmini M, Rufibach K, Salles G, Leoncini-Franscini L, Léger-Falandry C, Cogliatti S, Fey M, Martinelli G, Stahel R, Lohri A *et al*: Single agent rituximab in patients with follicular or mantle cell lymphoma: clinical and biological factors that are predictive of response and event-free survival as well as the effect of rituximab on the immune system: a study of the Swiss Group for Clinical Cancer Research (SAKK). *Annals of oncology : official journal of the European Society for Medical Oncology* 2005, 16(10):1675-1682.
37. Váróczy L, Zilahi E, Gyetvai A, Kajtár B, Gergely L, Sipka S, Illés A: Fc-gamma-receptor IIIa polymorphism and gene expression profile do not predict the prognosis in diffuse large B-cell lymphoma treated with R-CHOP protocol. *Pathology oncology research : POR* 2012, 18(1):43-48.
38. Castro F, Dirks WG, Fahnrich S, Hotz-Wagenblatt A, Pawlita M, Schmitt M: High-throughput SNP-based authentication of human cell lines. *Int J Cancer* 2013, 132(2):308-314.
39. Ruprecht B, Koch H, Medard G, Mundt M, Kuster B, Lemeer S: Comprehensive and reproducible phosphopeptide enrichment using iron immobilized metal ion affinity chromatography (Fe-IMAC) columns. *Mol Cell Proteomics* 2015, 14(1):205-215.
40. Kokubu M, Ishihama Y, Sato T, Nagasu T, Oda Y: Specificity of Immobilized Metal Affinity-Based IMAC/C18 Tip Enrichment of Phosphopeptides for Protein Phosphorylation Analysis. *Analytical Chemistry* 2005, 77(16):5144-5154.
41. Ruprecht B, Wang D, Chiozzi RZ, Li L-H, Hahne H, Kuster B: Hydrophilic Strong Anion Exchange (hSAX) Chromatography Enables Deep Fractionation of Tissue Proteomes. In: *Proteomics: Methods and Protocols.* edn. Edited by Comai L, Katz JE, Mallick P. New York, NY: Springer New York; 2017: 69-82.
42. Cox J, Mann M: MaxQuant enables high peptide identification rates, individualized p.p.b.-range mass accuracies and proteome-wide protein quantification. *Nature biotechnology* 2008, 26:1367.
43. Cox J, Neuhauser N, Michalski A, Scheltema RA, Olsen JV, Mann M: Andromeda: a peptide search engine integrated into the MaxQuant environment. *J Proteome Res* 2011, 10(4):1794-1805.
44. Tyanova S, Temu T, Sinitcyn P, Carlson A, Hein MY, Geiger T, Mann M, Cox J: The Perseus computational platform for comprehensive analysis of (prote)omics data. *Nat Meth* 2016, 13(9):731-740.
45. Ritz C, Baty F, Streibig JC, Gerhard D: Dose-Response Analysis Using R. *PLoS One* 2015, 10(12):e0146021.
46. Jassal B, Matthews L, Viteri G, Gong C, Lorente P, Fabregat A, Sidiropoulos K, Cook J, Gillespie M, Haw R *et al*: The reactome pathway knowledgebase. *Nucleic Acids Res* 2020, 48(D1):D498-d503.
47. Kanehisa M, Goto S, Kawashima S, Nakaya A: The KEGG databases at GenomeNet. *Nucleic Acids Res* 2002, 30(1):42-46.
48. Schindelin J, Arganda-Carreras I, Frise E, Kaynig V, Longair M, Pietzsch T, Preibisch S, Rueden C, Saalfeld S, Schmid B *et al*: Fiji: an open-source platform for biological-image analysis. *Nature methods* 2012, 9(7):676-682.

49. Neve RM, Chin K, Fridlyand J, Yeh J, Baehner FL, Fevr T, Clark L, Bayani N, Coppe J-P, Tong F *et al*: A collection of breast cancer cell lines for the study of functionally distinct cancer subtypes. *Cancer cell* 2006, 10(6):515-527.
50. Ginestier C, Adelaide J, Goncalves A, Repellini L, Sircoulomb F, Letessier A, Finetti P, Geneix J, Charafe-Jauffret E, Bertucci F *et al*: ERBB2 phosphorylation and trastuzumab sensitivity of breast cancer cell lines. *Oncogene* 2007, 26(50):7163-7169.
51. Nahta R, Hung MC, Esteva FJ: The HER-2-targeting antibodies trastuzumab and pertuzumab synergistically inhibit the survival of breast cancer cells. *Cancer Res* 2004, 64(7):2343-2346.
52. Tóth G, Szőőr Á, Simon L, Yarden Y, Szöllősi J, Vereb G: The combination of trastuzumab and pertuzumab administered at approved doses may delay development of trastuzumab resistance by additively enhancing antibody-dependent cell-mediated cytotoxicity. *mAbs* 2016, 8(7):1361-1370.
53. Meng Y, Zheng L, Yang Y, Wang H, Dong J, Wang C, Zhang Y, Yu X, Wang L, Xia T *et al*: A monoclonal antibody targeting ErbB2 domain III inhibits ErbB2 signaling and suppresses the growth of ErbB2-overexpressing breast tumors. *Oncogenesis* 2016, 5:e211.
54. Tagliabue E, Campiglio M, Pupa SM, Ménard S, Balsari A: Activity and resistance of trastuzumab according to different clinical settings. *Cancer treatment reviews* 2012, 38(3):212-217.
55. Lewis GD, Lofgren JA, McMurtrey AE, Nuijens A, Fendly BM, Bauer KD, Sliwkowski MX: Growth Regulation of Human Breast and Ovarian Tumor Cells by Heregulin: Evidence for the Requirement of ErbB2 as a Critical Component in Mediating Heregulin Responsiveness. *Cancer Research* 1996, 56(6):1457-1465.
56. Wilson TR, Lee DY, Berry L, Shames DS, Settleman J: Neuregulin-1-mediated autocrine signaling underlies sensitivity to HER2 kinase inhibitors in a subset of human cancers. *Cancer Cell* 2011, 20(2):158-172.
57. Epstein AL, Herman MM, Kim H, Dorfman RF, Kaplan HS: Biology of the human malignant lymphomas. III. Intracranial heterotransplantation in the nude, athymic mouse. *Cancer* 1976, 37(5):2158-2176.
58. Klein G, Giovanella B, Westman A, Stehlin JS, Mumford D: An EBV-genome-negative cell line established from an American Burkitt lymphoma; receptor characteristics. EBV infectibility and permanent conversion into EBV-positive sublines by in vitro infection. *Intervirology* 1975, 5(6):319-334.
59. Burk KH, Drewinko B, Turjillo JM, Ahearn MJ: Establishment of a human plasma cell line in vitro. *Cancer Res* 1978, 38(8):2508-2513.
60. Treon SP, Mitsiades C, Mitsiades N, Young G, Doss D, Schlossman R, Anderson KC: Tumor Cell Expression of CD59 Is Associated With Resistance to CD20 Serotherapy in Patients With B-Cell Malignancies. *Journal of Immunotherapy* 2001, 24(3):263-271.
61. Simons K, Toomre D: Lipid rafts and signal transduction. *Nature Reviews Molecular Cell Biology* 2000, 1(1):31-39.
62. Meyer zum Büschenfelde C, Feuerstacke Y, Götze KS, Scholze K, Peschel C: GM1 expression of non-Hodgkin's lymphoma determines susceptibility to rituximab treatment. *Cancer Res* 2008, 68(13):5414-5422.
63. Bruno R, Washington CB, Lu JF, Lieberman G, Banken L, Klein P: Population pharmacokinetics of trastuzumab in patients with HER2+ metastatic breast cancer. *Cancer chemotherapy and pharmacology* 2005, 56(4):361-369.

64. Spector NL, Robertson FC, Bacus S, Blackwell K, Smith DA, Glenn K, Cartee L, Harris J, Kimbrough CL, Gittelman M *et al*: Lapatinib Plasma and Tumor Concentrations and Effects on HER Receptor Phosphorylation in Tumor. *PloS one* 2015, 10(11):e0142845-e0142845.
65. Regazzi MB, Iacona I, Avanzini MA, Arcaini L, Merlini G, Perfetti V, Zaja F, Montagna M, Morra E, Lazzarino M: Pharmacokinetic behavior of rituximab: a study of different schedules of administration for heterogeneous clinical settings. *Therapeutic drug monitoring* 2005, 27(6):785-792.
66. Awasthi A, Rolland DCM, Ayello J, van de Ven C, Basrur V, Conlon K, Fermin D, Barth MJ, Klein C, Elenitoba-Johnson KSJ *et al*: A comparative global phosphoproteomics analysis of obinutuzumab (GA101) versus rituximab (RTX) against RTX sensitive and resistant Burkitt lymphoma (BL) demonstrates differential phosphorylation of signaling pathway proteins after treatment. *Oncotarget* 2017, 8(69):113895-113909.
67. Everton KL, Abbott DR, Crockett DK, Elenitoba-Johnson KS, Lim MS: Quantitative proteomic analysis of follicular lymphoma cells in response to rituximab. *Journal of chromatography B, Analytical technologies in the biomedical and life sciences* 2009, 877(13):1335-1343.
68. Moasser MM: The oncogene HER2: its signaling and transforming functions and its role in human cancer pathogenesis. *Oncogene* 2007, 26(45):6469-6487.
69. Patrussi L, Savino MT, Pellegrini M, Paccani SR, Migliaccio E, Plyte S, Lanfrancone L, Pelicci PG, Baldari CT: Cooperation and selectivity of the two Grb2 binding sites of p52Shc in T-cell antigen receptor signaling to Ras family GTPases and Myc-dependent survival. *Oncogene* 2005, 24(13):2218-2228.
70. Kovacina KS, Park GY, Bae SS, Guzzetta AW, Schaefer E, Birnbaum MJ, Roth RA: Identification of a Proline-rich Akt Substrate as a 14-3-3 Binding Partner. *Journal of Biological Chemistry* 2003, 278(12):10189-10194.
71. Dougherty MK, Müller J, Ritt DA, Zhou M, Zhou XZ, Copeland TD, Conrads TP, Veenstra TD, Lu KP, Morrison DK: Regulation of Raf-1 by direct feedback phosphorylation. *Mol Cell* 2005, 17(2):215-224.
72. Weigelt B, Lo AT, Park CC, Gray JW, Bissell MJ: HER2 signaling pathway activation and response of breast cancer cells to HER2-targeting agents is dependent strongly on the 3D microenvironment. *Breast Cancer Res Treat* 2010, 122(1):35-43.
73. Junttila TT, Akita RW, Parsons K, Fields C, Lewis Phillips GD, Friedman LS, Sampath D, Sliwkowski MX: Ligand-Independent HER2/HER3/PI3K Complex Is Disrupted by Trastuzumab and Is Effectively Inhibited by the PI3K Inhibitor GDC-0941. *Cancer Cell* 2009, 15(5):429-440.
74. Gijsen M, King P, Perera T, Parker PJ, Harris AL, Larijani B, Kong A: HER2 Phosphorylation Is Maintained by a PKB Negative Feedback Loop in Response to Anti-HER2 Herceptin in Breast Cancer. *PLoS Biology* 2010, 8(12):e1000563.
75. Xu Z-Q, Zhang Y, Li N, Liu P-J, Gao L, Gao X, Tie X-J: Efficacy and safety of lapatinib and trastuzumab for HER2-positive breast cancer: a systematic review and meta-analysis of randomised controlled trials. *BMJ Open* 2017, 7(3):e013053-e013053.
76. Chen CH, Hsia TC, Yeh MH, Chen TW, Chen YJ, Chen JT, Wei YL, Tu CY, Huang WC: MEK inhibitors induce Akt activation and drug resistance by suppressing negative feedback ERK-mediated HER2 phosphorylation at Thr701. *Molecular oncology* 2017, 11(9):1273-1287.
77. Chen PW, Lin SJ, Tsai SC, Lin JH, Chen MR, Wang JT, Lee CP, Tsai CH: Regulation of microtubule dynamics through phosphorylation on stathmin by Epstein-Barr virus kinase BGLF4. *J Biol Chem* 2010, 285(13):10053-10063.

78. Rubinfeld H, Seger R: The ERK cascade: a prototype of MAPK signaling. *Molecular biotechnology* 2005, 31(2):151-174.
79. Cuadrado A, Nebreda AR: Mechanisms and functions of p38 MAPK signalling. *The Biochemical journal* 2010, 429(3):403-417.
80. Hong J, Hu K, Yuan Y, Sang Y, Bu Q, Chen G, Yang L, Li B, Huang P, Chen D *et al*: CHK1 targets spleen tyrosine kinase (L) for proteolysis in hepatocellular carcinoma. *The Journal of Clinical Investigation* 2012, 122(6):2165-2175.
81. Yang EJ, Yoon J-H, Chung KC: Bruton's Tyrosine Kinase Phosphorylates cAMP-responsive Element-binding Protein at Serine 133 during Neuronal Differentiation in Immortalized Hippocampal Progenitor Cells. *Journal of Biological Chemistry* 2004, 279(3):1827-1837.
82. Procaccia S, Ordan M, Cohen I, Bendetz-Nezer S, Seger R: Direct binding of MEK1 and MEK2 to AKT induces Foxo1 phosphorylation, cellular migration and metastasis. *Sci Rep* 2017, 7:43078.
83. Ritt DA, Monson DM, Specht SI, Morrison DK: Impact of Feedback Phosphorylation and Raf Heterodimerization on Normal and Mutant B-Raf Signaling. *Molecular and Cellular Biology* 2010, 30(3):806.
84. Klaeger S, Heinzlmeir S, Wilhelm M, Polzer H, Vick B, Koenig P-A, Reinecke M, Ruprecht B, Petzoldt S, Meng C *et al*: The target landscape of clinical kinase drugs. *Science* 2017, 358(6367).
85. Bezombes C, Grazide S, Garret C, Fabre C, Quillet-Mary A, Muller S, Jaffrezou JP, Laurent G: Rituximab antiproliferative effect in B-lymphoma cells is associated with acid-sphingomyelinase activation in raft microdomains. *Blood* 2004, 104(4):1166-1173.
86. Jazirehi AR, Vega MI, Chatterjee D, Goodglick L, Bonavida B: Inhibition of the Raf–MEK1/2–ERK1/2 Signaling Pathway, Bcl-_{xL} Down-Regulation, and Chemosensitization of Non-Hodgkin's Lymphoma B Cells by Rituximab. *Cancer Research* 2004, 64(19):7117-7126.
87. Germann UA, Furey BF, Markland W, Hoover RR, Aronov AM, Roix JJ, Hale M, Boucher DM, Sorrell DA, Martinez-Botella G *et al*: Targeting the MAPK Signaling Pathway in Cancer: Promising Preclinical Activity with the Novel Selective ERK1/2 Inhibitor BVD-523 (Ulixertinib). *Molecular Cancer Therapeutics* 2017, 16(11):2351-2363.
88. Wainstein E, Seger R: The dynamic subcellular localization of ERK: mechanisms of translocation and role in various organelles. *Current opinion in cell biology* 2016, 39:15-20.
89. Stemmer PM, Klee CB: Dual calcium ion regulation of calcineurin by calmodulin and calcineurin B. *Biochemistry* 1994, 33(22):6859-6866.
90. Jain J, McCafffrey PG, Miner Z, Kerppola TK, Lambert JN, Verdine GL, Curran T, Rao A: The T-cell transcription factor NFATp is a substrate for calcineurin and interacts with Fos and Jun. *Nature* 1993, 365(6444):352-355.
91. Okamura H, Aramburu J, García-Rodríguez C, Viola JPB, Raghavan A, Tahiliani M, Zhang X, Qin J, Hogan PG, Rao A: Concerted Dephosphorylation of the Transcription Factor NFAT1 Induces a Conformational Switch that Regulates Transcriptional Activity. *Mol Cell* 2000, 6(3):539-550.
92. Aramburu J, García-Cózar F, Raghavan A, Okamura H, Rao A, Hogan PG: Selective Inhibition of NFAT Activation by a Peptide Spanning the Calcineurin Targeting Site of NFAT. *Mol Cell* 1998, 1(5):627-637.
93. Daniels I, Turzanski J, Haynes AP: A requirement for calcium in the caspase-independent killing of Burkitt lymphoma cell lines by Rituximab. *British journal of haematology* 2008, 142(3):394-403.

94. Xu S, Huo J, Lee K-G, Kurosaki T, Lam K-P: Phospholipase Cgamma2 is critical for Dectin-1-mediated Ca2+ flux and cytokine production in dendritic cells. *The Journal of biological chemistry* 2009, 284(11):7038-7046.
95. Goodridge HS, Reyes CN, Becker CA, Katsumoto TR, Ma J, Wolf AJ, Bose N, Chan ASH, Magee AS, Danielson ME *et al*: Activation of the innate immune receptor Dectin-1 upon formation of a 'phagocytic synapse'. *Nature* 2011, 472(7344):471-475.
96. Müller MR, Rao A: NFAT, immunity and cancer: a transcription factor comes of age. *Nature Reviews Immunology* 2010, 10(9):645-656.
97. Bucher P, Erdmann T, Grondona P, Xu W, Schmitt A, Schürch C, Zapukhlyak M, Schönfeld C, Serfling E, Kramer D *et al*: Targeting chronic NFAT activation with calcineurin inhibitors in diffuse large B-cell lymphoma. *Blood* 2020, 135(2):121-132.
98. Giacinti C, Giordano A: RB and cell cycle progression. *Oncogene* 2006, 25(38):5220-5227.
99. Burkhart DL, Sage J: Cellular mechanisms of tumour suppression by the retinoblastoma gene. *Nat Rev Cancer* 2008, 8(9):671-682.
100. Chytil A, Waltner-Law M, West R, Friedman D, Aakre M, Barker D, Law B: Construction of a cyclin D1-Cdk2 fusion protein to model the biological functions of cyclin D1-Cdk2 complexes. *J Biol Chem* 2004, 279(46):47688-47698.
101. Parker LL, Piwnica-Worms H: Inactivation of the p34cdc2-cyclin B complex by the human WEE1 tyrosine kinase. *Science* 1992, 257(5078):1955-1957.
102. Tedder TF, Forsgren A, Boyd AW, Nadler LM, Schlossman SF: Antibodies reactive with the B1 molecule inhibit cell cycle progression but not activation of human B lymphocytes. *Eur J Immunol* 1986, 16(8):881-887.

Abbreviations

ACN	Acetonitrile
ADCC	Antibody-dependent cellular cytotoxicity
ADCP	Antibody-dependent cellular phagocytosis
AGC	Automatic gain control
ATP	Adenosine triphosphate
CAA	Chloroacetamide
CDC	Complement-dependent cytotoxicity
CID	Collision-induced dissociation
DDA	Data-dependent acquisition
DMEM	Dulbecco's modified Eagle's medium
DMSO	Dimethylsulfoxide
EC50	Half maximal effective concentration
EDTA	Ethylenediaminetetraacetic acid
FA	Formic acid
FBS	Fetal bovine serum
FC	Fold change
FDR	False discovery rate
HCD	Higher energy collision-induced dissociation
HEPES	4-(2-hydroxyethyl)-1-piperazineethanesulfonic acid
HPLC	High performance liquid chromatography
IC50	Half maximal inhibitory concentration
IMAC	Immobilized metal ion affinity chromatography
LC-MS/MS	Liquid chromatography tandem mass spectrometry
LTQ	linear trap quadropole
mAb	Monoclonal antibody
MS1	Mass spectrum of intact peptides
MS2	Fragment mass spectrum of MS1 precursor
MS3	Fragment mass spectrum of MS2 precursor
nanoLC	Nano flow liquid chromatography
NCE	Normalized collision energy
PBS	Phosphate-buffered saline
P-peptide	Phosphorylated peptide
PPM	Parts per million
P-proteins	Phosphorylated protein
P-site	Phosphorylation site
pY-IP	Phosphotyrosine peptide-immunoprecipitation
SD	Standard deviation
SDS-PAGE	Sodiumdodecylsulfate polyacrylamide gel electrophoresis
SPE	Solid phase extraction
STR	Short tandem repeat
TBS	Tris-buffered saline
TFA	Trifluoroacetic acid
TMT	Tandem mass tags
Tris	Tris(hydroxymethyl)aminomethane

List of figures

List of tables

V General discussion

Table of contents

General discussion

Several dozens of targeted drugs are approved for the treatment of cancer. Despite their apparent success in the clinic, the detailed mode of actions are yet not fully understood. Mass spectrometry-based phosphoproteomics enables a global view on kinase activity and therefore, holds promise to elucidate molecular actions of these agents. In this thesis, phosphoproteomics was applied to reveal the mode of actions of selected targeted cancer drugs, including small molecule kinase inhibitors and monoclonal antibodies (mAbs) in various disease settings. Thereby, a greater understanding of putative radioresistance mechanisms and radiosensitizers (chapter II), and the action of AKT inhibitors (chapter III) and of anti-HER2 and anti-CD20 mAbs (chapter IV) was created. However, the application of phosphoproteomics harbors general obstacles such as low reproducibility (section 1), missing functional annotations (section 2), and biological fidelity (section 3) that need to be overcome for successful mode of action studies. These issues will be discussed in more detail on the basis of both the results of this thesis and literature. Finally, the potential of phosphoproteomics for the application in drug discovery programs and personalized cancer medicine will be highlighted (section 4).

1 Depth and reproducibility of phosphoproteomic identifications

The general depth of phosphoproteomic identifications of the discussed datasets was considerably high, reaching up to 12,000 phosphorylation sites (p-sites) in ten tandem mass tag (TMT)-multiplexed phosphoproteomes. The phosphoproteomic analysis of pancreatic cancer cells in chapter II, for instance, currently represents the most comprehensive dataset among published studies about phosphoproteomic responses towards radiation. In fact, the numbers achieved in this thesis can be regarded as a good compromise between the complexity of the datasets and the measurement time that has been spent (16 h /ten phosphoproteomes). Still, the dynamic nature and sub-stoichiometry of protein phosphorylation demand a high dynamic range that is not easily achieved with data-dependent acquisition (DDA) used here. The underlying difficulty is that the selection of ions for isolation and fragmentation for the final identification step in MS2 scans are based on their MS1 intensity. Most of the very low abundant phosphorylated peptides might therefore never have the chance to be sampled for identification. Consequently, reproducibility is compromised. This is commonly occurring despite the utilization of dynamic exclusion leading to the refusal of already sampled peptides from fragmentation for a fixed time.

Missing values across the datasets were a difficulty seen in the phosphoproteomic datasets generated in this thesis. This issue is especially of importance for large datasets as it severely diminishes the fraction of the phosphoproteome that can be compared between different samples and conditions. Thereby, a bias towards high abundant phosphorylated peptides is introduced. In chapter IV, only one third of the total numbers of all identified p-sites in each of the B-cell lines were found in all eight datasets. For the comparison across breast cancer cell lines of different subtypes this has even worsened the reproducibility (chapter III). Here, 16 % of the total p-sites were identified across the three cell lines perturbed by three different drugs. A look into a comprehensive collection of p-sites reflects this issue even in a bigger picture. PhosphoSitePlus is one of the largest and most updated databases for post-translational modifications (PTMs) of proteins and comprises a total number of 239,027 human p-sites, of which only 71,336 p-sites (~ 30 %) were identified in more than one MS-based dataset (status of May 2020; [1]). This lack of reproducibility highlights the various context-dependent mechanisms of phosphorylation leading to the vast dynamic nature of protein phosphorylation. To overcome this issue, targeted MS workflows offer a high quantification robustness and enhanced sampling reproducibility compared to DDA approaches. While they have been already applied successfully on sets of several hundreds of phosphorylated peptides [2, 3], they still require prior knowledge about the analytes and, thus, are not suited for discovery-based research. In this thesis, a parallel reaction monitoring (PRM) assay was set up as a follow-up experiment subsequent to a DDA-based phosphoproteomic experiment to robustly cover AKT signaling (chapter III). In such order, the DDA experiment enabled to include not only known but also so far unknown AKT pathway members, and the PRM assay facilitated the reproducible identification and quantification of the phosphorylated peptides in an efficient time frame. The assay was applied to determine the action of multiple AKT inhibitors on the signaling pathway and could be extended to study AKT signaling under other aspects, such as in different cell lines, patient samples or upon other drug treatments.

Other recent mass spectrometric approaches might enable an increased dynamic range for the global analysis of protein phosphorylation. The BoxCar data acquisition method makes use of multiple segmented windows to increase MS1 fill times. Consequently, the signal-to-noise and dynamic range of MS1 scans is improved [4]. Data-independent acquisition (DIA) methods combine comprehensive proteome coverage of DDA with the sensitivity and reproducibility of targeted proteomics [5]. These approaches have not been used frequently on phosphoproteomic samples yet. However, recent publications suggested novel tools for the quantification and localization of modified peptides, which have been challenging so far [6-8].

Given these points, the multiplexing strategy with TMT in conjunction with the DDA, which was the applied approach for this thesis, is an adequate strategy to analyze (up to 16) conditions side-by-side without missing values and with reduced measurement time. However, with increasing number of TMT-datasets, the overlapping phosphoproteomes between experiments become smaller. Other MS techniques could overcome this DDA-intrinsic problem of irreproducibility, and might be technically mature for large-scale phosphoproteomic studies in the future.

2 Functional annotation of protein phosphorylation

Despite thousands of p-sites of phosphoproteomic datasets are in theory available for analyses, most of them belong to the so-called 'dark phosphoproteome' [9]. This term describes the dilemma that upstream kinases and downstream functions of protein phosphorylation are to a dramatic extent unknown, which hampers the biological interpretation of a large part of acquired phosphoproteomes. Following an 80:20 rule, just 20 % of the human kinases are annotated to phosphorylate 87% of currently known kinase substrates. Furthermore, 80 % of the kinases have fewer than 20 known substrates [9]. It has been speculated that this is predominantly the result of research biased towards only a limited set of proteins [10]. 30% of the kinases lack an assigned substrate, which suggests that many kinase-substrate relationships are yet to be discovered. Therefore, the sizes of substrate spectra might eventually harmonize among the kinome. Moreover, the biological function of most of the reported p-sites is not annotated. The PhosphoSitePlus database describes a functional role for only 8097 human p-sites, which equals < 4 % of total human p-sites. The apparent lack of knowledge of the consequences of a large part of protein phosphorylation caused speculations whether 'silent phosphorylation', meaning phosphorylation without any functional relevance, exist [11]. The identification of substrates is especially important for those kinases for which information on their cellular function is scarce. Uncovering the substrates will consequently imply the regulation of biological functions that are harbored by these substrates. Similarly, proteins with unknown function benefit from an assignment of an upstream kinase or attributed function of phosphorylation.

Concentration- and time-dependent drug treatments represent the chance to prioritize the perturbations of phosphoproteomes without the need to fully understand the function of specific phosphorylation a priori. Such phosphoproteomic data was presented in chapter IV and enabled an insight into the hundreds and thousands of significantly regulated p-sites according to the potency and dynamic action of the studied anti-HER2 and anti-CD20 drugs. In this way, several p-sites were

identified to undergo significant regulation after a few minutes rituximab treatment, which were enriched in NFAT signaling-related proteins. This highlighted the importance of early calcium-mediated signaling for the action of rituximab. Similarly, machine learning of global phosphoproteomic profiles may allow the discovery of direct kinase substrates as well as phosphorylation events with functional relevance. This was recently demonstrated by a study that took the data of > 100,000 p-sites across different biological contexts into account leading to the systemic ranking of p-sites for subsequent validation [11].

From another perspective, the data of drug-perturbed phosphoproteomes collected in this thesis offered to shed light on so far unresolved substrates of selected kinases in the context of cancer treatments. *In vitro* kinase assays are a widely used approach to uncover kinase-substrate relationships utilizing synthetic peptides with putative substrate sites and recombinant kinases. Conserved linear sequence motifs that surround the phosphorylated residue in substrates [12] commonly guide the choice of putative peptide substrates. I*n vitro* kinase assays with LC-MS/MS readout were performed on significantly regulated p-sites upon radiation (chapter II) and pharmacological AKT inhibition (chapter III) that were assumed to be regulated by increased ATM or decreased AKT kinase activity, respectively. In particular, potential ATM and AKT substrates were identified in the datasets since they harbor well-established linear motifs. Thereby, 10 novel ATM and 15 novel AKT substrates were uncovered. This can be considered a great achievement as it puts these proteins, some of which indeed with unknown function, into the context of ATM and AKT signaling as well as radiation and AKT inhibitor treatment, respectively. Furthermore, it proves the fact that novel substrates of even already well studied kinases can be uncovered, and rises hope to find substrates for the so far non-annotated kinases.

Since substrate recognition by kinases is complex and additionally includes the binding of non-canonical linear sequences under distinct biological contexts and of folded, structural motifs [13], many kinases are overlooked when just taking linear motifs into account. To overcome this intricacy, peptide arrays using a synthetic peptide libraries with randomized sequences could ease the identification of substrates for kinases with unknown linear motifs [14]. Others have introduced large-scale kinase assays on dephosphorylated lysate harboring native proteins, which enables kinases to bind to structural motifs [15]. However, *in vitro* kinase assays still suffer from limitations that might drive false positives. In this regard, the biological context of phosphorylation is completely neglected. Among other factors, concentration of the kinase and substrate, co-factors and activation state of the kinase within the assay might not mimic the cellular situation. Other experimental means are available to validate the direct

interaction of the kinase substrates and its aftermath. Analysis of interactions that are specific to phosphorylated residues can be performed in large scale and unbiased manner with synthesized phosphorylated peptides via affinity purification with LC-MS/MS readout [16]. Moreover, the phosphoproteomic data can prompt experiments leading to insights into the molecular consequences of specific protein phosphorylation such as enzymatic activity by metabolomics [17], protein stability by measuring thermal melting curves [18, 19] and localization by organelle-resolved proteomics [20].

In summary, the concentration- and time-dependent drug-perturbed phosphoproteomes presented in this thesis highlighted the possibility to prioritize responsive p-sites according to their relevance for drug action. Moreover, *in vitro* kinase assays confirmed drug-responsive novel kinase substrates, which supports the illumination of the 'dark phosphoproteome'. Against the background of the multitude of possible techniques to functionalize phosphorylation, the data of this thesis can be regarded as a rich resource for even further exploitation to uncover the role of specific phosphorylation events in the context of targeted cancer drugs.

3 Biological fidelity of cancer cell lines

While the phosphoproteomic data of the thesis was based on the treatment of cancer cell lines, the ultimate goal of the mode of action study of the drugs is the transfer to the situation in patients. The ability of cell lines to provide unlimited amount of proteins in a short time frame and uncomplicated application of drugs for the phosphoproteomic analyses are major advantages compared to other biological matrices. In order to include a comprehensive biological background for screening the agents, cancer cell lines of different molecular subtypes were the basis for all three studies. In particular, four molecularly different pancreatic cancer cell lines (chapter II), three HER2-positive breast cancer cell lines of different breast cancer subtypes (chapter III) and three CD20-positive B-cell lines (chapter IV) were chosen to study the action of the drugs. In that way, different sensitivity levels towards the drugs were included that enabled the analysis of resistance mechanisms and common actions of the drugs thereby strengthening the results.

However, cancer cell lines experience to different extents molecular drifts causing altered genomes, transcriptomes or proteomes compared to their *in vivo* counterpart [21]. Furthermore, especially the two-dimensional (2D) monolayer culture of the adherent cancer cells suffer from the lack of tissue-specific architecture, mechanical and biochemical signals, and cell-to-cell and cell-to-matrix interactions leading to the altered molecular setup of the cells compared to the *in vivo* situation [22]. As an example,

HER2-positive cells undergo a shift from AKT- to MAPK-driven signaling and subsequent altered response towards pharmacological HER2 inhibition when brought into three-dimensional (3D) growth [23]. Future phosphoproteomic mode of actions studies will benefit from biological samples that resemble the *in vivo* situation more resulting in improved prediction accuracy of drug action. Patient-derived cancer cells *in vitro* as 2D cultures [24] or 3D organoids [25], and *in vivo* as mouse [26] or zebrafish [27] xenografts offer the chance to study the action of drugs in a biological system that better recapitulates the nature of cancer cells in the patient. While the biological fidelity of these approaches as a proxy for the action of drugs in patients is increased, duration of the cultivation, cost and scalability will be challenging. That is because phosphoproteomics generally requires a high amount of protein to enrich sub-stoichiometric phosphorylated peptides from protein digests. Particularly, down-scaling of input material in conjunction with automation of sample processing protocols will enable the introduction of more sophisticated biological matrixes for future phosphoproteomic studies.

To conclude, a shift from simple cell models to more sophisticated model systems is necessary to better understand the actions of applied drugs in patients. However, these more complex models introduce major experimental challenges, which need to be addressed in further research.

4 Phosphoproteomics for drug discovery and precision cancer medicine

The data of this thesis has demonstrated the ability of phosphoproteomics to study the action of kinase inhibitors and mAbs as targeted cancer drugs in an unbiased, global manner. In this regard, implementation of phosphoproteomics in drug discovery workflows could allow to acquire the action of molecules of interest on a global, signaling network-wide scale in an early stage. This is highly relevant since it has been proposed that most clinical drugs exert their action via off-target effects [28]. Similarly, it has been shown that most clinical kinase inhibitors bind to more proteins than just the intended ones [29]. In particular, phosphoproteomic analysis of drug discovery might help to exclude molecules with unwanted off-target effects or low target/pathway engagement from costly research at an early stage. Moreover, molecule libraries can be screened with the ambition to discover agents that enable the perturbation of complex signaling networks instead of only a single target and its direct downstream partners. Phosphoproteomics will furthermore facilitate the recommendation of highly effective target combinations that are necessary to address the ever challenging emergence of resistances during cancer treatment. Progress in drug development is especially of importance for those genomic alterations that have not been pharmacologically engaged in patients yet. As an example, Ras is a key component in

MAPK signaling that is mutated in the extent of one-quarter of all cancers and even in the majority of certain cancer types, such as in 95 % of pancreatic cancer patients [30]. To date, current drug development approaches have not been successful to design inhibitors of Ras. Promising candidates such as farnesyl transferase inhibitors, which prevent the activation of Ras oncogenes, have seen little clinical activity without a clear reason [31]. Phosphoproteomics could help to understand why these drugs have failed clinical reviewing and might suggest other agents.

Phosphoproteomics also rises hope to spur precision cancer medicine (PCM). While targeted cancer therapy and PCM were formerly used interchangeably, targeted therapies are defined to be applied to rather large groups of patients. Clinical efficacy and safety of targeted drugs and companion diagnostics are proven in prospective trials. PCM, in contrast, aims to administer one or more targeted agents to a patient with genomic alterations that are actionable [32]. The assignment of a specific drug is mostly justified by a 'levels-of-evidence' approach. This term describes a decision-support framework that estimates the likelihood of the biological relevance of genomic alterations found in a patient's tumor. Furthermore, the likelihood that a targeted drug will exert efficacy in a patient will be described [33]. However, supporting information for both layers of the framework are often limited to findings in cell lines and animal models, and anecdotal reports of clinical responses. Thus, a high risk of both low efficacy and toxic side effects are major difficulties of PCM. The sheer complexity of this endeavor still precludes standardized decisions, which necessitates molecular tumor boards that recommend therapeutic options on a case-by-case basis. Meta-analysis of personalized approaches in oncology trials generally support the application of PCM strategies to different patient populations [34, 35]. First PCM trials that were based on a combination of genomics and transcriptomics highlighted the benefits of additional 'omic data' for the characterization of tumors [32]. Additional levels of tumor data will strengthen the evidence for actionable targets and could include transcriptomics, proteomics and epigenomics. Especially the analysis of phosphoproteomic profiles of patients will contribute to reveal perturbed signaling pathways that are actionable by targeted drugs. Moreover, PCM will profit from phosphoproteomic mode of action studies, which uncover the action of drugs on a global scale and in the background of frequently occurring genomics alterations.

Major challenges regarding the application of phosphoproteomics in routine drug discovery and oncology still remain for the future and have been discussed. In particular, improvements in sample preparation and mass spectrometric analysis including an increase in the sensitivity, reproducibility, and throughput are required to meet the demands of industrial and clinical workflows. From the perspective

of the final data analysis, advanced computational methods such as machine learning will be obligatory to handle the increasingly complex phosphoproteomic data and to extract relevant findings.

References

1. Hornbeck PV, Kornhauser JM, Tkachev S, Zhang B, Skrzypek E, Murray B, Latham V, Sullivan M: PhosphoSitePlus: a comprehensive resource for investigating the structure and function of experimentally determined post-translational modifications in man and mouse. *Nucleic Acids Res* 2012, 40(Database issue):D261-270.
2. Lawrence RT, Searle BC, Llovet A, Villén J: Plug-and-play analysis of the human phosphoproteome by targeted high-resolution mass spectrometry. *Nat Methods* 2016, 13(5):431-434.
3. de Graaf EL, Kaplon J, Mohammed S, Vereijken LA, Duarte DP, Redondo Gallego L, Heck AJ, Peeper DS, Altelaar AF: Signal Transduction Reaction Monitoring Deciphers Site-Specific PI3K-mTOR/MAPK Pathway Dynamics in Oncogene-Induced Senescence. *J Proteome Res* 2015, 14(7):2906-2914.
4. Meier F, Geyer PE, Virreira Winter S, Cox J, Mann M: BoxCar acquisition method enables single-shot proteomics at a depth of 10,000 proteins in 100 minutes. *Nat Methods* 2018, 15(6):440-448.
5. Chapman JD, Goodlett DR, Masselon CD: Multiplexed and data-independent tandem mass spectrometry for global proteome profiling. *Mass Spectrom Rev* 2014, 33(6):452-470.
6. Rosenberger G, Liu Y, Röst HL, Ludwig C, Buil A, Bensimon A, Soste M, Spector TD, Dermitzakis ET, Collins BC *et al*: Inference and quantification of peptidoforms in large sample cohorts by SWATH-MS. *Nature biotechnology* 2017, 35(8):781-788.
7. Sidoli S, Fujiwara R, Kulej K, Garcia BA: Differential quantification of isobaric phosphopeptides using data-independent acquisition mass spectrometry. *Molecular bioSystems* 2016, 12(8):2385-2388.
8. Bekker-Jensen DB, Bernhardt OM, Hogrebe A, Martinez-Val A, Verbeke L, Gandhi T, Kelstrup CD, Reiter L, Olsen JV: Rapid and site-specific deep phosphoproteome profiling by data-independent acquisition without the need for spectral libraries. *Nature Communications* 2020, 11(1):787.
9. Needham EJ, Parker BL, Burykin T, James DE, Humphrey SJ: Illuminating the dark phosphoproteome. *Science Signaling* 2019, 12(565):eaau8645.
10. Edwards AM, Isserlin R, Bader GD, Frye SV, Willson TM, Yu FH: Too many roads not taken. *Nature* 2011, 470(7333):163-165.
11. Ochoa D, Jarnuczak AF, Viéitez C, Gehre M, Soucheray M, Mateus A, Kleefeldt AA, Hill A, Garcia-Alonso L, Stein F *et al*: The functional landscape of the human phosphoproteome. *Nature biotechnology* 2020, 38(3):365-373.
12. Miller ML, Jensen LJ, Diella F, Jørgensen C, Tinti M, Li L, Hsiung M, Parker SA, Bordeaux J, Sicheritz-Ponten T *et al*: Linear motif atlas for phosphorylation-dependent signaling. *Sci Signal* 2008, 1(35):ra2.
13. Miller CJ, Turk BE: Homing in: Mechanisms of Substrate Targeting by Protein Kinases. *Trends in biochemical sciences* 2018, 43(5):380-394.
14. Mok J, Kim PM, Lam HY, Piccirillo S, Zhou X, Jeschke GR, Sheridan DL, Parker SA, Desai V, Jwa M *et al*: Deciphering protein kinase specificity through large-scale analysis of yeast phosphorylation site motifs. *Sci Signal* 2010, 3(109):ra12.
15. Sugiyama N, Imamura H, Ishihama Y: Large-scale Discovery of Substrates of the Human Kinome. *Scientific Reports* 2019, 9(1):10503.
16. Sharma K, Weber C, Bairlein M, Greff Z, Kéri G, Cox J, Olsen JV, Daub H: Proteomics strategy for quantitative protein interaction profiling in cell extracts. *Nat Methods* 2009, 6(10):741-744.

17. Yugi K, Kubota H, Toyoshima Y, Noguchi R, Kawata K, Komori Y, Uda S, Kunida K, Tomizawa Y, Funato Y *et al*: Reconstruction of insulin signal flow from phosphoproteome and metabolome data. *Cell Rep* 2014, 8(4):1171-1183.
18. Martinez Molina D, Jafari R, Ignatushchenko M, Seki T, Larsson EA, Dan C, Sreekumar L, Cao Y, Nordlund P: Monitoring drug target engagement in cells and tissues using the cellular thermal shift assay. *Science* 2013, 341(6141):84-87.
19. Jarzab A, Kurzawa N, Hopf T, Moerch M, Zecha J, Leijten N, Bian Y, Musiol E, Maschberger M, Stoehr G *et al*: Meltome atlas—thermal proteome stability across the tree of life. *Nature Methods* 2020, 17(5):495-503.
20. Krahmer N, Najafi B, Schueder F, Quagliarini F, Steger M, Seitz S, Kasper R, Salinas F, Cox J, Uhlenhaut NH *et al*: Organellar Proteomics and Phospho-Proteomics Reveal Subcellular Reorganization in Diet-Induced Hepatic Steatosis. *Dev Cell* 2018, 47(2):205-221.e207.
21. Gillet J-P, Varma S, Gottesman MM: The clinical relevance of cancer cell lines. *J Natl Cancer Inst* 2013, 105(7):452-458.
22. Breslin S, O'Driscoll L: Three-dimensional cell culture: the missing link in drug discovery. *Drug discovery today* 2013, 18(5-6):240-249.
23. Pickl M, Ries CH: Comparison of 3D and 2D tumor models reveals enhanced HER2 activation in 3D associated with an increased response to trastuzumab. *Oncogene* 2009, 28(3):461-468.
24. Strauss DG, Blinova K: Clinical Trials in a Dish. *Trends Pharmacol Sci* 2017, 38(1):4-7.
25. Drost J, Clevers H: Organoids in cancer research. *Nat Rev Cancer* 2018, 18(7):407-418.
26. Clohessy JG, Pandolfi PP: Mouse hospital and co-clinical trial project--from bench to bedside. *Nature reviews Clinical oncology* 2015, 12(8):491-498.
27. Fazio M, Ablain J, Chuan Y, Langenau DM, Zon LI: Zebrafish patient avatars in cancer biology and precision cancer therapy. *Nature Reviews Cancer* 2020, 20(5):263-273.
28. Lin A, Giuliano CJ, Palladino A, John KM, Abramowicz C, Yuan ML, Sausville EL, Lukow DA, Liu L, Chait AR *et al*: Off-target toxicity is a common mechanism of action of cancer drugs undergoing clinical trials. *Science Translational Medicine* 2019, 11(509):eaaw8412.
29. Klaeger S, Heinzlmeir S, Wilhelm M, Polzer H, Vick B, Koenig PA, Reinecke M, Ruprecht B, Petzoldt S, Meng C *et al*: The target landscape of clinical kinase drugs. *Science* 2017, 358(6367).
30. Prior IA, Lewis PD, Mattos C: A comprehensive survey of Ras mutations in cancer. *Cancer research* 2012, 72(10):2457-2467.
31. Adjei AA, Mauer A, Bruzek L, Marks RS, Hillman S, Geyer S, Hanson LJ, Wright JJ, Erlichman C, Kaufmann SH *et al*: Phase II study of the farnesyl transferase inhibitor R115777 in patients with advanced non-small-cell lung cancer. *J Clin Oncol* 2003, 21(9):1760-1766.
32. Moscow JA, Fojo T, Schilsky RL: The evidence framework for precision cancer medicine. *Nature Reviews Clinical Oncology* 2018, 15(3):183-192.
33. Meric-Bernstam F, Johnson A, Holla V, Bailey AM, Brusco L, Chen K, Routbort M, Patel KP, Zeng J, Kopetz S *et al*: A decision support framework for genomically informed investigational cancer therapy. *J Natl Cancer Inst* 2015, 107(7).
34. Schwaederle M, Zhao M, Lee JJ, Eggermont AM, Schilsky RL, Mendelsohn J, Lazar V, Kurzrock R: Impact of Precision Medicine in Diverse Cancers: A Meta-Analysis of Phase II Clinical Trials. *J Clin Oncol* 2015, 33(32):3817-3825.
35. Jardim DL, Schwaederle M, Wei C, Lee JJ, Hong DS, Eggermont AM, Schilsky RL, Mendelsohn J, Lazar V, Kurzrock R: Impact of a Biomarker-Based Strategy on Oncology Drug Development: A Meta-analysis of Clinical Trials Leading to FDA Approval. *J Natl Cancer Inst* 2015, 107(11).

Abbreviations

2D	Two-dimensional
3D	Three-dimensional
DDA	Data-dependent acquisition
DIA	Data-independent acquisition
LC-MS/MS	Liquid chromatography tandem mass spectrometry
mAB	Monoclonal antibodie
PCM	Precision cancer medicine
PRM	Parallel reaction monitoring
P-site	Phosphorylation site
TMT	Tandem mass tag

Danksagung

An erster Stelle möchte ich meinem Doktorvater Bernhard meinen Dank aussprechen. Danke, dass ich an diesem spannenden Thema arbeiten durfte. Danke für dein ehrliches Feedback, die Zeit, die du für die vielen Meetings mit mir genommen hast, die motivierenden Gespräche am Morgen vor der Kaffeemaschine, deine Ideen in Projekten und den Freiraum, den du mir während der Jahre gelassen hast. Dies alles ist nicht selbstverständlich.

Danke an all meine lieben Kollegen. Solch einen Zusammenhalt, gegenseitige Unterstützung und Spaß bei der Arbeit findet man selten. Und ohne die sich die Jahre sicherlich nicht so leicht angefühlt hätten. Guillaume und Karl, danke für die positive Atmosphäre in unserem Büro und die vielen Gespräche über wissenschaftliche und nicht so wissenschaftliche Dinge. Merci beaucoup. Danke an Silvia und Gabi für die Unterstützung bei den administrativen Erledigungen der letzten Jahre und die vielen netten Plausche. Andi, Michaela und Andrea, danke für eure Hilfe bei allerlei kleineren und größeren Aufgaben im Labor und die Unterstützung bei Experimenten. Julia und Chien-Yun, danke, dass ihr euch Zeit und Muße für das Korrekturlesen meiner Arbeit genommen habt. Steffi, danke für die großartige Unterstützung in den Zeiten, auf die es ankommt.

Ich danke auch PD Dr. Günter Schneider meine Arbeit zu begutachten, und Prof. Dr. Angelika Schnieke für die Übernahme des Prüfungsvorsitz. Außerdem möchte ich meinen externen Kollaborationspartnern für die ausgezeichnete Zusammenarbeit danken.

Auch bin ich überaus dankbar, so engagierte Studierende in ihren Praktika, Masterarbeiten und Hiwis begleitet haben zu dürfen. Theresa, Leonie, Mona, Nicola und Nicolas, lieben Dank, dass ihr mit mir gearbeitet und einen wichtigen Beitrag zu dieser Arbeit geleistet habt.

Zu guter Letzt möchte ich mich bei meinen Freunden und meiner Familie nah und fern bedanken. Ihr seid immer für mich da gewesen. Danke Mama und Papa für eure immerwährende Unterstützung. Toby und Florentin, danke für den Rückhalt und die Liebe. Ohne euch wäre alles nichts.

List of publications

- Dietinger V, García de Durango CR, Wiechmann S, Boos SL, Michl M, Neumann J, Hermeking H, Kuster B, Jung P: Wnt-driven LARGE2 mediates laminin-adhesive O-glycosylation in human colonic epithelial cells and colorectal cancer. Cell Commun Signal 2020, 18(1):102.
- Bian Y, Zheng R, Bayer FP, Wong C, Chang YC, Meng C, Zolg DP, Reinecke M, Zecha J, Wiechmann S et al: Robust, reproducible and quantitative analysis of thousands of proteomes by micro-flow LC-MS/MS. Nat Commun 2020, 11(1):157.
- Reinecke M, Ruprecht B, Poser S, Wiechmann S, Wilhelm M, Heinzlmeir S, Kuster B, Medard G: Chemoproteomic Selectivity Profiling of PIKK and PI3K Kinase Inhibitors. ACS Chem Biol 2019.
- Yu P, Petzoldt S, Wilhelm M, Zolg DP, Zheng R, Sun X, Liu X, Schneider G, Huhmer A, Kuster B: Trimodal Mixed Mode Chromatography That Enables Efficient Offline Two-Dimensional Peptide Fractionation for Proteome Analysis. Anal Chem 2017, 89(17):8884-8891.
- Klaeger S, Heinzlmeir S, Wilhelm M, Polzer H, Vick B, Koenig P-A, Reinecke M, Ruprecht B, Petzoldt S, Meng C et al: The target landscape of clinical kinase drugs. Science 2017, 358(6367).
- Feil G, Horres R, Schulte J, Mack AF, Petzoldt S, Arnold C, Meng C, Jost L, Boxleitner J, Kiessling-Wolf N et al: Bacterial Cellulose Shifts Transcriptome and Proteome of Cultured Endothelial Cells Towards Native Differentiation. Mol Cell Proteomics 2017, 16(9):1563-1577.
- Petzoldt S, Kahra D, Kovermann M, Dingeldein AP, Niemiec MS, Aden J, Wittung-Stafshede P: Human cytoplasmic copper chaperones Atox1 and CCS exchange copper ions in vitro. Biometals 2015, 28(3):577-585.